

Synthesis and investigation of artificial metallonucleases

Noel Byrne

Thesis for the Degree of PhD



Supervisor: Dr. Andrea Erxleben

April 2015

School of Chemistry

National University of Ireland, Galway

Abstract

The aim of this work is the synthesis and investigation of artificial metallonucleases. In the first part of this work a simple model system was used allowing for the quantification of the artificial nucleases ability. In the second part of the work the synthesis of artificial metallonucleases with the ability to target specific cells was explored.

In the first part the synthesis of three dinucleating ligands, which structurally consist of a 4-methyl phenol “body” and two mononucleating ligand “arms” are described. This “body” allowed for the generation of dinuclear complexes with both metal atoms in close contact. Using a DNA and RNA analogue the nuclease ability of the complexes was quantified. It was found that complexes of the unsymmetrical ligand were more reactive and had higher optimum pH than the corresponding symmetrical complexes. Using both pH rate profiles and solution behaviour a mechanism of action based on an aqua-hydroxo species was proposed. The metals investigated were copper due to its Lewis acidity, gallium due to its potential to mimic the more biologically relevant Fe^{3+} and magnesium due to its involvement in nucleases.

In the second part the synthesis of a mononucleating ligand with an amine moiety is described, to allow for greater synthetic versatility this was further derivatized with a carboxylic acid moiety. Using the amine moiety the mononucleating ligand was linked to cholic acid and TSPO ligands generating 4 novel mononucleating ligands. Monocopper complexes of these ligands were synthesised using 1,10-phenanthroline as a co-ligand the synthesis of which is described. These novel complexes combine both an artificial nuclease and a targeting unit, potentially allowing for the selective targeting of tumour cells.

Acknowledgements

I firstly want to thank my supervisor Dr. Andrea Erxleben, for her help, guidance and patience during my PhD.

I also want to thank my co-workers and fellow students within the School of Chemistry for the good times. Special thanks must go to; Dr. Fergal Coleman for helping me at the start of my PhD, Nora Crushell for her help in deciphering other peoples writing, Dr. Pól MacFhionnaighle and Rob Whiriskey for the craic and good chats. I would also like to thank all the members, past and present, of the Erxleben group.

Thanks also must go to the Irish Research Council (formerly) IRCSET for funding this work. Without that none of this could have being performed.

I also want to thank the technical staff in NUIG without whose help and presence none of this work could be performed. Special thanks must go to Jim Cotter for his enthusiasm, energy and entertainment that made working in the Inorganic lab enjoyable. Seamus Collier for running my NMR samples no matter how terrible they were. Dr. Roisin Doohan and Ger Fahy for helping with my MS work. Marian Vignoles for running my elemental analyses and listening to all my complaints whenever the instrument broke.

Finally I would like to thank my family both close and extended for their support, understanding, encouragement and listening to all my complaints throughout my PhD. I also want to thank my parents for instilling the value of education and hard work which helped me get through my studies.

Table of contents

Abstract	i
Acknowledgments	ii
Table of contents	iii
Glossary of symbols and abbreviations	ix
Chapter 1. Introduction	
1.1. Phosphate group in biology	1
1.1.1. DNA and RNA structure	2
1.1.2. DNA/RNA phosphodiester bond stability	3
1.1.3. DNA/RNA function	4
1.2. Nucleic acid enzymes	4
1.2.1. Nucleases	5
1.2.1.1. Metal-free nucleases	6
1.2.1.2. Metal dependent nucleases	8
1.2.1.2.1. Dimetallic nucleases	8
1.2.1.2.2. Trimetallic nucleases	9
1.2.1.2.3. Monometallic nucleases	10
1.3. Artificial nucleases	11
1.3.1. Artificial nucleases as potential drugs	12
1.3.2. Hydrolytic cleavage	13
1.3.2.1. Leaving group activation	13
1.3.2.2. Lewis acid activation	14
1.3.2.3. Metal hydroxide activation	15
1.3.2.4. Metal hydroxide activation coupled with Lewis acid activation	15
1.3.3. Oxidative cleavage	16
1.3.3.1. Oxidative cleavage mechanism	17
1.3.4. Photoinduced cleavage	18
1.4. References	20

Chapter 2. Synthesis of dinuclear complexes as artificial nucleases

2.1	Introduction	23
2.1.1.	Free ions as artificial nucleases	23
2.1.2.	Complexes of f-block metals	23
2.1.3.	Complexes of d-block metals	24
2.1.4.	Complexes of p-block metals	26
2.1.5.	Synergy	28
2.1.5.1.	Multinuclear complexes	28
2.1.5.2.	Dinuclear complexes based on 4-methyl phenol	29
2.1.6.	Kinetic and mechanistic methods	32
2.2.	Aims and objectives	34
2.3.	Results	35
2.3.1.	Synthesis of ligands	35
2.3.1.1.	Synthesis of symmetrical ligands \mathbf{HL}^1 and $\mathbf{H}_3\mathbf{L}^2$	35
2.3.1.2.	Synthesis of unsymmetrical ligand $\mathbf{H}_3\mathbf{L}^3$	37
2.3.2.	Dinuclear \mathbf{Mg}^{II} complex studies	38
2.3.2.1.	\mathbf{HL}^1	38
2.3.2.1.1.	Complex synthesis and stability	38
2.3.2.2.	$\mathbf{H}_3\mathbf{L}^2$	40
2.3.2.2.1.	Complex synthesis and stability	40
2.3.2.2.2.	Kinetic investigations	41
2.3.2.3.	$\mathbf{H}_3\mathbf{L}^3$	45
2.3.2.3.1.	Complex synthesis and stability	45
2.3.2.3.2.	Kinetic investigations	47
2.3.3.	Dinuclear \mathbf{Cu}^{II} complex studies	50
2.3.3.1.	$\mathbf{H}_3\mathbf{L}^2$	50
2.3.3.1.1.	Complex synthesis	50
2.3.3.1.2.	X-ray structure	50
2.3.3.1.3.	Solution behaviour	52

2.3.3.1.4. Kinetic investigations	54
2.3.3.2. H_3L^3	57
2.3.3.2.1. Complex synthesis	57
2.3.3.2.2. Kinetic investigations	57
2.3.4. Dinuclear Ga^{III} complex studies	59
2.3.4.1. Complex synthesis and stability	59
2.3.4.2. Kinetic investigations	61
2.4. Discussion and conclusions	64
2.5. References	70

Chapter 3. Synthesis of mononucleating ligands linked to targeting units

3.1. Introduction	75
3.1.1. Metallodrugs	75
3.1.1.1. Pt^{II} chemotherapeutics	76
3.1.2. Targeting	77
3.1.2.1. Passive targeting	78
3.1.2.2. Active targeting	79
3.1.2.2.1. Receptor overexpression	79
3.1.2.2.2. Nutrient hijacking	81
3.1.2.2.3. Specific organ targeting	82
3.1.2.3. Prodrugs	83
3.1.2.4. Synergistic pharmaceutical behaviour	84
3.1.2.4.1. HDAC inhibitors	84
3.1.2.4.2. NAMI-A	85
3.1.2.5. Combination of targeting and synergistic pharmacological behaviour	86
3.1.3. Benzodiazepine receptors	88
3.1.3.1. CBR structure and role	88
3.1.3.2. Translocator protein structure and role	88
3.1.3.2.1. TSPO ligands	89

3.1.3.2.2.	TSPO overexpression	91
3.1.3.2.3.	TSPO ligand cytotoxicity	91
3.1.3.2.4.	TSPO ligand cytotoxicity mechanism	92
3.1.3.2.5.	TSPO ligand pharmacophore model	92
3.1.3.2.6.	Alpidem	93
3.1.3.2.6.1.	Pharmacophore model of Alpidem	93
3.1.3.2.6.2.	Alpidem structural activity relationships	94
3.1.3.2.6.3.	Alpidem derivatives	94
3.1.3.2.6.4.	Metalloodrugs based on Alpidem derivatives	95
3.1.3.2.7.	PK11195	96
3.2.	Objectives	97
3.3.	Results and discussion	98
3.3.1.	Synthesis of mononucleating ligand	98
3.3.1.1.	Synthesis of HL ⁴	98
3.3.1.2.	Addition of carboxylic acid moiety to HL ⁴	98
3.3.2.	TSPO ligand synthesis	99
3.3.2.1.	Synthesis of Alpidem derivative	99
3.3.2.2.	Synthesis of PK11195 derivative	100
3.3.3.	Amide coupling	101
3.3.3.1.	Synthesis of HL ⁷ and HL ⁸	101
3.3.3.2.	Synthesis of HL ⁹ and HL ¹⁰	103
3.3.3.2.1.	Unsuccessful synthesis of HL ⁹ and HL ¹⁰	103
3.3.3.2.2.	Successful synthesis of HL ⁹ and HL ¹⁰	104
3.3.3.3.	Ligand characterisation by MS	105
3.3.4.	Synthesis of monocopper complexes	110
3.4.	Conclusion	111
3.5.	References	115

Chapter 4. Experimental

4.1. General information	124
4.2. Kinetic studies	126
4.3. Materials	128
4.4. Synthetic procedures	128
4.4.1. Chapter 2. Synthesis of dinuclear complexes as artificial nucleases	128
4.4.1.1. Preparation of 1	128
4.4.1.2. Preparation of 2	129
4.4.1.3. Preparation of 3	130
4.4.1.4. Preparation of 4	131
4.4.1.5. Preparation of HL ¹	132
4.4.1.6. Preparation of 5	132
4.4.1.7. Preparation of Na₃L ²	133
4.4.1.8. Preparation of 6	134
4.4.1.9. Preparation of 7	135
4.4.1.10. Preparation of 8	136
4.4.1.11. Preparation of 10	136
4.4.1.12. Preparation of 11	137
4.4.1.13. Preparation of Na₃L ³	138
4.4.1.14. Preparation of [Mg₂(L¹)(acetate)₂](BF₄)	139
4.4.1.15. Preparation of [Cu₂(L²)(H₂O)₂](NO₃)	140
4.4.1.16. Preparation of [Cu₂(L³)(H₂O)₂](NO₃)	141
4.4.1.17. Preparation of [Ga₂(L¹)(acetate)₂](ClO₄)₃	142
4.4.2. Chapter 3. Synthesis of mononucleating ligands linked to targeting units	143
4.4.2.1. Preparation of 12	143
4.4.2.2. Preparation of 13	144
4.4.2.3. Preparation of HL ⁴	145
4.4.2.4. Preparation of H₂L ⁵	146
4.4.2.5. Preparation of H₂L ⁶	147

4.4.2.6.	Preparation of 14	148
4.4.2.7.	Preparation of 15	149
4.4.2.8.	Preparation of 16	150
4.4.2.9.	Preparation of 17	151
4.4.2.10.	Preparation of 18	152
4.4.2.11.	Preparation of 19	152
4.4.2.12.	Preparation of 20	153
4.4.2.13.	Preparation of 21	154
4.4.2.14.	Preparation of HL ⁷	154
4.4.2.15.	Preparation of HL ⁸	156
4.4.2.16.	Preparation of 22	157
4.4.2.17.	Preparation of 23	158
4.4.2.18.	Preparation of HL ⁹	159
4.4.2.19.	Preparation of HL ¹⁰	161
4.4.2.20.	Preparation of [Cu(HL⁷)(phen)](PF₆)₂	162
4.4.2.21.	Preparation of [Cu(HL⁸)(phen)](PF₆)₂	163
4.4.2.22.	Preparation of [Cu(HL⁹)(phen)](PF₆)₂	164
4.4.2.22.	Preparation of [Cu(HL¹⁰)(phen)](PF₆)₂	165
4.5.	References	167
Appendices		
Appendix 1.	pH rate profiles for auto-hydrolysis of substrates	170
Appendix 2.	Cu coordination environment within [Cu₂(L²)(H₂O)₂](NO₃)	171
Appendix 3.	Crystallographic data for [Cu₂(L²)(H₂O)₂](NO₃)	172
Appendix 4.	MS characterisation of compounds 16, 17, 19, 22 and 23	173
Appendix 5.	Tables of predicted versus measured MS data for generated ligands	178

Glossary of symbols and abbreviations

°C	degrees Celsius
Å	Angstrom
α	Alpha, Largest angle in penta-coordinate geometry
A	Adenine
ACN	Acetonitrile
AIF	Apoptosis inducing factor
AMU	Atomic mass unit
Anal.	analysis
AR	Androgen receptor
Asp	Aspartate
ATP	Adenosine triphosphate
β	Beta, Second largest angle in penta-coordinate geometry
BDNP	Bis-dinitrophenol phosphate
BNPP	Bis-nitrophenol phosphate
BOC	Tert-butyloxycarbonyl
Bpy	2,2'-bipyridine
C	Cytosine
calcd.	Calculated
cAMP	Cyclic adenosine monophosphate
CAPS	N-cyclohexyl-3-aminopropanesulfonic acid
CBR	Central benzodiazepine receptor
CHES	N-cyclohexyl-2-aminoethanesulfonic acid
cm	Centimetre
cm ⁻¹	Wavenumber (IR)
CNS	Central nervous system
CNT	Carbon nanotubes
COSY	Correlation spectroscopy
d	Doublet (spectral)

Da	Dalton (Atomic mass unit) 1.66×10^{-27} Kg
DACH	Trans-1,2-diaminocyclohexane
DCC	Dicyclohexylcarbodiimide
DCM	Dichloromethane
dd	Doublet of doublets (spectral)
ddd	Doublet of doublets of doublets (spectral)
DEPT	Distortionless enhancement by polarisation transfer
DIC	N.N'-diisopropylcarbodiimide
DIEA	Diisopropylethylamine
dione	1,10-phenanthroline-5,6-dione
DMF	Dimethylformamide
DMP	Dimethylphosphate
DMSO	Dimethylsulfoxide
DNA	Deoxyribonucleic acid
DNase	Deoxyribonuclease
DPA	Bis(2-picoyl)amine
dppn	Benzo[<i>i</i>]dipyrido[3,2- <i>a</i> :2',3'- <i>c</i>]phenazine
dppz	Dipyrido[3,2- <i>a</i> :2',3'- <i>c</i>]phenazine
dpq	Dipyrido[3,2- <i>f</i> :2',3'- <i>h</i>]quinoxaline
dq	Doublet of quartets (Spectral)
DSC	Differential scanning calorimetry
dt	Doublet of triplets (Spectral)
<i>E. coli</i>	Escherichia coli
EDTA	Ethylenediaminetetraacetic acid
EEDQ	Ethyl 1,2-dihydro-2-ethoxy-1-quinolinecarboxylate
EPSP	4-(2-hydroxyethyl)-1-piperazinepropanesulfonic acid
Eq.	Equation
eq.	Equivalent
ER	Oestrogen receptor

ERZ	Electron rich zone
ESI	Electron spray ionisation
FDA	Food and drugs administration
FRA	Freely rotating aromatic
g	gram
G	Guanine
Glu	Glutamic acid
IR	Infra-red
H-bonds	Hydrogen bonds
HDAC	Histone deacetylase
His	Histidine
HOBT	Hydroxybenzotriazole
HMBC	Heteronuclear multiple bond correlation
HPLC	High pressure liquid chromatography
HPNP	2-hydroxypropyl-para-nitrophenol
hr	Hour
HRMS	High resolution mass spectrometry
HSAB	Hard and soft Lewis acid and base
HSQC	Heteronuclear single quantum correlation
HXTA	5-methyl-2-hydroxy-1,3-xylene- α,α -diamine-N,N,N',N'-tetraacetic acid
Hz	Hertz (s^{-1})
<i>I</i>	Ionic strength
<i>J</i>	Coupling constant in Hertz (Spectral)
k	Rate constant
K_a	Acid dissociation constant
K_d	Dissociation constant
kDa	kilo Dalton (1×10^3 Da)
k_{obs}	Pseudo first-order rate constant
L	Litre

LA	Lipophilic area
LRMS	Low resolution mass spectrometry
m	Multiplet (spectral)
M	Molar
mBzR	Mitochondrial benzodiazepine receptor
MDR	Mitochondrial diazepam binding inhibitor receptors
MES	2-(N-morpholino)ethanesulfonic acid
MIA	Molecular imaging agent
mg	Milligram (1×10^{-3} g)
MHz	Megahertz (1×10^6 Hz)
ml	Millilitre (1×10^{-3} L)
mM	Millimolar (1×10^{-3} M)
mmol	Millimole (1×10^{-3} mol)
mol	Mole
MOPS	(N-morpholino)propanesulfonic acid
mPBR	Mitochondrial peripheral benzodiazepine receptors
MPTP	Mitochondrial permeability transitions pore
MRI	Magnetic resonance imaging
mRNA	Messenger RNA
MS	Mass spectrometry
<i>m/z</i>	Ratio of mass to charge (Mass spectrometry)
NADH	Nicotinamide adenine dinucleotide
NAMI-A	New anti-metastasis agent
nM	Nanomolar (1×10^{-9} M)
nm	Nanometre
NMR	Nuclear magnetic resonance
NP	Nanoparticle
NPP	Nitrophenol phosphate
NUIG	National University of Galway

OPR	Out-of-plane region
PAP	Purple acid phosphatase
PAR	Planar aromatic region
PBBS	Peripheral benzodiazepine binding site
PBR	Peripheral benzodiazepine receptors
pD	negative logarithm of deuterium, ^2H , ion concentration
PET	Positron emission topography
pH	negative logarithm of hydrogen ion concentration
Phen	1,10 phenantroline
PIPES	Piperazine-N,N'-bis(2-ethanesulfonic acid)
pK _a	negative logarithm of the dissociation constant, K _a
PNS	Peripheral nervous system
RCSI	Royal College of Surgeons Ireland
R _f	Retention factor
RNA	Ribonucleic acid
RNase	Ribonuclease
ROS	Reactive oxygen species
rRNA	Ribosomal RNA
q	Quartet (spectral)
qd	Quartet of doublets (spectral)
δ	Chemical shift in ppm downfield from TMS
s	Second, singlet (spectral)
SAHA	Zolinza
SAR	Structure activity relationship
Ser	Serine
sRNA	Small RNA
τ	Tau, penta-coordinate geometry parameter
t	Triplet (spectral)
T	Thymine

TACH	Cis,cis-1,3,5-triaminocyclohexane
TACN	1.4.7-triazacyclononane
td	Triplet of doublets (Spectral)
TFA	Trifluoroacetic acid
TGA	Thermogravimetric analysis
THF	Tetrahydrofuran
TLC	Thin layer chromatography
TMP	Trimethylphosphate
TMS	Trimethylsilane
TOF	Time of flight
tRNA	Transfer RNA
TSP	Trimethylsilyl propanoic acid
TSPO	Translocator protein
Tyr	Tyrosine
U	Uracil
UCC	University College Cork
μl	Microliters (1×10^{-6} L)
μm	Micrometre (1×10^{-6} m)
μM	Micromolar (1×10^{-6} M)
μmol	Micromole (1×10^{-6} mol)
UPNP	Uridine para nitro phenol
UV-Vis	Ultraviolet-visible

Chapter 1. Introduction

Life can take a multitude of forms from microscopic to macroscopic. But however complex it may appear, life can be described in terms of molecules and chemical reactions. The molecules used can range from small molecules to incredibly large polymer-like biomolecules such as proteins, sugars and nucleic acids. These biopolymers are favoured for the majority of tasks and roles. In these biopolymers the functional groups used to link the monomers are: amide bond in proteins, glycosidic linkage in sugars and phosphate diester (phosphodiester) in nucleic acids. The phosphate diester group (phosphodiester) is based on the inorganic phosphate group (**Figure 1.1**). Phosphate monoesters (phosphomonoester) and triesters (phosphotriester) are also possible (**Figure 1.1**).

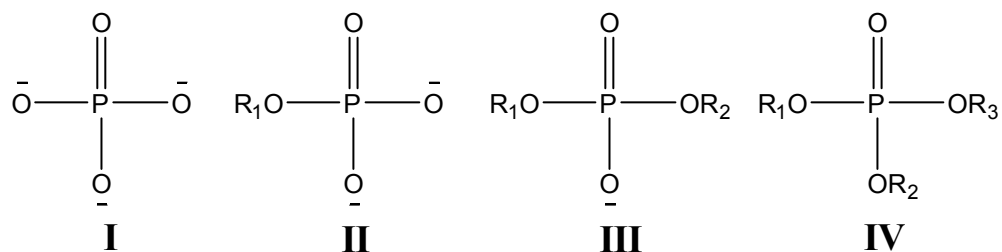


Figure 1.1: I phosphate group; II phosphate monoester; III phosphate diester; IV phosphate triester. R₁, R₂, R₃=any organic group.

1.1. Phosphate Group in Biology

Phosphate esters are found in numerous fundamental biomolecules. Adenosine triphosphate (ATP) (**Figure 1.2**) is involved in the transport of chemical energy around cells. Cyclic adenosine monophosphate (cAMP), (**Figure 1.2**), is involved in messaging and signalling processes. Phospholipids which are mainly involved in the formation of cell membranes can contain both phosphomonoesters and phosphodiester. The nucleic acids deoxyribonucleic acid (DNA) and ribonucleic acid (RNA) (**Figure 1.3**) are perhaps the most widely known biomolecules. They are involved in information storage and transfer.

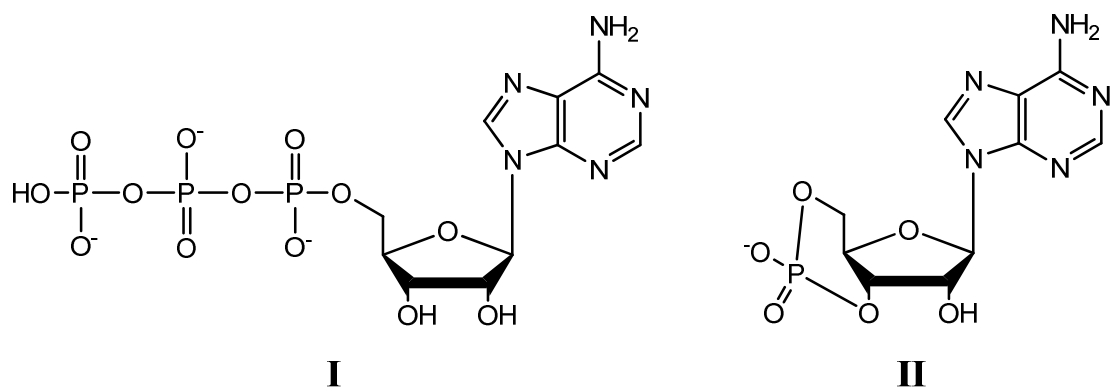


Figure 1.2: I Structure of ATP, II Structure of cAMP

1.1.1. DNA and RNA structure

RNA and DNA are found in all living organisms. The only exception is viruses, which only contain RNA. In terms of chemical structure they are very similar. Both consist of a repeating chain of a 5 membered sugar ring and phosphate diester unit (**Figure 1.3**). In DNA the sugar is deoxyribose and in RNA the sugar is ribose. Attached to the sugar is a heterocyclic base group termed as nucleobase. Together the phosphate group, sugar and nucleobase form a nucleotide. Due to their polymeric nature DNA and RNA can also be referred to as polynucleotides.

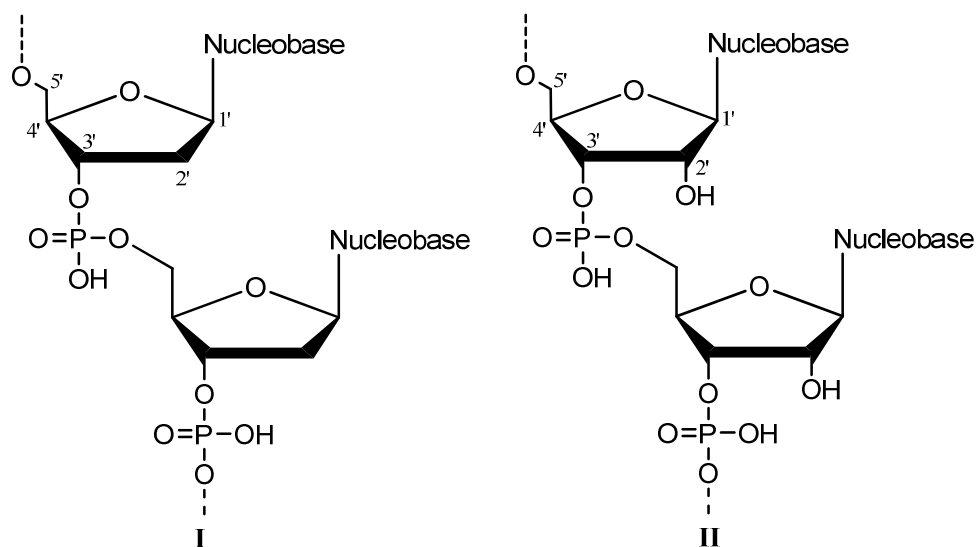


Figure 1.3: I Structure of DNA; II Structure of RNA. Numbering scheme of sugar included.

Both RNA and DNA only use four nucleobases. In DNA they are adenine (A), guanine (G), cytosine (C) and thymine (T). While RNA also uses A, C and G, thymine is replaced by uracil (U).

In the cell DNA exists as a dimer and in 1953 it was shown that the DNA dimer is a double helix¹. The nucleobases are in the centre of the helix with the sugar and phosphate diester on the outside. The two separate DNA strands are held together by hydrogen bonds (H-bonds) between nucleobases. The nucleobases are paired together in a complementary fashion termed Watson-Crick base pairing (**Figure 1.4**).

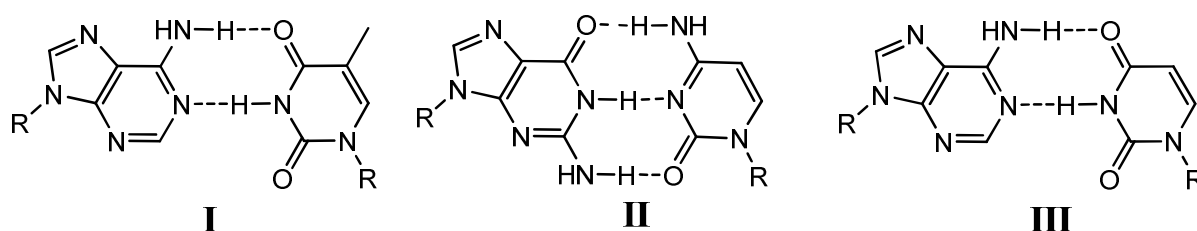


Figure 1.4: Watson-Crick base pairing: **I** Adenine:Thymine; **II** Guanine:Cytosine; **III** Adenine:Uracil. H-bonds are represented as dashed lines, R represents the sugar.

Unlike DNA, RNA is usually found as a monomer. Like DNA there is the possibility of H-bonds between complementary nucleobases to form supramolecular structures. In these, uracil replaces thymine in the adenine:thymine base pairing (**Figure 1.4, structure III**). A potential supramolecular structure is a “hairpin”, arising when there are complementary nucleotides in a single-strand.

1.1.2. DNA/RNA phosphodiester bond stability

DNA and RNA differ in their stability and location where they are found in eukaryotic cells. Humans have the vast majority of their DNA in the nucleus of the cell (≈ 3 billion base pairs) with a smaller amount found in the mitochondria (≈ 16 thousand base pairs). RNA on the other hand can be found throughout the cell.

Due to the presence of an OH group on the C2' position in ribose (**Figure 1.3, structure II**), RNA is less stable relative to DNA. The OH group can act as an internal nucleophile decreasing the stability. This can be observed by comparing the half-life of the phosphodiester linker in RNA and DNA at pH 7 and 25 °C, 110years² and 200 million years³ respectively.

1.1.3. DNA, RNA function

DNA's primary function is the storage and transfer of genetic material in living organisms. DNA can be thought of as the blueprints with the information encoded for protein structure in specific nucleotide sequences.

RNA has several functions. The main function is the synthesis of proteins which occurs in the ribosome. Several types of RNA exist for this role. Ribosomal RNA, rRNA, is an integral part of the ribosome. Transfer RNA, tRNA, which carries activated peptides to the ribosome. Messenger RNA, mRNA, is involved in DNA transcription and the carrying of the information encoded on DNA out of the nucleus to the ribosome. Short length RNA chains termed small RNA (sRNA) are present in bacteria and are involved in orchestrating stress responses⁴.

1.2. Nucleic acid enzymes

There are numerous different enzymes that are involved in the biochemistry of nucleic acids and phosphate esters e.g. nucleases, polymerases, phosphodiesterase, phosphatases and integrases. Nucleases cleave the phosphodiester bond in polynucleotides. Polymerases are involved in the synthesis of polynucleotides. Phosphatases hydrolyse phosphate monoesters. Phosphodiesterases cleave the phosphodiester bond in cyclic nucleotides such as cAMP. Integrase is a viral enzyme that allows the virus's genetic material to be integrated into the DNA of an infected cell.

Most enzymes in the previous examples usually require a divalent metal ion to promote activity^{5,6}. Magnesium is by far the most utilised. A combination of properties explains magnesium's prominence:

- High natural abundance
- Redox inertness
- Hard Lewis acid, due to high charge density
- Slow solvent exchange rates⁵
- Reduction of H₂O pK_a, from 16.0 (free solution) to 11.4 i.e. Mg-OH₂⁷

1.2.1. Nucleases

As stated previously a nuclease cleaves the phosphodiester bond in polynucleotides. The half-life of a phosphodiester bond in RNA and DNA at pH 7 and 25 °C is 110 years² and 200 million years³ respectively. So for nucleases to be biologically useful there must be very large rate accelerations. Nucleases can be divided into several categories based on a variety of properties. Firstly based on the substrate they act on; deoxyribonuclease (DNase) hydrolyses DNA and ribonuclease (RNase) hydrolyses RNA. They can also be classed on where the cleavage occurs: endonucleases cleave within the chain and exonucleases cleave at the end of the chain. Endonucleases can be further divided into non-specific or specific. Specific endonucleases will cleave a polynucleotide chain only at a very specific nucleotide sequences. Also from a bioinorganic point of view nucleases can be divided into metal free and metal dependent enzymes.

Nucleases can also be selective for which bond they cleave. There are two potential bonds, 3'-O-P and 5'-O-P, for nucleases to break. These can be distinguished by the products formed. Cleavage of the 3'-O-P bond forms 3'-OH and 5'-phosphate products. Cleavage of the 5'-O-P bond forms 3'-phosphate and 5'-OH products (**Figure 1.6**).

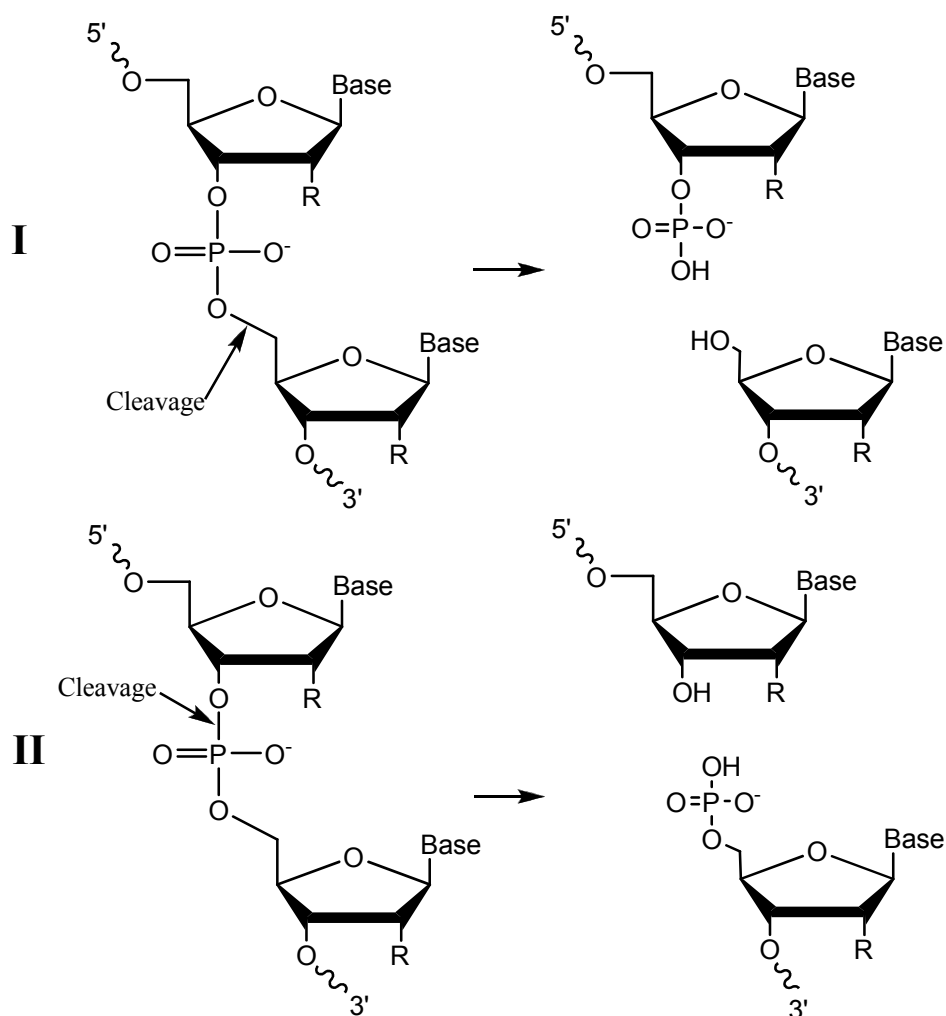


Figure 1.6: Potential hydrolysis reaction of polynucleotides (R = H DNA, R = OH RNA). **I** cleavage of 5'-O-P bond; **II** cleavage of 3'-O-P bond.

1.2.1.1. Metal-free nucleases

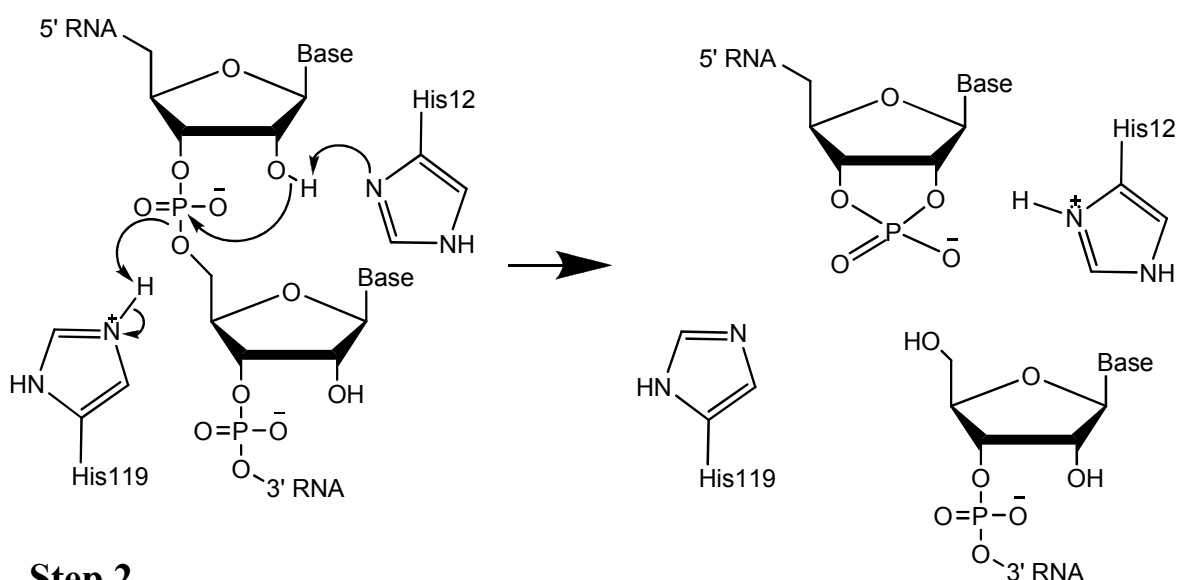
As stated earlier (**Section 1.1.2**) RNA is less stable relative to DNA due to the presence of an internal nucleophile. It has been found that metal-independent RNases utilize this moiety in their function to generate a 2'-3' cyclic phosphate intermediate. DNases which do not have this internal nucleophile moiety to exploit, form phosphoenzyme covalent intermediates with amino acid side chains such as histidine (His)⁸ and tyrosine (Tyr)⁹ on the enzyme. An example of a metal-independent nuclease is ribonuclease A (RNase A).

RNase A is an endonuclease that cleaves single stranded RNA and it is a very widely studied nuclease¹⁰. It selectively cleaves the 5'-O-P bond and operates through a two-step mechanism¹⁰⁻¹² (**Figure 1.7**). Two histidines are essential to the

mechanism. In the first step His12 acting as a general base abstracts hydrogen from 2'-OH. The 2'-O⁻ nucleophile then attacks the phosphorus atom while the His119 acting as a general acid protonates the 5'-O displacing a 5'-OH capped nucleoside and generating a 2'-3' cyclic phosphate intermediate.

In the second step the now basic His119 deprotonates a H₂O molecule generating an OH⁻ nucleophile. This nucleophile targets the phosphorus atom of the cyclic intermediate, while the acidic His12 protonates the 2'-O'. This generates the 5'-phosphate product.

Step 1



Step 2

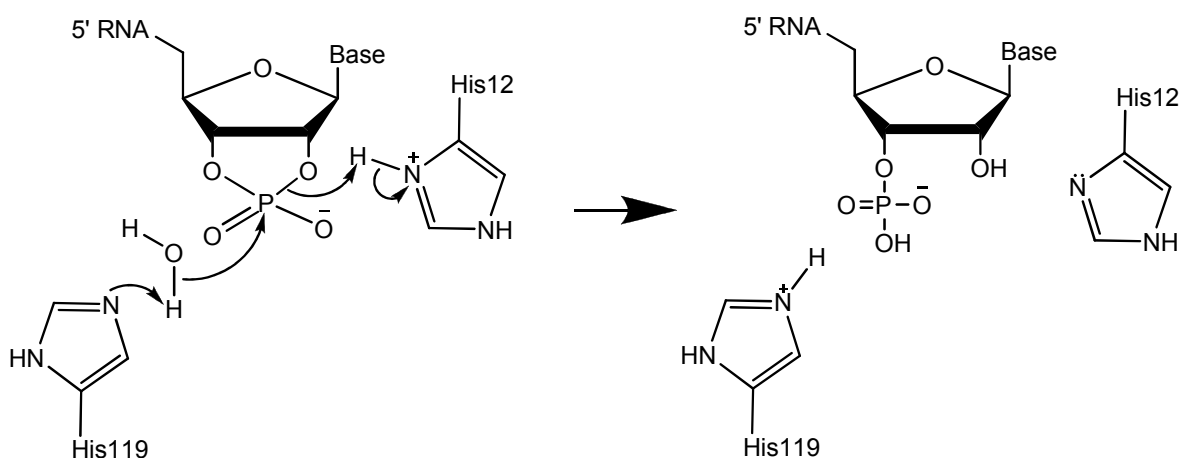


Figure 1.7: Mechanism of RNase A¹⁰⁻¹².

1.2.1.2. Metal dependent nucleases

Numerous examples of nucleases utilise metals in their active sites. From a bioinorganic point of view they can be classified in terms of how many metal atoms are in the active site. The most prevalent examples are dimetallic nucleases. Tri- and mono- metallic examples will also be discussed.

1.2.1.2.1. Dimetallic nucleases

Usually in dimetallic nucleases, both metals will coordinate the same phosphate oxygen activating the phosphodiester for nucleophilic attack. One metal will position and/or activate a nucleophile which can then attack the phosphorus atom. The other metal can coordinate to the substrate stabilising the negatively charged transition state and facilitating the reaction. An example of a dimetallic nuclease is DNA polymerase I.

DNA polymerase I is an enzyme that can catalyse both the cleavage and production of DNA. It has been shown that the active sites for both of these functions reside in separate areas of the enzyme¹³, have separate binding sites and can function independently of each other¹⁴. It is an exonuclease which selectively cleaves the 3' O-P bond. It has been shown that it requires two divalent metal atoms (Mg^{II} , Mn^{II} or Zn^{II}) to be active¹⁵.

From structural studies and x-ray crystallography data a two metal mechanism has been proposed^{13,16} (**Figure 1.8**). In the proposed mechanism two divalent ions (M_A and M_B) are coordinated by aspartic acid (Asp) residues. The metal atoms coordinate a single phosphate oxygen activating the phosphodiester bond. A hydroxide nucleophile held in place by co-ordination to M_A and H-bonds to glutamic acid (Glu) and tyrosine (Tyr) residues is able to attack the phosphorus atom. Coordination of M_B with the 3'-O facilitates the leaving of the observed products.

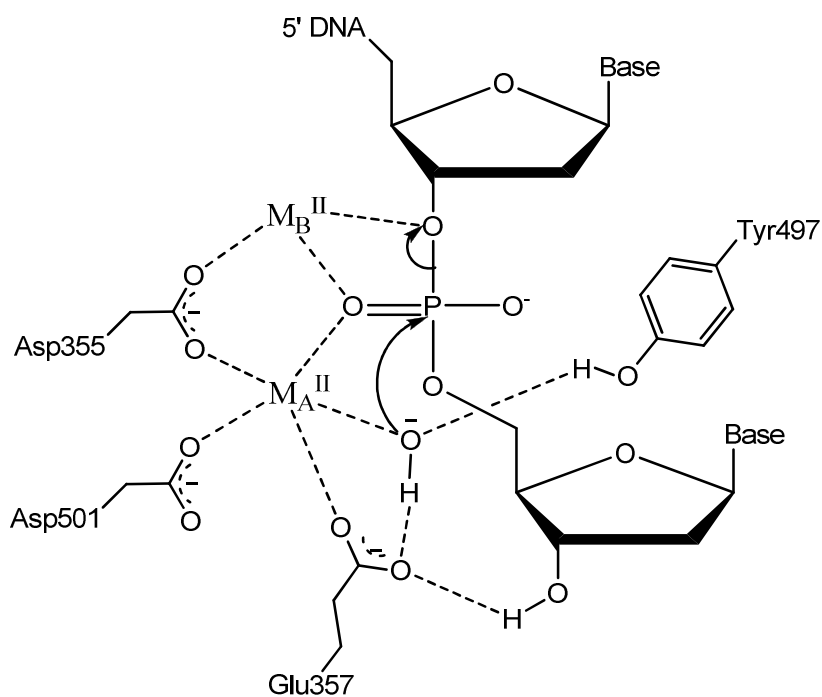


Figure 1.8: Proposed mechanism for DNA Polymerase I reaction^{13,16}.

1.2.1.2.2. Trimetallic nucleases

The mechanism of trimetallic nucleases can be thought of as a variation of the dimetallic mechanism. Two of the metal atoms have the same function as they do in the dimetallic nuclease mechanism. The third metal atom can stabilise the transition state. An example of a trimetallic nuclease is ribonuclease P (RNase P).

RNase P is an endonuclease occurring in a wide range of organisms such as archaea, bacteria and eukaryotes¹⁷. It is unusual in that it consists mainly of a single large RNA chain with one or more protein sections¹⁸. Its function is to cleave a specific phosphodiester in precursor tRNA to generate the mature tRNA. It was shown that RNase P requires the presence of divalent metal atoms (Mg^{II} or Mn^{II})¹⁹. It has also been shown that the RNA section of RNase P is able to carry out its function without the protein subunit¹⁹.

The exact mechanism is unknown but from biochemical studies proposed mechanisms involving two metals²⁰ were proposed and more recently a three metal¹⁷ variation has been proposed (**Figure 1.9**). In the proposed trimetallic mechanism a phosphate oxygen is bridged by two magnesium ions (Mg_A and Mg_B). Mg_A activates and positions the hydroxide nucleophile while Mg_B stabilises the transition state and

activates the 3'-O leaving group. The third metal atom Mg_C coordinates the 2'-OH through an inner sphere water. Mg_C contributes to the activation of the leaving group by lowering the pK_a of the coordinated water and so alleviating the proton transfer to the 3'-O.

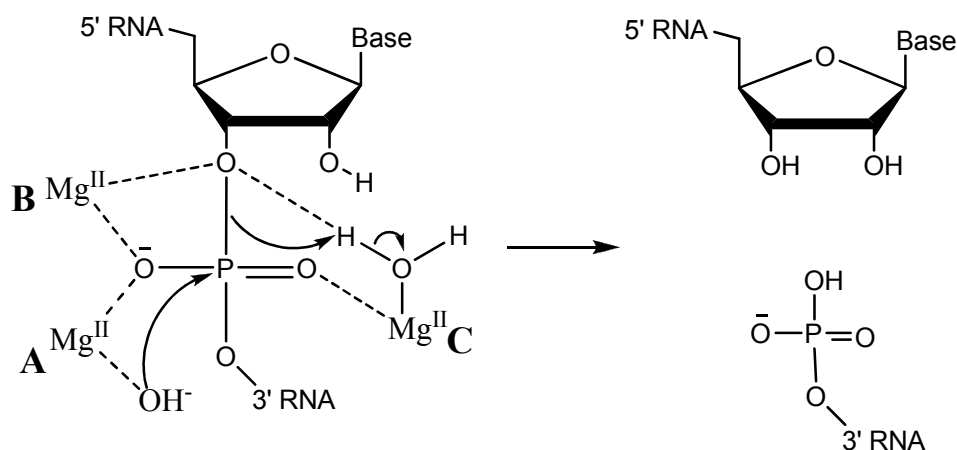


Figure 1.9: Mechanism of RNase P¹⁷.

1.2.1.2.3. Monometallic nucleases

Ribonuclease H (RNase H) is a non-specific endonuclease. It selectively cleaves the 3'-O-P bond and targets RNA strands in DNA/RNA hybrids²¹. It also requires Mg^{II} as a co-factor and is present in a wide variety of organisms from *Escherichia coli* (*E. Coli*) to humans.

RNase H is a very widely studied nuclease and several different mechanisms have been proposed²¹⁻²⁴. One proposed mechanism for *E. coli* RNase H is a general acid mechanism, with the Mg atom only influencing by outer sphere interactions²⁴ (**Figure 1.10**).

In the proposed mechanism His124 acting as a base deprotonates a water (B) which is held in place by H-bonding with Asp134. This generates a hydroxide nucleophile. This nucleophile then attacks the phosphorus. A water molecule (A) which is held in place by H-bonding with Glu48 acting as a general acid protonates the 3'-O generating the observed products. Through outer sphere interactions with Mg and 2'-OH the transient intermediate is stabilised.

This outer sphere interaction role for magnesium is reinforced by studies where substitutionally inert $[\text{Co}(\text{NH}_3)_6]^{3+}$ and $[\text{Co}(\text{en})_3]^{3+}$ also acted as metal co-factors²⁵. It is unlikely that these inert complexes are degraded *in situ* and so an outer sphere mechanism is inferred.

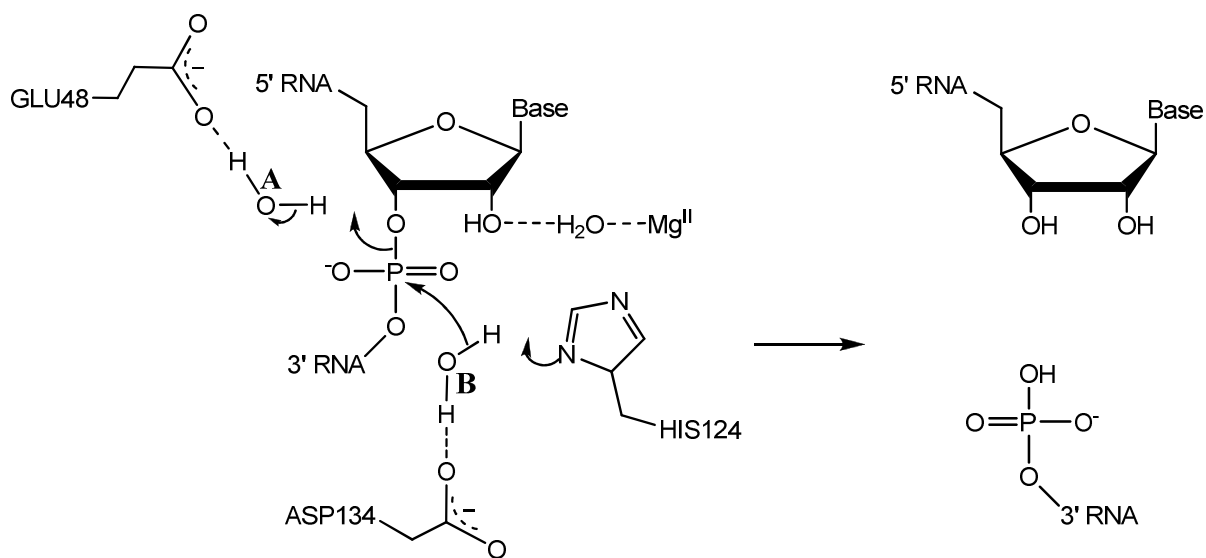


Figure 1.10: Mechanism of RNase H²⁴.

1.3. Artificial Nucleases

Artificial nucleases as indicated by their name are entities which cleave RNA and DNA but are not used by living organisms. They can include: free ions, metal complexes and organic molecules. The study of artificial nucleases is driven by many motivations: elucidation of enzyme mechanisms, generation of customised restriction enzymes and as potential antibiotic or chemotherapeutic drugs²⁶. The use of metal complexes allows for the use of elements which have little or no biological relevance. Artificial nucleases also have the potential to be produced at a much lower cost and have a higher stability than natural nucleases. They can also use oxidative and photocleavage mechanisms.

1.3.1. Artificial nucleases as potential drugs

Artificial nucleases also have the potential to be used as antisense drugs. Antisense drugs are designed oligonucleotides that can form a stable duplex with specific mRNA chains by exploiting Watson-Crick base pairing. The formation of the duplex stops translation and hence halts the production of harmful proteins (**Figure 1.11**). They are being proposed to treat a wide variety of diseases ranging from Ebola²⁷, glioma cancer²⁸ to HIV/AIDS²⁹. An antisense drug currently on the market is Vitravene which is used to treat cytomegalovirus retinitis in HIV/AIDS patients.

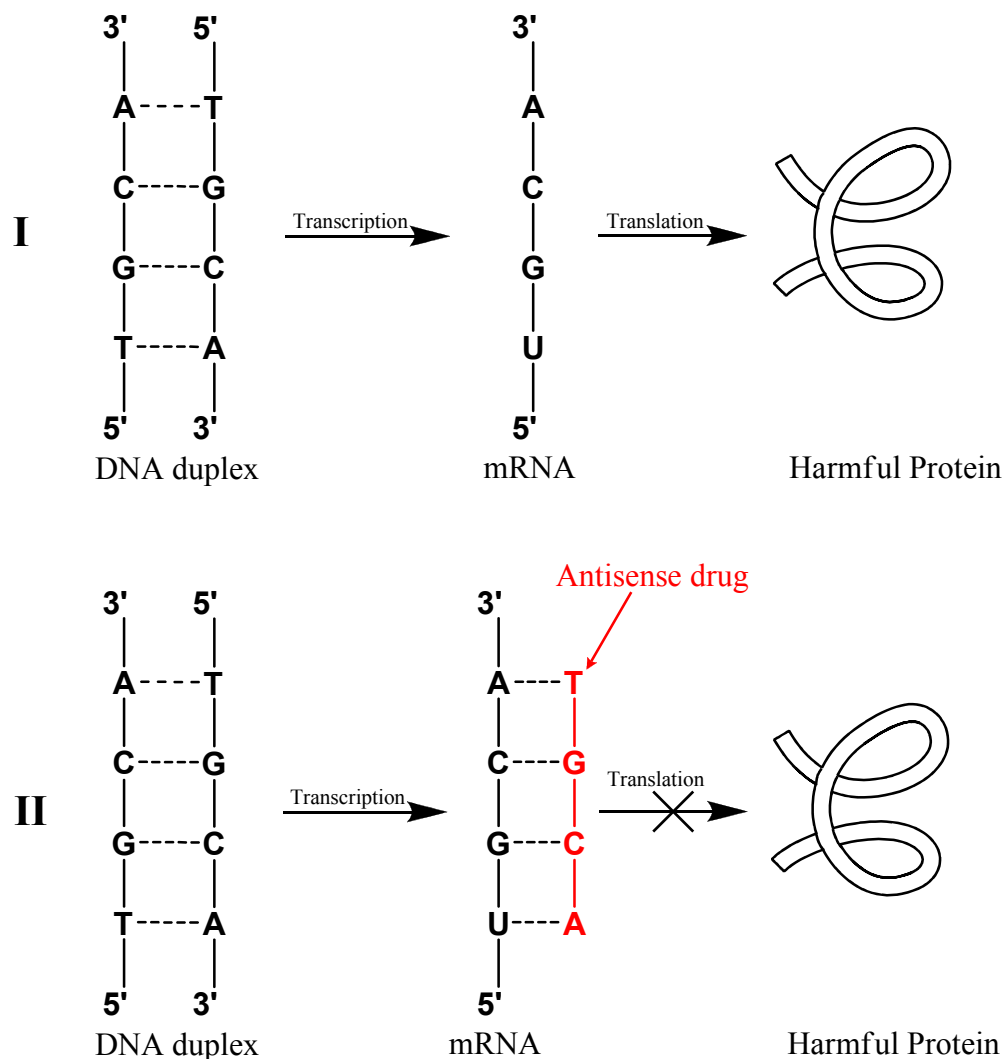


Figure 1.11: Mechanism of action of antisense drugs. **I** Process of transcription and translation producing harmful proteins; **II** antisense drug forming a duplex with mRNA halting translation.

Artificial nucleases can be transformed into antisense therapeutics by the addition of an appropriate targeting unit. These have an added benefit over traditional antisense therapeutics because the targeted mRNA chain will also be cleaved. Some examples from literature include a Cu^{II} complex³⁰ and trivalent lanthanide complexes^{31,32} (**Figure 1.12**). In the mentioned examples a known metal-binding ligand was functionalised and attached to a designed DNA chain ranging from 15 to 20 nucleotides in length. They all are found to hydrolyse the targeted RNA chain with varying success.

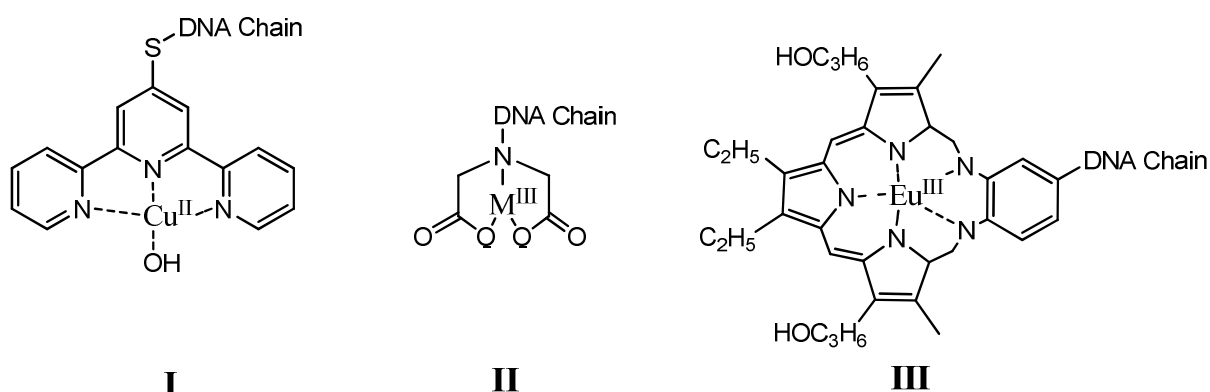


Figure 1.12: Structure of artificial nucleases linked to recognition agents. **II** $\text{M}^{\text{III}} = \text{La}^{\text{III}}, \text{Lu}^{\text{III}}, \text{Eu}^{\text{III}}, \text{Tm}^{\text{III}}$.

1.3.2. Hydrolytic cleavage

Hydrolytic cleavage involves the targeting of the phosphodiester to cleave polynucleotides. Metal complexes have several properties that enhance their cleavage ability. These are: leaving group activation, Lewis acid activation, metal-hydroxide activation and metal-hydroxide activation coupled with Lewis acid activation.

1.3.2.1. Leaving group activation

As discussed in the mechanism of DNA polymerase I (**Section 1.2.1.2.1**) it is proposed that due to the leaving group being coordinated to a metal ion the transition state is stabilised and hence the rate of hydrolysis is enhanced^{13,16}. But designing model compounds to explore this mode of activation is difficult due to the low affinity of the non-basic leaving group oxygen towards metal coordination.

In work by the group of Prof. Jik Chin a linear free energy relationship between the rate (k) of hydroxide-catalysed catalysis of phosphodiester and the pK_a of the conjugate acid of the leaving group at 25°C was determined³ (**Eq 1**).

Equation 1: $\text{Log}k = 0.69 - 0.76 pK_a$

So for each pK_a unit decrease there will be rate enhancement of approx. 5.75-fold i.e. if pK_a is lowered by 1 unit there is 5.75-fold rate enhancement, if pK_a is lowered by 2 units there is a 33-fold rate enhancement, ($33 = 5.75^2$), and so on.

Leaving group activation was also demonstrated by the hydrolysis of bis-hydroxyquinoline phosphates in the presence of divalent metal ions³³. It was found that in the presence of M^{II} ions the hydrolysis of bis(6-hydroxyquinoline) phosphate is much slower than the hydrolysis of bis(8-hydroxyquinoline).

This is explained by the metal coordination site in bis(8-hydroxyquinoline) is able to stabilise the leaving group (**Figure 1.13**) enhancing the rate of hydrolysis.

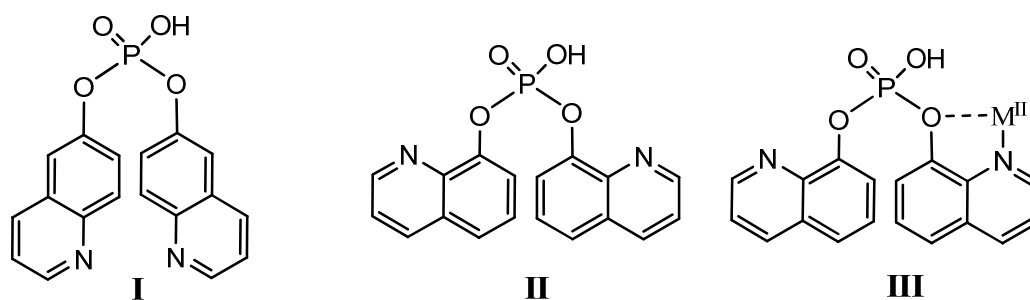


Figure 1.13: **I** structure of bis(6-hydroxyquinoline) phosphate; **II** structure of bis(8-hydroxyquinoline) phosphate; **III** divalent metal atom coordinated to bis(8-hydroxyquinoline) activating the leaving group.

1.3.2.2. Lewis acid activation

Lewis acid activation is a common method for catalysis. For artificial nucleases the phosphodiester coordinates to a metal ion thus electron density is withdrawn from the phosphorus atom making nucleophilic attack more favourable. This effect was quantified by the use of a substitutionally inert penta amine Ir^{III} complex. This complex is able to coordinate to a phosphate oxygen and gives a 400-fold rate enhancement in the rate of hydrolysis of trimethylphosphate (TMP) to yield dimethylphosphate (DMP) relative to uncoordinated TMP³⁴. The coordination makes

the phosphate more susceptible to nucleophilic attack by a solvent hydroxide (Figure 1.14). It was also shown for a substitutionally inert penta amine Co^{III} complex³⁵. This gave a 100 fold rate increase for the hydrolysis of bis(4-nitrophenol) phosphate (BNPP) (Figure 1.14).

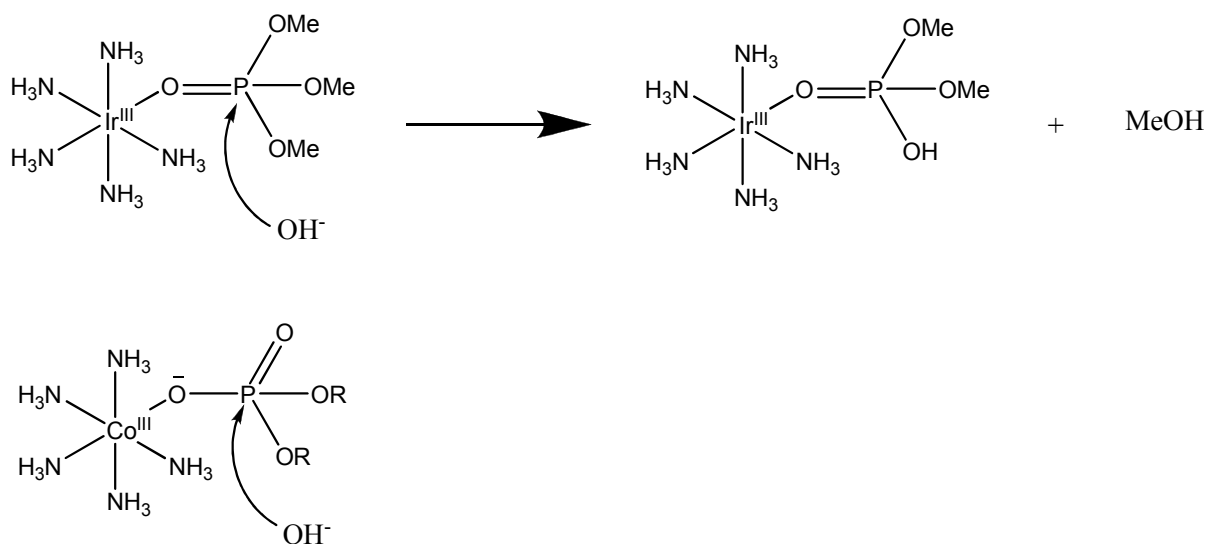


Figure 1.14: Lewis acid activation of phosphate group leading to hydrolysis.

1.3.2.3. Metal hydroxide activation

Metal ions can also generate a hydroxide nucleophile which can subsequently hydrolyse a phosphodiester. Upon coordination to a metal ion the pK_a for the reaction $2\text{H}_2\text{O} \rightleftharpoons \text{OH}^- + \text{H}_3\text{O}^+$ is lowered³⁶. Therefore metal ions can increase the concentration of hydroxide species at neutral pH. But metal coordinated hydroxide is approximately 100-times less nucleophilic than free hydroxide³³.

1.3.2.4. Metal hydroxide activation coupled with Lewis acid activation

Combination of metal hydroxide activation and Lewis acid activation by substrate binding is how metal complexes can get the greatest rate enhancement. As the activated substrate will now be in close proximity to the nucleophile there is a greater probability of hydrolysis and hence enhancing the hydrolysis rate.

This was illustrated by studies into the hydrolysis of DMP by two structurally analogous Co^{III} complexes (Figure 1.15)³⁷. DMP is a hydrolytically stable phosphodiester, the second-order rate constant for hydroxide catalysed hydrolysis of which at 25°C is $6.08 \times 10^{-12} \text{ M}^{-1}\text{s}^{-1}$ ³⁸. The main structural difference between the

Co^{III} complexes is that in **I** there are two free positions *cis* to each other while in **II** there is only one position free. It was observed that **I** gave a 90,000-fold rate enhancement over spontaneous hydrolysis. While for **II** there was no DMP hydrolysis observed even after heating at 100 °C for 1 month. This can be explained by the fact that while both **I** and **II** can coordinate the phosphate ester only in **I** is the phosphate brought into close proximity to a coordinated nucleophile (**Figure 1.15**).

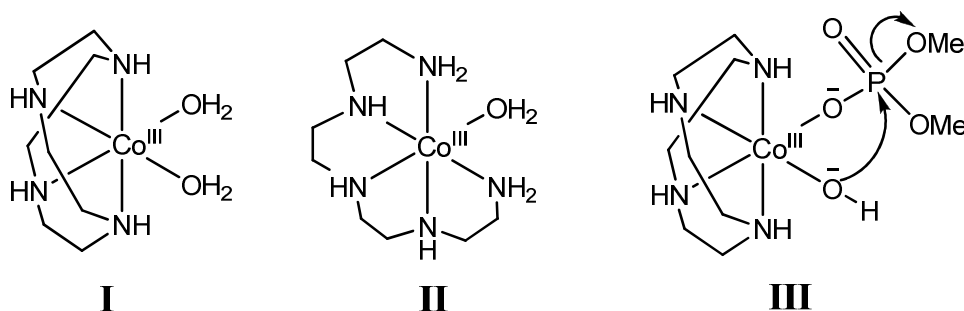


Figure 1.15: Structure of Co^{III} complexes: **I** 2 positions are taken by aqua ligands; **II** only 1 position is taken by an aqua ligand; **III** Mechanism of DMP hydrolysis by **I**.

1.3.3. Oxidative cleavage

While enzymes cleave nucleotides by hydrolytic mechanisms, the use of redox active transition metals opens the possibility of exploiting oxidative mechanisms. The first described example was a Cu^I phenanthroline complex³⁹, other examples from literature include a Fe-EDTA⁴⁰ complex and metalloporphyrins^{41,42} (**Figure 1.16**). Oxidative cleavage differs greatly from hydrolytic cleavage. While hydrolytic cleavage involves attack at the phosphodiester, oxidative cleavage involves attack of the sugar.

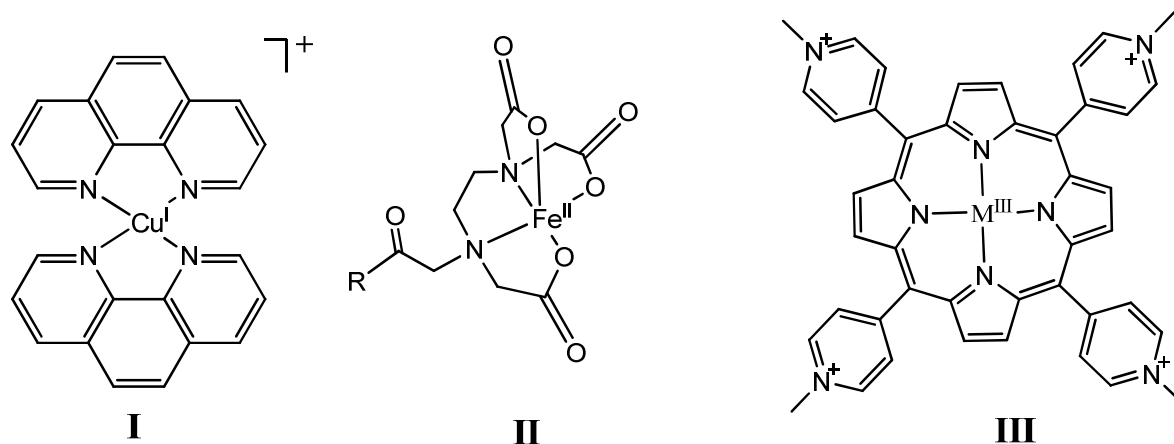


Figure 1.16: Structure of complexes that oxidatively cleave nucleic acids: **I** $[\text{Cu}(\text{phen})_2]^+$; **II** Fe-EDTA, R=DNA intercalator agent; **III** metalloporphyrins, $\text{M}^{\text{III}}=\text{Mn}^{3+}$, Fe^{3+} and Co^{3+} .

1.3.3.1. Oxidative cleavage mechanism

The first example of a complex that cleaved DNA by a purely oxidative mechanism was the Cu^{I} complex $[\text{Cu}(\text{phen})_2]^+$ ³⁹ (**Figure 1.16, structure I**). From studies it was found the reaction was dependent on the presence of an oxidising agent (O_2 or H_2O_2)³⁹ and a reducing agent (NADH)⁴³. The major products formed by the reaction are the free nucleobase, 5-methylenfuranone and the 3' and 5' phosphomonoesters⁴⁴ (**Figure 1.17**).

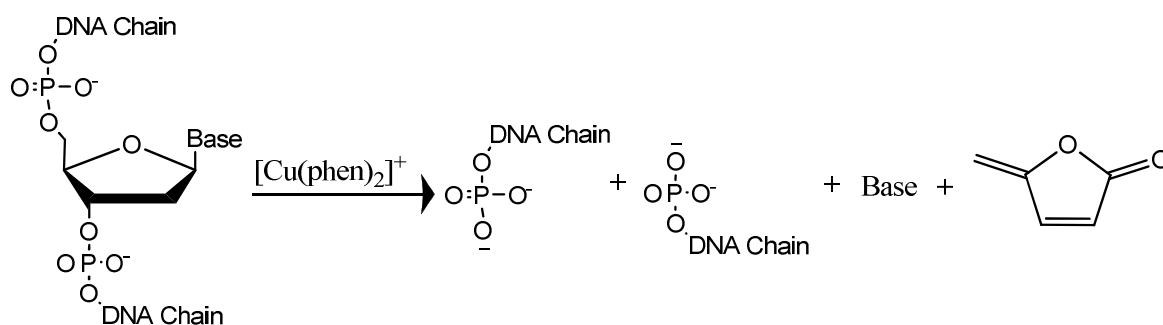


Figure 1.17: Major products of the oxidative cleavage of a DNA chain by $[\text{Cu}(\text{phen})_2]^+$

The proposed mechanism involves the reduction of Cu^{II} to Cu^{I} by the reducing agent NADH ⁴³, then through a series of reactions with H_2O_2 the active Cu-oxo species are formed or the starting Cu^{II} species can be regenerated. The active species is then able to abstract hydrogen from the deoxyribose ring. Through rearrangements and oxidation by the Cu the DNA is broken down and the observed products are

formed⁴⁵. Hydrogen abstraction primarily happens at the C1' position of the deoxyribose ring giving the major products (**Figure 1.17**). Attack is also possible at the C4' or C5' positions⁴⁶ but it is much less prevalent.

In the proposed mechanism the active site is centred on the copper atom and so is non-diffusible. The presence of the phenanthroline ligands allows $[\text{Cu}(\text{phen})_2]^+$ to intercalate DNA^{47,48}. Intercalation is the insertion between two adjacent nucleobases. It has been shown that $[\text{Cu}(\text{phen})_2]^{1+}$ interacts with the minor groove of DNA⁴⁹. This is consistent with the mechanism as the C1' carbon is only accessible in the minor groove.

1.3.4. Photoinduced cleavage

Another potential cleavage mechanism is photoinduced cleavage. Photodynamic therapy as it is termed is of particular interest for drug development as the location and timing of illumination and hence of cleavage can be easily controlled allowing for on-demand drug dosing⁵⁰. The localising of the irradiation allows for high selectivity as only targeted tissue can be irradiated.

While photoinduced cleavage has been observed for free ions such as U^{VI} ⁵¹ the most commonly explored are Ru^{II} complexes^{52,53} (**Figure 1.18**). There are two potential mechanisms for photoactive complexes to cleave DNA. These can occur together or separately. Photoinduced electron transfer to the excited complex can occur and hence the polynucleotide is cleaved by an oxidative process⁵⁴. Or singlet oxygen ($^1\text{O}_2$) is produced by the excited complex and cleaves the polynucleotide⁵⁵.

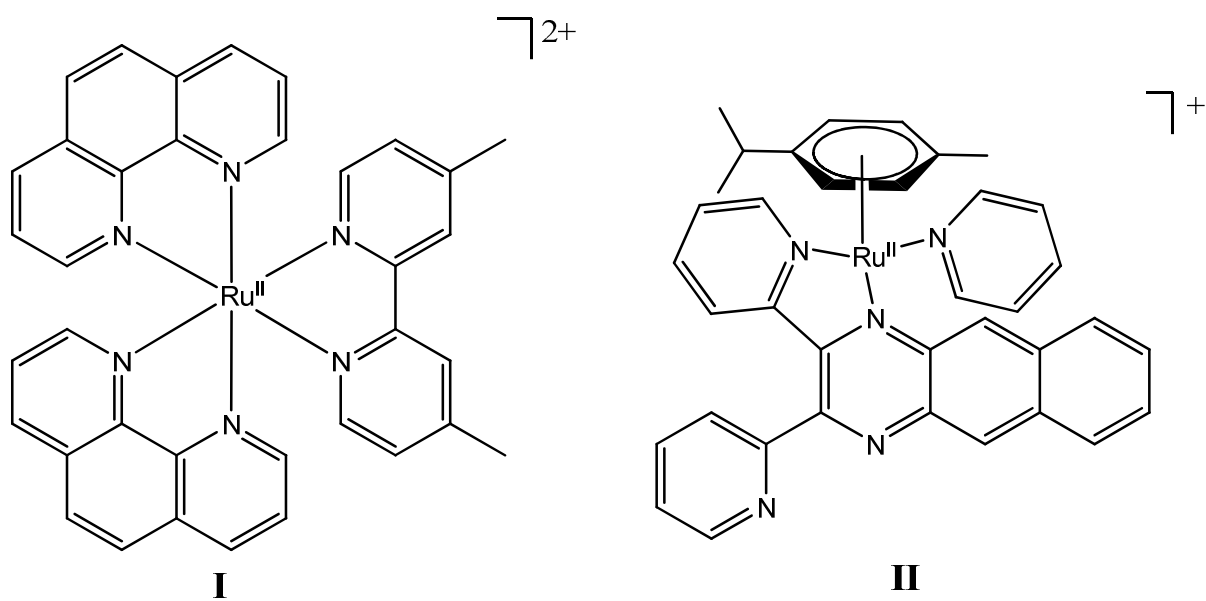


Figure 1.18 Structure of selected photoactive Ru^{II} complexes: **I** [Ru(phen)₂(dmbpy)]²⁺⁵⁶; **II** [(η⁶-*p*-cymene)Ru(dpbb)(py)]²⁺⁵⁷.

1.4. References

- (1) Watson, J. D.; Crick, F. H. *Nature* **1953**, *171*, 737-738.
- (2) Williams, N. H.; Chin, J. *Chem. Commun.* **1996**, 131-132.
- (3) Chin, J.; Banaszczyk, M.; Jubian, V.; Zou, X. *J. Am. Chem. Soc.* **1989**, *111*, 186-190.
- (4) Hoe, C.; Raabe, C. A.; Rozhdestvensky, T. S.; Tang, T. *Int. J. Med. Microbiol.* **2013**, *303*, 217-229.
- (5) Cowan, J. A., Ed. *The Biological Chemistry of Magnesium*, Wiley-VCH **1995**.
- (6) Wilcox, D. E. *Chem. Rev.* **1996**, *96*, 2435-2458.
- (7) Pontius, B. W.; Lott, W. B.; Von Hippel, P. H. *Proc. Natl. Acad. Sci. U.S.A.* **1997**, *94*, 2290-2294.
- (8) Gottlin, E. B.; Rudolph, A. E.; Zhao, Y.; Matthews, H. R.; Dixon, J. E. *Proc. Natl. Acad. Sci. U.S.A.* **1998**, *95*, 9202-9207.
- (9) Grindley, N. D.; Whiteson, K. L.; Rice, P. A. *Annu. Rev. Biochem.* **2006**, *75*, 567-605.
- (10) Raines, R. T. *Chem. Rev.* **1998**, *98*, 1045-1066.
Findlay, D.; Mathias, A. P.; Rabin, B. R. *Nature* **1960**, *187*, 601-602
- (12) Richards, F. M.; Wyckoff, H. W., in *The Enzymes, Volume 4* (Ed.: D. B. Paul), Academic Press, **1971**, 647-806
- (13) Ollis, D.; Brick, P.; Hamlin, R.; Xuong, N.; Steitz, T. *Nature* **1985**, *313*, 762-766.
- (14) Catalano, C. E.; Benkovic, S. J. *Biochemistry* **1989**, *28*, 4374-4382.
- (15) Kornberg, A.; Bagker, T. A. *DNA Replication*, University Science books **1980**.
- (16) Beese, L. S.; Steitz, T. A. *EMBO J.* **1991**, *10*, 25-33.
- (17) Kazantsev, A. V.; Pace, N. R. *Nature Rev. Microbiol.* **2006**, *4*, 729-740.
- (18) Mondragón, A. *Annu. Rev. Biophys.* **2013**, *42*, 537-557.
- (19) Guerrier-Takada, C.; Gardiner, K.; Marsh, T.; Pace, N.; Altman, S. *Cell* **1983**, *35*, 849-857.
- (20) Steitz, T. A.; Steitz, J. A. *Proc. Natl. Acad. Sci. USA* **1993**, *90*, 6498-6502.
- (21) Oda, Y.; Yoshida, M.; Kanaya, S. *J. Biol. Chem.* **1993**, *268*, 88-92.

- (22) Yang, W.; Hendrickson, W. A.; Crouch, R. J.; Satow, Y. *Science* **1990**, *249*, 1398-1405.
- (23) Nakamura, H.; Oda, Y.; Iwai, S.; Inoue, H.; Ohtsuka, E.; Kanaya, S.; Kimura, S.; Katsuda, C.; Katayanagi, K.; Morikawa, K. *Proc. Natl. Acad. Sci. U.S.A.* **1991**, *88*, 11535-11539.
- (24) Kanaya, S.; Oobatake, M.; Liu, Y. *J. Biol. Chem.* **1996**, *271*, 32729-32736.
- (25) Jou, R.; Cowan, J. A. *J. Am. Chem. Soc.* **1991**, *113*, 6685-6686.
- (26) Mancin, F.; Scrimin, P.; Tecilla, P.; Tonellato, U. *Chem. Commun.* **2005**, 2540-2548.
- (27) Barton, S. *Nat. Rev. Drug Discov.* **2006**, *5*, 106.
- (28) Hau, P.; Stockhammer, G.; Kunst, M.; Mahapatra, A.; Sastry, K.; Parfenov, V.; Leshinsky, V.; Jachimczak, P.; Bogdahn, U.; Schlingensiepen, K. In *ASCO Meeting Abstracts, Vol 24*, Am Soc Clin Oncol, **2006**, 1566.
- (29) Lu, X.; Yu, Q.; Binder, G. K.; Chen, Z.; Slepushkina, T.; Rossi, J.; Dropulic, B. *J. Virol.* **2004**, *78*, 7079-7088.
- (30) Bashkin, J. K.; Frolova, E. I.; Sampath, U. *J. Am. Chem. Soc.* **1994**, *116*, 5981-5982.
- (31) Matsumura, K.; Endo, M.; Komiyama, M. *J. Chem. Soc. Chem. Comm.* **1994**, 2019-2020.
- (32) Magda, D.; Miller, R. A.; Sessler, J. L.; Iverson, B. L. *J. Am. Chem. Soc.* **1994**, *116*, 7439-7440.
- (33) Browne, K. A.; Bruice, T. C. *J. Am. Chem. Soc.* **1992**, *114*, 4951-4958.
- (34) Hendry, P.; Sargeson, A. M. *J. Chem. Soc., Chem. Commun.* **1984**, 164-165.
- (35) Hendry, P.; Sargeson, A. M. *Progress in Inorganic Chemistry: Bioinorganic Chemistry, Volume 38* (Ed. S. J. Lippard) **1990**, 201-258.
- (36) Buckingham, D. A.; Harrowfield, J. M.; Sargeson, A. M. *J. Am. Chem. Soc.* **1974**, *96*, 1726-1729.
- (37) Kim, J. H.; Chin, J. *J. Am. Chem. Soc.* **1992**, *114*, 9792-9795.
- (38) Guthrie, J. P. *J. Am. Chem. Soc.* **1977**, *99*, 3991-4001.
- (39) Sigman, D. S.; Graham, D. R.; D'Aurora, V.; Stern, A. M. *J. Biol. Chem.* **1979**, *254*, 12269-12272.
- (40) Hertzberg, R. P.; Dervan, P. B. *J. Am. Chem. Soc.* **1982**, *104*, 313-315.
- (41) Ward, B.; Skorobogaty, A.; Dabrowiak, J. C. *Biochem. J.* **1986**, *25*, 6875-6883.

- (42) Trung Le, D.; Perrouault, L.; Helene, C.; Chassignol, M.; Nguyen Thanh, T. *Biochem. J.* **1986**, *25*, 6736-6739.
- (43) Reich, K. A.; Marshall, L. E.; Graham, D. R.; Sigman, D. S. *J. Am. Chem. Soc.* **1981**, *103*, 3582-3584.
- (44) Pope, L. M.; Reich, K. A.; Graham, D. R.; Sigman, D. S. *J. Biol. Chem.* **1982**, *257*, 12121-12128.
- (45) Meijler, M. M.; Zelenko, O.; Sigman, D. S. *J. Am. Chem. Soc.* **1997**, *119*, 1135-1136.
- (46) Oyoshi, T.; Sugiyama, H. *J. Am. Chem. Soc.* **2000**, *122*, 6313-6314.
- (47) Marshall, L. E.; Graham, D. R.; Reich, K. A.; Sigman, D. S. *Biochem. J.* **1981**, *20*, 244-250.
- (48) Veal, J. M.; Rill, R. L. *Biochem. J.* **1991**, *30*, 1132-1140.
- (49) Kuwabara, M.; Yoon, C.; Goyne, T.; Thederahn, T.; Sigman, D. S. *Biochem. J.* **1986**, *25*, 7401-7408.
- (50) Rai, P.; Mallidi, S.; Zheng, X.; Rahmanzadeh, R.; Mir, Y.; Elrington, S.; Khurshid, A.; Hasan, T. *Adv. Drug Deliv. Rev.* **2010**, *62*, 1094-1124.
- (51) Nielsen, P. E.; Jeppesen, C.; Buchardt, O. *FEBS Lett.* **1988**, *235*, 122-124.
- (52) Gao, F.; Chao, H.; Ji, L.-N. *Chem. Biodivers.* **2008**, *5*, 1962-1979.
- (53) Chao, H.; Ji, L.-N. *Bioinorg. Chem. Appl.* **2005**, *3*, 15-28.
- (54) Lecomte, J.-P.; Mesmaeker, A. K.-D.; Kelly, J. M.; Tossi, A. B.; Görner, H. *Photochem. Photobiol.* **1992**, *55*, 681-689.
- (55) Hergueta-Bravo, A.; Jiménez-Hernández, M. E.; Montero, F.; Oliveros, E.; Orellana, G. *J. Phys. Chem. B* **2002**, *106*, 4010-4017.
- (56) Bouskila, A.; Drahi, B.; Amouyal, E.; Sasaki, I.; Gaudemer, A. *J. Photochem. Photobiol. A* **2004**, *163*, 381-388.
- (57) Chen, Y.; Lei, W.; Jiang, G.; Hou, Y.; Li, C.; Zhang, B.; Zhou, Q.; Wang, X. *Dalton Trans.* **2014**, *43*, 15375-15384.

Chapter 2. Synthesis of dinuclear complexes as artificial nucleases

2.1. Introduction

As discussed previously the study of artificial nucleases is driven by a variety of reasons. Metal complexes are attractive due to their ability to utilise hydrolytic, oxidative, photoinduced or combination mechanisms. Also if the metal is substitutionally labile it will allow for rapid turnover and hence greater nuclease activity. There are numerous examples of artificial nucleases, these include: free metal ions, f-block complexes, p-block complexes and d-block complexes.

2.1.1. Free ions as artificial nucleases

It was found that free metal ions and metal salts can cause a rate enhancement of the hydrolysis of DNA. Examples include high oxidation state actinides¹, U^{VI}, and trivalent lanthanides^{2,3}. With the exception of the higher lanthanides (Tm^{III}, Yb^{III} and Lu^{III}) it was found that the rate enhancement follows the position in the series, i.e. Er^{III} gives a greater rate enhancement than La³⁺.

Similar rate enhancements have also been shown for the stable tetravalent lanthanide Ce^{IV}, which has been shown to hydrolyse DNA⁴. Ce is the only lanthanide to have a stable +4 oxidation state and it was found to be more efficient than the trivalent lanthanides towards linear DNA⁵. The catalytic ability of Ce^{IV} is best demonstrated by the 10¹¹-fold rate enhancement of the hydrolysis of the dinucleotide TpT^{4,6}.

Due to the toxicity of aqueous lanthanide metal ions they are not suitable for use as therapeutics but are still suitable and useful for biochemical applications. In all the cases discussed only hydrolytic cleavage was observed, no oxidative cleavage was observed.

2.1.2. Complexes of f-block metals

By using lanthanide complexes the toxicity would be decreased so these have also been studied. Ligands used range from macrocycles (aza-crowns and schiff bases) to modified phenols (**Figure 2.1**). Using an aza-crown (**Figure 2.1 structure I**) dinuclear Eu^{III} and Pr^{III} complexes were studied⁷. It was found that at pH 7 and 37 °C

the Pr^{III} complex caused a 2×10^6 rate enhancement for the hydrolysis of double stranded DNA. But no synergy between the metal centres was observed as the activity of the complex was only twofold of the free ion. Using a macrocyclic schiff base (**Figure 2.1 structure II**) dinuclear Ho^{III} and Er^{III} complexes were studied⁸. At pH 7 and 37 °C the complexes promoted complete hydrolysis of supercoiled DNA to either nicked or linear DNA. But there was low affinity for substrate, therefore necessitating high concentrations of complex for effective hydrolysis. Using a modified 4-methyl phenol (**Figure 2.1 structure III**), a dinuclear Ce^{IV} complex was studied⁹. At pH 8 and 37 °C the complex cleaved plasmid DNA with a rate constant of $1.4 \times 10^{-4} \text{ s}^{-1}$. It was found that the complex was selective for double stranded DNA and regioselectively hydrolysed the O3'-P bond.

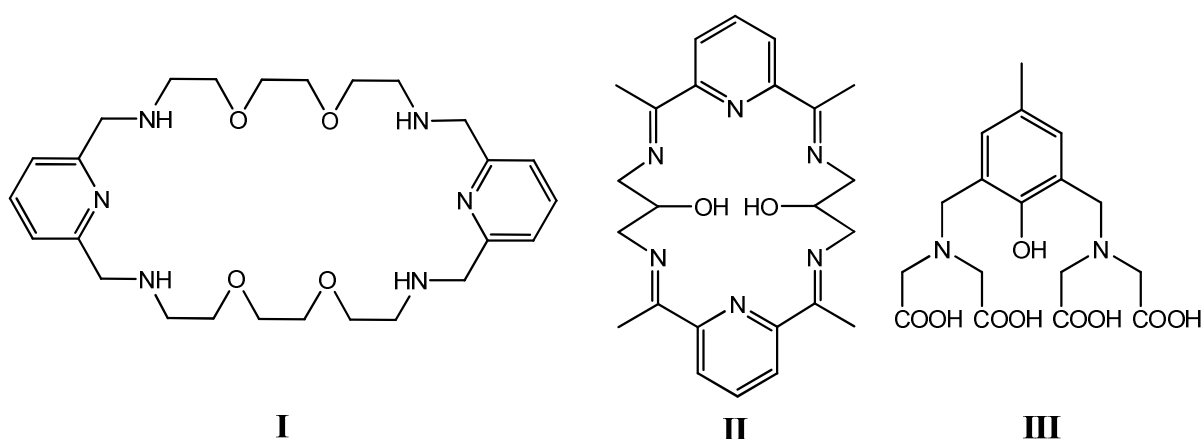


Figure 2.1: I Macrocyclic aza crown; II Macrocyclic schiff base; III Modified 4-methyl phenol ligand.

2.1.3. Complexes of d-block metals

Due to their Lewis acidity and redox chemistry transition metal containing complexes are attractive targets for artificial nucleases. Selected transition metal ions are well tolerated by the body and are involved in numerous metalloenzymes.

Copper is one of the most widely studied transition metals. One of the main reasons is that the first described oxidative nuclease was $[\text{Cu}(\text{phen})_2]^+$ ¹⁰ (**Figure 1.15 structure I, Section 1.3.3.1**). Much work has been done on this system and numerous mononuclear Cu complexes have been generated. One of the problems with $[\text{Cu}(\text{phen})_2]^+$ has been its low specificity and so work has been undertaken to make the system more selective. Phenanthroline derivatives with targeting substituents such as peptide and nucleotide chains have been investigated¹¹ (**Figure**

2.2, structure I). Also explored is the replacement of one phenanthroline with a different copper binding ligand. This can increase specificity and/or allow for introduction of additional behaviour. Ligands used include: doxycycline (antibacterial agent)¹² (**Figure 2.2, structure II**), alanine (amino acid)¹³, photosensitive ligands¹⁴ and redox compounds such as ferrocene¹⁵. In all these examples oxidative cleavage was observed. But replacement of a phenanthroline ligand can change the observed mechanism, for example when replaced by 1,2,4-triazole, hydrolytic cleavage is observed¹⁶.

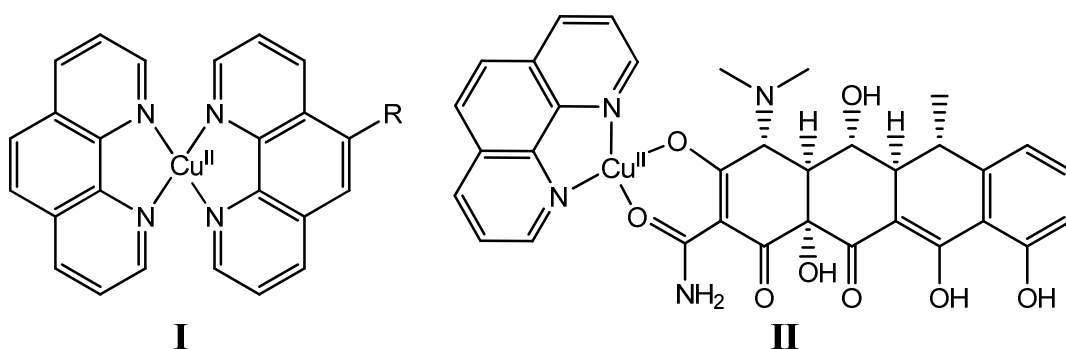


Figure 2.2: I R = peptide or nucleotide chain II [Cu(phen)(doxycycline)]²⁺.

Numerous other mononuclear Cu complexes have been explored. Ligands used include: 1,4,7-triazacyclononane, (TACN)¹⁷, *cis,cis*-1,3,5-triaminocyclohexane (TACH)¹⁸, 2,2'-bipyridine (bpy)¹⁹, ammonium bpy (a-bpy)²⁰, bis(2-picoyl)amine (DPA)²¹, methylated DPA (mDPA)²², ethylated DPA (eDPA)²², guanidinium DPA (gDPA)²³ and phenylated DPA (pDPA)²⁴ (**Figure 2.3**). In all those examples the mono-Cu²⁺ complexes generated were shown to cleave polynucleotides.

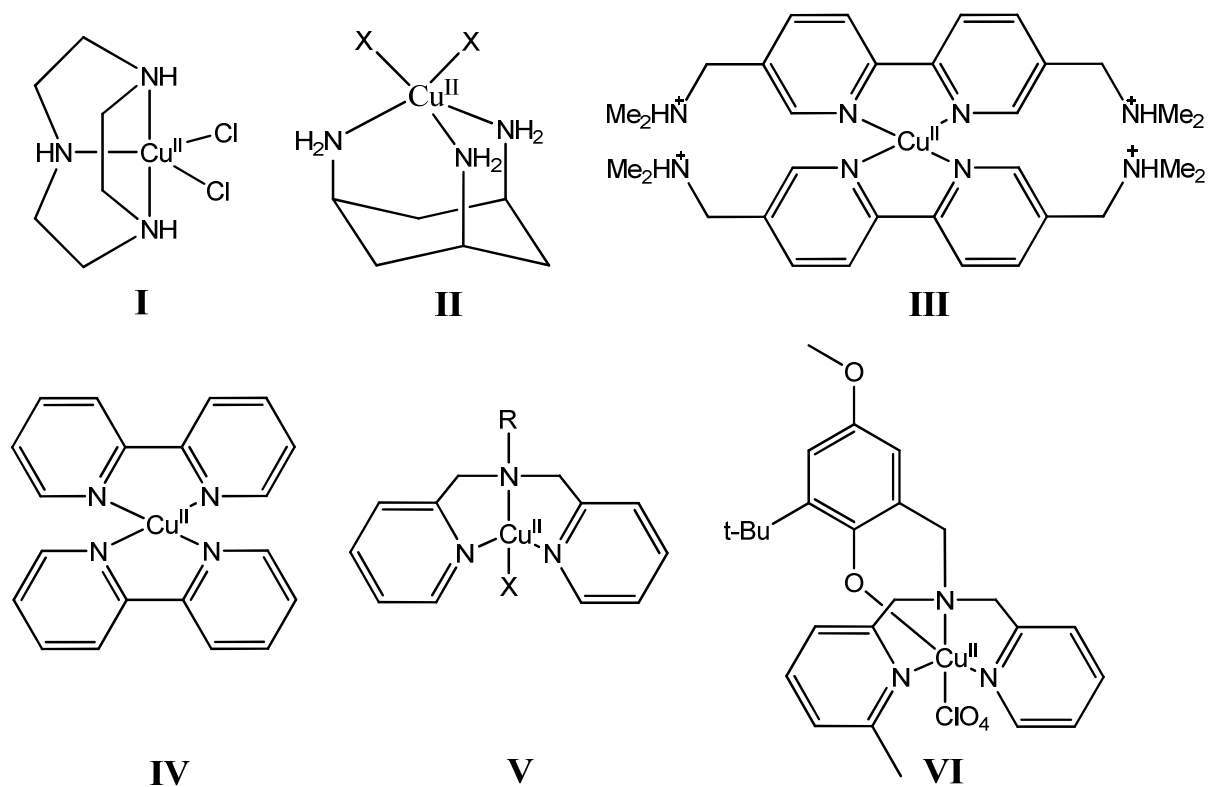


Figure 2.3: Structure of monocopper complexes: **I** [Cu(TACN)Cl₂]; **II** [Cu(TACH)]²⁺; **III** [Cu(a-bpy)₂]⁶⁺; **IV** [Cu(bpy)₂]²⁺; **V** [Cu(DPA)X]¹⁺ X= Cl, Br, R= H, methyl, ethyl, guanidium; **VI** [Cu(pDPA)ClO₄].

2.1.4. Complexes of p-block metals

Complexes of the post-transition metals are also possible. The most widely studied are gallium complexes. Gallium in its +3 oxidation state (Ga^{III}) has a well-defined coordination chemistry, it also has a similar ionic radius and Lewis acidity to the more biologically relevant Fe^{III}. Unlike the ferromagnetic Fe^{III}, gallium complexes can be investigated by routine NMR spectroscopy experiments (¹H, ¹³C and ⁷¹Ga); also there is no accessible redox chemistry thus eliminating the possibility of oxidative cleavage interfering with reactivity studies.

Fe^{III} is of interest due to its involvement in the dinuclear Fe^{III} – M^{II} (M^{II} = Fe^{II}, Zn^{II} or Mn^{II}) active site of purple acid phosphatase (PAP)²⁵ (**Figure 2.4**). PAP is an enzyme found in animals, plants, fungi and bacteria and catalyses the hydrolysis of a variety of phosphate ester substrates. It has been shown that Ga^{III} can replace Fe^{III} in PAP²⁶.

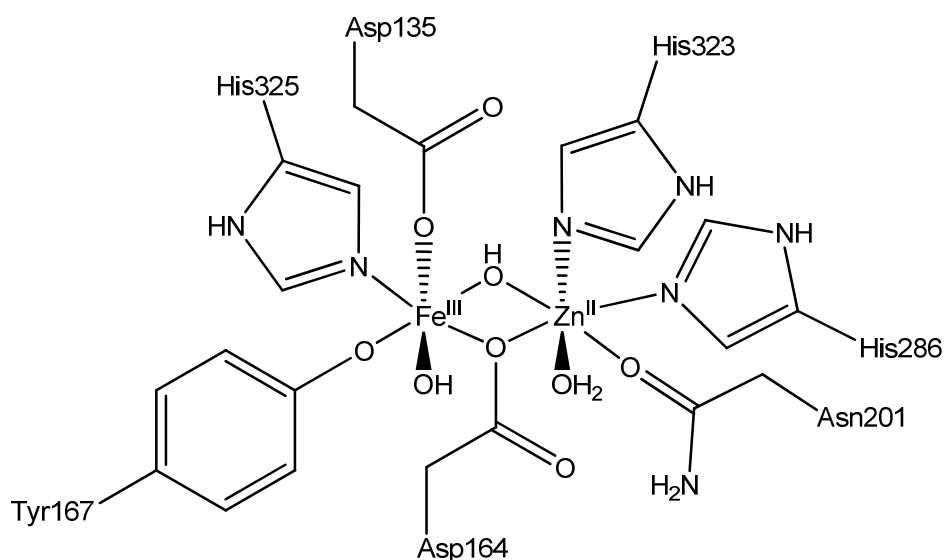


Figure 2.4: Active site of red kidney bean PAP ²⁷.

Using dinucleating and mononucleating ligands the mechanism of PAP has been investigated^{25,26,28-30}. An example of a PAP mimic is the dinuclear $\text{Fe}^{\text{III}}(\mu\text{-OH})\text{Zn}^{\text{II}}$ complex ^{29,30} (**Figure 2.5 structure I**). This complex showed activity against bis-dinitrophenol phosphate (BDNP) and also double stranded DNA. Using the same ligand an analogous $\text{Ga}^{\text{III}}\text{-Zn}^{\text{II}}$ complex was investigated²⁶ (**Figure 2.5 structure II**). This allowed for the analysis of the complex by ¹H, ¹³C and ⁷¹Ga NMR spectroscopy.

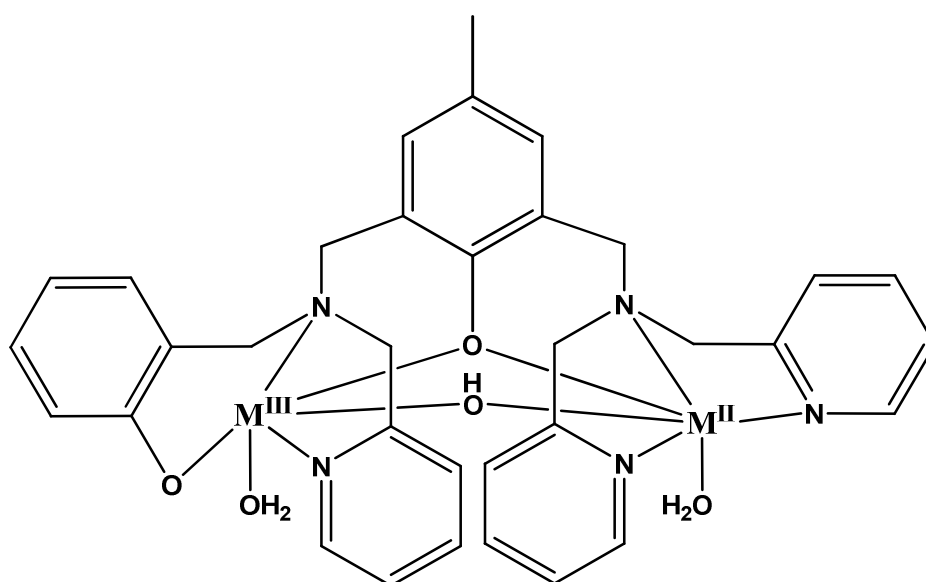


Figure 2.5: Structure of PAP biomimetics. **I** $\text{Fe}^{\text{III}}(\mu\text{-OH})\text{Zn}^{\text{II}}$ complex, $\text{M}^{\text{III}} = \text{Fe}^{\text{III}}$, $\text{M}^{\text{II}} = \text{Zn}^{\text{II}}$; **II** $\text{Ga}^{\text{III}}\text{-Zn}^{\text{II}}$ complex, catalytic active species $\text{M}^{\text{III}} = \text{Ga}^{\text{III}}$, $\text{M}^{\text{II}} = \text{Zn}^{\text{II}}$.

2.1.5. Synergy

As discussed earlier, metal centres have several means to enhance the hydrolytic cleavage rate and having multiple metal centres in close proximity, can allow for synergy between the metal centres. This is demonstrated in the fact that it has been found that dinuclear catalysts are generally more reactive than the mononuclear version³¹.

Two reasons can explain this phenomenon. The phosphodiester can coordinate to both metal atoms leading to double Lewis acid activation (**Figure 2.6, structure I**). This can allow for RNA hydrolysis due to the presence of the internal nucleophile at 2'-OH. Or the phosphodiester may coordinate a single metal atom with a hydroxide coordinated to the other metal atom (**Figure 2.6, structure II**). This will result in single Lewis acid activation combined with metal hydroxide activation. DNA hydrolysis requires both Lewis acid activation and nucleophile activation to occur³¹.

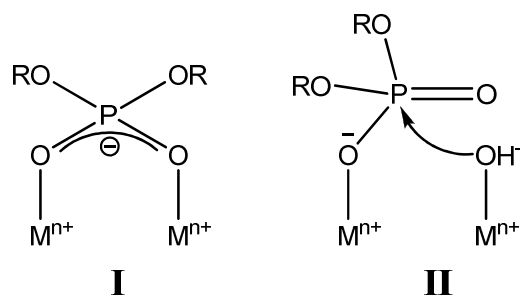


Figure 2.6: **I** Double Lewis acid activation; **II** Single Lewis acid activation with metal-bound hydroxide attack.

2.1.5.1. Multinuclear complexes

There has been extensive work done on generating di-, tri and multinuclear complexes. Due to its effectiveness (**Section 2.1.4.**) and the body's tolerance multinuclear Cu complexes have been thoroughly explored.

A di- and trinuclear Cu complex was generated by linking DPA ligands with a terpyridine ligand as a spacer group³² (**Figure 2.7**). Both were able to cleave plasmid DNA and as expected the trinuclear complex was more active than the dinuclear counterpart. The trinuclear complex showed high cytotoxicity against cisplatin-resistant leukaemia cell lines. It is able to bind to DNA either by intercalation or

groove binding. But due to the chemical structure the metal centres are relatively far apart and are unable to interact directly.

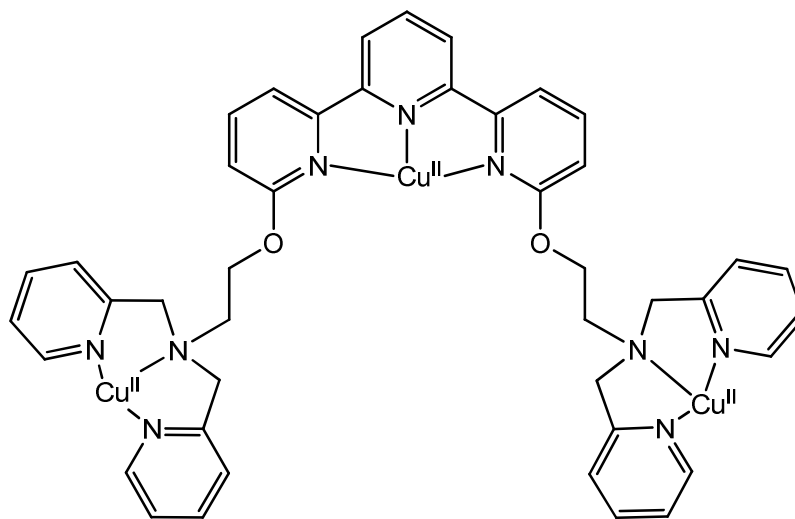


Figure 2.7: Structure of trinuclear copper complex.

2.1.5.2. Dinuclear complexes based on 4-methyl phenol

Dinucleating ligands based on 4-methyl phenol (**Figure 2.8**) have been extensively studied. 4-methyl phenol has several advantages: the phenol group is rigid, the methyl group will not interfere in the metal coordination, the phenolic oxygen has the potential to bridge two separate metals, the bridged metals will be at a distance similar to that in dinuclear enzymes and generation of dinucleating ligands is synthetically easily accessed. So the bridging phenol will bring in multiple metal centres into close contact. Symmetrical ($R_1 = R_2$) and unsymmetrical ($R_1 \neq R_2$) ligands are possible. Mixed metal complexes ($M_1^{n+} \neq M_2^{n+}$) are also possible. Summarised in **Table 2.1** are a brief selection of R groups, complexes generated and the method by which their nuclease activity was quantified.

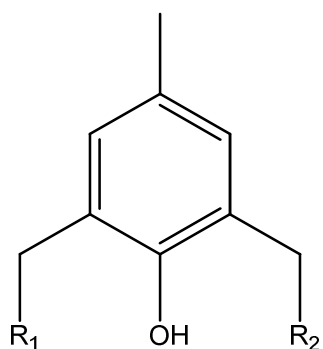
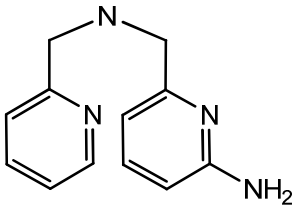
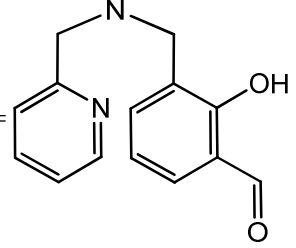
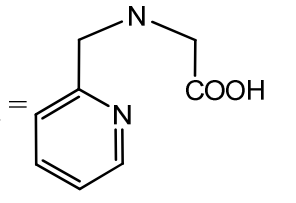
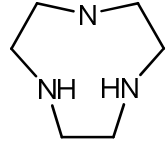
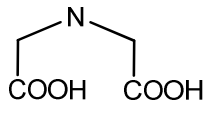
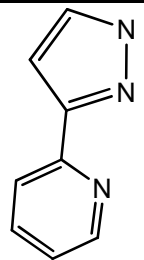
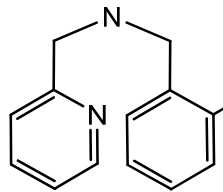
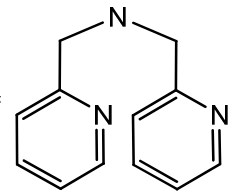
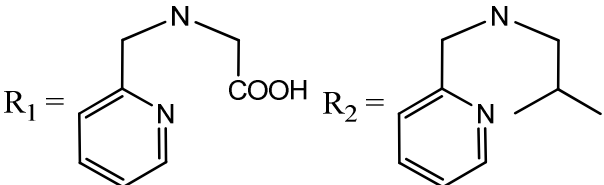


Figure 2.8: Generic structure of 4-methyl phenol dinucleating ligands, R_1 and R_2 mononucleating binding sites.

Table 2.1: Structure of different R groups in 4-methyl phenol based dinuclear complexes with nuclease activity.

Structure of R groups	Complexes	Substrate studied
$R_1 = R_2 =$	$M_1 = M_2 = Cu^{II}$ ³³	HPNP
$R_1 = R_2 =$	$M_1 = M_2 = Cu^{II}$ ³⁴ $M_1 = M_2 = Fe^{III}$ ³⁵	Plasmid DNA BNPP
$R_1 = R_2 =$	$M_1 = Fe^{III}, M_2 = Fe^{II}$ ³⁶ $M_1 = M_2 = Zn^{II}$ ³⁷	BDNP, DNPP HPNP
$R_1 = R_2 =$	$M_1 = Fe^{III}, M_2 = Fe^{II}$ ³⁶	BDNP, DNPP

$R_1 = R_2 =$ 	$M_1 = Fe^{III}, M_2 = Fe^{II}$ ³⁶	BDNP, DNPPP
$R_1 = R_2 =$ 	$M_1 = Fe^{III}, M_2 = Zn^{II}$ ³⁸	BDNP
$R_1 = R_2 =$ 	$M_1 = M_2 = Zn^{II}$ ^{39,40}	BDNP, HPNP
$R_1 = R_2 =$ 	$M_1 = M_2 = Zn^{II}$ ⁴¹ $M_1 = M_2 = Cu^{II}$ ⁴²	BDNP, HPNP BDNP, HPNP
$R_1 = R_2 =$ 	$M_1 = M_2 = Ce^{IV}$ ⁴³ $M_1 = M_2 = Zr^{IV}$ ⁴⁴	Plasmid DNA NPP
$R_1 = R_2 =$ 	$M_1 = M_2 = Mn^{II}$ ⁴⁵ $M_1 = M_2 = Co^{II}$ ⁴⁵ $M_1 = M_2 = Zn^{II}$ ⁴⁵	HPNP HPNP HPNP
$R_1 =$  $R_2 =$ 	$M_1 = Co^{II}, M_2 = Fe^{III}$ ⁴⁶ $M_1 = Co^{II}, M_2 = Ga^{III}$ ⁴⁶ $M_1 = Fe^{III}, M_2 = Fe^{II}$ ⁴⁷ $M_1 = Fe^{III}, M_2 = Cd^{II}$ ⁴⁸ $M_1 = Fe^{III}, M_2 = Hg^{II}$ ⁴⁸ $M_1 = Fe^{III}, M_2 = Zn^{II}$ ³⁰ $M_1 = Ga^{III}, M_2 = Zn^{II}$ ²⁶	BDNP BDNP BDNP BDNP BDNP BDNP, d.s. DNA BDNP

	$M_1 = M_2 = \text{Zn}^{\text{II}}$ ^{39,40}	BDNP, HPNP
---	--	------------

As can be seen in **Table 2.1** there are a wide range of dimetallic complexes based on 4-methyl phenol. In all these examples the two metals are bridged by the phenol, thereby bringing the metal centres into close contact and allowing for synergy.

2.1.6. Kinetic and mechanistic methods

There are several methods to study the nuclease ability of artificial nucleases. One method is to work with polynucleotide strands. Different polynucleotide types can be used; single-stranded DNA, single-stranded RNA, double-stranded DNA, double-stranded DNA/RNA hybrids, simple dinucleotides and most commonly plasmid DNA. The reaction can then be monitored by electrophoresis⁴⁹ or HPLC².

There are different methods to distinguish between hydrolytic and oxidative reaction mechanisms. The reaction can be monitored in both aerobic and anaerobic conditions¹⁷. It can also be performed in the presence of radical scavengers¹. An alternative method is to treat the products of the reaction with a ligase enzyme such as T4 DNA ligase¹². These methods can distinguish between an oxidative and hydrolytic mechanism and also determine the contribution due to each in a combination mechanism.

But the most common method to determine hydrolytic ability is the use of phosphodiester or phosphomonoester analogues^{28,39,44}. These range from DNA analogues (bis-dinitrophenol phosphate (BDNP), bis-nitrophenol phosphate (BNPP)) to RNA analogues (uridine para-nitro phenol phosphate (UPNP) and 2-hydroxypropyl-para-nitrophenol (HPNP)) to monoester analogue nitrophenol phosphate (NPP) (**Figure 2.9**).

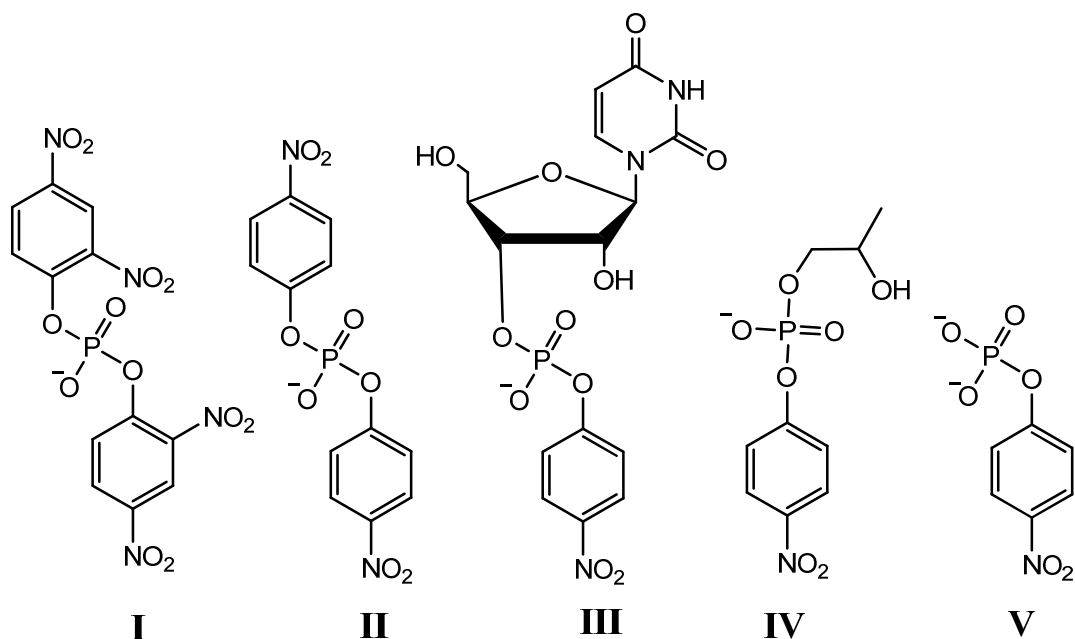
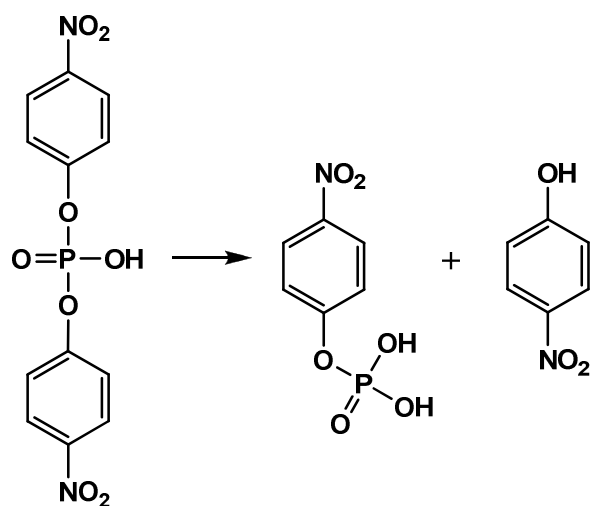


Figure 2.9: Structure of selected phosphodiester and phosphomonoesters analogues. **I** BDNP; **II** BNPP; **III** UPNP; **IV** HPNP; **V** NPP.

For all of the analogues, when hydrolysed they will release a nitro- or dinitrophenol (**Scheme 2.1**). Due to high extinction coefficients of the released nitro- or dinitrophenol the reaction can be monitored using UV-Vis spectroscopy.



Scheme 2.1: Hydrolysis of DNA analogue BDNP releasing a nitrophenol.

2.2. Aims and objectives

The objective of this study is to generate several dinucleating ligands based on 4-methyl phenol. The ligands will consist of a “body” based on 4-methyl phenol and two mononucleating ligand “arms” which consist of varying amounts of pyridine and carboxylic acid metal binding moieties. This will allow for the generation of symmetrical and unsymmetrical ligands (**Figure 2.10**). The symmetrical tetracarboxylic acid ligand (HXTA) was previously studied within the group⁵⁰ and so will not be part of this study.

Dinuclear complexes of Mg^{II} , Cu^{II} and Ga^{III} will be generated and where possible isolated. Magnesium is of interest due to its role in enzymes and in particular nucleic acid enzymes (**Section 1.2**). Copper is of interest due to its Lewis acidity and potential as a therapeutic. Gallium is of interest due its potential as a mimic for the more biologically relevant Fe^{III} ion (**Section 2.1.4**). Their stability over a range of pH will also be studied. The ability of the dinuclear complexes to mediate the hydrolysis of phosphodiester bonds in DNA and RNA will be measured using analogues BDNP and HPNP respectively.

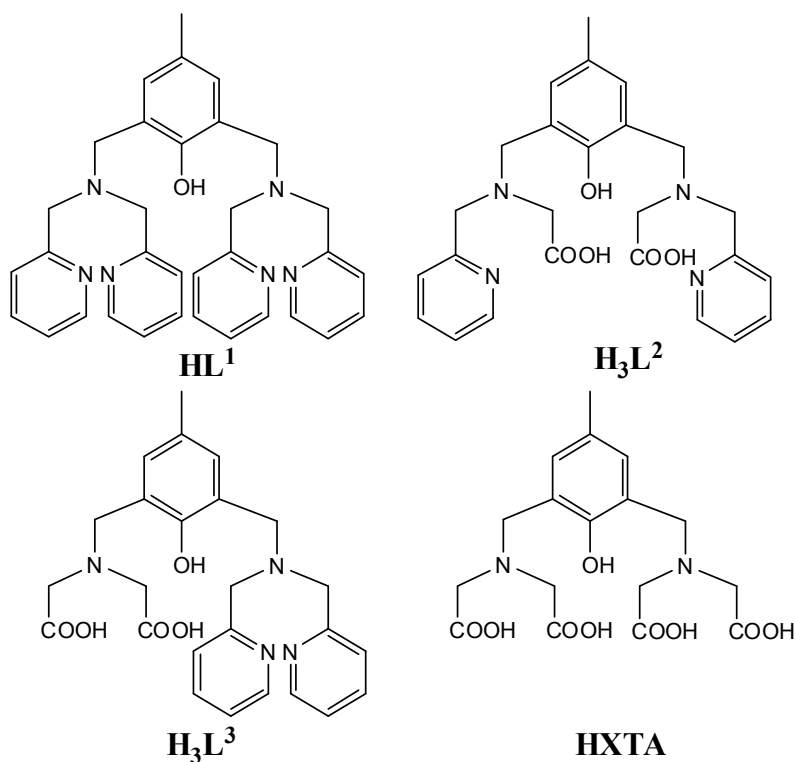


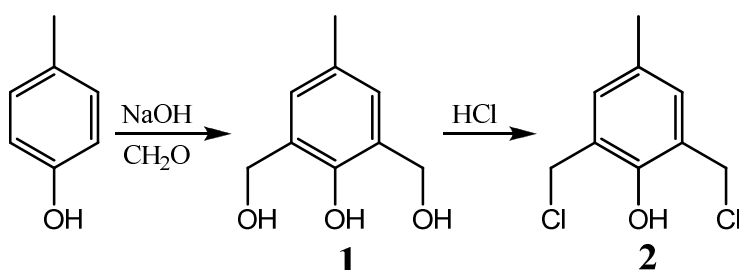
Figure 2.10: Structure of ligands used in this study (**HL¹**, **H₃L²** and **H₃L³**) and HXTA.

2.3. Results

2.3.1. Synthesis of ligands

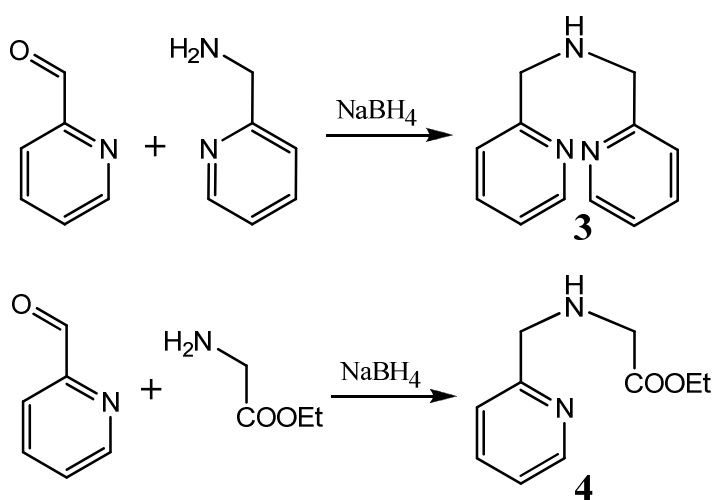
2.3.1.1 Synthesis of symmetrical ligands HL^1 and H_3L^2

The symmetrical ligands HL^1 and H_3L^2 were synthesised in a similar convergent manner. Following literature procedures the body of the ligand was synthesised from the starting material, 4-methyl phenol. By reaction with formaldehyde in basic conditions compound **1** was obtained⁵¹. This was subsequently reacted with HCl to generate **2**⁵² (Scheme 2.1).



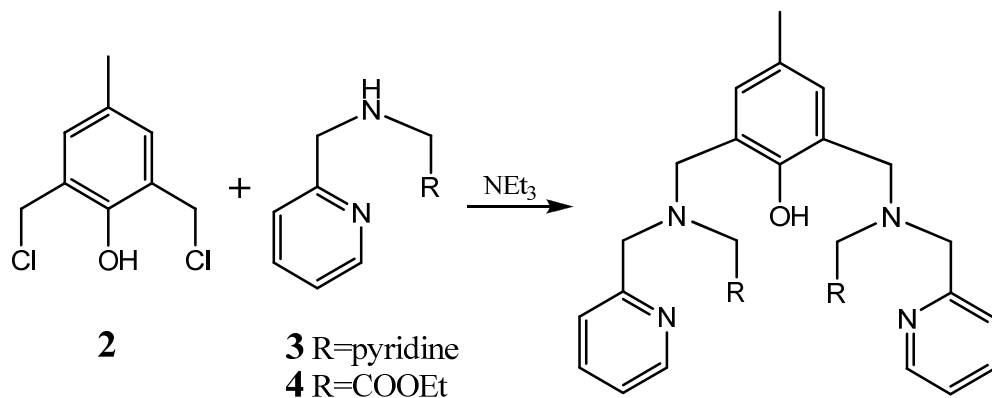
Scheme 2.2: Synthesis of symmetrical ligand body.

The mononucleating ligand arms were synthesised by a schiff base reaction. In a one-pot reaction the appropriate amine and pyridine-2-carbaldehyde were reacted to generate an imine which was then reduced by NaBH₄ to generate the desired secondary amines **3** and **4** (Scheme 2.2).



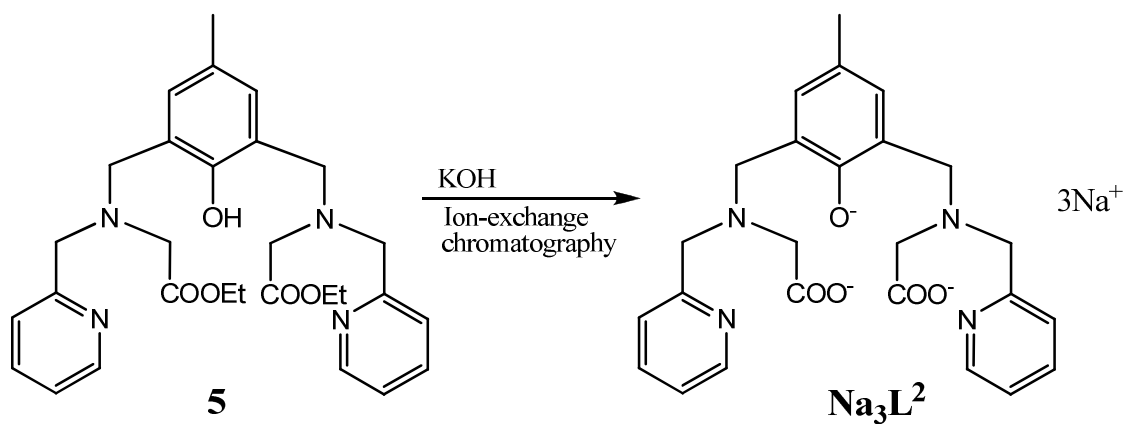
Scheme 2.3: Synthesis of mononucleating ligand "arm".

Then by reaction of **2** and the appropriate secondary amine ligand **HL**¹ and the ethyl ester of **H₃L**², **5**, were generated (**Scheme 2.3**). Both of these were purified by column chromatography.



Scheme 2.4: Synthesis of symmetrical ligands. **H₁L**¹ R=pyridine, **5** R=COOEt.

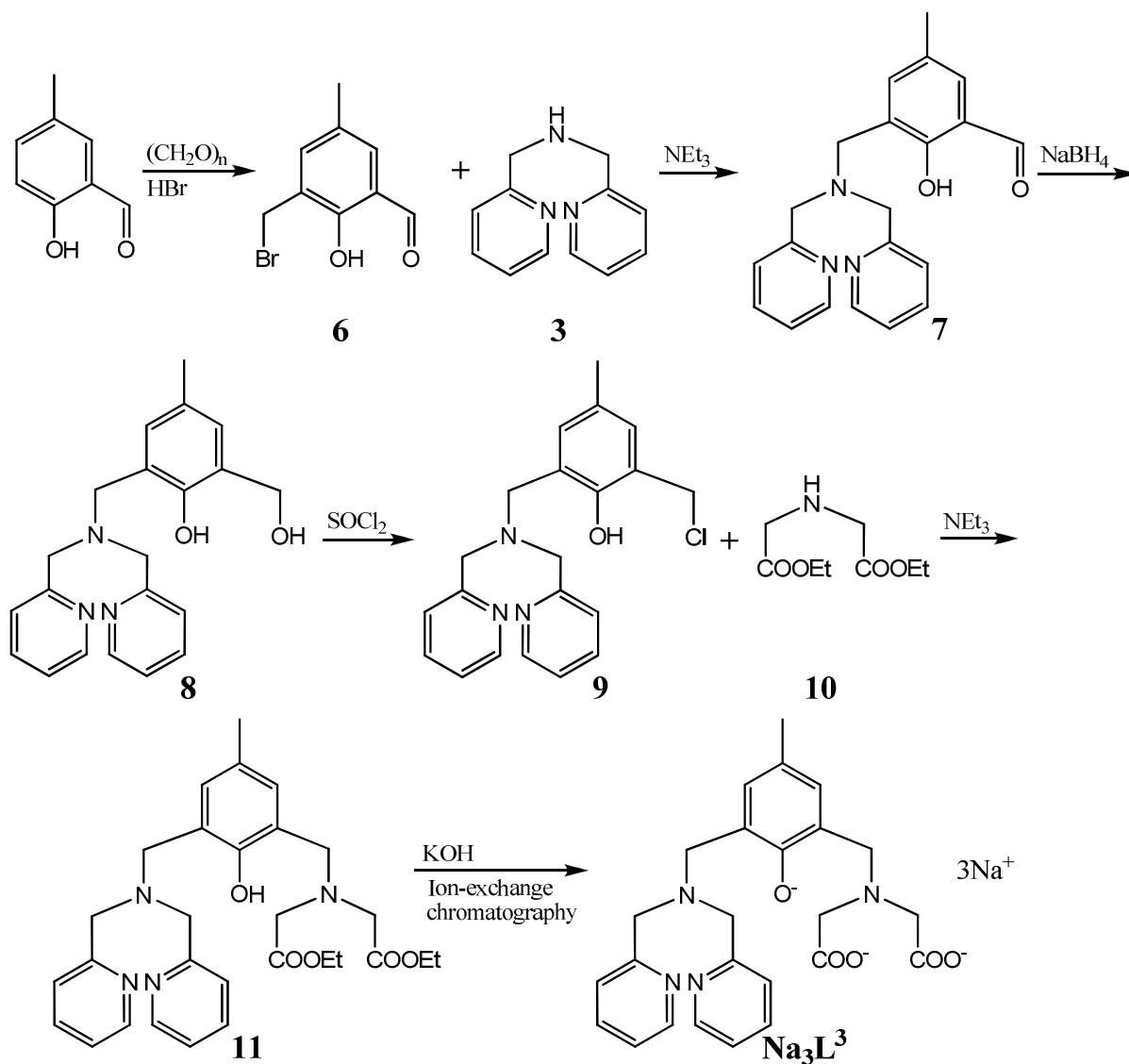
The dinucleating ligand **H₃L**² was generated by base hydrolysis of **5** (**Scheme 2.4**) and was isolated as the tri-sodium salt by ion-exchange chromatography. Acid hydrolysis using 1 M HCl was attempted but it was found to degrade **5** cleaving the C-C bond linking the phenol to the mononucleating ligand “arm”.



Scheme 2.5: Base hydrolysis of **5**.

2.3.1.2. Synthesis of unsymmetrical ligand H_3L^3

The unsymmetrical ligand H_3L^3 was synthesised in a linear fashion (Scheme 2.5). The starting material 5-methyl salicylaldehyde was reacted with paraformaldehyde and HBr to give **6**⁵³. In the presence of NEt_3 **6** was reacted with dipicolylamine, **3**, to give **7**⁵⁴. The aldehyde group of **7** was reduced by NaBH_4 to give the corresponding alcohol **8**⁵⁵. In a one pot reaction **8** was reacted with thionyl chloride to give **9**⁵⁴ which was then reacted with diethyl iminodiacetate in the presence of NEt_3 to give the ethyl ester version of H_3L^3 , **11**. This was purified by column chromatography. The dinucleating ligand H_3L^3 was generated by base hydrolysis of **11** and was isolated as the tri-sodium salt by ion-exchange chromatography.



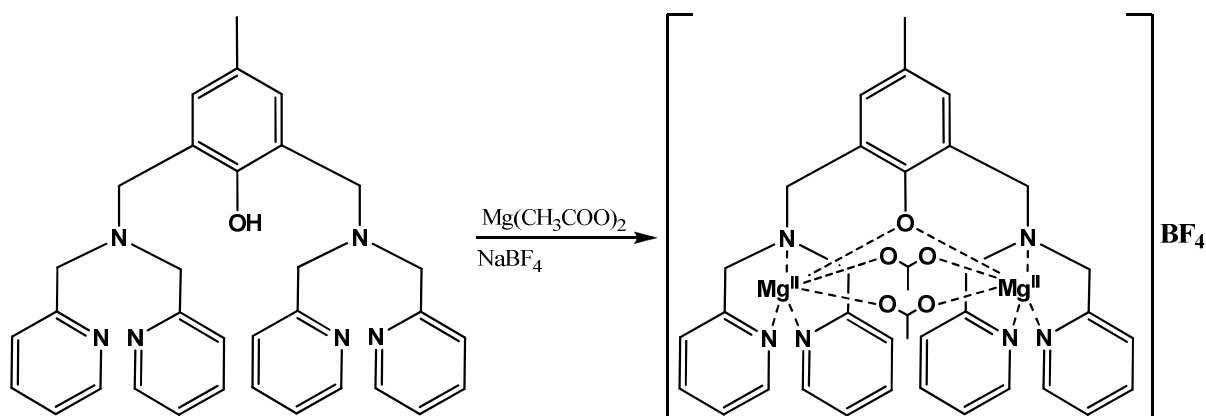
Scheme 2.6: Synthesis of Na_3L^3 .

2.3.2 Dinuclear Mg^{II} complex studies

2.3.2.1. HL¹

2.3.2.1.1. Complex synthesis and stability

Using a literature procedure for the preparation of a di-Zn^{II} complex⁵⁶, a di-Mg^{II} complex of HL¹ with formula [Mg₂L¹(CH₃CO₂)₂]BF₄ was isolated and fully characterised (Scheme 2.6).



Scheme 2.7: Synthesis of [Mg₂(L¹)(acetate)₂]BF₄.

As can be seen from the ¹H NMR of the isolated complex (Figure 2.11) there is a large difference between the spectra of the free ligand and isolated complex. There is a significant upfield shift of the phenol, CH, peak from 6.94 ppm for the free ligand to 6.42 ppm for the complex. This confirms deprotonation of the phenol and hence that the magnesium atoms are bridged by the phenolic oxygen. The presence of two bridging acetates was confirmed by the presence of a singlet at 2.02 ppm which integrates for 6 hydrogens. The main feature of the ¹H spectra of the complex is the additional peaks compared to the free ligand. This is due to the pyridines rings within each dipicolylamine arm not being equivalent hence giving 8 signals rather than 4. The singlet peaks of the CH₂'s in the aliphatic regions have been split into doublets due to geminal coupling. This is similar to the corresponding di-Zn^{II} complex⁵⁶.

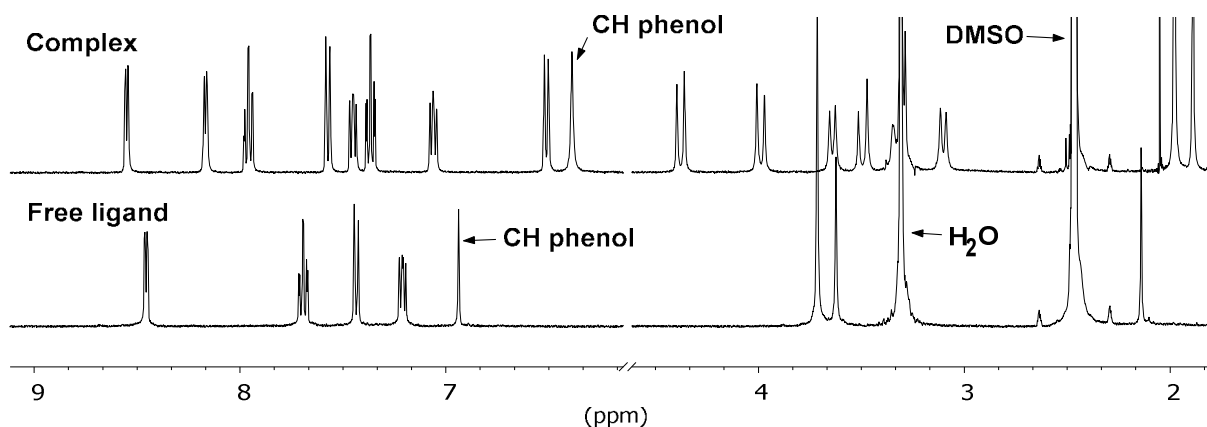


Figure 2.11: Stacked NMR of HL^I and di-Mg^{II} complex (DMSO-d₆, 400MHz).

Using ¹H NMR the stability of the complex was investigated over a range of pD (Figure 2.12). Due to solubility issues samples were dissolved in a 1:1 D₂O:CD₃OD mixture. As can be seen from the diagram the complex is not stable and readily forms the free ligand.

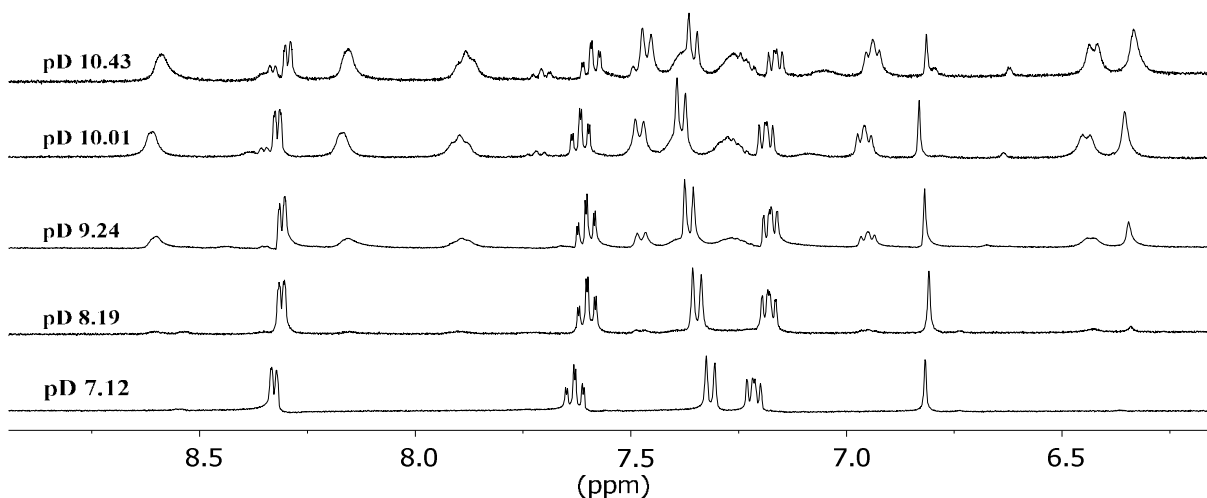


Figure 2.12: Stacked NMR spectra of [Mg₂(L^I)(CH₃CO₂)₂]₂BF₄ over a range of pD (1:1 D₂O:CD₃OD, 400 MHz).

Using the integration of the signals the ratio of ligand:complex was determined (Table 2.2). It was found that at pD 10.4 the ratio of ligand:complex was 1:2.5 and at pD 7.1 the complex was fully dissociated and so only peaks for the free ligand were observed. Due to this instability at physiologically relevant pH the ability of the complex to mediate phosphodiester hydrolysis was not investigated

Table 2.2: Ratio of ligand:complex over a range of pD for di-Mg^{II} complex of HL¹.

pD	Ligand:Complex
10.43	1: 2.5
10.01	1: 2
9.24	1: 1.25
8.19	1: 0.125
7.12	1: 0

2.3.2.2 H₃L²

2.3.2.2.1. Complex synthesis and stability

On the basis of the “hard and soft Lewis acid and base” (HSAB) concept it was expected that the carboxylic acid moiety containing H₃L² would give a stable dinuclear Mg^{II} complex. Several attempts were made to synthesis and isolate the complex but no product was generated or isolated.

A ¹H NMR titration was performed where increasing equivalents (eq.) of Mg²⁺ were added to a solution of H₃L² but was inconclusive. The pH stability of the di-Mg^{II} adduct was also investigated by ¹H NMR spectroscopy. A fresh mixture of 2:1 Mg²⁺: Na₃L² was generated in 1:1 D₂O:DMSO-d₆ and the ¹H NMR spectra were taken over a range of pD values. The spectra were compared to ¹H spectra of free ligand (Na₃L³) at similar pD values and in the same solvent mixture (**Figure 2.13**).

As can be seen in **Figure 2.13** at pD 6.23 the ¹H spectra of the mixture resembles the ¹H spectra of free ligand at pD 5.59 indicating only free ligand is present. As the pD is raised the spectrum changes and at pD 7.52 only peaks corresponding to adduct are observed. When the pD is raised to pD 11.84 no further changes are observed in the spectra. This spectrum is very different from the ¹H spectra of free ligand at pD 9.61 and 14.00. This indicates that the peaks are due to the formation of a di-Mg^{II} adduct. This shows that the adduct is stable from pD 7.52 and upwards. As can be seen in the spectra of the adduct there is a significant upfield shift in the phenol peak indicating that the phenolic oxygen is involved in bridging the metal centres. As can also be seen in the adduct spectra the pyridine peaks are broad indicating that there is rapid exchange.

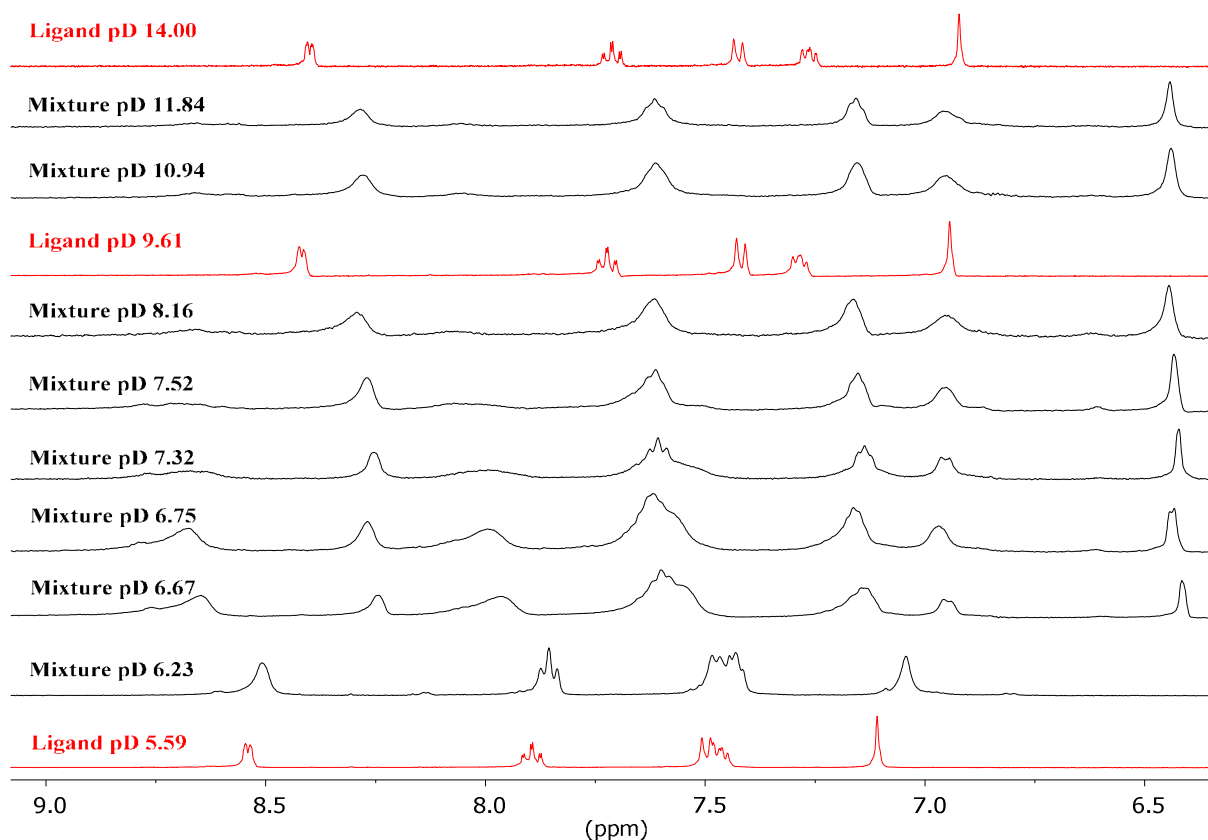


Figure 2.13: Stacked NMR of ligand, Na_3L^2 , and mixture, 1eq. Na_3L^2 and 2 eq. Mg^{2+} , over a range of pD (1:1 DMSO- d_6 : D_2O , 400MHz)

2.3.2.2.2. Kinetic investigations

The ability of the di- Mg^{II} adduct to mediate the hydrolysis of the phosphodiester group in DNA and RNA was investigated using the analogues BDNP and HPNP respectively (Section 2.1.6.). As discussed previously when hydrolysed BDNP and HPNP will release a nitrophenol or dinitrophenol. Due to the large extinction coefficient for nitrophenols the progress of the reaction can be monitored relatively easily by a UV-Vis spectrophotometer.

The pH rate profile for the hydrolysis by the di- Mg^{II} adduct was investigated (BDNP Figure 2.14, HPNP Figure 2.15). For comparison the rate due to free Mg^{2+} was also investigated. Free Mg^{2+} hydrolysis of phosphodiester has been previously reported but with different substrates and under dissimilar conditions^{57,58}. No measurements were taken above pH 11 due to the lack of an appropriate ‘Goods’ buffer and due to the increasingly large substrate auto-hydrolysis rate (see Appendix 1 for pH auto-hydrolysis profiles). The di- Mg^{II} adduct was generated by mixing 1 eq. Na_3L^2 and

2eq. Mg^{2+} and incubating for 1 hr prior to the experiment. For both adduct and free Mg^{2+} a similar activity is exhibited up to pH 8.5. For both BDNP and HPNP the free Mg^{2+} exhibits a bell-shaped pH-rate profile. The pH-rate profile for the di- Mg^{II} adduct is very different only exhibiting an exponential increase. The adduct may exhibit a bell-shaped or sinusoidal graph but as discussed earlier no points for pH greater than 11.0 could be taken. For both BDNP above pH 10 the dinuclear complex is more active than free Mg^{2+} . This is also observed with HPNP but from pH 9.5 and higher.

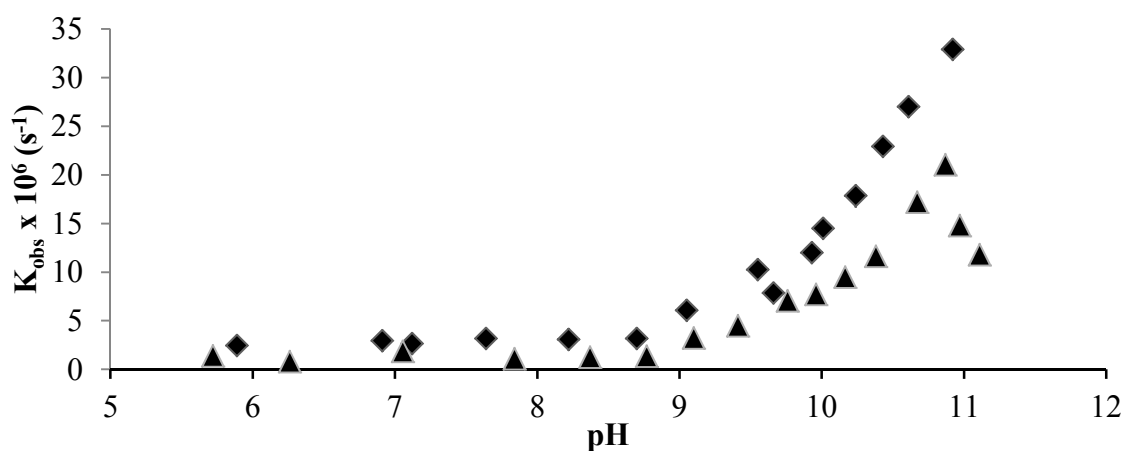


Figure 2.14: pH-rate profiles for cleavage of BDNP [5×10^{-5} M] with 1 mM di- Mg^{II} adduct (◆) and 2 mM $\text{Mg}(\text{CH}_3\text{CO}_2)(\text{NO}_3)$ (▲) at 40 °C in 1:1 DMSO: H_2O . $I = 0.1$ M (KNO_3), [buffer] = 50 mM (buffer = MES (pH 5.5 – 6.7), PIPES (pH 6.2 – 7.4), MOPS (pH 6.6 – 7.8), HEPES (pH 6.9 – 8.1), EPPS (pH 7.4 – 8.6), CHES (pH 8.7 – 9.9) and CAPS (pH 9.8 – 11.0)).

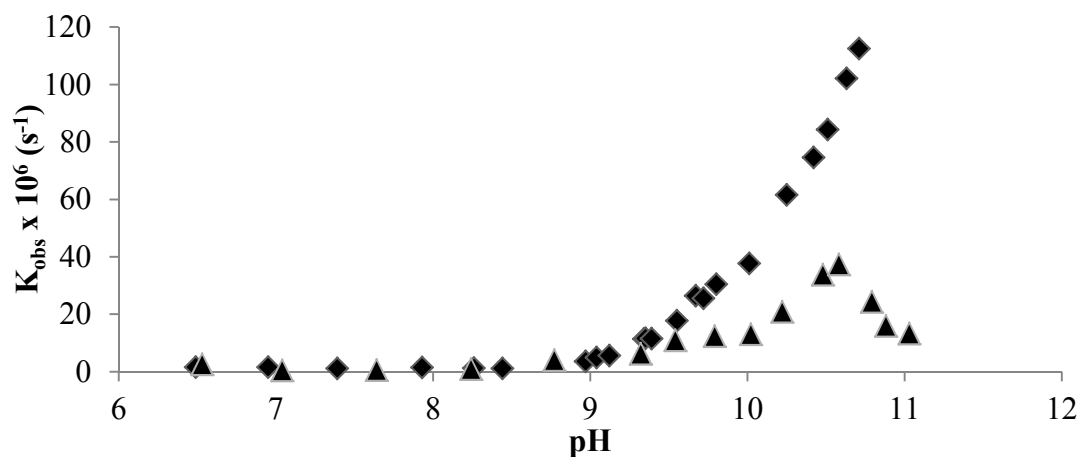


Figure 2.15: pH-rate profiles for cleavage of HPNP [5×10^{-5} M] with 2 mM di-Mg^{II} adduct (◆) and 4 mM Mg(CH₃CO₂)(NO₃) (▲) at 40 °C in 1:1 DMSO: H₂O. $I = 0.1$ M (KNO₃), [buffer] = 50 mM (buffer = MES (pH 5.5 – 6.7), PIPES (pH 6.2 – 7.4), MOPS (pH 6.6 – 7.8), HEPES (pH 6.9 – 8.1), EPPS (pH 7.4 – 8.6), CHES (pH 8.7 – 9.9) and CAPS (pH 9.8 – 11.0)).

The dependence of the rate of analogue hydrolysis with adduct concentration was investigated (BDNP **Figure 2.17**, HPNP **Figure 2.18**). This was done at pH 9.5 for BDNP and pH 9.3 for HPNP. It was not investigated at a higher pH due to large auto-hydrolysis of substrate at high pH. The rate was found to increase linearly with increasing adduct concentration indicating 2nd order kinetics rather than Michaelis-Menten behaviour. The rate constant was calculated to be $2.8 \times 10^{-3} \text{ s}^{-1}\text{M}^{-1}$ and $4.3 \times 10^{-3} \text{ s}^{-1}\text{M}^{-1}$ for BDNP and HPNP hydrolysis respectively.

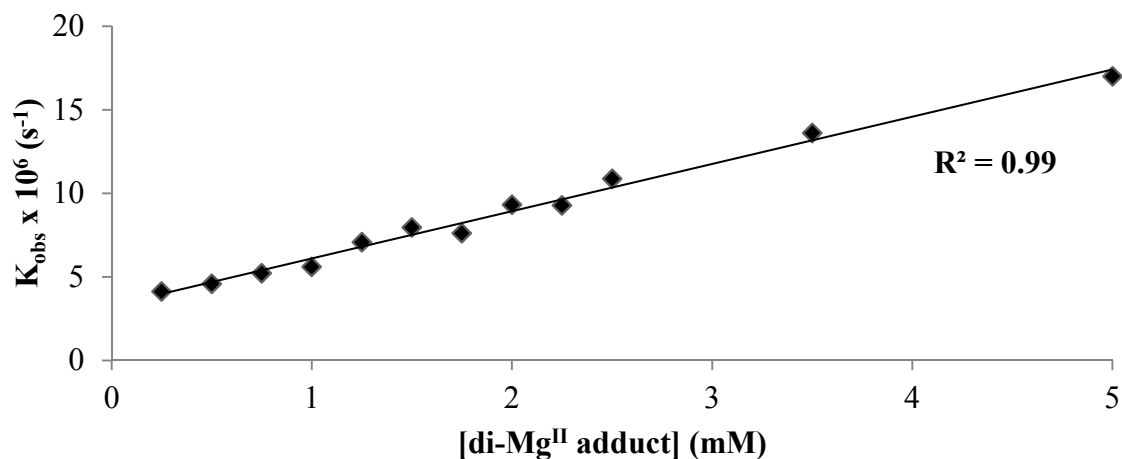


Figure 2.16: Dependence of the rate of cleavage of BDNP [5×10^{-5} M] on the concentration of di-Mg^{II} adduct at pH 9.5 and 40 °C in 1:1 DMSO: H₂O. $I = 0.1$ M (KNO₃), [buffer] = 50 mM (CHES)

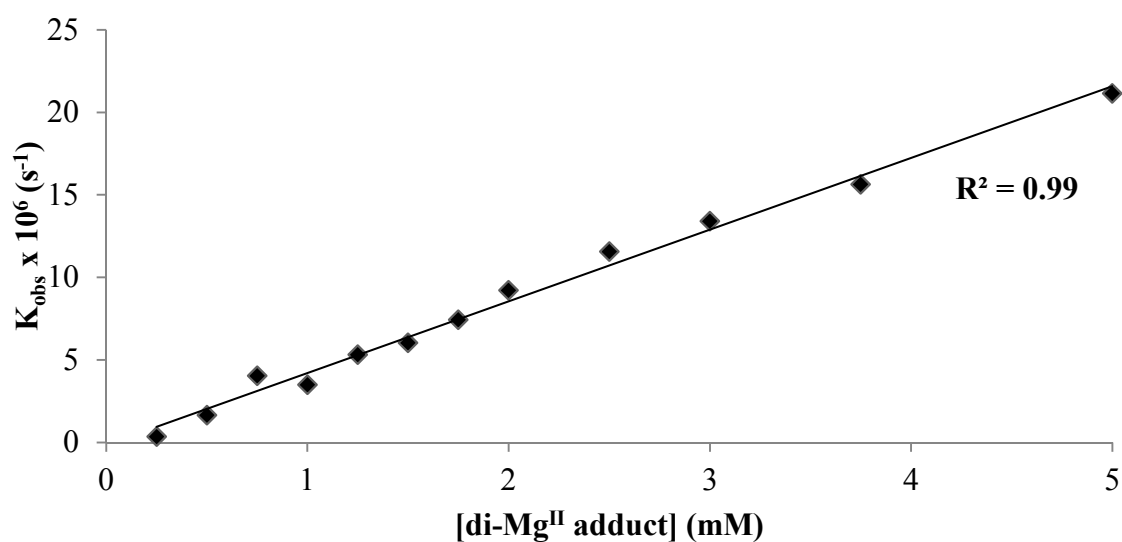


Figure 2.17: Dependence of the rate of cleavage of HPNP [5×10^{-5} M] on the concentration of di-Mg^{II} adduct at pH 9.3 and 40 °C in 1:1 DMSO: H₂O. $I = 0.1$ M (KNO₃), [buffer] = 50 mM (CHES)

2.3.2.3. H_3L^3

2.3.2.3.1. Complex synthesis and stability

As with H_3L^2 , H_3L^3 would be expected to give a stable di- Mg^{II} complex. Unfortunately as with H_3L^2 numerous synthetic attempts were undertaken but no complex was isolated.

To show the Mg^{2+} binding affinity of H_3L^3 a NMR titration was performed where increasing equivalents of Mg^{2+} were added to a solution of Na_3L^3 and the ^1H NMR spectra was taken (**Figure 2.18**). To prevent any contribution due to pH the titration was performed in CD_3OD .

As can be seen in **Figure 2.18** with 1 eq of Mg^{2+} there is broadening of signals which are only resolved in the presence of 2 eq of Mg^{2+} . There is no further change observed when increasing equivalents of Mg^{2+} are added. This resolution indicates that H_3L^3 will form a dinuclear Mg^{II} complex.

Similar to HL^1 (**Section 2.3.2.1.1.**) when the di- Mg^{II} adduct is formed the pyridines within each mononucleating ligand “arm” are no longer equivalent. By examination of the splitting patterns and by the use of a COSY experiment peak assignment within the aromatic region was determined (**Figure 2.19**).

Peak movement is also observed with the phenol CH peak. For the free ligand the phenol peaks are two overlapping singlets at 7.034 and 7.029 ppm. Upon formation of the di- Mg^{II} adduct the singlets separate and shift upfield to 6.75 and 6.36 ppm. This large shift upfield indicates that the phenolic oxygen is involved in bridging the metal centres.

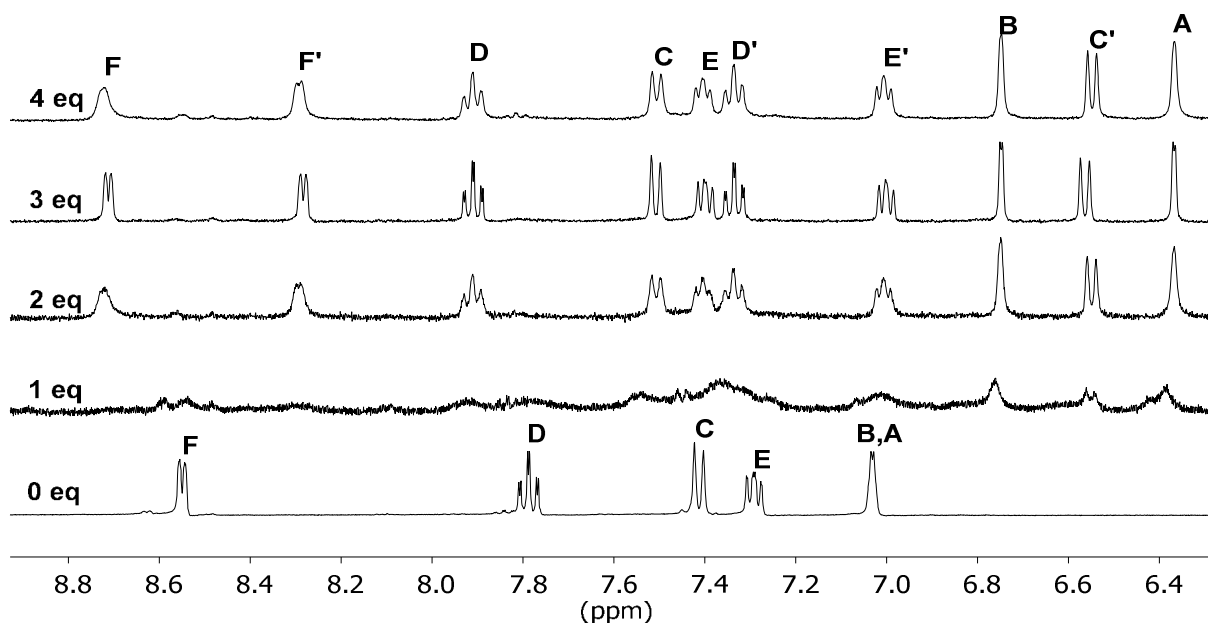


Figure 2.18: Stacked NMR showing Mg^{2+} binding affinity of H_3L^3 (MeOH- d_4 , 400 MHz).

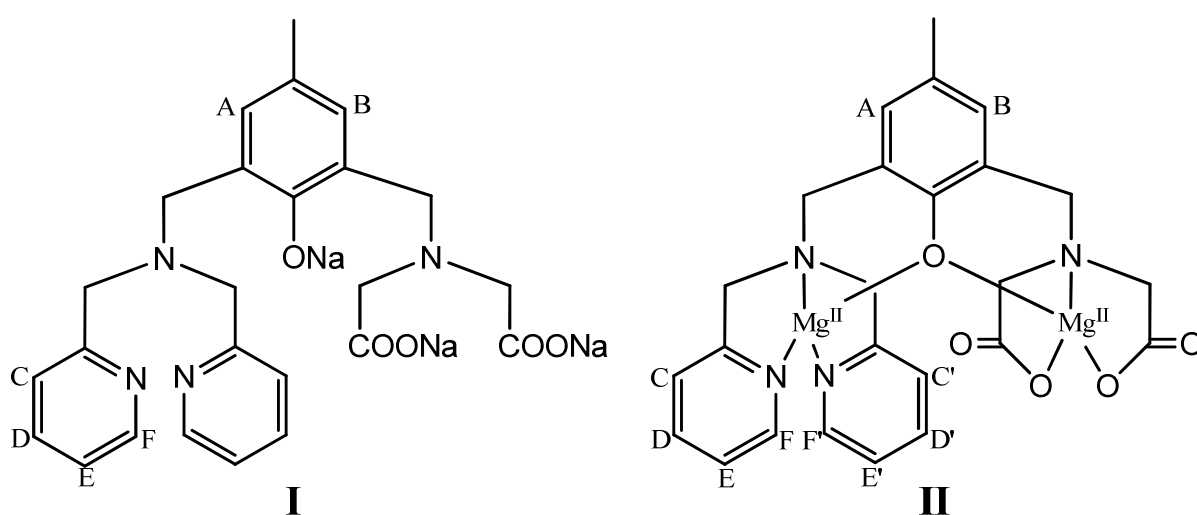


Figure 2.19: Aromatic peak positions for: **I** Na_3L^3 ; **II** proposed di- Mg^{II} adduct of H_3L^3 .

The pH stability of the di- Mg^{II} adduct was also investigated by ^1H NMR spectroscopy. A freshly generated mixture of 2:1 Mg^{2+} :ligand was generated and the ^1H NMR spectra taken over a range of pD values (**Figure 2.20**). As can be seen from the stacked ^1H NMR spectra at low pD, pD 6.21, there are very broad peaks indicating that there is exchange from the adduct to ligand. As the pD is raised the spectra become sharper and at pD 8.04 only peaks corresponding to adduct are

observed. There is no further change with increasing pD. This shows that the di-Mg^{II} adduct is stable from pD 8.04 and higher.

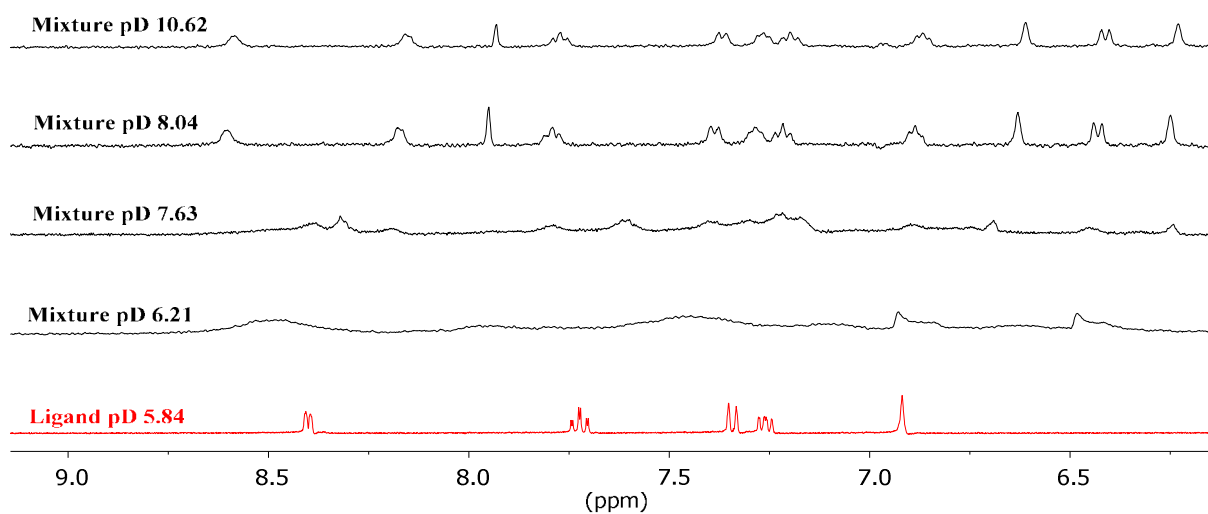


Figure 2.20: Stacked NMR of ligand, Na_3L^3 , and mixture, 1 eq. Na_3L^3 and 2 eq. Mg^{2+} over a range of pD (1:1 DMSO- d_6 : D_2O , 400 MHz).

2.3.2.3.2. Kinetic investigations

Similar to H_3L^2 (Section 2.3.2.2.2.) the ability of the di-Mg^{II} adduct to mediate the hydrolysis of the phosphodiester group in DNA and RNA was investigated using the analogues BDNP and HPNP respectively (BDNP **Figure 2.21**, HPNP **Figure 2.22**). The di-Mg^{II} adduct was generated by mixing 1 eq. of Na_3L^3 and 2 eq. Mg^{2+} and incubating for 1 hr. prior to the experiment. For both the di-Mg^{II} adduct and free Mg^{2+} a similar activity is exhibited up to pH 9.0. For both BDNP and HPNP the free Mg^{2+} exhibits a bell-shaped pH-rate profile. The pH-rate profile for the di-Mg^{II} adduct is very different only exhibiting an exponential increase. The adduct may exhibit a bell-shaped or sinusoidal graph but as discussed earlier (Section 2.3.2.2.2.) no points for pH greater than 11.0 could be taken. As seen with H_3L^2 (Section 2.3.2.2.2.) the di-Mg^{II} adduct is significantly more active than free Mg^{2+} . For BDNP the di-Mg^{II} adduct is more active above pH 10.5 and for HPNP the di-Mg^{II} adduct is more active above pH 10.

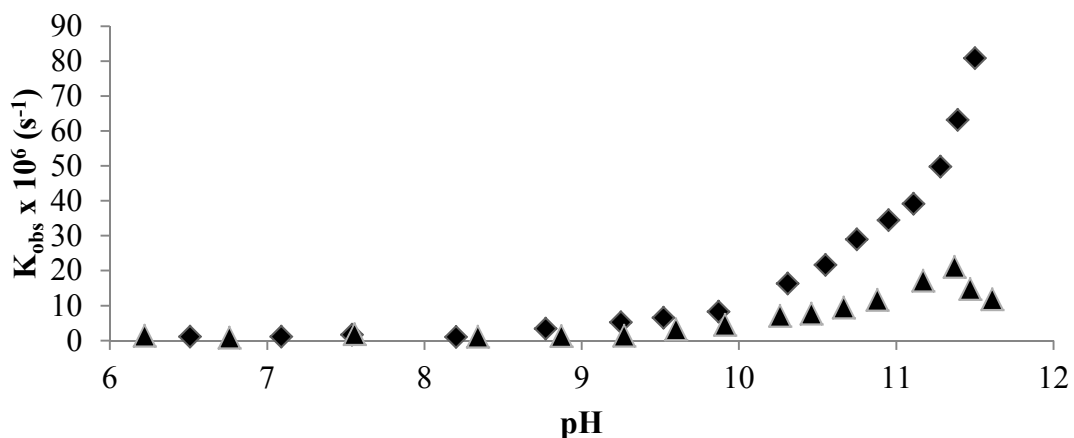


Figure 2.21: pH-rate profiles for cleavage of BDNP [5×10^{-5} M] with 1 mM di-Mg^{II} adduct (◆) and 2 mM Mg(CH₃CO₂)(NO₃) (▲) at 40 °C in 1:1 DMSO: H₂O. $I = 0.1$ M (KNO₃), [buffer] = 50 mM (buffer = MES (pH 5.5 – 6.7), PIPES (pH 6.2 – 7.4), MOPS (pH 6.6 – 7.8), HEPES (pH 6.9 – 8.1), EPPS (pH 7.4 – 8.6), CHES (pH 8.7 – 9.9) and CAPS (pH 9.8 – 11.0)).

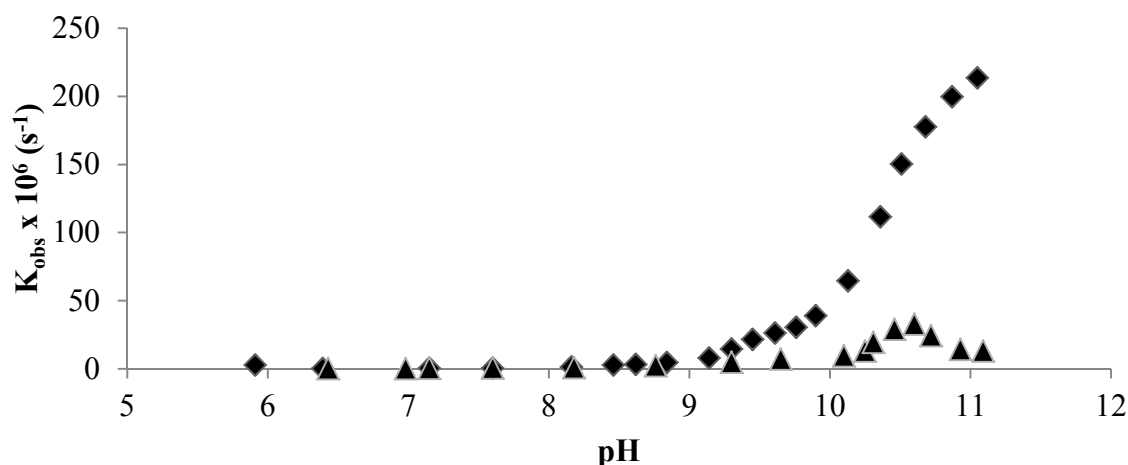


Figure 2.22: pH-rate profiles for cleavage of HPNP [5×10^{-5} M] with 1 mM di-Mg^{II} adduct (◆) and 2 mM Mg(CH₃CO₂)(NO₃) (▲) at 40 °C in 1:1 DMSO: H₂O. $I = 0.1$ M (KNO₃), [buffer] = 50 mM (buffer = MES (pH 5.5 – 6.7), PIPES (pH 6.2 – 7.4), MOPS (pH 6.6 – 7.8), HEPES (pH 6.9 – 8.1), EPPS (pH 7.4 – 8.6), CHES (pH 8.7 – 9.9) and CAPS (pH 9.8 – 11.0)).

The dependence of the rate of analogue hydrolysis with di-Mg^{II} adduct concentration was investigated (BDNP **Figure 2.23**, HPNP **Figure 2.24**). This was done at pH 9.4 for BDNP and pH 9.3 for HPNP. It was not investigated at a higher pH due to large

auto-hydrolysis of substrate at high pH. The rate was found to increase linearly with increasing di-Mg^{II} adduct concentration indicating 2nd order kinetics rather than Michaelis-Menten behaviour. The rate constant was calculated to be $1.12 \times 10^{-2} \text{ s}^{-1} \text{ M}^{-1}$ and $2.7 \times 10^{-2} \text{ s}^{-1} \text{ M}^{-1}$ for BDNP and HPNP hydrolysis respectively.

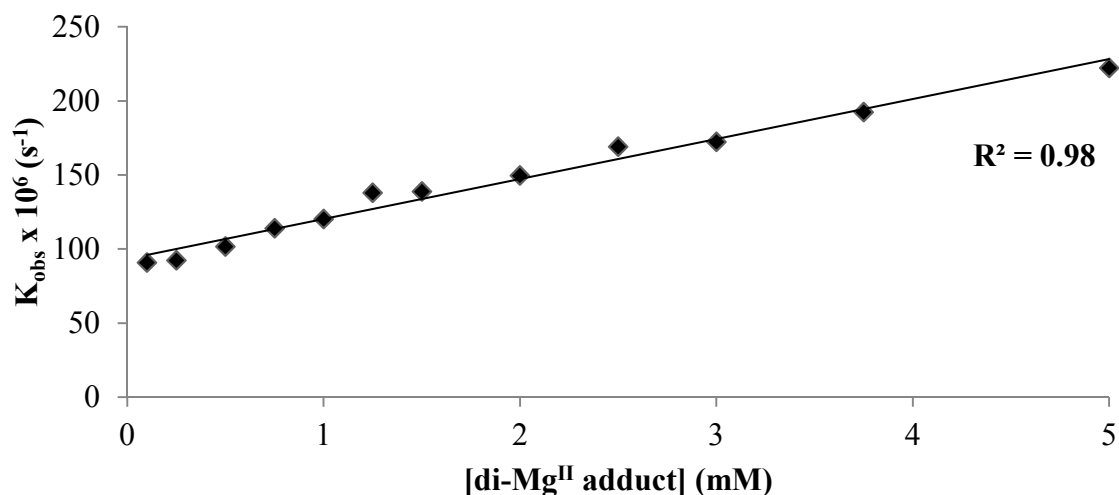


Figure 2.23: Dependence of the rate of cleavage of BDNP [$5 \times 10^{-5} \text{ M}$] on the concentration of di-Mg^{II} adduct at pH 9.4 and 40 °C in 1:1 DMSO: H₂O. $I = 0.1 \text{ M}$ (KNO₃), [buffer] = 50 mM (CHES).

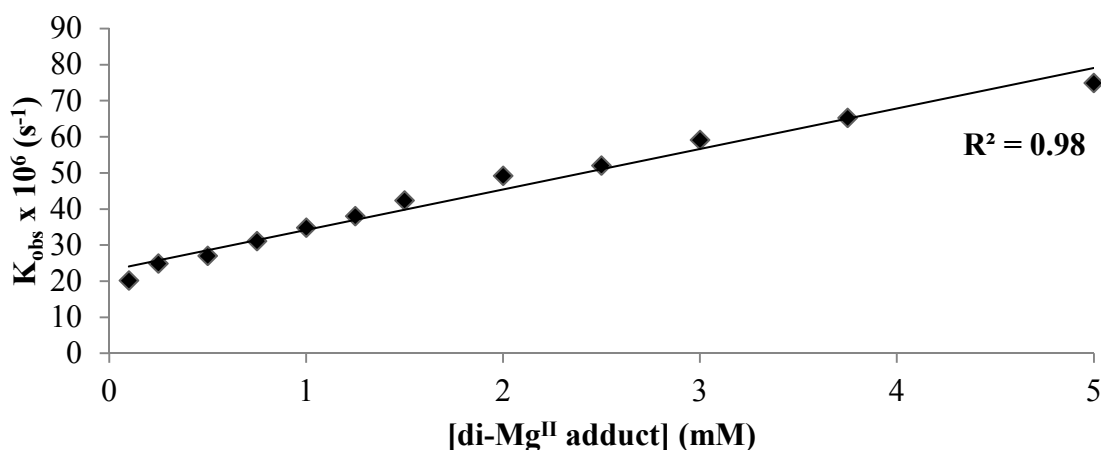


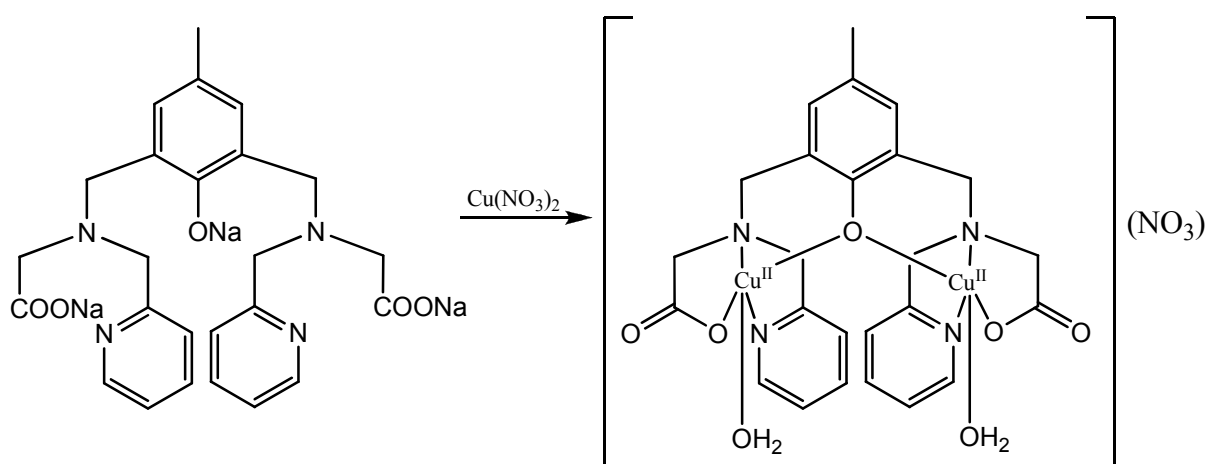
Figure 2.24: Dependence of the rate of cleavage of HPNP [$5 \times 10^{-5} \text{ M}$] on the concentration of di-Mg^{II} adduct at pH 9.3 and 40 °C in 1:1 DMSO: H₂O. $I = 0.1 \text{ M}$ (KNO₃), [buffer] = 50 mM (CHES).

2.3.3. Dinuclear Cu^{II} complex studies

2.3.3.1. H₃L²

2.3.3.1.1. Complex synthesis

A di-Cu^{II} complex of H₃L² was synthesised by mixing 1 equivalent of the trisodium salt of the ligand (Na₃L²) and 2 equivalents of Cu(NO₃)₂ and heating at 60 °C for 4 hrs (**Scheme 2.8**). The complex was isolated in crystalline form by filtration from slightly acidic solution (pH 4.03). From X-ray and elemental analysis the molecular formula of [Cu₂(L²)(H₂O)₂](NO₃) was determined.



Scheme 2.8: Synthesis of [Cu₂(L²)(H₂O)₂](NO₃).

2.3.3.1.2. X-ray structure

Repeating the synthesis on a smaller scale gave crystals suitable for analysis by X-ray crystallography. The complex crystallised in the triclinic crystal system and space group P-1. As expected the ligand binds two Cu atoms with the Cu atoms being bridged by the phenolic oxygen bringing them into close contact. The Cu···Cu distance is 3.769 Å (**Table 2.3**).

Both of the Cu atoms are in similar penta-coordinate N₂O₃ donor sets. They are coordinated by the bridging phenolic oxygen, mononucleating ligand “arm” and by a terminal water molecule each.

While the ligand is symmetrical there is asymmetry in the synthesised di-Cu^{II} complex. By calculation of the geometric parameter Tau (τ)⁵⁹ the geometry and measure of the distortion of that geometry if any around the Cu atoms can be determined. τ is defined as:

$$\tau = \frac{\beta - \alpha}{60} \text{ where } \beta \text{ and } \alpha \text{ are the largest and second largest angle respectively}$$

For a perfect square pyramidal geometry $\tau = 0$, for a perfect trigonal bipyramidal geometry $\tau = 1$ and for an intermediate geometry $\tau = 0.5$. It is found that Cu(1) is in a distorted square pyramidal environment ($\tau = 0.16$), while Cu(2) is in a considerably more distorted square pyramidal environment ($\tau = 0.44$). The value of τ for Cu(2) indicates that it more accurately would be described as a penta-coordinate geometry intermediate between square planar and trigonal bipyramidal, for descriptive purposes it will be treated as square pyramidal.

For Cu(1) the square plane is made up of the aqua oxygen, O(7), the pyridine nitrogen, N(4), the tertiary amine nitrogen, N(3) and the phenolic oxygen, O(1). With the apex for Cu(1) being the carboxylic oxygen, O(4). For Cu(2) the square plane is made of the aqua oxygen, O(6), the pyridine nitrogen, N(2), the tertiary amine nitrogen, N(1) and the carboxylic oxygen, O(2). With the apex for Cu(2) being the phenolic oxygen, O(1). For clarity only selected bond distances and bond angles are in **Table 2.3**, all bond distances and angles can be found in **Appendix 2**.

There is also H-bonding present within the complex. It is found that the O \cdots O separation for O(7) \cdots O(2) and for O(7) \cdots O(6) is 2.809(3) Å and 3.477 Å respectively. This indicates the presence of moderate and weak H-bonding respectively being present⁶⁰.

Full crystallographic data for [Cu₂(L²)(H₂O)₂](NO₃) is presented in **Appendix 3**.

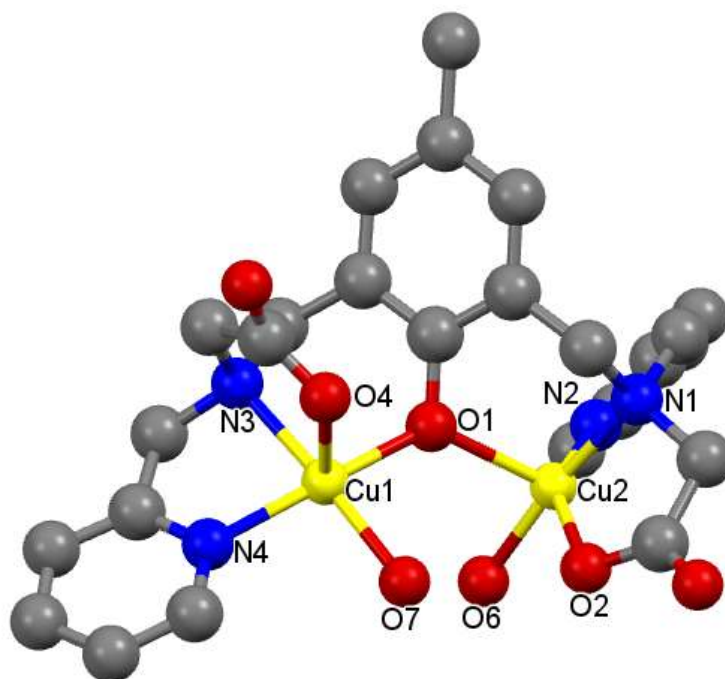


Figure 2.25: Molecular structure of $[\text{Cu}_2(\text{L}^2)(\text{H}_2\text{O})_2](\text{NO}_3)$ with atom numbering scheme included. Hydrogen atoms and Nitrate counter-ion are omitted for clarity.

Table 2.3: Selected bond lengths (Å) and angles (°) for $[\text{Cu}_2(\text{L}^2)(\text{H}_2\text{O})_2](\text{NO}_3)$.

Bond distances (Å)		Bond angles (°)	
Cu(1)-O(1)	1.945(2)	N(3)-Cu(1)-O(7)	176.17(10)
Cu(2)-O(1)	2.185(2)	N(4)-Cu(1)-O(1)	166.51(10)
Cu(1)⋯Cu(2)	3.769	N(1)-Cu(2)-O(6)	173.12(12)
O(7)⋯O(2)	2.809(3)	N(2)-Cu(2)-O(2)	146.64(10)
O(7)⋯O(6)	3.477	Cu(1)-O(1)-Cu(2)	131.67(11)

2.3.3.1.3. Solution behaviour

To determine the pKa of the coordinated waters a potentiometric titration was performed (**Figure 2.26**). From the titration two titratable protons, as expected were determined. The pKa of the coordinated waters were determined to be 6.65(2) and 7.65(2). Using this data a species distribution plot (**Figure 2.27**) was computed using a program based on the COMICS algorithm⁶¹. These values are similar to the pKa values for coordinated waters in a similarly constructed di-Cu^{II} complex based on 4-methyl phenol³³.

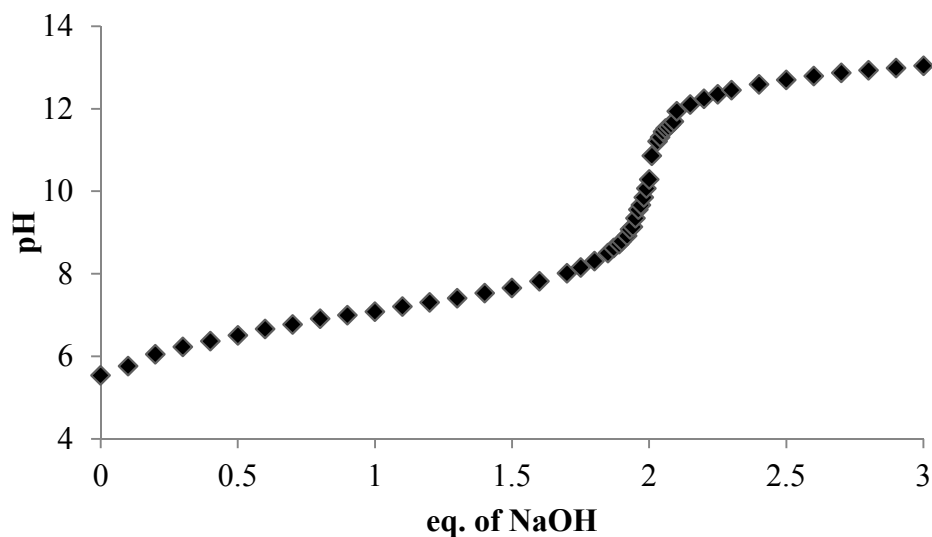


Figure 2.26: pH titration curve of $[\text{Cu}_2(\text{L}^2)(\text{H}_2\text{O})_2](\text{NO}_3)$.

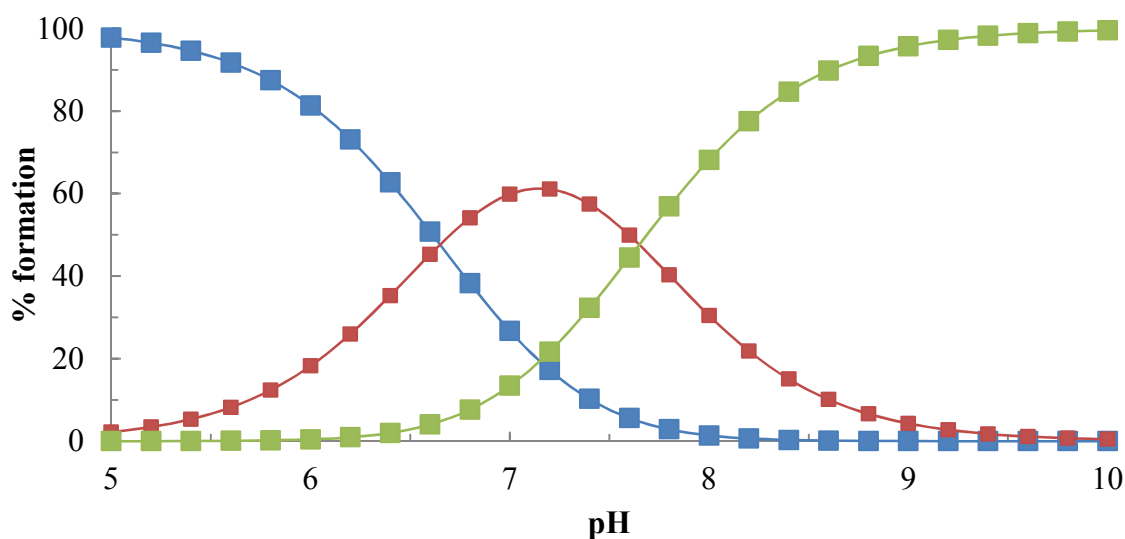


Figure 2.27: Species distribution curves for (■) $[\text{Cu}_2(\text{L}^2)(\text{H}_2\text{O})_2]^{2+}$, (■) $[\text{Cu}_2(\text{L}^2)(\text{H}_2\text{O})(\text{OH})]$, (■) $[\text{Cu}_2(\text{L}^2)(\text{OH})_2]^-$.

As can be seen from the distribution curve at lower pH the di-aqua species predominates, at neutral pH the aqua-hydroxo species predominates and then at higher pH the di-hydroxo species predominates.

2.3.3.1.4. Kinetic investigations

Using the same methods as for the di-Mg^{II} adducts (Section 2.3.2.2.2.) the ability of the complex to mediate the hydrolysis of the phosphodiester group in DNA and RNA was investigated using the analogues BDNP and HPNP, respectively (BDNP Figure 2.28, HPNP Figure 2.29). For both analogues the complex exhibits a bell-shaped pH-rate profile with optimum pH at 7.3 and 8 for BDNP and HPNP respectively.

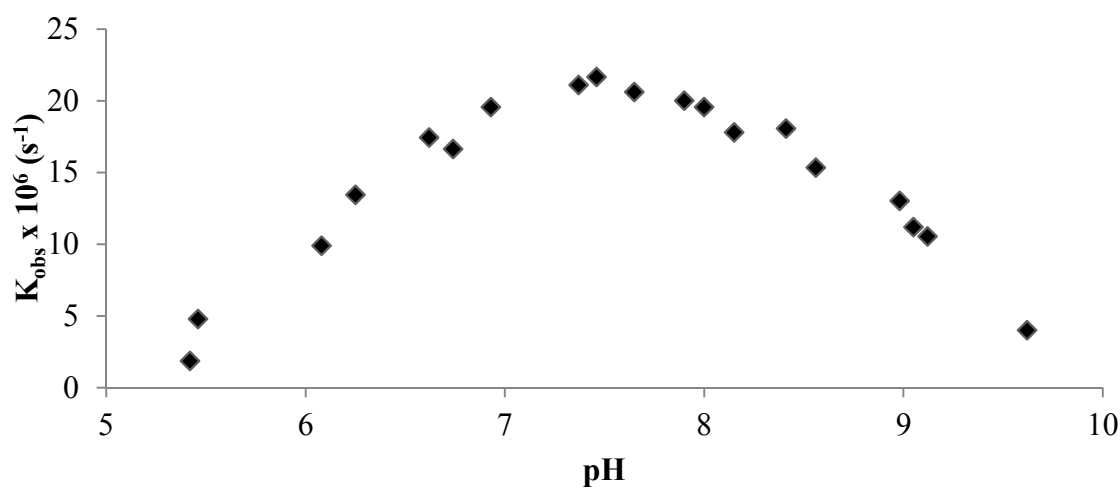


Figure 2.28: pH-rate profiles for cleavage of BDNP [5×10^{-5} M] with 0.5 mM complex at 40 °C in H₂O. $I = 0.1$ M (KNO₃), [buffer] = 50 mM (buffer = MES (pH 5.5 – 6.7), PIPES (pH 6.2 – 7.4), MOPS (pH 6.6 – 7.8), HEPES (pH 6.9 – 8.1), EPPS (pH 7.4 – 8.6) and CHES (pH 8.7 – 9.9)).

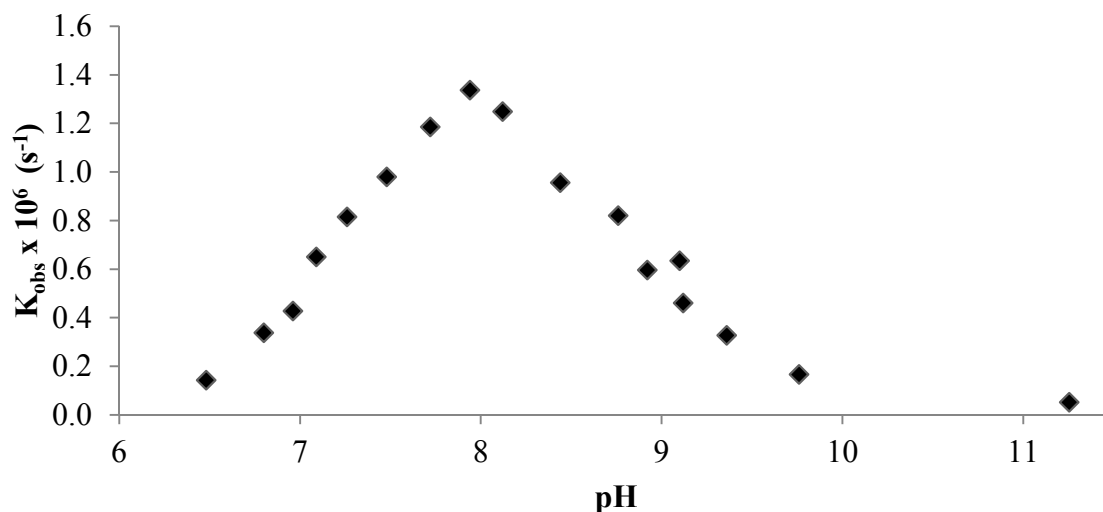


Figure 2.29: pH-rate profiles for cleavage of HPNP [5×10^{-5} M] with 0.5 mM complex at 40 °C in H₂O. $I = 0.1$ M (KNO₃), [buffer] = 50 mM (buffer = MES (pH 5.5 – 6.7), PIPES (pH 6.2 – 7.4), MOPS (pH 6.6 – 7.8), HEPES (pH 6.9 – 8.1), EPPS (pH 7.4 – 8.6) and CHES (pH 8.7 – 9.9)).

The dependence of the rate of analogue hydrolysis with complex concentration was investigated (BDNP **Figure 2.30**, HPNP **Figure 2.31**). This was done at the optimum pH). The rate was found to increase linearly with increasing complex concentration indicating 2nd order kinetics rather than Michaelis-Menten behaviour. The rate constants were calculated to be $4.625 \times 10^{-3} \text{ M}^{-1}\text{s}^{-1}$ and $1.729 \times 10^{-3} \text{ M}^{-1}\text{s}^{-1}$ for BDNP and HPNP hydrolysis respectively.

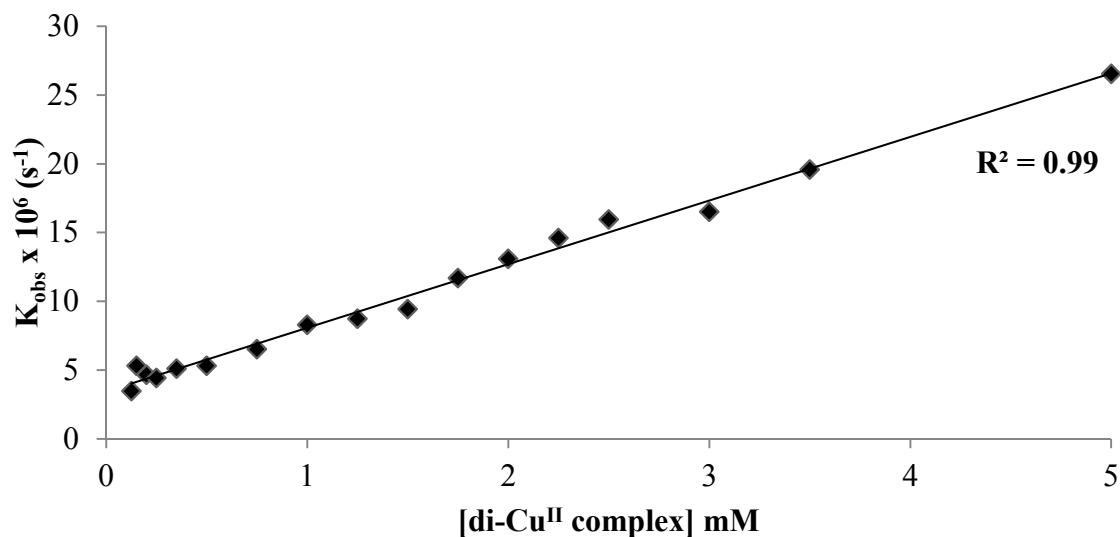


Figure 2.30: Dependence of the rate of cleavage of BDNP [5×10^{-5} M] on the concentration of di-Cu^{II} complex at pH 7.3 and 40 °C in H₂O. $I = 0.1$ M (KNO₃), [buffer] = 50 mM (HEPES).

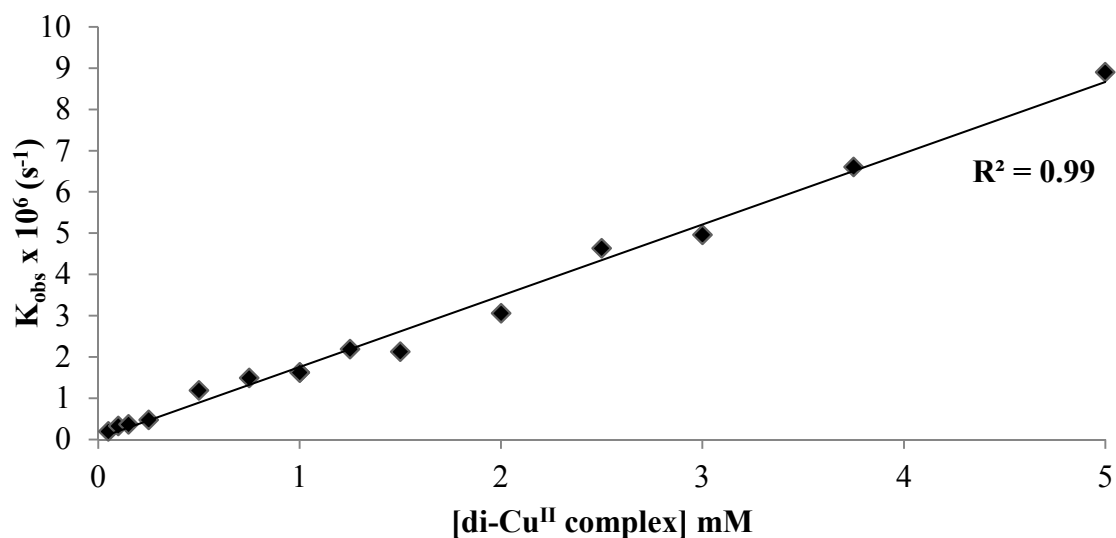
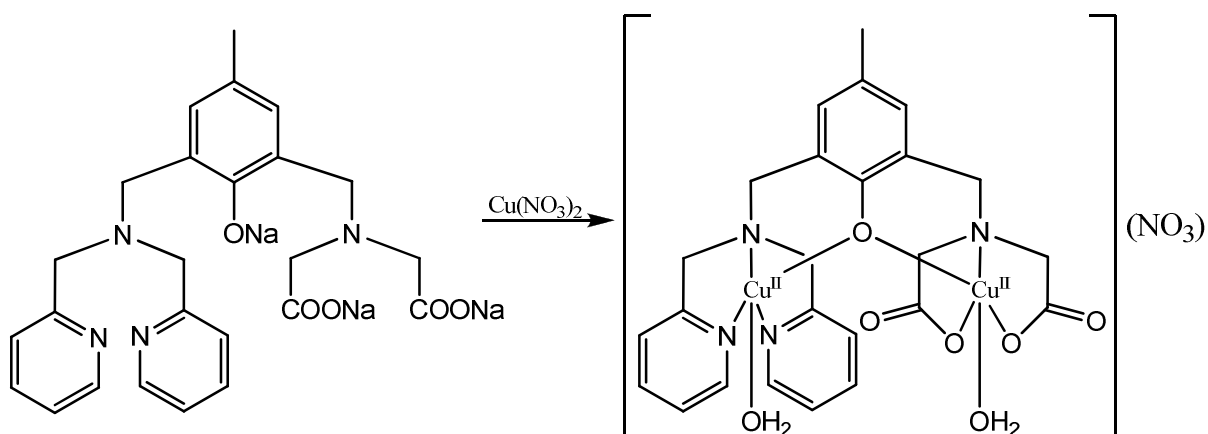


Figure 2.31: Dependence of the rate of cleavage of HPNP [5×10^{-5} M] on the concentration of di-Cu^{II} complex at pH 8.0 and 40 °C in H₂O. $I = 0.1$ M (KNO₃), [buffer] = 50 mM (EPPS).

2.3.3.2. H_3L^3

2.3.3.2.1. Complex synthesis

A di- Cu^{II} complex of H_3L^2 was synthesised by mixing 1 equivalent of the trisodium salt of the ligand (Na_3L^3) and 2 equivalent of $Cu(NO_3)_2$ and heating at 60 °C for 4 hrs (**Scheme 2.9**). The complex was isolated in crystalline form by filtration from slightly acidic solution (pH 6.18). From mass spectrometry and elemental analysis the molecular formula of $[Cu_2(L^3)(H_2O)_2](NO_3)$ was determined.



Scheme 2.9: Synthesis of $[Cu_2(L^3)(H_2O)_2](NO_3)$.

While the di- Cu^{II} complex was isolated in crystalline form, no crystals suitable for single crystal X-ray crystallography were obtained. The crystals obtained were found to be an amalgamation of several single crystals and hence were unsuitable for analysis.

Due to lack of complex no potentiometric titrations were able to be performed.

2.3.3.2.2. Kinetic investigations

Using the same method as for the H_3L^2 (**Section 2.3.3.1.2.**) The ability of the complex to mediate the hydrolysis of the phosphodiester group in DNA and RNA was investigated using the analogues BDNP and HPNP respectively (BDNP **Figure 2.32**, HPNP **Figure 2.33**). BDNP has optimum pH at 8.0 and HPNP has optimum pH at 8.5.

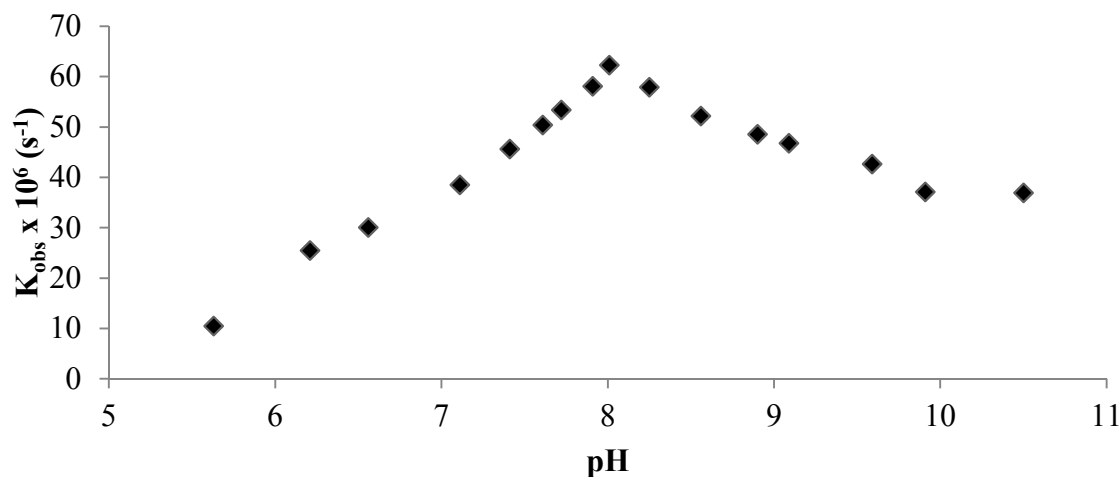


Figure 2.32: pH-rate profiles for cleavage of BDNP [5×10^{-5} M] with 1 mM complex at 40 °C in 1:1 DMSO: H₂O. $I = 0.1$ M (KNO₃), [buffer] = 50 mM (buffer = MES (pH 5.5 – 6.7), PIPES (pH 6.2 – 7.4), MOPS (pH 6.6 – 7.8), HEPES (pH 6.9 – 8.1), EPPS (pH 7.4 – 8.6) and CHES (pH 8.7 – 9.9)).

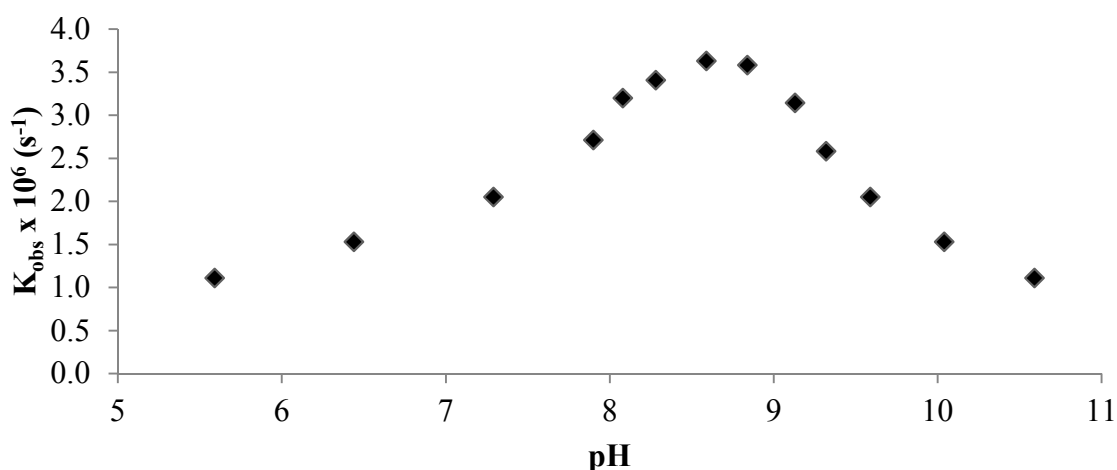


Figure 2.33: pH-rate profiles for cleavage of HPNP [5×10^{-5} M] with 1 mM complex at 40 °C in 1:1 DMSO: H₂O. $I = 0.1$ M (KNO₃), [buffer] = 50 mM (buffer = MES (pH 5.5 – 6.7), PIPES (pH 6.2 – 7.4), MOPS (pH 6.6 – 7.8), HEPES (pH 6.9 – 8.1), EPPS (pH 7.4 – 8.6) and CHES (pH 8.7 – 9.9)).

The dependence of the rate of analogue hydrolysis with complex concentration was investigated (BDNP **Figure 2.34**, HPNP **Figure 2.35**). This was done at the optimum pH. The rate was found to increase linearly with increasing complex concentration indicating 2nd order kinetics rather than Michaelis-Menten behaviour.

The rate constants were calculated to be $24.1 \times 10^{-3} \text{ M}^{-1}\text{s}^{-1}$ and $7.12 \times 10^{-3} \text{ M}^{-1}\text{s}^{-1}$ for BDNP and HPNP hydrolysis respectively.

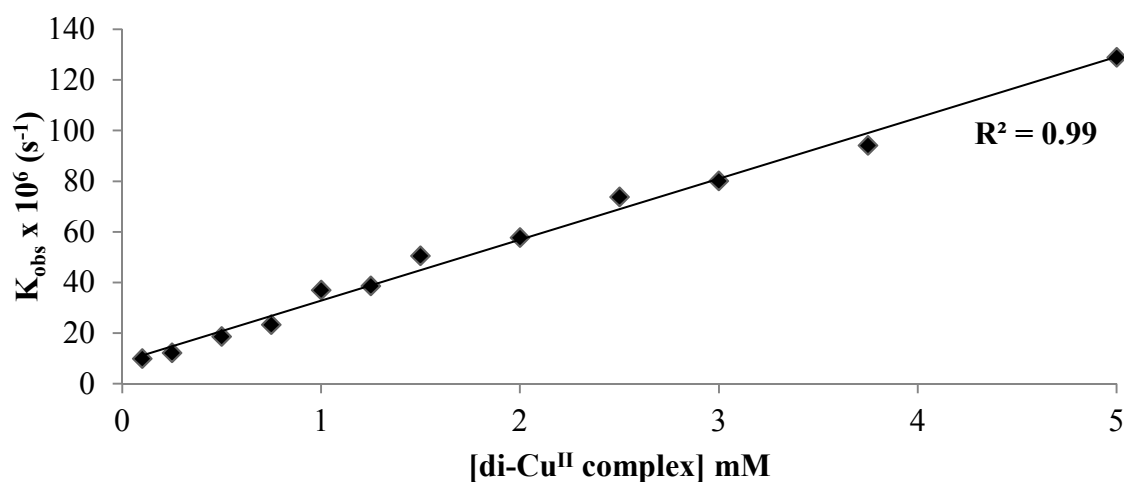


Figure 2.34: Dependence of the rate of cleavage of BDNP [$5 \times 10^{-5} \text{ M}$] on the concentration of di-Cu^{II} complex at pH 8.0 and 40 °C in 1:1 DMSO: H₂O. $I = 0.1 \text{ M}$ (KNO₃), [buffer] = 50 mM (EPPS).

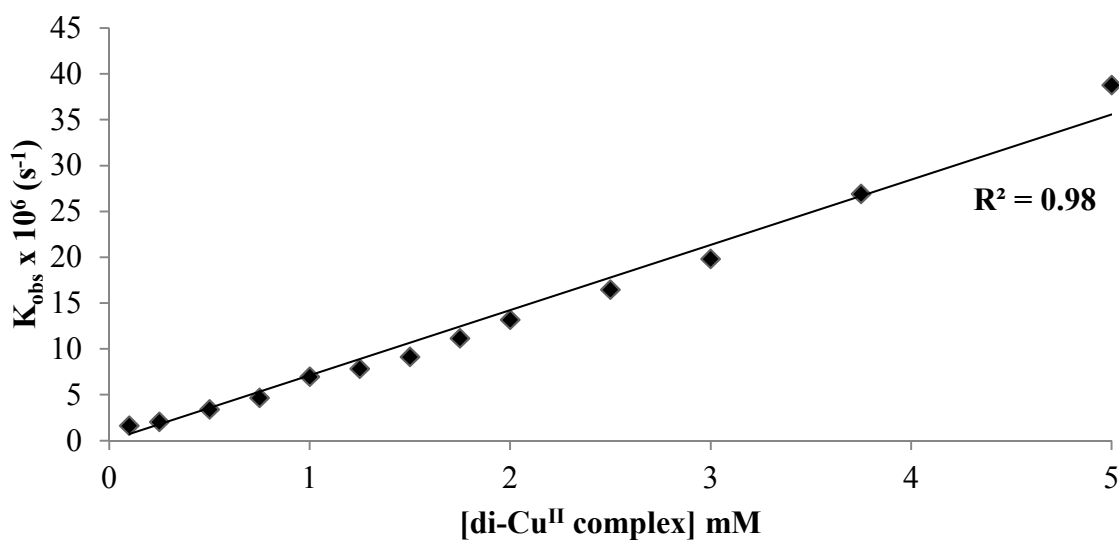
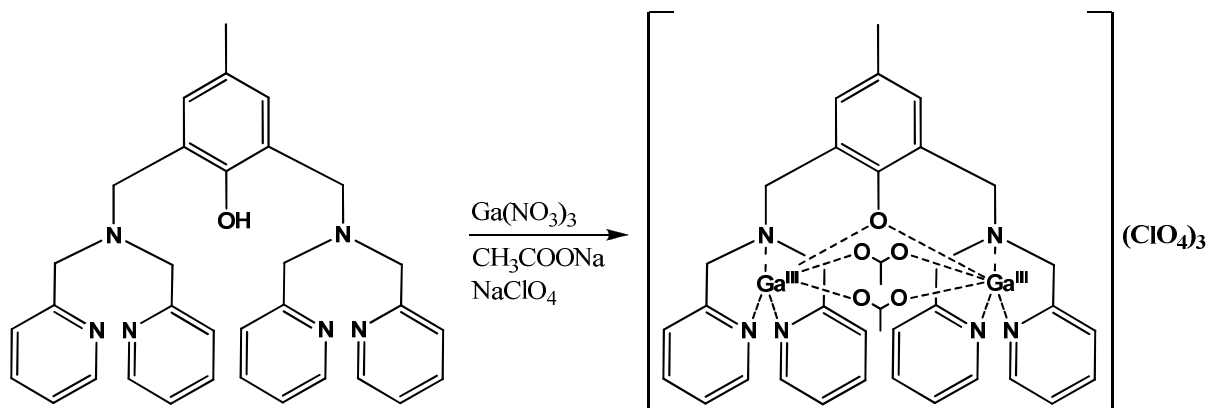


Figure 2.35: Dependence of the rate of cleavage of HPNP [$5 \times 10^{-5} \text{ M}$] on the concentration of di-Cu^{II} complex at pH 8.5 and 40 °C in 1:1 DMSO: H₂O. $I = 0.1 \text{ M}$ (KNO₃), [buffer] = 50 mM (EPPS).

2.3.4. Dinuclear Ga^{III} complex studies

2.3.4.1. Complex synthesis and stability

Due to Ga^{III}'s ability to mimic Fe³⁺ and its potential involvement in the active site of PAP (**Section 2.1.4.**) investigations were undertaken with a dinuclear Ga^{III} complex of **HL**¹. Following a literature procedure the dinuclear Ga^{III} complex of **HL**¹, [Ga₂(L¹)(acetate)₂](ClO₄)₃, was generated²⁶ (**Scheme 2.10**).



Scheme 2.10: Synthesis of [Ga₂(L¹)(acetate)₂](ClO₄)₃.

As the yield for the synthesis of [Ga₂(L¹)(acetate)₂](ClO₄)₃ was low it was proposed to determine the nuclease ability of the complex by generating a di-Ga^{III} adduct *in situ*. The ability of **HL**¹ to bind Ga³⁺ *in situ* was determined by a ¹H NMR titration. To prevent any contribution from pH the titration was performed in MeOH-d₁. Unfortunately this led to large residual solvent and water peaks which overlapped with the aliphatic region. Increasing equivalents of Ga(NO₃)₃ were added and the ¹H NMR spectra were taken (**Figure 2.36**). As can be seen from the stacked NMR spectra there is a large difference in the aromatic region with increasing equivalents of Ga³⁺. After 2 equivalents of Ga³⁺ were added there was no further change in the ¹H NMR spectra. This indicates that **HL**¹ will form a di-Ga^{III} adduct *in situ*. But after 1 equivalent of Ga³⁺ was added there was no broadening of the signals as was seen previously (**Section 2.3.2.3.1.**). This is due to the presence of a 1:1 adduct and free ligand. Even though the titration is performed in non-aqueous conditions there are shifts in the peak positions observed.

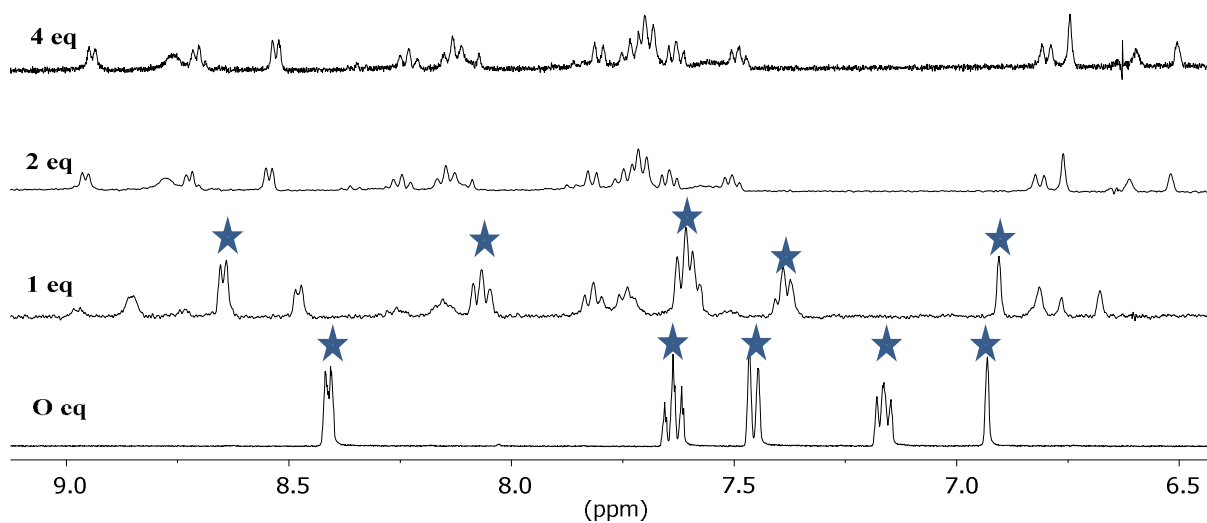


Figure 2.36: Stacked NMR showing **HL¹** with increasing equivalents of Ga³⁺ (MeOH-d₁, 400 MHz) (★= free ligand).

Since the nuclease ability will be studied in aqueous conditions the pH stability of the di-Ga^{III} adduct was also studied by ¹H NMR spectroscopy (**Figure 2.37**). The ¹H NMR spectra of a freshly mixed solution of 2:1 Ga³⁺:**HL¹** was taken over a range of pD. Due to solubility issues of **HL¹** the solution was made in 1:1 MeOH-d₁:D₂O. As can be seen from the stacked ¹H NMR there is no change in the peak positions. Indicating that the di-Ga^{III} adduct is stable from pH 2.09 to pH 9.58.

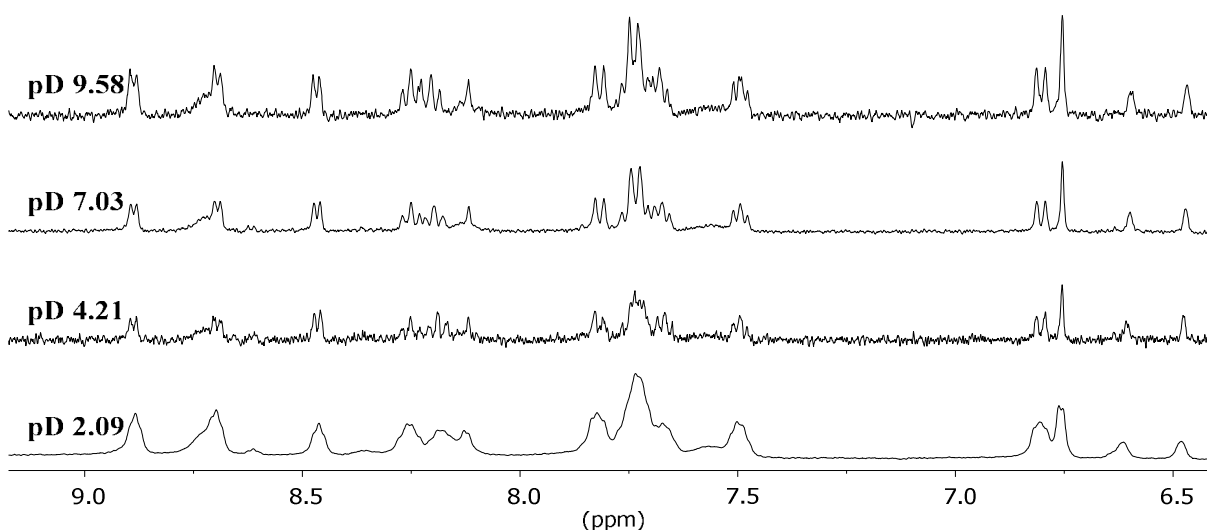


Figure 2.37: Stacked NMR showing the stability of [Ga₂L¹] over a range of pD (1:1 MeOH-d₁: D₂O, 400 MHz).

2.3.4.2. Kinetic investigations

Using the same method as for the di-Mg^{II} adducts (Section 2.3.2.2.2.) The ability of the complex to mediate the hydrolysis of the phosphodiester group in DNA was investigated using the analogues BDNP (Figure 2.38). The di-Ga^{III} adduct was generated by mixing 1 eq. of HL¹ and 2 eq. of Ga³⁺ and incubating for 1 hr. prior to the experiment. The complex exhibits a bell-shaped pH-rate profile with optimum pH at 6.0. The ability of the complex to mediate the hydrolysis of the phosphodiester group in RNA was also investigated using HPNP but the complex was found to be inactive.

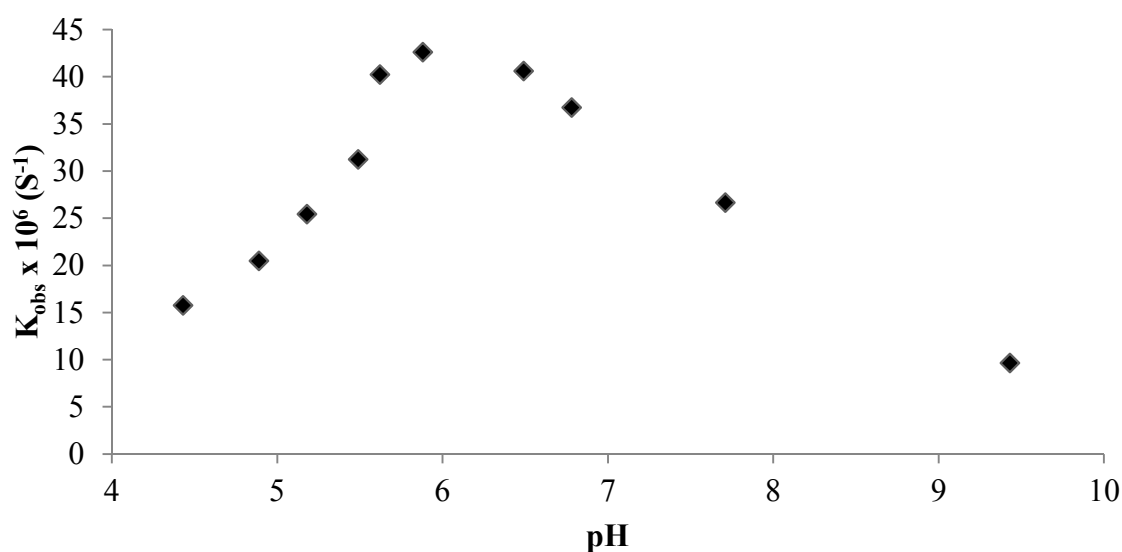


Figure 2.38: pH-rate profiles for cleavage of BDNP [5×10^{-5} M] with 1 mM di-Ga^{III} adduct at 40 °C in 1:1 MeOH: H₂O. $I = 0.1$ M (KNO₃), [buffer] = 50 mM (buffer = MES (pH 5.5 – 6.7), PIPES (pH 6.2 – 7.4), MOPS (pH 6.6 – 7.8), HEPES (pH 6.9 – 8.1), EPPS (pH 7.4 – 8.6) and CHES (pH 8.7 – 9.9)).

The dependence of the rate of analogue hydrolysis with complex concentration was investigated (Figure 2.39). This was done at the optimum pH. The rate was found to increase linearly with increasing complex concentration indicating 2nd order kinetics rather than Michaelis-Menten behaviour. The rate constants were calculated to be $5.0 \times 10^{-3} \text{ s}^{-1}\text{M}^{-1}$.

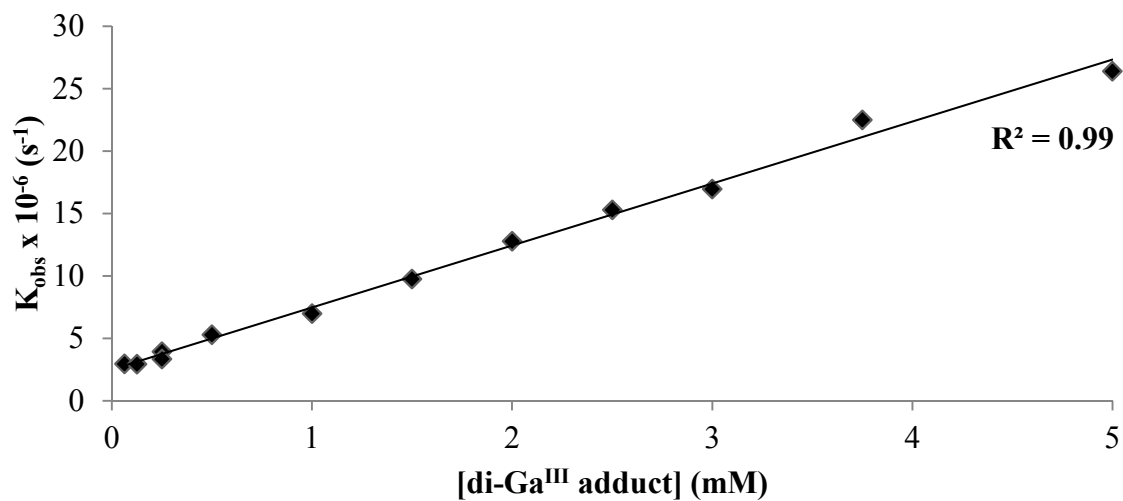


Figure 2.39: Dependence of the rate of cleavage of BDNP [$5 \times 10^{-5} \text{ M}$] on the concentration of di-Ga^{III} adduct at pH 6.0 and 40 °C in 1:1 MeOH: H₂O. $I = 0.1 \text{ M}$ (KNO₃), [buffer] = 50 mM (CHES).

2.4. Discussion and conclusions

Using either literature procedures or by modified means three dinucleating ligands have been synthesised. All three consist of a 4-methyl phenol body and metal binding “arms”. The presence of the phenol will bring the metal ions into close contact and promote synergy. The metal binding “arms” are mononucleating ligands which have various amounts of pyridine and carboxylic acid metal binding moieties arranged symmetrically or unsymmetrically.

For all three ligands the di-Mg^{II} adducts were studied by either synthesis or by generation *in situ*. For the complex with the tetra-pyridine ligand **HL**¹, it was found to be unstable at neutral pH and only at very high pH there is an appreciable amount of complex present. The carboxylic acid containing ligands, **H₃L**² and **H₃L**³, were found to generate di-Mg^{II} adducts *in situ* that were stable from pH 7.5 upwards. This is in keeping with the HSAB theory and is also consistent with electrostatic effects.

The nuclease ability of the proposed di-Mg^{II} adducts of **H₃L**² and **H₃L**³ was investigated. For both an exponential increase from pH 9 and higher was exhibited. Due to the inability to measure above pH 11.0 it is not possible to determine if a bell-shaped or sinusoidal pH rate curve would be exhibited, and so it is difficult to assign any potential mechanism to the cleavage.

The di-Cu^{II} complexes of the carboxylic acid containing ligands, **H₃L**² and **H₃L**³ were synthesised. Unfortunately no suitable single crystal of the unsymmetrical complex, **[Cu₂(L³)(H₂O)₂](NO₃)**, was obtained and so the solid-state structure could not be investigated. But crystals suitable for analysis were obtained for the symmetrical complex, **[Cu₂(L²)(H₂O)₂](NO₃)**, were obtained.

It was found that the two Cu atoms were bridged by the phenolic oxygen bringing them into close contact (3.769 Å) which is similar but slightly larger than literature values (3.56 Å – 3.67 Å)^{33,34,42} for Cu···Cu distances in similarly constructed ligands with nuclease ability. The Cu···Cu distance is also comparable to the observed M···M distance in the dimetallic enzyme, DNA polymerase I (Section 1.2.1.2.1), which is 3.9 Å⁶². For comparison with the analogous di-Zn^{II} complex the M···M is 3.50 Å³⁹ with both Zn atoms in an octahedral coordination environment with a N₂O₄ donor set³⁹. In the symmetrical complex both Cu atoms are in similar penta-

coordinate N_2O_3 donor sets. The difference in the donor set between the di- Zn^{II} complex and di- Cu^{II} complex is due to the presence of two bridging acetate moieties in the di- Zn^{II} complex.

By calculation of the geometric parameter τ ⁵⁹ it was found that both metal centres are in different coordination environments. Cu(1) is in a distorted square pyramidal while Cu(2) is in an intermediate geometry between square pyramidal and trigonal bipyramidal. This difference in τ for the two Cu atoms has also been observed in other di- Cu^{II} complexes with nuclease activity but in those instances the difference in τ was much smaller³⁴.

As with the di- Mg^{II} adducts the nuclease ability of the symmetrical and unsymmetrical complex were investigated. For the symmetrical complex a bell-shaped pH rate curve was obtained for the hydrolysis of BDNP and HPNP with optimum pH of 7.3 and 8.0 respectively (**Section 2.3.3.1.4.**). This indicates that the active species is the aqua-hydroxo species, with an aqua ligand on one metal centre and a hydroxide on the other metal centre.

Cleavage occurs by coordination of the substrate displacing the aqua ligand. Subsequent nucleophile attack by the hydroxide coordinated to the neighbouring metal centre causes cleavage of the phosphate group. For both complexes the optimum pH for the different substrates is similar indicating that the active species is the same.

Further evidence for the aqua-hydroxo species being the catalytically active species comes from the potentiometric titration and species distribution curve (**Section 2.3.3.1.3.**). From the titration the pK_a of the waters was determined to be 6.65(2) and 7.65(2). These values indicate that at the optimum hydrolysis pH the aqua-hydroxo species predominates which is in keeping with the proposed mechanism.

The nuclease ability of the unsymmetrical complex was also investigated. As with the di- Mg^{II} studies the unsymmetrical complex was found to be substantially more active, approx. 3 times more active, than the symmetrical complex. It was also found that the optimum pH for the unsymmetrical complex was higher than the symmetrical complex.

While both ligands have a similar charge and have the same overall donor set, due to the structural difference between the symmetrical and unsymmetrical ligand there are two very different coordination environments for the Cu atoms in the unsymmetrical complex. This dissimilar binding environments is also seen in numerous active sites of dimetallic enzymes including DNA polymerase I (**Section 1.2.1.2.1.**)^{62,63} and alkaline phosphatase⁶⁴.

In the symmetrical complex both Cu atoms are in similar N_2O_3 donor sets, with both metal atoms coordinated by a carboxylic acid (**Figure 2.40 structure I**). This decreases the Lewis acidity for both Cu atoms. In the unsymmetrical complex Cu_1 is in a N_3O_2 donor set coordinated by two pyridines while Cu_2 is in a NO_4 donor set coordinated to two carboxylic (**Figure 2.40 structure II**). So while the Lewis acidity of Cu_2 will be reduced due to the carboxylic acids, the Lewis acidity of Cu_1 will be unchanged.

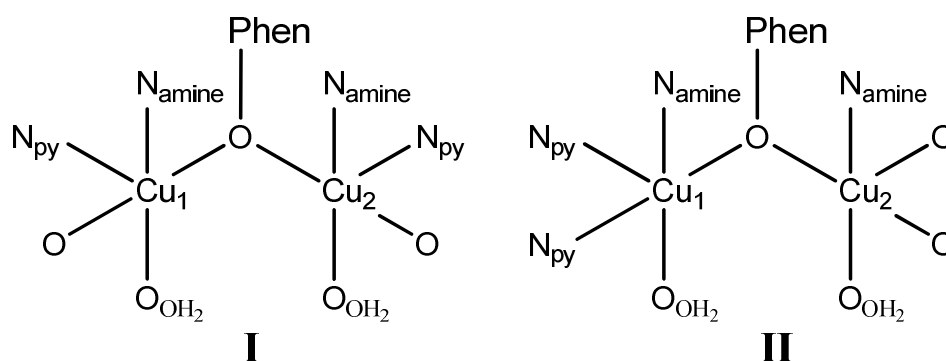


Figure 2.40: Coordination environment of Cu atoms in: **I** symmetrical complex $[Cu_2(L^2)(H_2O)_2](NO_3)$; **II** unsymmetrical complex $[Cu_2(L^3)(H_2O)_2](NO_3)$.

The dissimilar binding environment will raise the pK_a of the coordinated water to Cu_2 . So relative to the symmetrical complex will the aqua-hydroxo species predominate at higher pH. So if the aqua-hydroxo species is the active species for the unsymmetrical complex it would be expected that the optimum pH would be higher than the symmetrical complex and that it would be more reactive due to the unchanged Lewis acidity of Cu_1 . This matches the kinetic data so for the unsymmetrical as was found for the symmetrical complex the aqua-hydroxo species is the active species.

For both the symmetrical and unsymmetrical complexes 2nd order kinetics was exhibited rather than Michaelis-Menten behaviour indicating that the complex is not saturable in the concentration range 0 – 5mM.

The nuclease ability of the di-Ga^{III} adduct of the tetra pyridine ligand **HL**¹ was also investigated. For the hydrolysis of BDNP it exhibited a bell-shaped pH-rate profile indicating a similar mechanism as the di-Cu^{II} complexes. But when the reactivity with the RNA analogue, HPNP, was investigated it was found to be inactive. As with the di-Cu^{II} complexes it exhibited 2nd order kinetics rather than Michaelis-Menten behaviour indicating that the adduct is not saturable in the concentration range 0 – 5 mM.

From the literature artificial nucleases which include Ga^{III} are either mixed metal systems^{26,46} based on PAP or mononuclear complexes²⁸ so it is difficult to directly compare the activity against literature examples.

As discussed earlier (**Section 1.3.**) the study of artificial nucleases is driven by many motivations. But whether to be used for the elucidation of enzyme mechanisms or as potential therapeutics, complexes which are stable and active at physiological pH are desired.

For both of the di-Cu^{II} complexes and the di-Ga^{III} complex studied they were found to be active at pH values relatively similar to physiological pH. But for the di-Mg^{II} adducts generated *in situ* this was not the case. It was found for all the dinucleating ligands studied that the di-Mg^{II} adducts were only stable and/or active at pH values much greater than physiological pH. This was disappointing as one of the main reasons magnesium was studied was its relatively high abundance in the body. So any potential therapeutic developed could be utilised as a metal free agent and would bind magnesium atoms *in vitro*. The use of a metal-free agent is desirable as it would potentially be able to permeate cellular membranes much easier than a metal complex.

The main structural difference between the ligands is the replacement of two pyridine moieties with carboxylic acids. So potentially by full replacement of all the pyridine moieties with carboxylic acids a stable and active di-Mg^{II} complex could be obtained. This tetra-carboxylic acid ligand, 5-methyl-2-hydroxy-1,3-xylene- α,α -

diamine- N,N,N',N' -tetraacetic acid (HXTA) (Ligand 9, **Table 2.1.**, **Figure 2.10**) has been previously studied within the group the di- Mg^{II} and di- Zn^{II} complex of HXTA was investigated⁵⁰. It was found to be inactive towards the transesterification of HPNP and no coordination of the inactive phosphate DPP was observed. It was proposed that this was due to the reduced electrophilicity of the divalent metal ions and the large negative charge of the carboxylate donors interfering with the coordination of the negatively charged phosphate diester.

Rather than replacing the pyridines with carboxylic acids they could be replaced by amines (**Figure 2.41**). From the HSAB theory this should generate a ligand that will form a stable complex which could potentially be active. But due to the large number of functional groups synthesis of such ligands could be difficult.

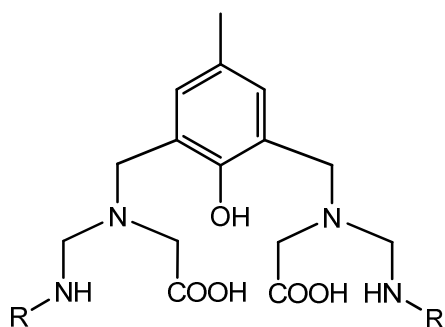


Figure 2.41: Structure of proposed changed ligand, R = H, alkyl chain.

Also possible would be to utilise a known ligand of completely different design. Mono- Mg^{II} complexes based on macrocycle⁶⁵ or modified schiff bases^{66,67} have been reported. While these are monometallic complexes by modification of the ligand additional metal binding sites could be introduced to generate di or tri- Mg^{II} complexes that could potentially be effective ligands. But a downside of using these ligands could be the difficulty to get the metal atoms in close contact and, hence, the degree of synergy could be low.

To ensure that the metal atoms are in close contact a calixarene could be used. Calixarenes are cone shaped supramolecules (**Figure 2.42**). Metal binding groups can be added at the top or bottom of the cone to allow for complexation. Previously it was found that carboxylic acid containing calixarenes are effective complexing agents for alkaline earth elements⁶⁸ and there has also been reported di- Zn^{II} and tri- Zn^{II} complexes which are effective catalysts for the transesterification of HPNP⁶⁹. A

benefit of using a calixarene ligand is the large synthetic versatility and that the metal centres would be in close contact allowing synergy between the metal ions. Numerous example of calixarenes have being reported for their use in metal based catalysis⁷⁰ this would help greatly in the generation of a suitable ligand.

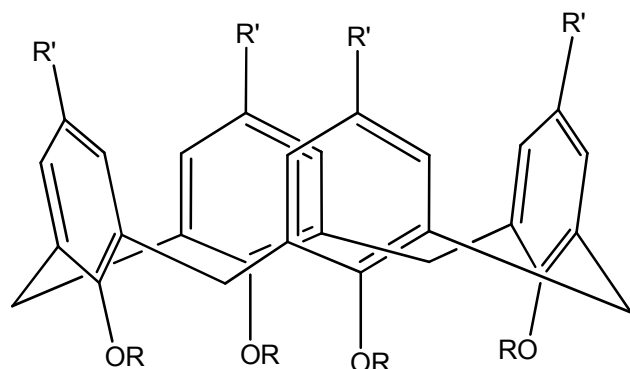


Figure 2.42: Schematic structure of calix-4-arene; R, R' = potential metal binding groups.

In this work all the ligands generated include a 4-methyl phenol as the body. For artificial nucleases to be transformed to antisense therapeutic a targeting unit needs to be incorporated (**Section 1.3.1.**). The ligands in this work do not allow for addition of a targeting unit but modification of the methyl group to an amine or carboxylic acid would allow for linking to targeting units. This topic is the subject of the next chapter.

2.5. References

- (1) Nielsen, P. E.; Jeppesen, C.; Buchardt, O. *FEBS Letters* **1988**, *235*, 122-124.
- (2) Takasaki, B. K.; Chin, J. *J. Am. Chem. Soc.* **1994**, *116*, 1121-1122.
- (3) Roigk, A.; Hettich, R.; Schneider, H.-J. *Inorg. Chem.* **1998**, *37*, 751-756.
- (4) Komiyama, M.; Takeda, N.; Takahashi, Y.; Uchida, H.; Shiiba, T.; Kodama, T.; Yashiro, M. *J. Chem. Soc., Perkin. Trans. 2* **1995**, 269-274.
- (5) Igawa, T.; Sumaoka, J.; Makot, K. *Chem. Lett.* **2000**, 356-357.
- (6) Sumaoka, J.; Azuma, Y.; Komiyama, M. *Chem. Eur. J.* **1998**, *4*, 205-209.
- (7) Raganathan, K. G.; Schneider, H.-J. *Angew. Chem. Int. Ed.* **1996**, *35*, 1219-1211.
- (8) Zhu, B.; Zhao, D.-Q.; Ni, J.-Z.; Zeng, Q.-H.; Huang, B.-Q.; Wang, Z.-L. *Inorg. Chem. Commun.* **1999**, *2*, 351-353.
- (9) Branum, M. E.; Tipton, A. K.; Zhu, S.; Que, L. *J. Am. Chem. Soc.* **2001**, *123*, 1898-1904.
- (10) Sigman, D. S.; Graham, D. R.; D'Aurora, V.; Stern, A. M. *J. Biol. Chem.* **1979**, *254*, 12269-12272.
- (11) Chen, C. H. B.; Mazumder, A.; Constant, J. F.; Sigman, D. S. *Bioconjugate Chem.* **1993**, *4*, 69-77.
- (12) Silva, P. P.; Guerra, W.; Silveira, J. N.; Ferreira, A. M. d. C.; Bortolotto, T.; Fischer, F. L.; Terenzi, H. n.; Neves, A.; Pereira-Maia, E. C. *Inorg. Chem.* **2011**, *50*, 6414-6424.
- (13) Chetana, P. R.; Rao, R.; Roy, M.; Patra, A. K. *Inorg. Chim. Acta* **2009**, *362*, 4692-4698.
- (14) Patra, A. K.; Bhowmick, T.; Ramakumar, S.; Nethaji, M.; Chakravarty, A. R. *Dalton Trans.* **2008**, 6966-6976.
- (15) Goswami, T. K.; Roy, M.; Nethaji, M.; Chakravarty, A. R. *Organometallics* **2009**, *28*, 1992-1994.
- (16) Tabassum, S.; Asim, A.; Arjmand, F.; Afzal, M.; Bagchi, V. *Eur. J. Med. Chem.* **2012**, *58*, 308-316.
- (17) Hegg, E. L.; Burstyn, J. N. *Inorg. Chem.* **1996**, *35*, 7474-7481.
- (18) Itoh, T.; Hisada, H.; Sumiya, T.; Hosono, M.; Usui, Y.; Fujii, Y. *Chem. Commun.* **1997**, 677-678.

- (19) Stern, M. K.; Bashkin, J. K.; Sall, E. D. *J. Am. Chem. Soc.* **1990**, *112*, 5357-5359.
- (20) Li, J.-H.; Wang, J.-T.; Hu, P.; Zhang, L.-Y.; Chen, Z.-N.; Mao, Z.-W.; Ji, L.-N. *Polyhedron* **2008**, *27*, 1898-1904.
- (21) Ibrahim, M. M.; Ramadan, A.-M. M.; Mersal, G. A. M.; El-Shazly, S. A. *J. Mol. Struct.* **2011**, *998*, 1-10.
- (22) Qian, J.; Wang, L.-P.; Tian, J.-L.; Yan, S.-P. *J. Coord. Chem.* **2011**, *64*, 1991-2001.
- (23) Belousoff, M. J.; Tjioe, L.; Graham, B.; Spiccia, L. *Inorg. Chem.* **2008**, *47*, 8641-8651.
- (24) Berthet, N.; Martel-Frchet, V.; Michel, F.; Philouze, C.; Hamman, S.; Ronot, X.; Thomas, F. *Dalton Trans.* **2013**, *42*, 8468-8483.
- (25) Mitic, N.; Smith, S. J.; Neves, A.; Guddat, L. W.; Gahan, L. R.; Schenk, G. *Chem. Rev.* **2006**, *106*, 3338-3363.
- (26) Smith, S. J.; Casellato, A.; Hadler, K. S.; Mitic, N.; Riley, M. J.; Bortoluzzi, A. J.; Szpoganicz, B.; Schenk, G.; Neves, A.; Gahan, L. R. *J. Biol. Inorg. Chem.* **2007**, *12*, 1207-1220.
- (27) Klabunde, T.; Sträter, N.; Fröhlich, R.; Witzel, H.; Krebs, B. *J. Mol. Biol.* **1996**, *259*, 737-748.
- (28) Coleman, F.; Hynes, M. J.; Erxleben, A. *Inorg. Chem.* **2010**, *49*, 6725-6733.
- (29) Neves, A.; Lanznaster, M.; Bortoluzzi, A. J.; Peralta, R. A.; Casellato, A.; Castellano, E. E.; Herrald, P.; Riley, M. J.; Schenk, G. *J. Am. Chem. Soc.* **2007**, *129*, 7486-7487.
- (30) Peralta, R. A.; Bortoluzzi, A. J.; de Souza, B.; Jovito, R.; Xavier, F. R.; Couto, R. A.; Casellato, A.; Nome, F.; Dick, A.; Gahan, L. R.; Schenk, G.; Hanson, G. R.; de Paula, F. C.; Pereira-Maia, E. C.; de, P. M. S.; Severino, P. C.; Pich, C.; Bortolotto, T.; Terenzi, H.; Castellano, E. E.; Neves, A.; Riley, M. J. *Inorg. Chem.* **2010**, *49*, 11421-11428.
- (31) Williams, N. H.; Takasaki, B.; Wall, M.; Chin, J. *Acc. Chem. Res.* **1999**, *32*, 485-493.
- (32) Suntharalingam, K.; Hunt, D. J.; Duarte, A. A.; White, A. J. P.; Mann, D. J.; Vilar, R. *Chem. Eur. J.* **2012**, *18*, 15133-15141.
- (33) Wall, M.; Hynes, R. C.; Chin, J. *Angew. Chem. Int. Edit.* **1993**, *32*, 1633-1635.

- (34) Banerjee, A.; Singh, R.; Colacio, E.; Rajak, K. K. *Eur. J. Inorg. Chem.* **2009**, *2009*, 277-284.
- (35) Chen, X.-Q.; Peng, X.-J.; Wang, J.-Y.; Wang, Y.; Wu, S.; Zhang, L.-Z.; Wu, T.; Wu, Y.-K. *Eur. J. Inorg. Chem.* **2007**, *2007*, 5400-5407.
- (36) Comba, P.; Gahan, L. R.; Mereacre, V.; Hanson, G. R.; Powell, A. K.; Schenk, G.; Zajaczkowski-Fischer, M. *Inorg. Chem.* **2012**, *51*, 12195-12209
- (37) Selmeczi, K.; Michel, C.; Milet, A.; Gautier-Luneau, I.; Philouze, C.; Pierre, J. L.; Schnieders, D.; Rompel, A.; Belle, C. *Chem. Eur. J.* **2007**, *13*, 9093-9106.
- (38) Zee, Y. L. M.; Gahan, L. R.; Schenk, G. *Aust. J. Chem.* **2011**, *64*, 258-264.
- (39) Jarenmark, M.; Kappen, S.; Haukka, M.; Nordlander, E. *Dalton Trans.* **2008**, 993-996.
- (40) Jarenmark, M.; Csapo, E.; Singh, J.; Wockel, S.; Farkas, E.; Meyer, F.; Haukka, M.; Nordlander, E. *Dalton Trans.* **2010**, *39*, 8183-8194.
- (41) Montagner, D.; Gandin, V.; Marzano, C.; Erxleben, A. *Eur. J. Inorg. Chem.* **2014**, *2014*, 4084-4092.
- (42) Montagner, D.; Erxleben, A. Unpublished work.
- (43) Branum, M. E.; Tipton, A. K.; Zhu, S.; Que, L. *J. Am. Chem. Soc.* **2001**, *123*, 1898-1904.
- (44) Coleman, F.; Erxleben, A. *Polyhedron* **2012**, *48*, 104-109.
- (45) Arora, H.; Barman, S. K.; Lloret, F.; Mukherjee, R. *Inorg. Chem.* **2012**, *51*, 5539-5553.
- (46) Xavier, F. R.; Neves, A.; Casellato, A.; Peralta, R. A.; Bortoluzzi, A. J.; Szpoganicz, B.; Severino, P. C.; Terenzi, H.; Tomkowicz, Z.; Ostrovsky, S.; Haase, W.; Ozarowski, A.; Krzystek, J.; Telsler, J.; Schenk, G.; Gahan, L. R. *Inorg. Chem* **2009**, *48*, 7905-7921.
- (47) Smith, S. J.; Peralta, R. A.; Jovito, R.; Horn, A.; Bortoluzzi, A. J.; Noble, C. J.; Hanson, G. R.; Stranger, R.; Jayaratne, V.; Cavigliasso, G.; Gahan, L. R.; Schenk, G.; Nascimento, O. R.; Cavalett, A.; Bortolotto, T.; Razzera, G.; Terenzi, H.; Neves, A.; Riley, M. J. *Inorg. Chem.* **2012**, *51*, 2065-2078.
- (48) Xavier, F. R.; Peralta, R. A.; Bortoluzzi, A. J.; Drago, V.; Castellano, E. E.; Haase, W.; Tomkowicz, Z.; Neves, A. *J. Inorg. Biochem.* **2011**, *105*, 1740-1752.
- (49) Hertzberg, R. P.; Dervan, P. B. *J. Am. Chem. Soc.* **1982**, *104*, 313-315.

- (50) Coleman, F. **2011**, Ga^{III} and Zr^{IV} Complexes as Phosphatase Analogues, PhD Thesis, NUI Galway, Eire
- (51) Van der Boom, M. E.; Liou, S. Y.; Ben-David, Y.; Shimon, L. J. W.; Milstein, D. *J. Am. Chem. Soc.* **1998**, *120*, 6531-6541.
- (52) Paine, R. T.; Tan, Y. C.; Gan, X. M. *Inorg. Chem.* **2001**, *40*, 7009-7013.
- (53) Wang, Q.; Wilson, C.; Blake, A. J.; Collinson, S. R.; Tasker, P. A.; Schröder, M. *Tetrahedron Lett.* **2006**, *47*, 8983-8987.
- (54) Lambert, E.; Chabut, B.; Chardon-Noblat, S.; Deronzier, A.; Chottard, G.; Bousseksou, A.; Tuchagues, J. P.; Laugier, J.; Bardet, M.; Latour, J. M. *J. Am. Chem. Soc.* **1997**, *119*, 9424-9437.
- (55) Huisman, M.; Koval, I. A.; Gamez, P.; Reedijk, J. *Inorg. Chim. Acta* **2006**, *359*, 1786-1794.
- (56) Adams, H.; Bradshaw, D.; Fenton, D. E. *Inorg. Chim. Acta* **2002**, *332*, 195-200.
- (57) Li, Y.; Breaker, R. R. *J. Am. Chem. Soc.* **1999**, *121*, 5364-5372.
- (58) Zagórowska, I.; Kuusela, S.; Lönnberg, H. *Nucleic Acids Res.* **1998**, *26*, 3392-3396.
- (59) Addison, A. W.; Rao, T. N.; Reedijk, J.; van Rijn, J.; Verschoor, G. C. *J. Chem. Soc., Dalton Trans.* **1984**, 1349-1356.
- (60) Jeffrey, G. A. *An introduction to hydrogen bonding*; Oxford university press New York, **1997**.
- (61) Ginzburg, G. *Talanta* **1976**, *23*, 149-152.
- (62) Beese, L. S.; Steitz, T. A. *EMBO J.* **1991**, *10*, 25-33.
- (63) Ollis, D.; Brick, P.; Hamlin, R.; Xuong, N.; Steitz, T. *Nature* **1985**, *313*, 762-766.
- (64) Coleman, J. E. *Annu. Rev. Biophys. Biomol. Struct.* **1992**, *21*, 441-483.
- (65) Kabay, N.; Karadeniz, H.; Demirayak, N.; Gök, Y. *Inorg. Chem. Commun.* **2011**, *14*, 641-644.
- (66) Coleman, F.; Dux, D.; Erxleben, A. *Z. Anorg. Allg. Chem.* **2013**, *639*, 1584-1589.
- (67) Corazza, F.; Floriani, C.; Chiesi-Villa, A.; Guastini, C.; Ciurli, S. *J. Chem. Soc., Dalton Trans.* **1988**, 2341-2345.
- (68) Arnaud-Neu, F.; Barrett, G.; Harris, S. J.; Owens, M.; McKerverey, M. A.; Schwing-Weill, M. J.; Schwinte, P. *Inorg. Chem.* **1993**, *32*, 2644-2650.

- (69) Cacciapaglia, R.; Casnati, A.; Mandolini, L.; Reinhoudt, D. N.; Salvio, R.; Sartori, A.; Ungaro, R. *J. Org. Chem.* **2004**, *70*, 624-630.
- (70) Homden, D. M.; Redshaw, C. *Chem. Rev.* **2008**, *108*, 5086-5130.

Chapter 3. Synthesis of mononucleating ligands linked to targeting units

3.1. Introduction

3.1.1. Metallodrugs

The vast majority of current pharmaceuticals are derived from organic chemistry and use only a small selection of elements from the periodic table. But as with artificial nucleases the use of metal atoms can greatly increase the scope and expand the potential mechanisms of action. Drugs containing metal atoms are termed metallodrugs. Historically metallodrugs have been used for a variety of purposes with little knowledge of the mode of action. An example is silver which was used for centuries as an antimicrobial agent¹. Numerous metallodrugs have been or are being developed for the treatment of a wide range of conditions ranging from diseases (diabetes)² to viruses (herpes)³ to microbes (malaria)⁴ (**Figure 3.1**).

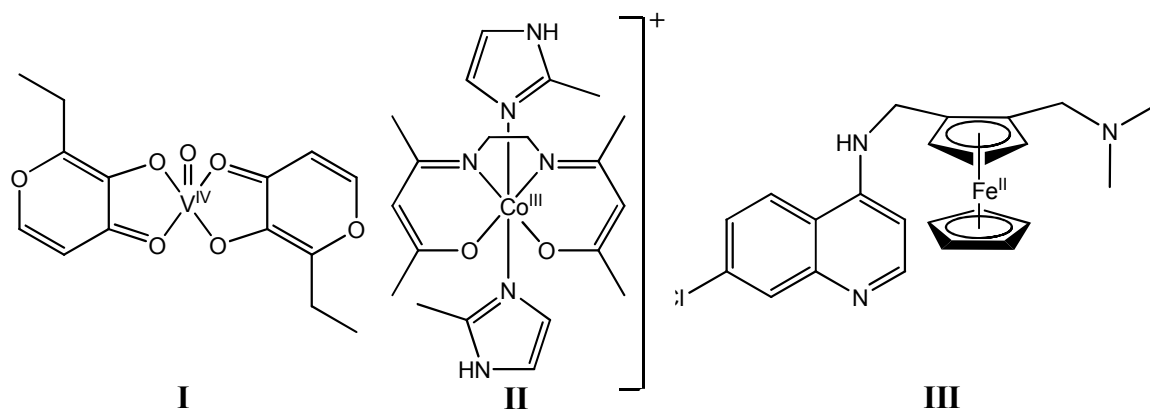


Figure 3.1: Structure of metallodrugs: **I** BEOV (diabetes); **II** Doxovir (herpes); **III** Ferroquine (malaria).

Traditionally a metallodrug will contain a metal ion but there are pseudo-metallodrugs which are given as metal-free agents and it is thought that they coordinate a metal ion *in situ* and so exhibit their pharmacological properties. The glycopeptide antibiotic bleomycin (**Figure 3.2**) is thought to act by this mechanism. Bleomycin is an antitumor agent which is able to bind to and degrade DNA by inducing strand breaks⁵. It was found that Fe²⁺ and O₂ are co-factors for this DNA degradation⁶. While the exact mechanism is unknown it is proposed that bleomycin

coordinates Fe^{2+} *in situ* to form a Fe^{II} -bleomycin complex. The Fe atom can then form reactive oxygen species (ROS) through the Fenton reaction or form reactive Fe-oxo species. Other metal co-factors including Cu, Co, Mn, Ru and V can also facilitate DNA degradation⁷.

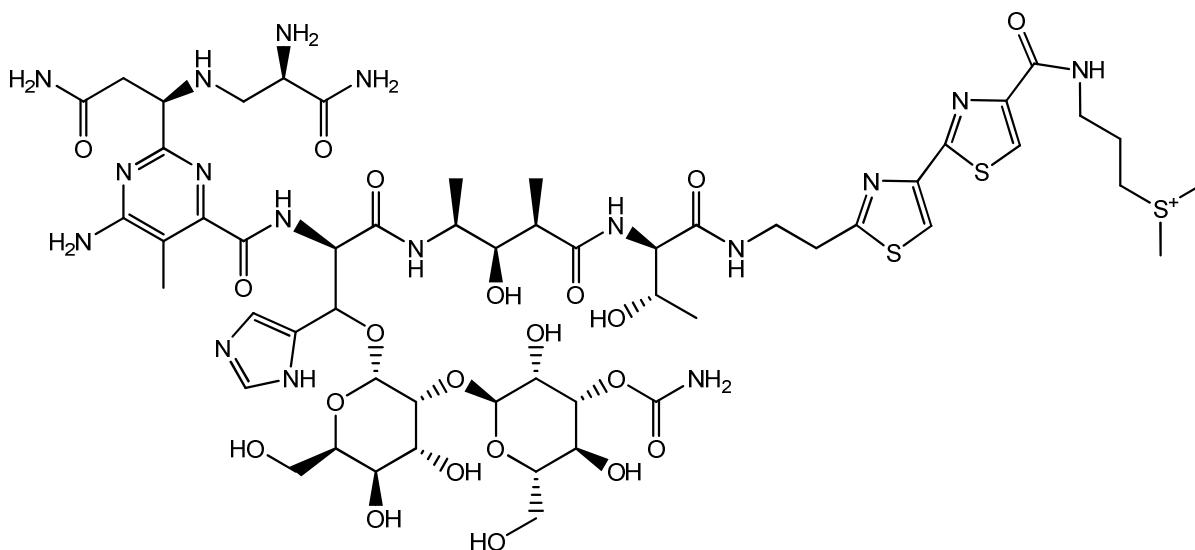


Figure 3.2: Structure of bleomycin.

Metallo drugs are an area of intense research for a number of reasons. They are able to target and damage specific structures in the cell such as phosphodiesterases causing cleavage and hence can have cytotoxic properties. Due to this they are used for the treatment of cancer as shown by bleomycin. Cancer is extremely prevalent in modern society, in 2010 it was the 2nd leading cause of death in Ireland⁸. Numerous metallo drugs are being used as chemotherapeutics the most famous class being Pt^{II} -based drugs.

3.1.1.1. Pt^{II} chemotherapeutics

Pt^{II} based complexes are extensively used ($\approx 50\%$) in cancer therapies⁹. The first and most widely known example is cisplatin (**Figure 3.3 structure I**). Cisplatin is currently used for the treatment of testicular, ovarian and bladder cancer. Only two other Pt^{II} complexes (carboplatin and oxaliplatin) are currently approved by the FDA (**Figure 3.3 structure II and III**). The cytotoxicity of cisplatin arises from its ability to crosslink DNA. It does this by coordinating two neighbouring guanine nucleobases at the N7 position¹⁰. This crosslinking inhibits cell division, may prevent DNA repair and induces apoptosis¹¹.

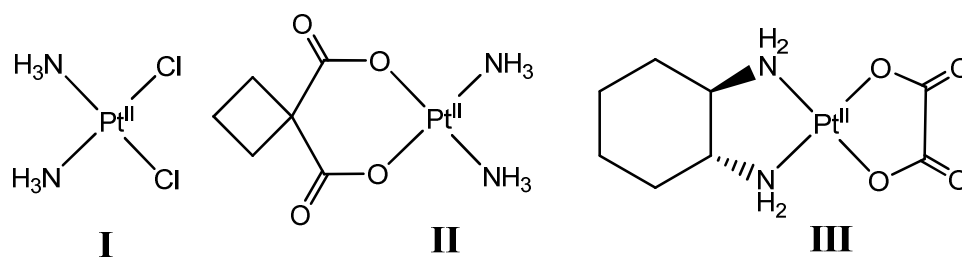


Figure 3.3: Structure of FDA approved Pt^{II} chemotherapeutics: **I** Cisplatin; **II** Carboplatin; **III** Oxaliplatin.

But cisplatin has several side-effects including kidney damage and nausea. Side-effects such as these can reduce the efficacy of the drug and can only be reduced by co-administration with other drugs. Amifostin and ondansetron are used to reduce kidney damage and nausea respectively¹². Side-effects can be blamed on the fact that chemotherapeutics do not selectively accumulate in tumour cells. This is shown by the finding that the dose that reaches tumours may be as low as 5 - 10% of that accumulated in normal cells¹³. But recent work has been done to design chemotherapeutics that selectively target tumour cells rather than normal cells.

3.1.2. Targeting

These targeting methods can be broken into two broad but not exclusive classes: passive and active targeting. Passive targeting utilises the physiological differences between normal tissue and tumours, while active targeting utilises the chemical differences between normal and cancer cells.

A separate tactic is to improve the efficacy of the drug. This can be done by coupling the drug with a unit with separate pharmacological behaviour. This unit can work by the same mechanism or by a completely separate mechanism. Both of these tactics will hopefully give greater efficacy than the parent drugs. This increased efficacy would allow for a lower dose to be administered and, hence, a decrease in side-effects would be observed.

3.1.2.1. Passive Targeting

Tumours by their very nature are abnormal and physiologically tumour tissues differ greatly from normal tissues. For example, due to their rapid growth, the normal vascular system is unable to provide adequate nutrient supply to the tumour, so cancer cells will start to die. As they die they release factors that promote the building of new blood vessels in a process called angiogenesis¹⁴. This forms new highly irregular blood vessels which have holes in them termed fenestrations. These fenestrations range from 0.2 to 1.2 μm in size¹⁵. Fenestrations increase the permeability of tumours relative to normal tissue. This has been exploited for delivery of chemotherapeutics.

The proposed targeting mechanism is to encapsulate, absorb or chemically bind a chemotherapeutic to a nanoparticle (NP). This drug-np would be of an appropriate size to enter a tumour but not normal tissue by use of the fenestrations. Therefore there would be accumulation of the drug-np in the tumour. Once in the tumour the drug would be released and kill the cancer cells. Different nanoparticles have been investigated. These include liposomes¹⁶, proteins¹⁷, bio-polymers¹⁸ and carbon nanotubes¹⁹.

Liposomes are artificially prepared spherical vessels similar in structure to cell membranes. Within their interior cavity they can encapsulate drug molecules. Commercial examples include Doxil® by Ortho Biotech for the delivery of doxorubicin¹⁶. Versions incorporating Pt^{II} chemotherapeutics have also been developed. SPI-77 is a liposomal version of cisplatin²⁰ and L-NDDP (Aroplatin®) developed by Antigenics is a liposomal version of oxaliplatin²¹.

With regards to proteins, human serum albumin is an attractive target²². Several properties explain this: it is native to the body, stability over a wide pH range (4-9), stability with regards to heating (up to 60 °C) and stability in the presence of solvents and denaturing agents^{23,24}. An example of a commercial albumin bound chemotherapeutic is Abraxane® developed by Abraxis BioScience¹⁷. This is an albumin-bound version of paclitaxel (Taxol). The concept has also been recently investigated for the delivery of several potential Pt^{IV} prodrugs²⁵

The use of biocompatible polymers has also been investigated. The use of polymers allows for greater control on the structure and chemical properties. Using hydroxypropyl methacrylamide (HPMA), Pt^{II} based chemotherapeutics have been investigated. AP5280 is a cisplatin derivative²⁶. Using *trans*-1,2-diaminocyclohexane (DACH), an oxaliplatin derivative, AP5346 (ProLindac®) was developed¹⁸. AP5346 was shown to deliver 16.3 times more platinum to tumours and 1.2 times more platinum to tumour DNA in comparison to oxaliplatin¹⁸.

Carbon nanotubes (CNTs) have also been investigated. They are attractive due to their biocompatibility and ability to be chemically modified. But the major challenge with CNTs is the ability to release the drugs on command. Cisplatin embedded CNTs have been shown to release cisplatin and cause inhibition of prostate cancer cells¹⁹. CNTs were also used to encapsulate chemotherapeutic drugs with low aqueous solubility. Taxol and C6-ceramide were contained in the same CNT²⁷. It was shown that the CNT-drug could be used at a 100 fold lower concentration than normal while still having comparable cytotoxicity.

3.1.2.2. Active targeting

Active targeting involves the use of active transport/targeting processes. Broadly these involve using the chemical differences between the target tumours and normal tissues.

3.1.2.2.1. Receptor overexpression

In numerous cancer types tumour cells overexpress certain receptors on their surface relative to normal cells. This has been explored for the active targeting of chemotherapeutics.

The folic acid receptor is found to be overexpressed in numerous malignant tissues²⁸. A folic acid functionalised liposome encapsulating cytotoxic Pt^{II} and As^{III} chemotherapeutics was developed²⁹. This liposome showed significantly enhanced cellular uptake and had comparable cytotoxicity values as their parent Pt^{II} and As^{III} chemotherapeutics.

Steroids can also be exploited. The oestrogen receptor (ER) is found to be overexpressed in 60-75% of all breast cancer tumours³⁰. Estrogen was functionalised with Pt^{2+} binding moieties to generate complexes structurally analogous to cisplatin³¹ (**Figure 3.4**). These complexes were found to be more cytotoxic than cisplatin and had comparable affinity to the estrogen binding receptor as unmodified estrogen.

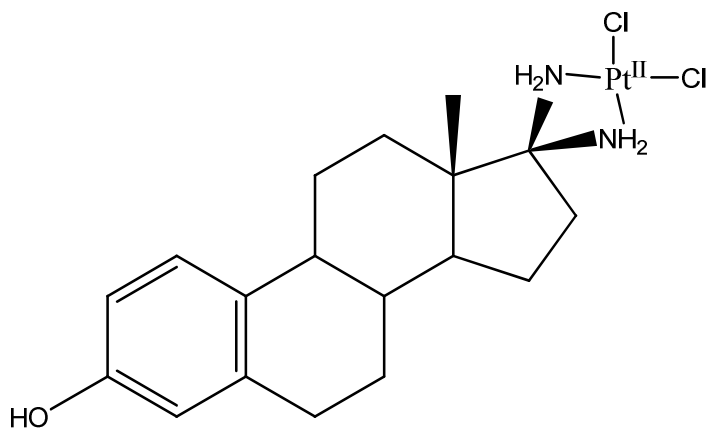


Figure 3.4: Structure of an Estrogen- Pt^{II} complex.

Overexpression of the androgen receptor (AR) is more widely found in tumours than ER. It occurs in approx. 80% of breast³², 90% of ovarian³³ and in nearly 100% of prostate tumours³⁴. To target these, testosterone was functionalised with Pt^{2+} binding moieties³⁵ (**Figure 3.5**). The testosterone- Pt^{II} complex showed improved delivery to tumour cells. Also while the parent Pt^{II} complexes were inactive the testosterone- Pt^{2+} were found to be highly cytotoxic. It is proposed there is a synergistic effect between the steroid and Pt^{2+} components³⁵.

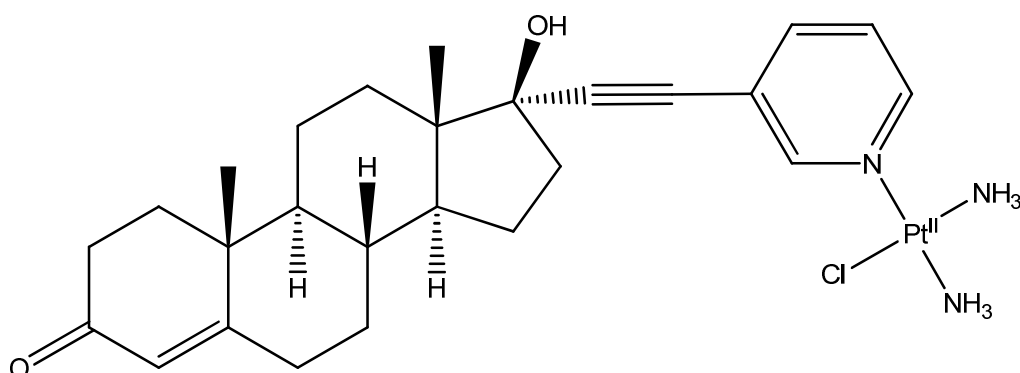


Figure 3.5: Structure of a Testosterone- Pt^{II} complex.

3.1.2.2.2. Nutrient hijacking

Tumours are sites of enhanced proliferation and increased growth. Due to this tumour cells show an enhanced demand for nutrients. These nutrients can be hijacked so as to specifically deliver chemotherapeutics to tumours.

Vitamin B₁₂ is an essential vitamin and consists of a cobalt atom coordinated to a modified corrin ring. To become biologically active cobalt must be reduced from Co^{III} to Co^{II}. In the Co^{III} form a coordination space is taken by a cyano (CN⁻) ligand but upon reduction to Co^{II} this is released. The cyano ligand has been used to attach different pharmacologically active metal complexes to B₁₂. The strategy is that the metal complex would only be released in the cell. Pt^{II} complexes analogous to cisplatin were linked to B₁₂³⁶ (**Figure 3.6 structure II**). It was found that B₁₂-Pt^{II} had a better *in vitro* cytotoxicity than cisplatin and that the Pt^{II} complex was only released after reduction of B₁₂³⁶. In a separate study the cyano ligand was used to coordinate a technetium complex³⁷ (**Figure 3.6 structure III**). Technetium is a synthetic radioactive element and its ^{99m}Tc isotope is widely used in medical imaging. It was found that the Tc^I complexes coordinated quantitatively to B₁₂ and were stable for up to 24 hrs.

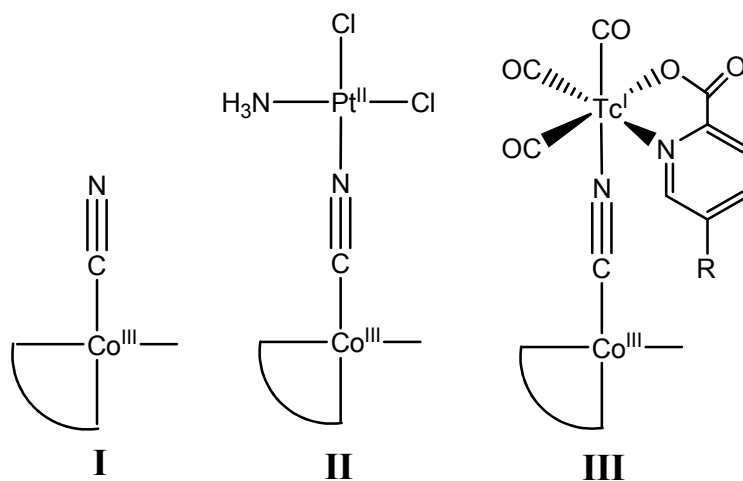


Figure 3.6: I Vitamin B₁₂; II B₁₂-Pt^{II} complex; III B₁₂-Tc^I complex.

3.1.2.2.3. Specific organ targeting

Different organs in the body have different specific chemical needs. As with the nutrient hijacking these can be hijacked for the delivery of chemotherapeutics.

Cholic acid is one of the major bile acids. Cholic acid and its derivatives represent 80% of all the bile acids. Bile is crucial for digestion of fat and vitamins in the small intestine. After being used for food absorption nearly all ($\approx 95\%$) of the bile acids are reabsorbed at the ileum (terminal of the small intestine). They are then transported back to the liver and are recycled. This localisation and non-excretion makes bile acids such as cholic acid interesting targets for the liver, kidney, small intestine and the biliary system (gall bladder and bile ducts). A literature example of this is a cholic acid derivative coupled to the leukaemia drug chlorambucil³⁸ (**Figure 3.7**). It was found that the drug was delivered specifically to the liver and biliary system.

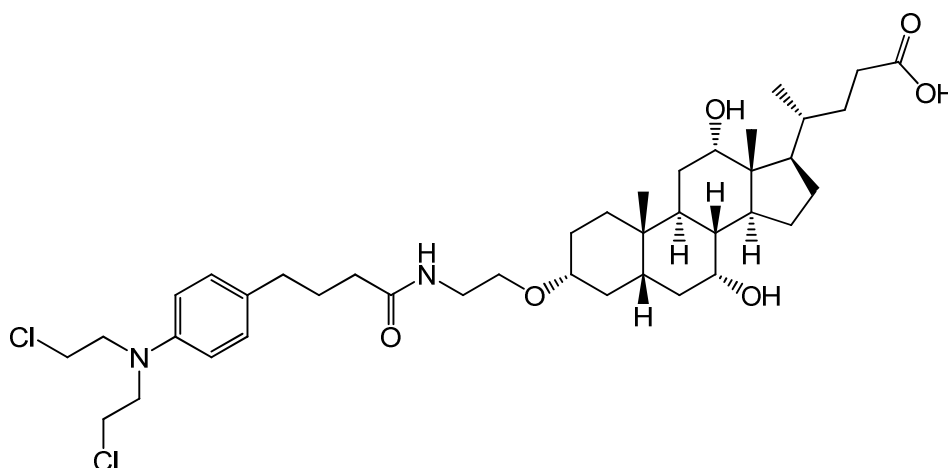


Figure 3.7: Structure of cholic acid-chlorambucil derivative

Cholic acid has also been used as a scaffold for the construction of new anticancer agents. The anticancer agent Tamoxifen was linked to a series of bile acids, including cholic acid. Monomer, dimer and trimers were synthesised (**Figure 3.8**)³⁹. In the 4T1 tumour model (breast cancer) the tri-Tamoxifen-cholic acid was found to be more effective than Tamoxifen³⁹. This shows that cholic acid and other bile acids can be used as scaffolds for the construction of effective anticancer agents.

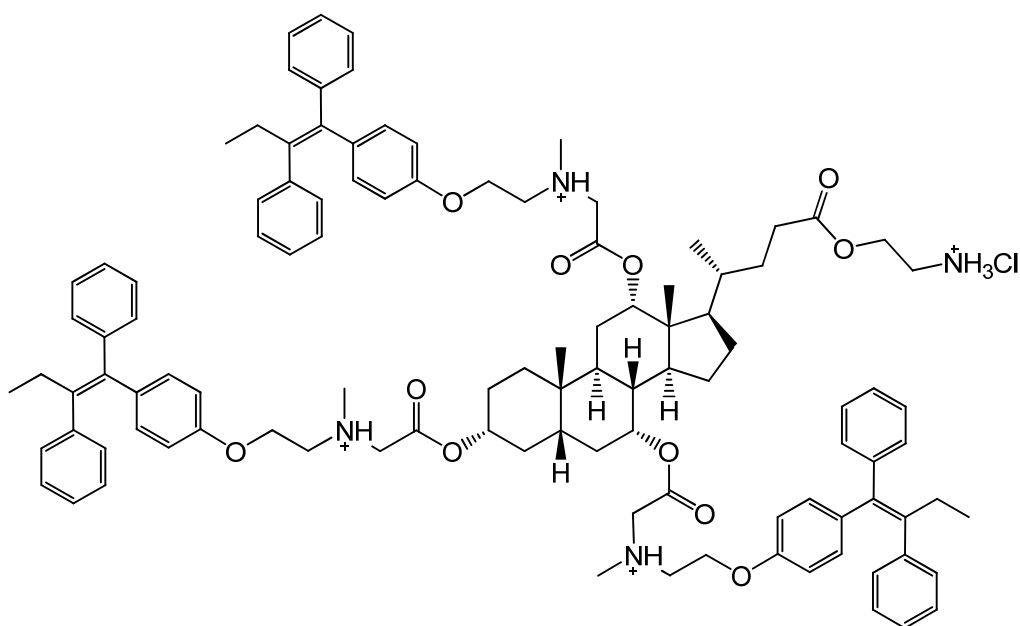


Figure 3.8: Structure of tri-tamoxifen-cholic acid derivative.

3.1.2.3. Prodrugs

An alternative to passive and active targeting is the use of prodrugs. Prodrugs can be thought of as a hybrid of passive and active targeting. The drug is linked to a unit rendering it inactive in normal tissues. But due to the chemical or physiological differences between normal and tumour cells the unit is removed and the drug is activated. So, while the inactive prodrug would be able to access all tissues the active drug would only be released in tumour cells.

Compared to normal tissues there is enhanced β -glucuronidase activity in several different tumour types^{13,40}. β -Glucuronidase is an enzyme that catalyses the hydrolysis of β -D-glucuronic acid. To create inactive prodrugs glucuronic acid has been linked to several chemotherapeutics. As example is HMR 1826 (**Figure 3.9**) which is glucuronic-doxorubicin prodrug¹³. It was found that doxorubicin was selectively deposited at tumour tissues rather than normal tissue¹³.

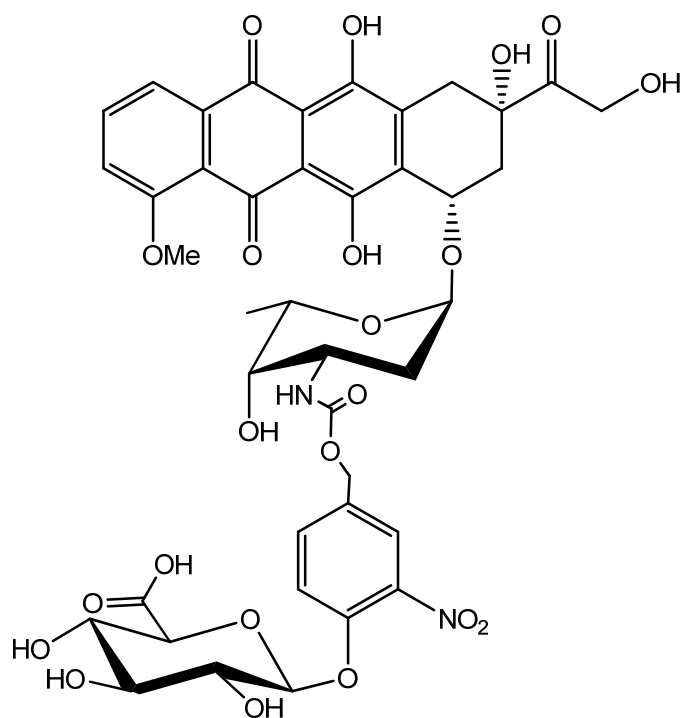


Figure 3.9: Structure of HMR 1826.

3.1.2.4. Synergistic pharmaceutical behaviour

Adding extra pharmaceutical moieties to a drug molecule can have a large effect on its behaviour. Coupling two drugs for the same condition but work by different means can also help overcome resistance. Also they may have a synergistic effect i.e. the two drugs linked will be more effective than both separately.

3.1.2.4.1. HDAC inhibitors

Histone deacetylase (HDAC) is an enzyme involved in the formation of chromatin. Chromatin is a supramolecular structure consisting of the DNA double helix coiled around histone proteins. Inhibition of HDAC can affect chromatin structure and function. HDAC inhibitors have been shown to cause cell cycle arrest, differentiation and/or apoptosis in tumour cells^{41,42}. HDAC inhibitors Zolinza (SAHA) and Depakote (valproic acid) have been approved for use and Belinostat is currently undergoing clinical trials.

Work by the group of Prof. Celine Marmion at RCSI has functionalised all three examples with Pt²⁺ binding moieties (**Figure 3.10**). The Pt^{II}-SAHA drug showed similar cytotoxicity values as the parent Pt^{II} drug and selectivity for tumour cells

over normal cells but no synergistic effect or increased effectiveness against resistant cells was observed^{43,44}. The Pt^{II}-Valproic acid showed enhanced cytotoxicity in comparison to the parent Pt^{II} drug⁴⁵. It also showed enhanced cytotoxicity against a cisplatin-resistant cell line. The Pt^{II}-Belinostat showed comparable *in vitro* cytotoxicity as the parent cisplatin and also *in-vitro* cytotoxicity against cisplatin resistant cells⁴⁶. It also showed selectivity for cancer cells over normal cells.

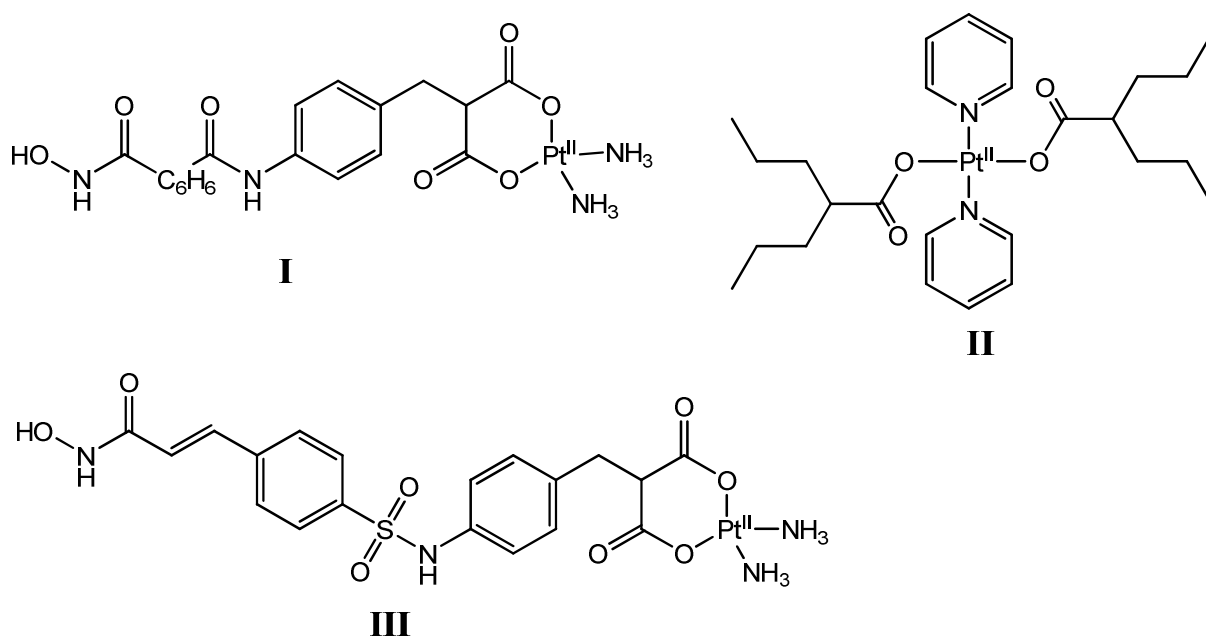


Figure 3.10: I Pt^{II}-SAHA; II Pt^{II}-Valproic acid; III Pt^{II}-Belinostat.

3.1.2.4.2. NAMI-A

NAMI-A (new anti-metathesis agent) is a ruthenium-based drug candidate currently in clinical trials. As indicated by its name it prevents the spread of cancer from the affected organ to healthy organs⁴⁷. In the parent form Ru is coordinated by an imidazole ligand (**Figure 3.11 Structure I**). By replacement of the imidazole by a pyrazine a Pt^{II} complex structurally analogous to cisplatin was generated⁴⁸ (**Figure 3.11 Structure II**). The Pt-NAMI A drug was found to be more effective than cisplatin and NAMI-A at inhibiting yeast growth and DNA synthesis.

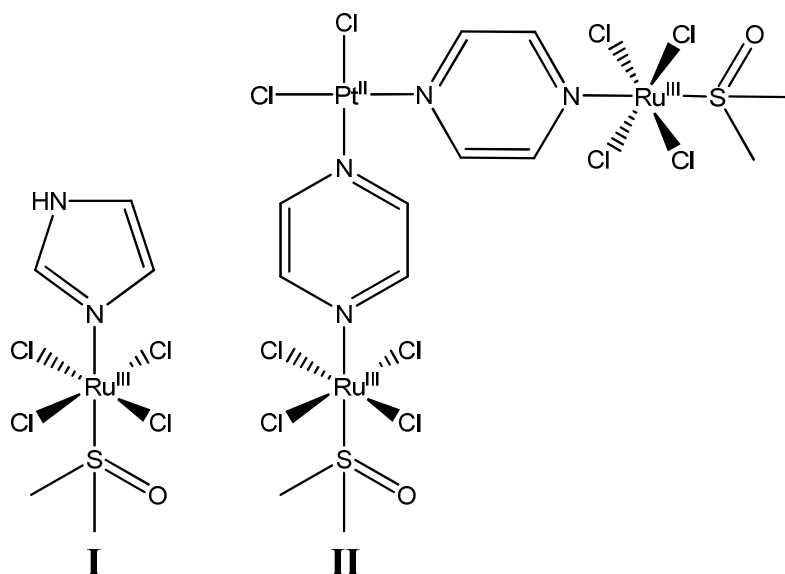


Figure 3.11: **I** Structure of NAMI-A; **II** Structure of Pt^{II}-NAMI A drug.

3.1.2.5. Combination of targeting and synergistic pharmacological behaviour

Combination of both targeting and additional pharmacological activity is very attractive. A drug with these properties would be selective for cancer cells and would have exceedingly high cytotoxicity. As discussed earlier (**Section 3.1.2.3**) glucuronic acid has been used to generate prodrugs which selectively deposits the active drug compound in tumours¹³.

Glucuronic acid has also been linked to two chemotherapeutic units. A homodimeric doxorubicin linked to glucuronic acid was investigated⁴⁹. The homodimer was found to be twice as effective as the monomeric version. This dimeric concept was further explored by the generation of a heterodimeric prodrug. This heterodimeric prodrug consisted of two chemotherapeutic units, doxorubicin and the HDAC inhibitor MS-275, linked to glucuronic acid⁵⁰ (**Figure 3.12**). The heterodimer was tested for its antiproliferative activity against H290 lung cancer. It was found that the heterodimer has an IC-50 of 48 nM which is 5 times more effective than the parent drugs IC-50, 221 nM. The proposed explanation of the enhanced activity is that during the cleavage of glucuronic acid, azaquinone methide a cytotoxic by-product is released. So rather than being a heterodimer it is a heterotrimer.

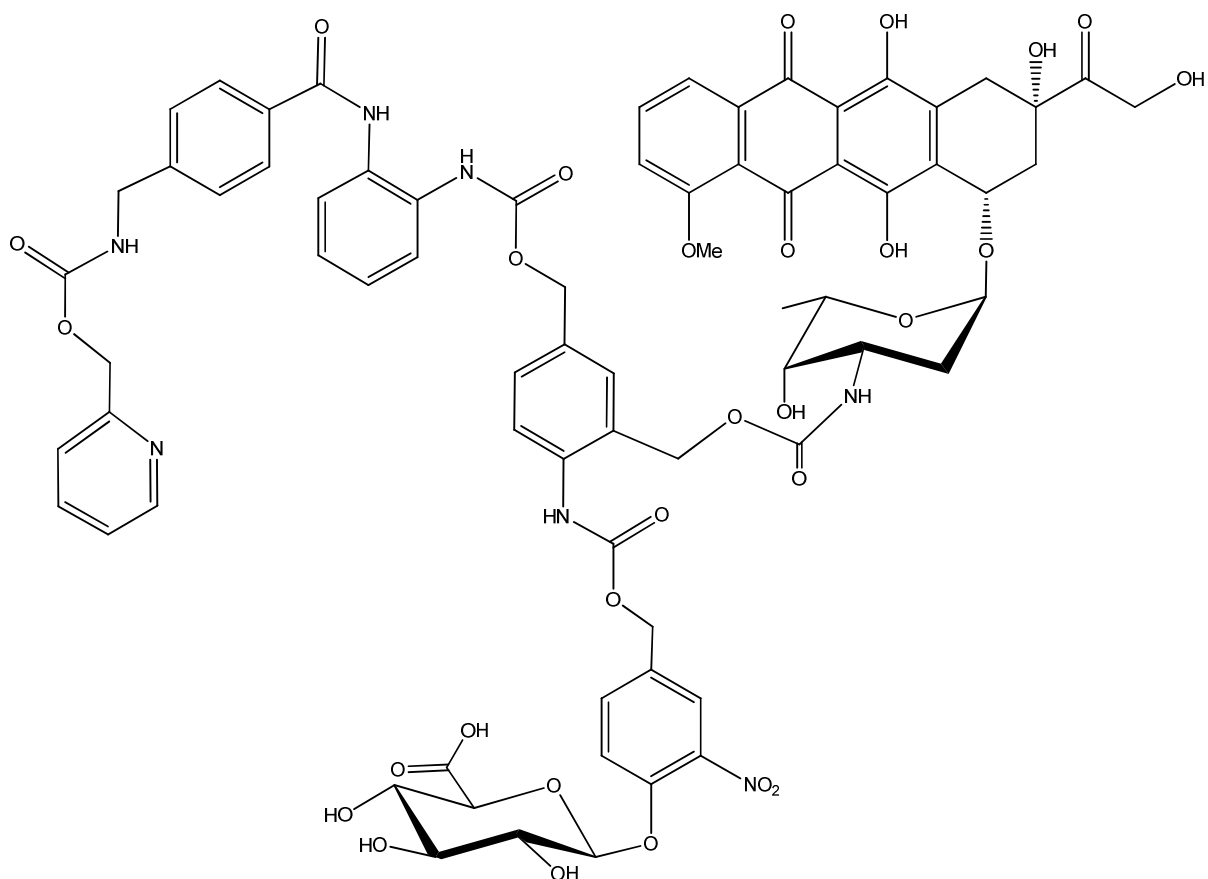


Figure 3.12: Structure of heterotrimer glucuronic acid prodrug.

As can be seen this combination strategy can yield extremely cytotoxic compounds. But having separate targeting and drug units can give drug candidates which are hard to access synthetically and also may have low aqueous solubility. So if possible a unit that combines both targeting and synergistic behaviour would be desirable. With regards to this, ligands for the translocator protein (TSPO) could satisfy both of these requirements.

3.1.3. Benzodiazepine receptors

In humans there exist two different forms of benzodiazepine receptors these are the central benzodiazepine receptor (CBR) and the peripheral benzodiazepine receptor (PBR). The PBR is now more commonly called the translocator protein (TSPO).

3.1.3.1. CBR structure and role

The CBR is a sub site of the GABA_A receptor-ionophore complex⁵¹ and is found in the central nervous system (CNS). They were first identified in human/mammal brains^{52,53}. Studies have shown that CBR are responsible for GABA_A induced anxiolytic and sedation⁵⁴ and so CBR ligands have been extensively used as therapeutics. Two of the most recognised drugs in the class are alprazolam and diazepam which are commercially known as Xanax and Valium. Ligands for the CBR increase the power of the inhibitory action of gamma-aminobutyric acid (GABA) in the brain^{55,56} giving rise to the observed pharmacological effects.

3.1.3.2. Translocator protein structure and role

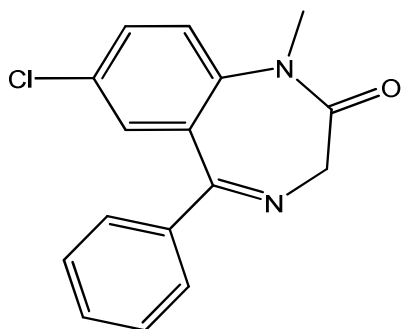
TSPO is a 18 kDa protein found in humans which has been found to be conserved throughout species⁵⁷. It was originally discovered when it was found that CBR ligands bound to sites not associated with the PNS⁵². The TSPO is found in peripheral organs of the body such as kidney, liver and lungs as well as glial cells of the central nervous system⁵⁸. Glial cells are found in the organs of the central nervous system, brain and spinal cord, but are not part of the CNS, their function is to provide support and protection for neurons/nerve cells. TSPO has also been linked with a variety of roles. These include cholesterol transport⁵⁹, steroid production⁶⁰, mitochondrial respiration⁶¹, cell growth and differentiation⁶² and response to stress⁶³.

Previously it has gone by several different names: peripheral-type benzodiazepine receptors (PBR), mitochondrial peripheral benzodiazepine receptor (mPBR), peripheral benzodiazepine binding site (PBBS), mitochondrial diazepam binding inhibitor receptors (MDR) and mitochondrial benzodiazepine receptor (mBzR). As stated earlier the name translocator protein is now commonly used.

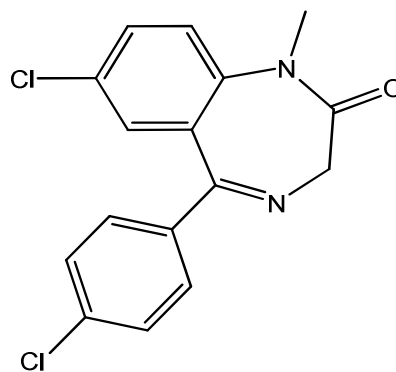
3.1.3.2.1. TSPO ligands

Several classes of molecules have been found to be TSPO ligands, these include: benzodiazepine (Diazepam), isoquinoline (PK 11195), indoleacetamide (FGIN-1-27), phenoxyphenylacetamide (DAA1097), imidazopyridine (Alpidem) and pyrazolopyrimidine (DPA-713) (**Figure 3.13**).

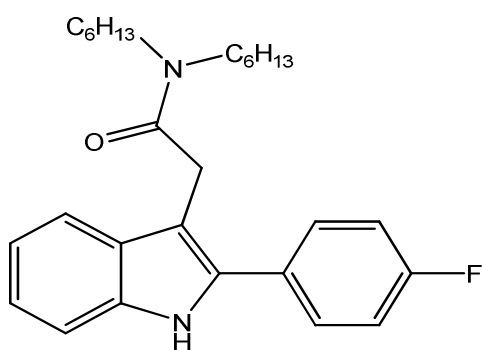
All of these are high affinity ligands for TSPO but selectivity is also of importance. Diazepam has an affinity of 40 nM for rat kidney but has a 3 nM affinity for rat brain⁶⁴, indicating that it is not selective. But the structure of the ligand can have a large effect on both affinity and selectivity, the Chloro derivative of Diazepam, Ro-54864⁵² (**Figure 3.13**), has a 7.3 nM affinity for TSPO⁶⁵ and 163 μ M affinity for CBR in rat brains⁶⁶ and so is a high affinity and highly selective ligand for TSPO.



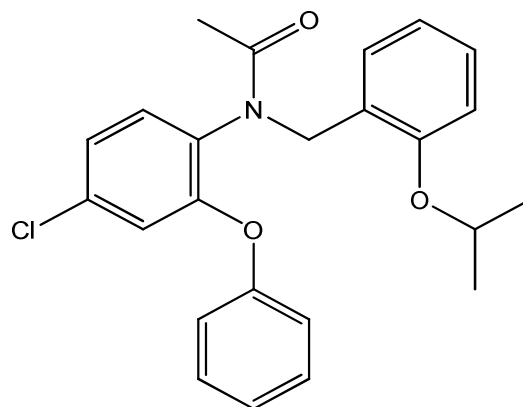
Diazepam



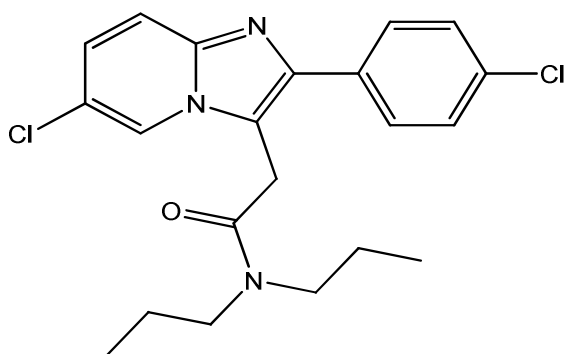
Ro-54864



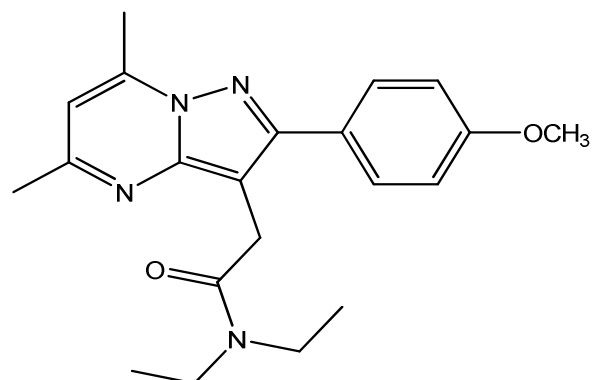
FGIN-1-27



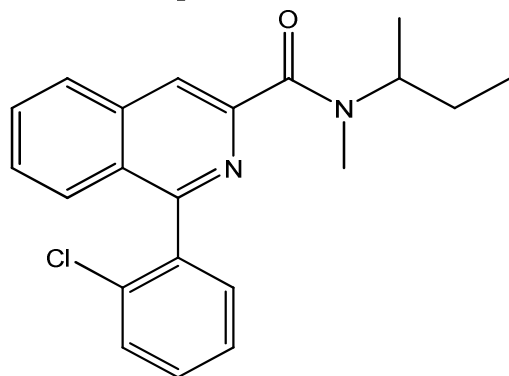
DAA1097



Alpidem



DPA-713



PK 11195

Figure 3.13: Structures and names of known TSPO ligands.

3.1.3.2.2. TSPO overexpression

Overexpression of TSPO has been observed in different diseases. These include neurological diseases such as Alzheimer's⁶⁷ and Huntington's⁶⁸. This has been exploited for imaging techniques such as autoradiography. Autoradiography is the production of an X-ray image due to radioactive decay processes. TSPO ligand DAA1106 with ¹²⁵I was used for imaging of Alzheimer's⁶⁹ and a version of Ro5-4864 with ³H was used to image Huntington's disease⁷⁰. But the main reason for the intense interest in TSPO and TSPO ligands is the overexpression of TSPO in different cancer types. TSPO is overexpressed in several different tumour types such as brain^{71,72}, colon⁷³, breast⁷⁴, liver⁷⁵ and ovarian⁷⁶ tumours.

3.1.3.2.3. TSPO ligand cytotoxicity

In several studies with different TSPO ligands and different cancer cell lines the TSPO ligands have been shown to be cytotoxic. Typically TSPO ligands have a pro-apoptotic effect⁷⁷⁻⁸⁰. But also necrosis has been proposed in some situations⁷⁸. Necrosis and apoptosis are two of the main mechanisms by which cells die. They differ greatly in their mechanism of action.

Necrosis is unregulated cell death and is usually caused by external factors. It is usually detrimental and fatal to organisms. The lethality of necrosis is demonstrated in the extreme cases of gangrene and frostbite. Removal of the necrotic tissue, i.e. amputation, is one of the primary means of treating both of these disorders. Physiologically in necrosis there is swelling of the cell and organelles, DNA is randomly digested and the products are released into the intracellular space.

Apoptosis on the other hand is programmed cell death. It is usually beneficial to the organism and in humans happens 50-70 billion times per day⁸¹. One of the crucial first steps is the change in the permittivity of a mitochondrial membrane. This allows certain molecules to be released from the mitochondria into the cellular fluid. Opening of the mitochondrial permeability transition pore (MPTP) can cause this. MPTP opening allows the passage of ions and solutes up to 1.5kda into the mitochondrion. This can cause the mitochondrion to swell and uncouple causing the membrane to burst. This bursting causes the release of proteins such as cytochrome c⁸² and apoptosis inducing factors (AIF) into the cell⁸³.

Cytochrome c acts in the cell to induce the caspase cascade which ultimately results in the destruction of the nucleus, cytoskeleton and plasma membrane⁸³. AIFs can migrate to the nucleus causing DNA fragmentation and chromatin condensation. The result of both of these actions is apoptosis, programmed cell death⁸³.

3.1.3.2.4. TSPO ligand cytotoxic mechanism

The proposed mechanism of action is based on TSPO's structure, location and interaction with neighbouring proteins. Structurally TSPO consists of 5 trans domain alpha-helices^{84,85} which are long enough to span a membrane bilayer⁸⁴. TSPO is located on the outer membrane of mitochondria primarily at the contact point between the inner and outer membrane⁸⁶. It is proposed that TSPO has role within the MPTP⁸⁷ and so binding of ligands to TSPO will cause opening of the MPTP and hence apoptosis.

But a recent study throws doubt on this proposed function for TSPO⁸⁸. In this study mice lacking the TSPO gene were generated and it was found that there was no functional difference between their liver mitochondria with and without TSPO. They propose that TSPO plays no structural role in the MPTP complex.

While the role of TSPO in mitochondrial function is still unclear but as has been shown in numerous studies TSPO ligands have a cytotoxic effect on numerous different cancer cell lines⁷⁷⁻⁸⁰.

3.1.3.2.5. TSPO ligand pharmacophore model

A pharmacophore model for TSPO ligands has been proposed^{89,90} (**Figure 3.14 structure I**). In the pharmacophore model there are 4 key regions: planar aromatic region (PAR), freely rotating aromatic (FRA), lipophilic area (LA) and an electron rich zone (ERZ). The PAR, FRA and LA all bind in lipophilic pockets⁹¹ and the electron rich zone is necessary for the formation of H-bonds⁹². Much work has been done with analogues to determine structure activity relationships (SAR) which will be discussed later.

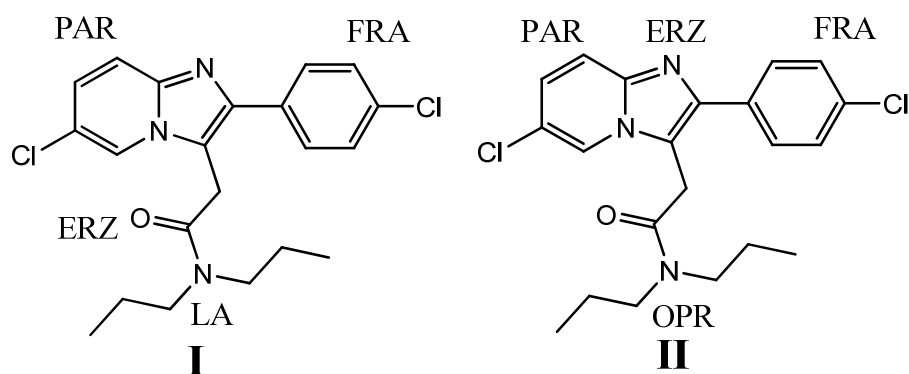


Figure 3.14: Pharmacophore models for Alpidem: **I** Interaction with TSPO; **II** Interaction with CBR. PAR planar aromatic region, FRA freely rotating aromatic ring, ERZ electron rich zone, LA lipophilic area, OPR out-of-plane region.

3.1.3.2.6. Alpidem

As mentioned earlier Alpidem is a TSPO ligand. It was approved in France in 1991 under the trade name Ananxyl as an antianxiety drug. But it was subsequently withdrawn from market in 1994 after it was found to cause liver damage⁹³. It is structurally very closely related to the more commonplace drug zolpidem (Ambien). Alpidem shows high affinity for both TSPO and CBR, with K_d of 0.33 nM and 1.67 nM respectively⁹⁴.

3.1.3.2.6.1. Pharmacophore model of Alpidem

The pharmacophore model described earlier was applied to explain the non-specificity of Alpidem (**Figure 3.14 structure II**). It was proposed that Alpidem could exist in two different conformations^{92,95}. The carbonyl could be in-plane or out-of-plane with respect to the PAR. When interacting with TSPO it's in plane, while interacting with CBR its out-of-plane. It was also proposed that the imidazole Nitrogen is the ERZ and engages in hydrogen bonding (**Figure 3.14 structure II**). Using this model as a basis work has being done on synthesising Alpidem derivatives with greater specificity and equal affinity for TSPO⁹⁵⁻¹⁰⁰.

3.1.3.2.6.2. Alpidem structure activity relationships

Investigation into Alpidem derivatives has established certain SAR's that have determined the key features needed for high affinity and TSPO selective ligands (**Figure 3.15**). The presence of a para-Cl phenyl ring on C2' (Z group) enhances selectivity and affinity to TSPO⁹⁷. Changing the methylene linker on C3' by either replacement of H with CH₃ or increasing the chain length leads to a slight decrease in affinity⁹⁸⁻¹⁰⁰. The length and presence of the alkyl chains (R₁ and R₂) also have an effect on affinity. Di-substitution is essential as mono-substitution leads to a large decrease in affinity⁹⁹. It was found that medium length chains such as n-propyl and n-butyl gave greater binding affinity than short alkyl chains (methyl, ethyl) or large bulky groups (n-hexyl, benzyl)^{95,100}. Also substitution at the C8' position is a key factor for improving affinity and selectivity^{97,98}.

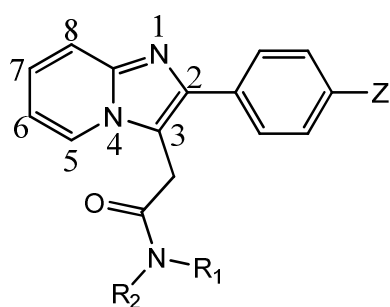


Figure 3.15: Schematic of Alpidem skeleton with numbering of all sites on the imidazopyridine ring.

3.1.3.2.6.3. Alpidem derivatives

As mentioned earlier the pharmacophore model of TSPO ligands the ligand binds in lipophilic binding pockets. As a consequence TSPO ligands have low aqueous solubility. Analogues of alpidem with hydrophilic groups have been investigated⁹⁶. From the SAR studies described above the only potential sites for hydrophilic moieties are the on the FRA or on the PAR. Three potential alpidem analogues with amines have been reported (**Figure 3.16**). They differ by the location of the amine moiety; **I** *meta*-position of the phenyl ring, **II** *para*-position of the phenyl ring and **III** C8' of the imidazopyridine ring. The amine allowed for the attachment of different hydrophilic groups such as carboxylic acids, free amines and esters to enhance aqueous solubility.

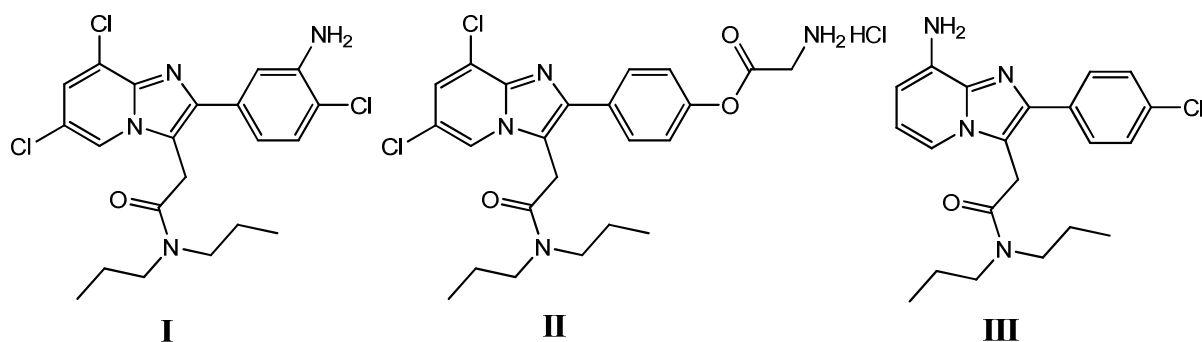


Figure 3.16: Structure of Alpidem derivatives with amine moieties.

From a linking motivation an amine is desirable as it allows for numerous potential linking motifs. The pharmacophore model would need to be taken into account for selection of the linking site; Compound **I** and **II** are not suitable as linking a large molecule as it would presumably interfere with the rotation. This only leaves **III**. Also as a consequence of the substitution they are TSPO selective ligands⁹⁶.

3.1.3.8.4. Metallodrugs based on Alpidem analogues

Alpidem derivatives have also been prepared with Pt^{2+} binding moieties to form a compound structurally analogous to cisplatin¹⁰¹ (**Figure 3.17**). This Pt^{II} -TSPO ligand complex showed high affinity and selectivity for TSPO. It was also found to be as cytotoxic as cisplatin and was equally active against cisplatin-sensitive and cisplatin-resistant cells.

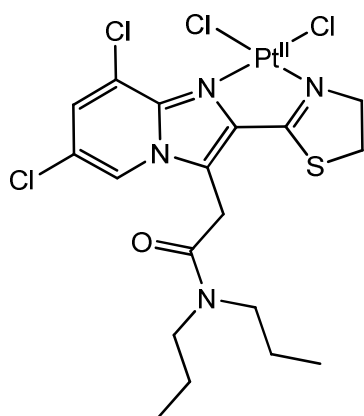


Figure 3.17: Structure of Pt^{II} - TSPO ligand complex.

3.1.3.2.7

PK11195

PK-11195 (**Figure 3.18 structure I**) is also an attractive molecule as it has a low nanomolar affinity for TSPO (0.63 - 2 nM)^{65,102} and much lower affinity for the CBR¹⁰². It is commonly used to determine the binding affinity of new proposed TSPO ligands. A ¹¹C analogue was used for *in vivo* marking of microglial activation in patients suffering from Huntington's¹⁰³ by the use of positron emission topography (PET). PK11195 derivatives linked to other functional molecules have been synthesised. A molecular imaging agent (MIA) was developed by coupling PK11195 to a lissamine dye¹⁰⁴. This allowed for confocal imaging of TSPO *in vitro*. Another MIA was developed by coupling PK11195 to cyclen¹⁰⁵. Cyclen is a large macrocycle which can be used as a ligand for Lanthanoids. Eu^{III} and Gd^{III} complexes of this conjugate showed fluorescence and Magnetic Resonance Imaging (MRI) signatures respectively in C6 glioma cells¹⁰⁵. In both of these cases a linkable form of PK11195 was used (**Figure 3.18 structure II**) and an amide linkage was used.

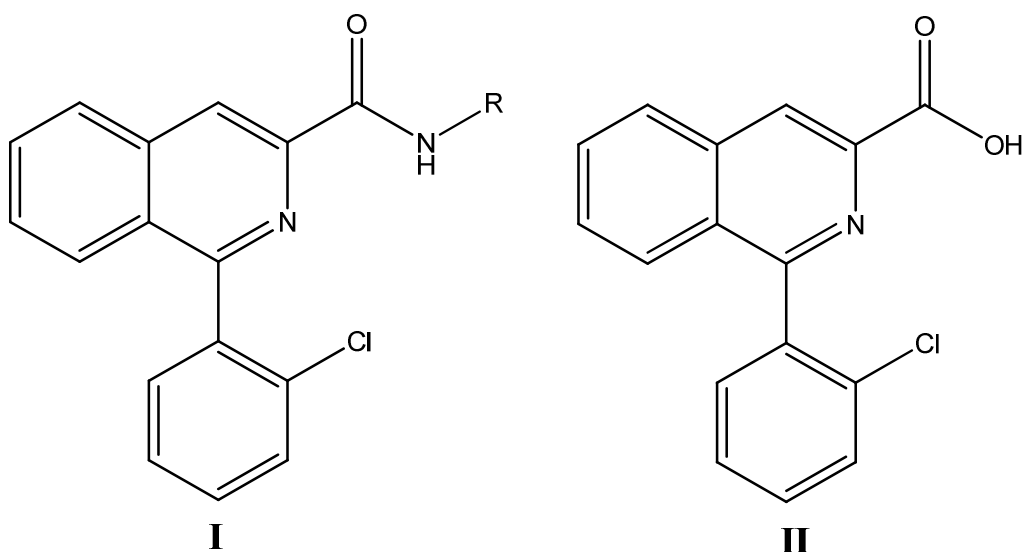


Figure 3.18: **I** Structure of PK11195 linked to functional molecules (R); **II** Carboxylic acid form of PK11195.

3.2 Aims and objectives

The objective of this study is to develop a mononucleating ligand based on the known Cu^{II} binding ligand dipicolylamine (DPA) (**Figure 3.19 structure I**). Mononuclear Cu^{II} complexes of DPA and DPA analogues have been shown to cleave DNA¹⁰⁶⁻¹⁰⁹ (**Section 2.1.3.**). In these complexes there is an open coordination site to allow for coordination of the substrate.

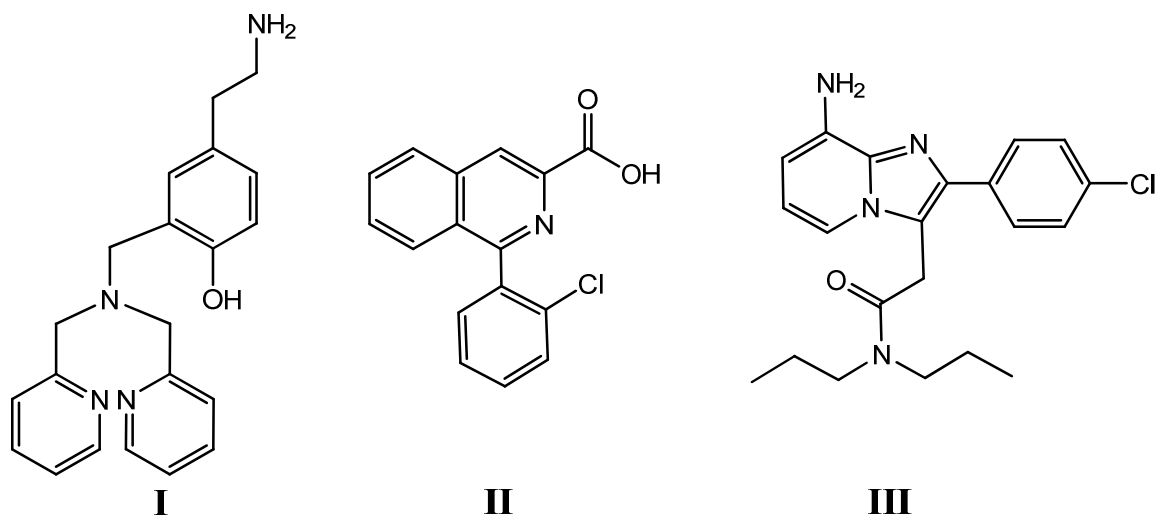


Figure 3.19: Structure of: **I** Mononucleating ligand; **II** PK11195 analogue; **III** Alpidem analogue.

Using the NH_2 moiety, the mononucleating ligand will be linked to several targeting units. The units used will be cholic acid and TSPO ligands. Cholic acid allows for specific organ targeting while TSPO ligands allow for both targeting and pharmacological behaviour. Linkable analogues of known TSPO ligands PK11195 and alpidem (**Figure 3.19 structure II and III**) will be used.

To isolate mononuclear Cu^{II} complexes 1,10-phenantroline (phen) will be used as a co-ligand. As has been shown for $[\text{Cu}(\text{phen})_2]^+$ this will potentially allow for intercalation into DNA¹¹⁰ (**Section 1.3.3.1.**) and hence bring the proposed metallodrug into close contact to their cellular target.

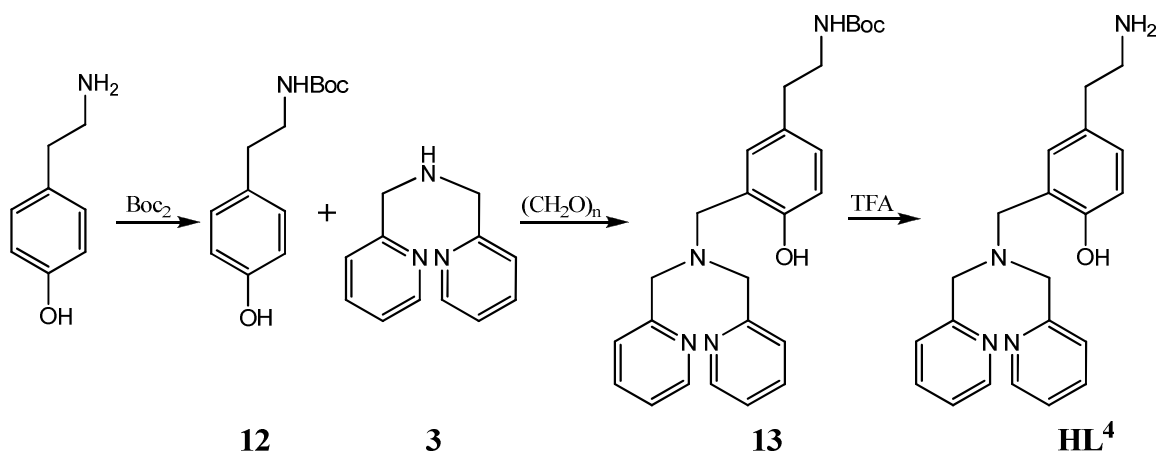
The aim is to generate new mononuclear Cu^{II} complexes as potential anticancer metallodrugs. This metallodrug will combine tumour cell targeting and synergistic pharmacological behaviour.

3.3. Results and discussion

3.3.1. Synthesis of mononucleating ligands

3.3.1.1 Synthesis of HL^4

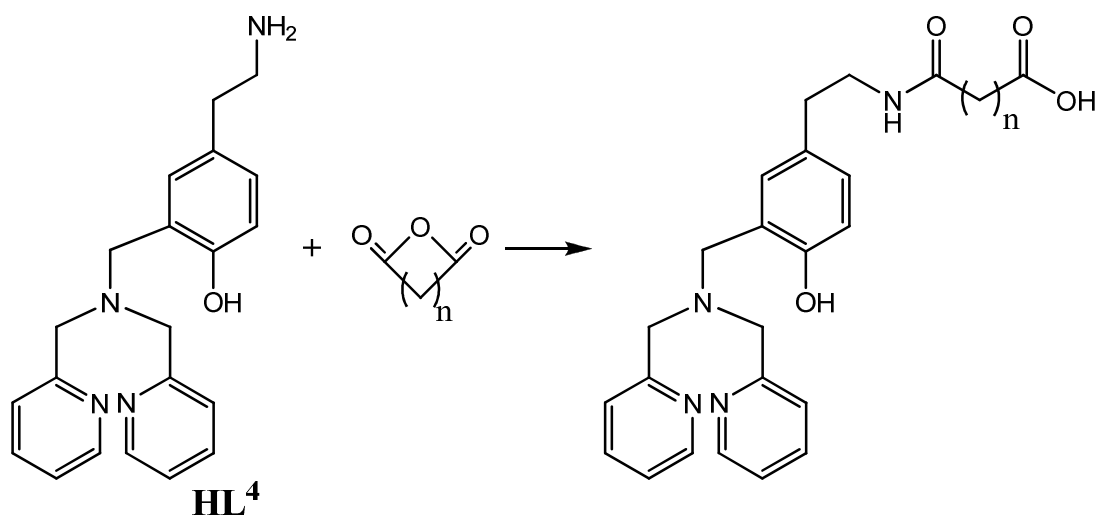
The mononucleating ligand HL^4 was synthesised in a convergent manner. Firstly the metal binding arm, **3**, was synthesised as described in **Section 2.3.1.1. (Scheme 2.2)**. The phenol body was synthesised from tyramine. Initially the amine moiety was protected with a *tert*-butyloxycarbonyl (BOC) group to generate **12**¹¹¹ (**Scheme 3.1**). In a Mannich reaction **12** was reacted with paraformaldehyde and **3** to generate **13**¹¹². The BOC protecting group was removed using trifluoroacetic acid (TFA) to give HL^4 ¹¹².



Scheme 3.1: Synthesis of mononucleating ligand HL^4 .

3.3.1.2 Addition of carboxylic acid moiety to HL^4

To increase the versatility of HL^4 the amine moiety was converted to a carboxylic acid. To allow for varying chain length HL^4 was reacted with succinic and glutaric anhydride to generate H_2L^5 and H_2L^6 respectively (**Scheme 3.2**). The resulting carboxylic acids were purified by column chromatography.

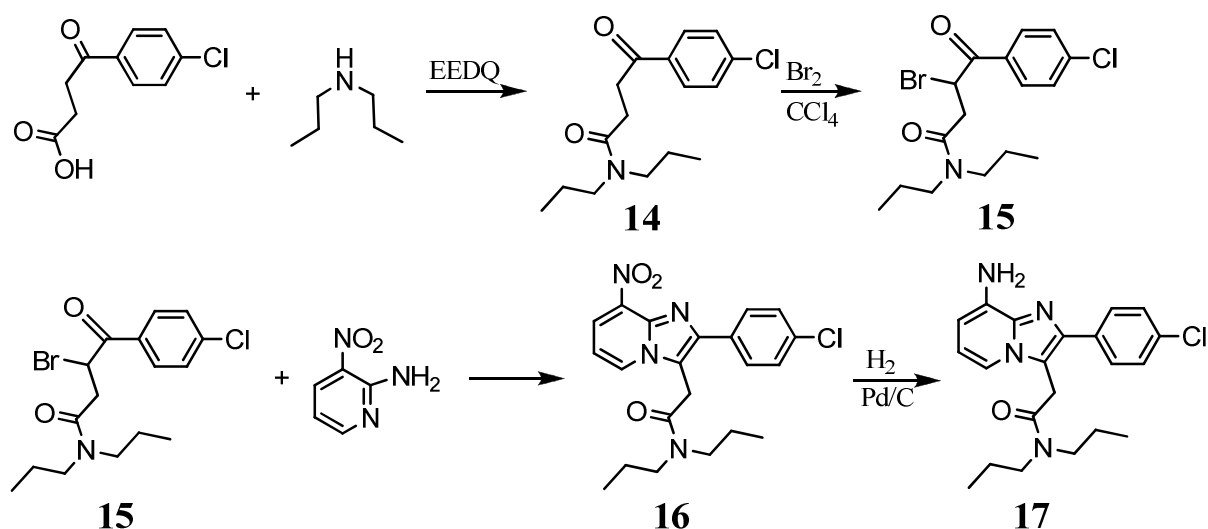


Scheme 3.2: Synthesis of **H₂L⁵** (n = 2) and **H₂L⁶** (n = 3).

3.3.2. TSPO Ligand synthesis

3.3.2.1. Synthesis of Alpidem derivative

The alpidem derivative was synthesised in a linear manner (**Scheme 3.3**). The starting material 3-(4-Chlorobenzoyl)propionic acid was reacted with dipropylamine in the presence of ethyl 1,2-dihydro-2-ethoxy-1-quinolinecarboxylate (EEDQ) as a dehydrating agent to give the amide **14**⁹⁸. **14** was then brominated to give **15**⁹⁸. In a condensation reaction **15** was reacted with 2-amino-3-nitro pyridine to generate the imidazopyridine **16**. By use of catalytic hydrogenation the nitro group in **16** was reduced to an amine to generate **17**⁹⁷.



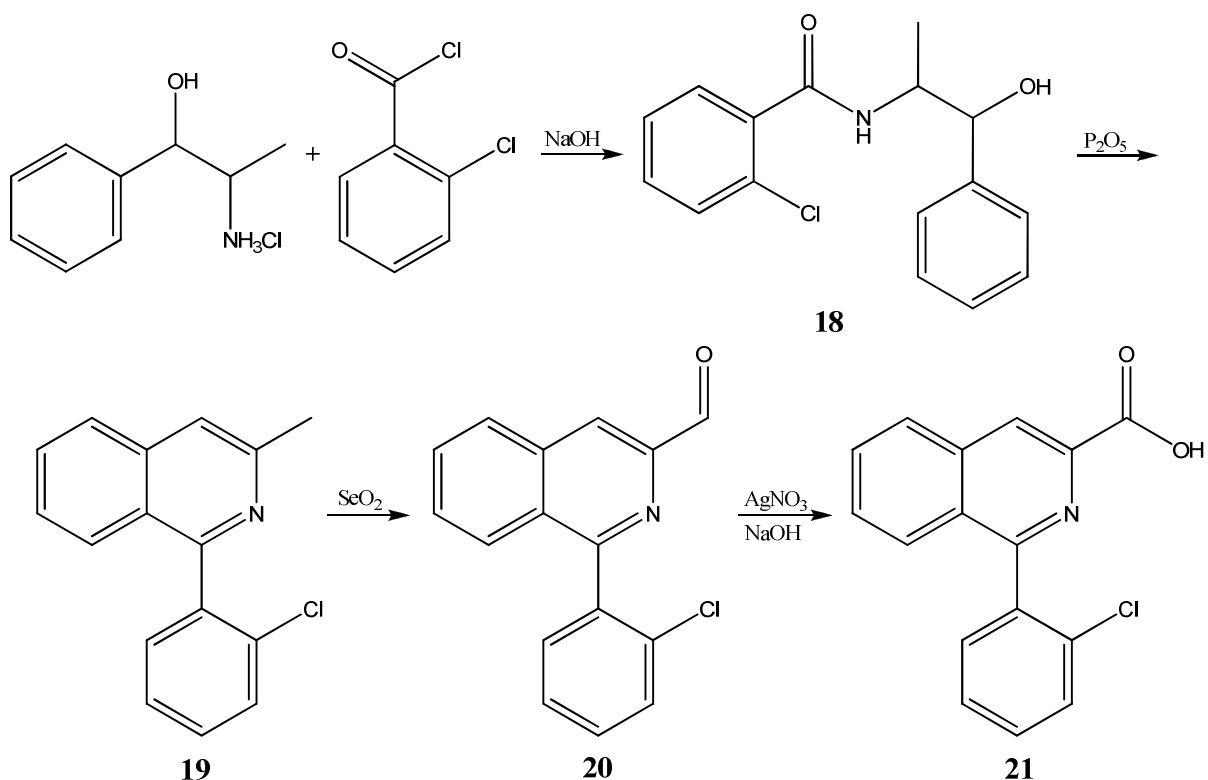
Scheme 3.3: Synthesis of alpidem derivative.

A modified literature procedure was used for the condensation reaction⁹⁷ but due to the difficulty in removal of DMF, the high boiling point alcohol Butan-1-ol was used instead. There was an associated reduction in yield from the reported 18%⁹⁷ to 6.2%. This decrease in yield may have been due to the change in reaction conditions and the need for two separate column chromatography steps to purify **16**.

The overall yield for the synthesis of **17** based upon the amount of 3-(4-Chlorobenzoyl)propionic acid used was 2.6%. The poor obtained yield is due to several reasons. As discussed earlier the decrease of yield in the production of **16**. For the purification of **14** it was necessary to perform several successive column chromatography steps to obtain pure compound. This was due to an impurity with a similar R_f value as **14**. Also for the production of **15**, the yield was poor. But by column chromatography the starting material, **14**, could be recovered from the reaction mixture and the reaction reset. But this added several extra purification steps as the reaction would be reset ≈ 4 times to obtain full conversion. As described in literature the more handling and purification needed the lower the yield¹¹³. Due to this the yield and hence amount of material obtained of **17** was poor.

3.3.2.2. Synthesis of PK11195 analogue

The PK11195 analogue was synthesised in a linear manner following previously published methodology¹¹⁴⁻¹¹⁶ (Scheme 3.4). The starting materials norephedrine (HCl salt) and 2-chlorobenzoyl chloride were coupled in basic conditions to give **18**¹¹⁵. To generate the isoquinoline ring **18** was treated with P_2O_5 in a condensation reaction to obtain **19**¹¹⁵. The methyl group was oxidised to the corresponding aldehyde by SeO_2 to give **20**¹¹⁴. By treatment with $AgNO_3$ in basic conditions the aldehyde group was further oxidised to the corresponding carboxylic acid to obtain **21**¹¹⁶. As with the Alpidem derivative poor yields were obtained in the condensation reaction and as with the Alpidem derivative it was difficult to obtain large amounts of product.



Scheme 3.4: Synthesis of PK11195 analogue, **21**.

3.3.3. Amide coupling

3.3.3.1. Synthesis of **HL**⁷ and **HL**⁸

The ligand **HL**⁴ was linked to Cholic acid and **21** to form **HL**⁷ and **HL**⁸ respectively (**Figure 3.20**). These were both synthesised following established methodology¹¹⁷. The amide bond was formed by reacting the carboxylic acid and the amine in the presence of a carbodiimide (N,N'-diisopropylcarbodiimide, DIC, or Dicyclohexylcarbodiimide, DCC) and 1-hydroxy-6-chloro-benzotriazole (6-Cl HOBt) (**Scheme 3.5 reaction I**). The carbodiimide helped activate the carboxylic acid and promote the formation of the amide bond. Both carbodiimides (DCC and DIC) gave similar yields but DIC was favoured as it is a liquid at room temperature and so there can be greater control over the amounts added. The additive 4-Cl HOBt was used to promote yields and to prevent the formation of undesired by-products such as N-acylureas (**Scheme 3.5 reaction II**). The ligands were purified by column chromatography on either alumina or silica gel.

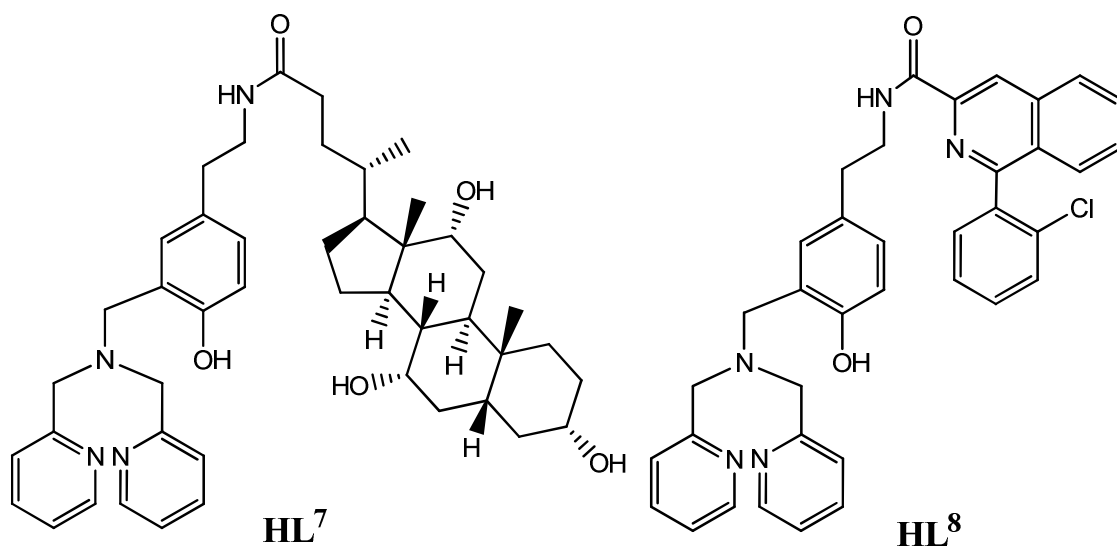
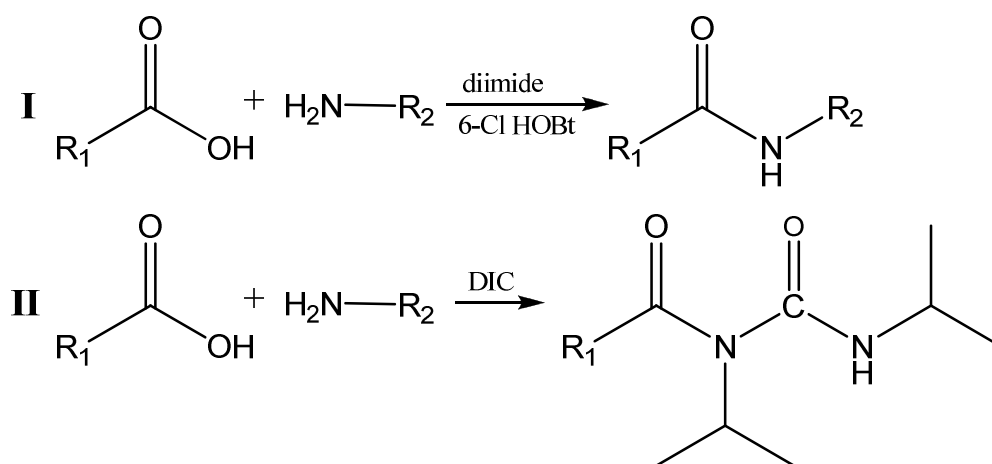


Figure 3.20: Mononucleating ligands generated: **HL⁷** Cholic acid-HL⁴; **HL⁸** PK11195-HL⁴.



Scheme 3.5: **I** amide coupling reaction using a diimide and 6-Cl HOBt; **II** the formation of N-acylurea by-product.

3.3.3.2. Synthesis of HL⁹ and HL¹⁰

Due to the presence of an amine on **17** it was proposed that **17** would be linked to **H₂L⁵** and **H₂L⁶** to form **HL⁹** and **HL¹⁰** respectively (**Figure 3.21**). Numerous different synthetic methods were explored.

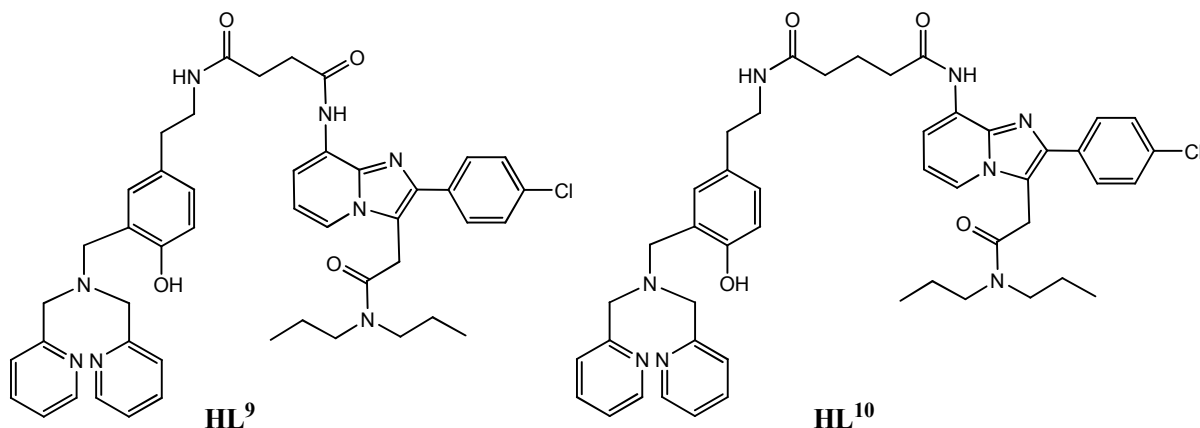


Figure 3.21: Mononucleating ligands generated: **HL⁹** Alpidem-H₂L⁵; **HL¹⁰** Alpidem-H₂L⁶.

3.3.3.2.1. Unsuccessful synthesis of HL⁹ and HL¹⁰

Initially the same methodology used for the successful synthesis of **HL⁷** and **HL⁸** was explored. In similar conditions (room temperature) no reaction was observed. The reaction was then repeated with varied conditions: different diimides, different equivalents of reagents, increased temperature, using anhydrous solvents and under Schlenk conditions. But for all no reaction was observed. Fortunately **17** could be isolated by column chromatography on Alumina gel with little loss.

The reaction was then attempted using the coupling reagent EEDQ¹¹⁸. The reaction was performed under both anhydrous conditions at ambient temperature and at reflux. But no reaction was observed. As before **17** could be isolated by column chromatography on Alumina gel with very little loss.

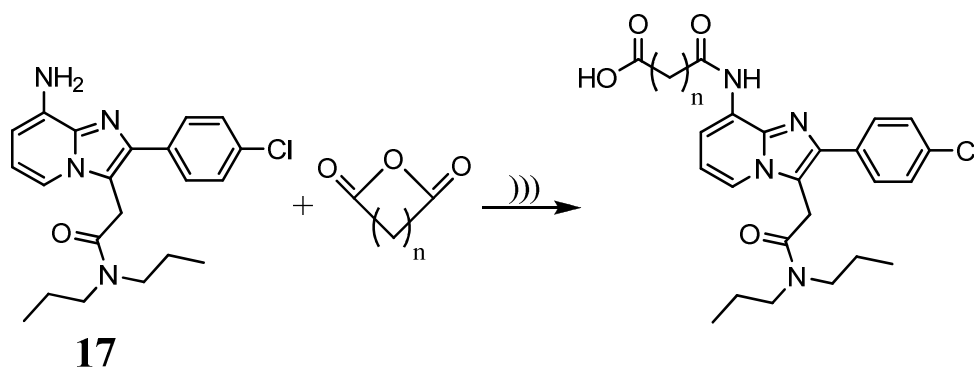
Formation of the amide bond was then attempted using an acid chloride. In the same pot **H₂L⁶** was treated with thionyl chloride (SOCl₂) which was removed by distillation under reduced pressure. After the removal of SOCl₂, **17** was added in the presence of triethylamine (NEt₃). As before no product was obtained. This may not have worked due to the degradation of **H₂L⁶** by SOCl₂.

The reactions (except acid chloride) were then repeated using Microwave irradiation. Microwave irradiation has been used in numerous different reactions to obtain increased yields and purity in comparison to conventional heating methods¹¹⁹. It has been used for the synthesis of several novel amide bond containing molecules^{120,121} and for the synthesis of peptides that were otherwise inaccessible¹²². But no product was generated.

3.3.3.2.2. Successful synthesis of HL⁹ and HL¹⁰

Due to the lack of success linking **17** to the carboxylic acid form of HL⁴, the synthesis plan was modified. Rather than converting the amine on HL⁴ to a carboxylic acid the amine on **17** was modified to a carboxylic acid. Using an ultrasonic bath **17** was reacted with succinic and glutaric anhydride to generate **22** and **23** respectively (Scheme 3.6). There was a slight reduction in yield in comparison to the reported synthesis⁹⁶ but there was a reduction in reaction time from overnight to 2 hrs and a reduction in reaction temperature from reflux to room temperature.

Then using the methodology used for the successful synthesis of HL⁷ and HL⁸, **22** and **23** were linked to HL⁴ to generate HL⁹ and HL¹⁰ respectively (Figure 3.21).



Scheme 3.6: Synthesis of **22** ($n = 2$) and **23** ($n = 3$).

3.3.3.3. Ligand characterisation by MS

The ligands were fully characterised by standard spectroscopic and analysis methods. The presence of the ligands was further confirmed by examining the isotopic distribution in the mass spectra (MS) (**Figure 3.22 – 3.25**). Using literature values for atomic masses and isotopic abundances¹²³⁻¹²⁶ it was also possible to identify the species observed. The same process was applied to compounds **16, 17, 22, 23** and **21** (**Appendix 4**) to confirm the presence of the alpidem derivative precursors and PK11195 derivative.

Isotopic distributions were observed due to the presence of atoms with isotopes of reasonably high abundance. The ligands **HL**⁸, **HL**⁹ and **HL**¹⁰ all contain a single chlorine atom. Chlorine has two main isotopes, ³⁵Cl and ³⁷Cl, which have a high abundance of 75.77% and 24.23% respectively¹²⁶. This generates two observable peaks in the MS for the ³⁵Cl species and ³⁷Cl species. Due to the difference in abundance the ratio of peak height for the ³⁵Cl species to ³⁷Cl species is approx. 3:1. Also all the ligands contain a large number of Carbon atoms. Carbon has two isotopes, ¹²C and ¹³C. While ¹³C has a low abundance, 1.1%¹²⁶, so normally the ¹³C species would not be observed. But due to the large number of Carbon atoms in the ligands the ¹³C species is readily observed. Also for **HL**⁷ the di-¹³C is observed. The tri-¹³C species was observed but fell below the peak threshold and so was hard to distinguish from the noise.

The observed distributions were compared to distributions predicted by the MassLynx program and were found to be in good agreement (**Appendix 5**). This further proves the presence of the ligands.

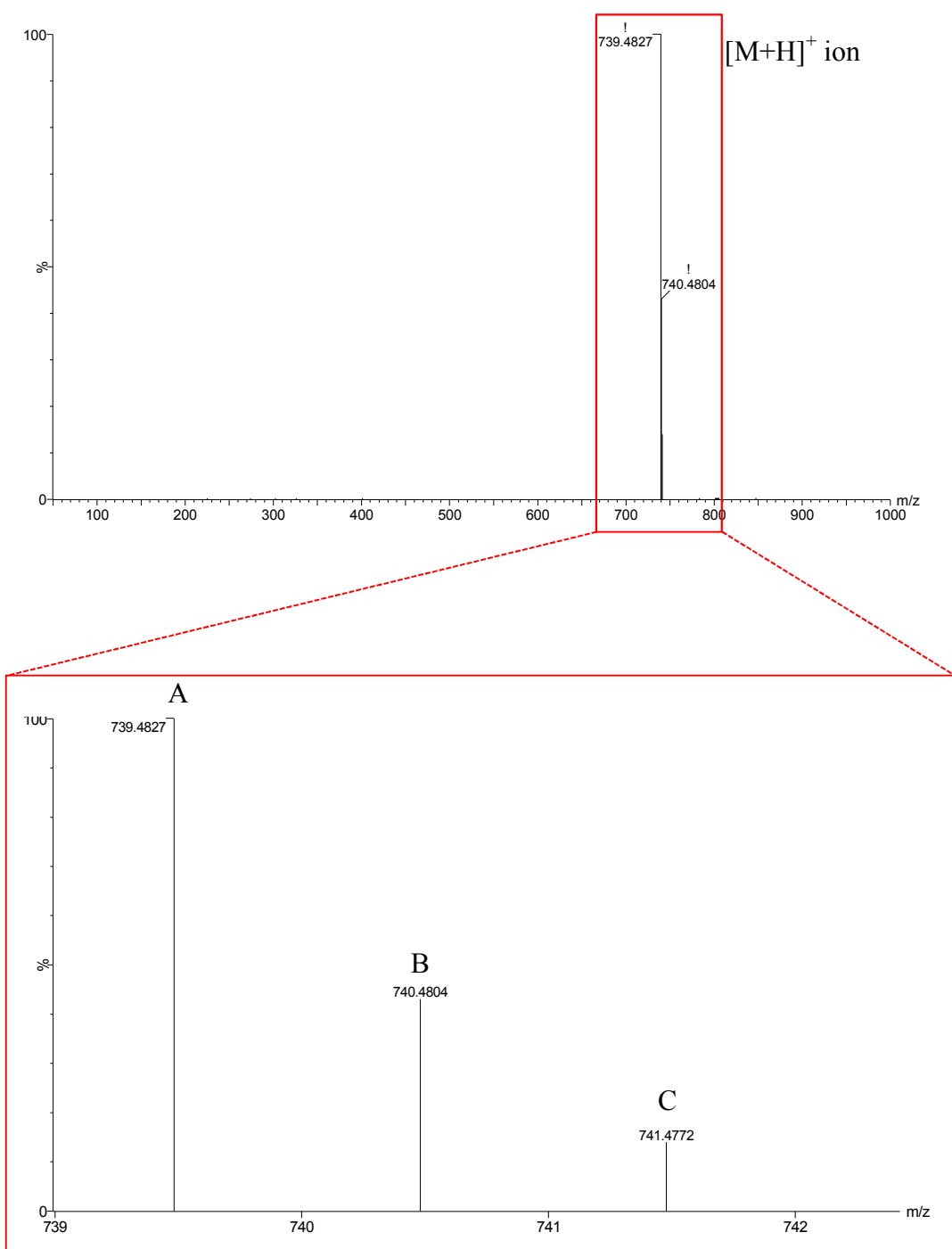


Figure 3.22: Measured positive ion MS for HL^7 , observed ion $[M+H]^+$. A = $^{12}C_{45}^1H_{63}^{14}N_4^{16}O_5$, B = $^{13}C_1^{12}C_{44}^1H_{63}^{14}N_4^{16}O_5$, C = $^{13}C_2^{12}C_{37}^1H_{63}^{14}N_4^{16}O_5$.

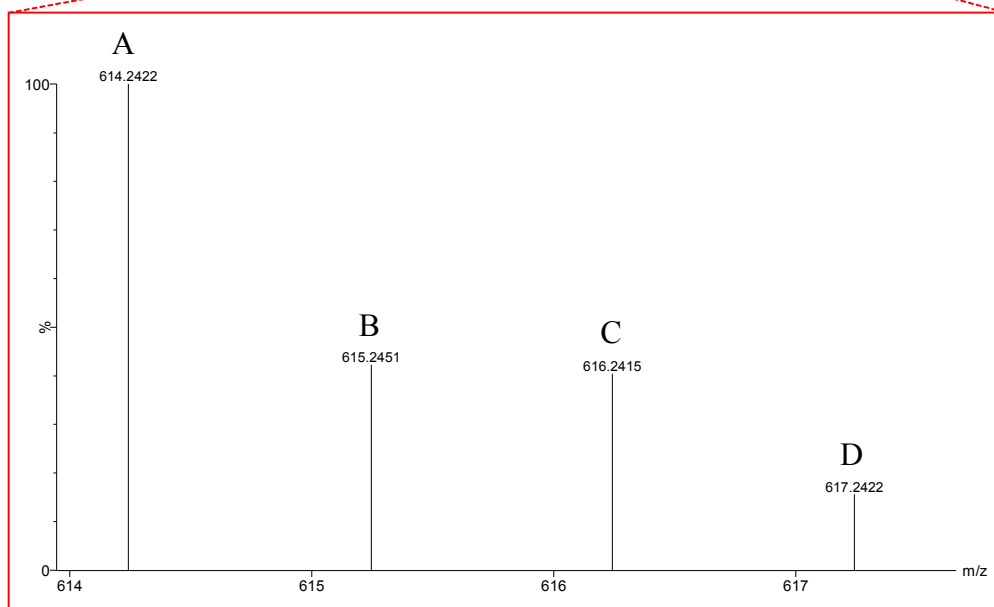
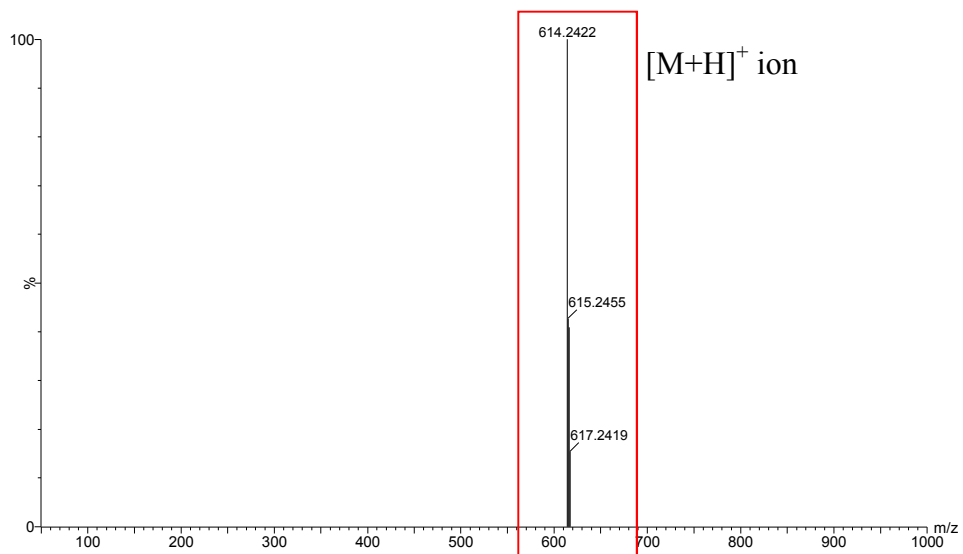
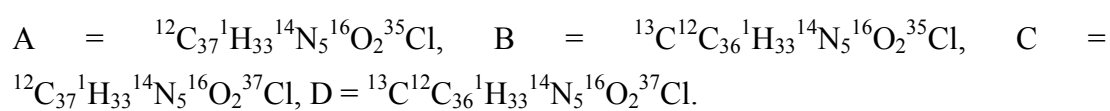


Figure 3.23: Expanded and zoomed positive ion MS for HL^8 , observed ion $[M+H]^+$.



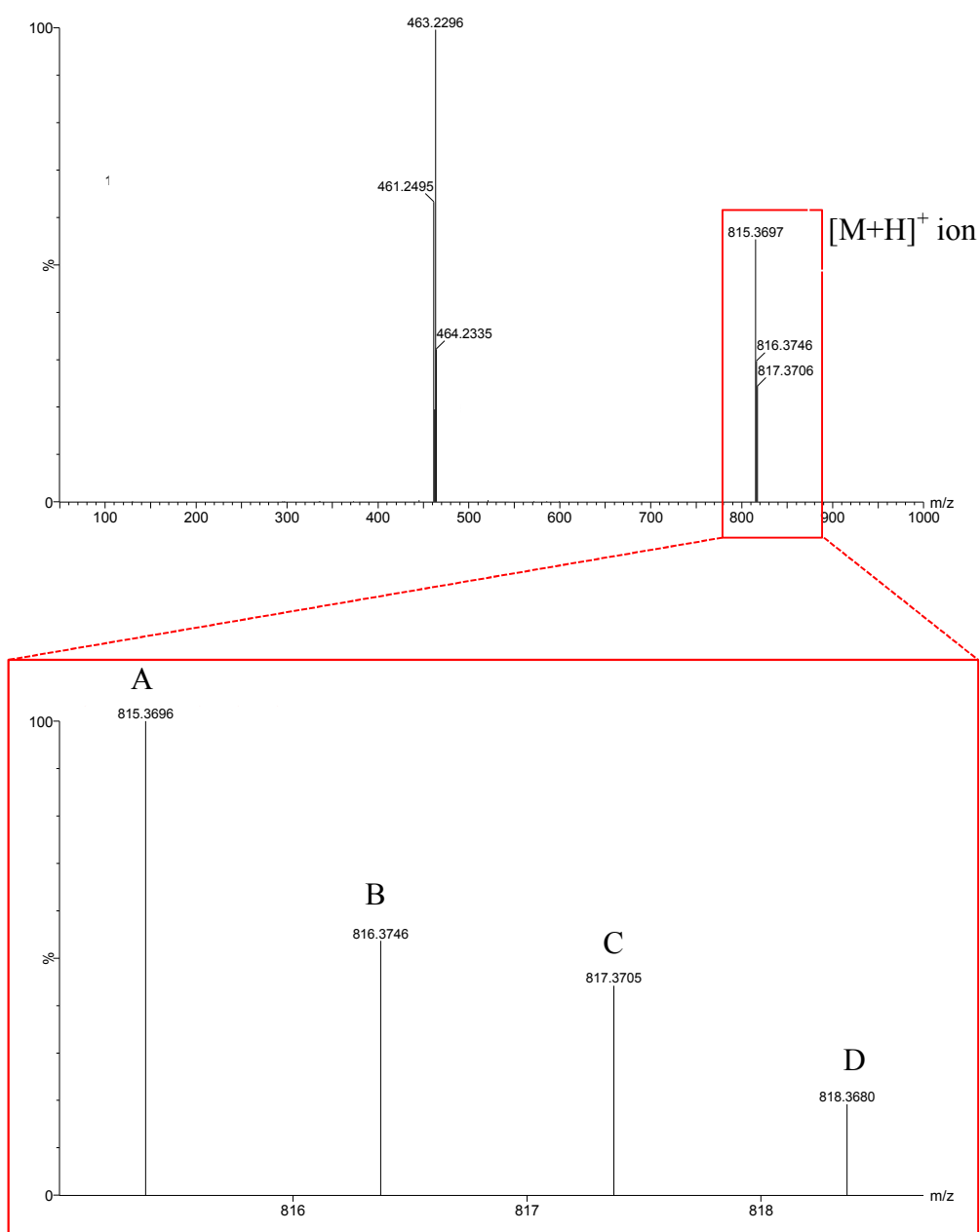
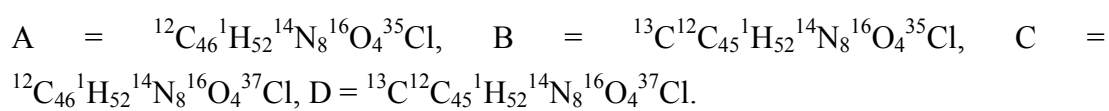


Figure 3.24: Expanded and zoomed positive ion MS for HL^9 , observed ion $[M+H]^+$.



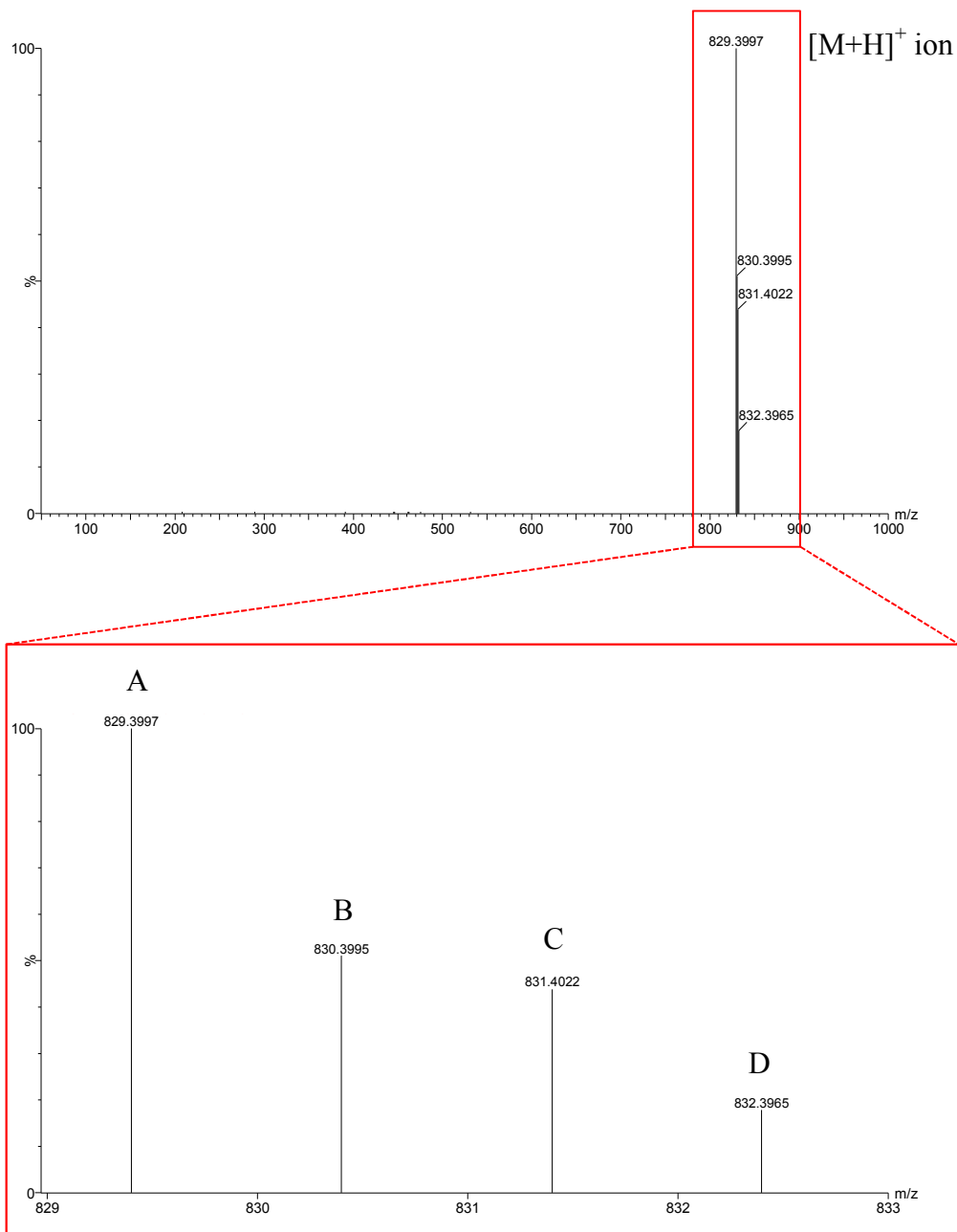
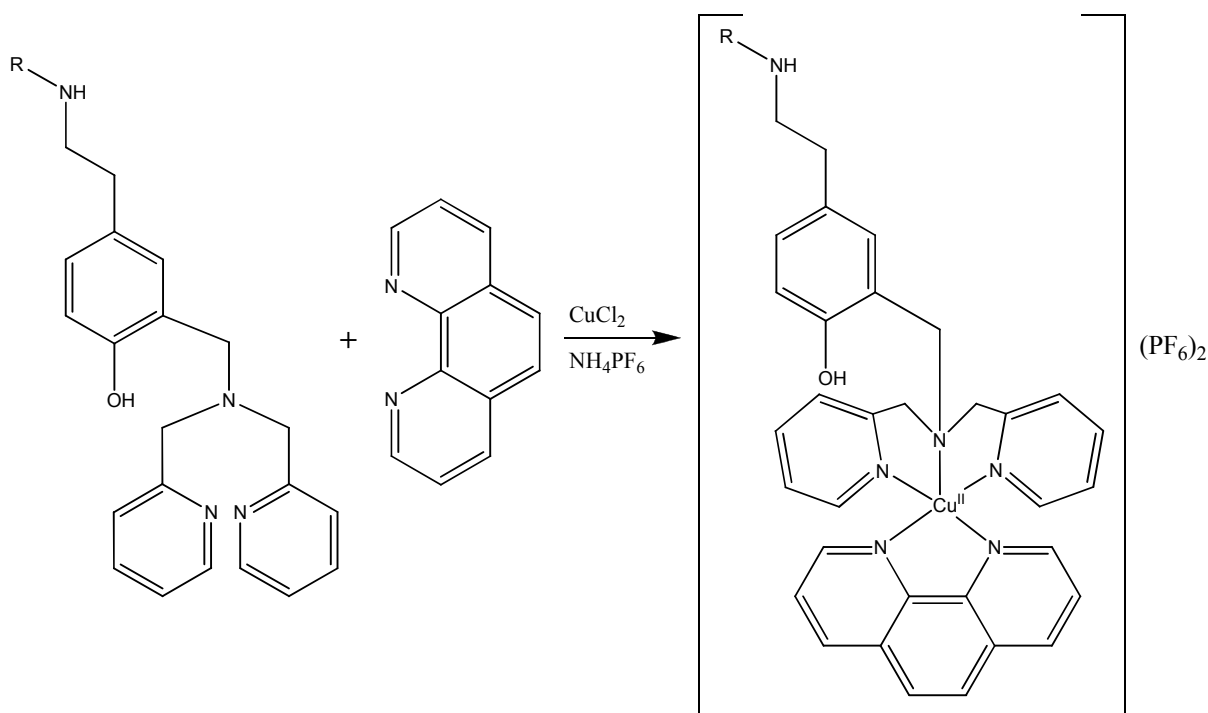


Figure 3.25: Expanded and zoomed positive ion MS for **HL¹⁰**, observed ion $[M+H]^+$. $A = {}^{12}\text{C}_{47}{}^1\text{H}_{54}{}^{14}\text{N}_8{}^{16}\text{O}_4{}^{35}\text{Cl}$, $B = {}^{13}\text{C}{}^{12}\text{C}_{46}{}^1\text{H}_{54}{}^{14}\text{N}_8{}^{16}\text{O}_4{}^{35}\text{Cl}$, $C = {}^{12}\text{C}_{47}{}^1\text{H}_{54}{}^{14}\text{N}_8{}^{16}\text{O}_4{}^{37}\text{Cl}$, $D = {}^{13}\text{C}{}^{12}\text{C}_{46}{}^1\text{H}_{54}{}^{14}\text{N}_8{}^{16}\text{O}_4{}^{37}\text{Cl}$.

3.3.4. Synthesis of monocopper complexes

Mono-Cu^{II} complexes of the ligands were synthesised by mixing 1 equivalent of ligand, 1 equivalent of Cu(Cl)₂ and 1 equivalent of 1,10-phenanthroline (phen). The resulting solution was heated at 60 °C for 4 hours and were then let cool, filtered and 2 equivalents of NH₄PF₆ were added (**Scheme 3.7**). After being left standing for several days the complexes were isolated as powders by filtration. From elemental analysis and mass spectrometry the general molecular formula of [Cu(HL^X)(phen)](PF₆)₂ was determined.



Scheme 3.7: Synthesis of [Cu(HL⁷)(phen)](PF₆)₂ (R = cholic acid), [Cu(HL⁸)(phen)](PF₆)₂ (R = 21), [Cu(HL⁹)(phen)](PF₆)₂ (R = 22), [Cu(HL¹⁰)(phen)](PF₆)₂ (R = 23).

From the analyses the phenolic oxygen is not involved in coordinating the Cu^{II}. Since the complexes were isolated as a powder no structural information could be obtained but based on the reported coordination environments for similarly constructed complexes¹²⁷⁻¹³² it can be presumed that the Cu^{II} is in a N₅ binding environment being coordinated by the dipodal 1,10-phenanthroline and the tripodal dipicolylamine “arm” (**Scheme 3.7**).

3.4 Conclusions and future work

The synthesis of the known mononucleating ligand **HL**⁴ has been described and fully characterised. To give greater synthetic versatility the amine moiety on **HL**⁴ was modified to a carboxylic acid, the synthesis of which has been fully described. To allow for different chain lengths various cyclic anhydrides were employed. In this work succinic (**H₂L**⁵) and glutaric anhydride (**H₂L**⁶) were used but malonic or adipic anhydride could easily be used to obtain a shorter (n = 1) or a longer (n = 4) chain respectively. Known TSPO ligands based on PK11195 and Alpidem were synthesised and fully characterised. By use of an amide bond these were linked to **HL**⁴ generating mononucleating ligands containing a targeting unit with pharmacological activity. **HL**⁴ was also linked to cholic acid to give a mononucleating ligand containing a targeting unit.

The original synthetic plan for the linkage of **HL**⁴ to the Alpidem derivatives was to use the carboxylic acid derivatized versions of **HL**⁴, **H₂L**⁵ and **H₂L**⁶. Several different synthetic methodologies were pursued but no product was found. For the diimide and EEDQ methodologies there are several dead-end by-products that may have formed but none of these were found in the reaction mixture by MS or after work-up. It was also attempted to form the amide bond by use of an acid chloride. But as before no product was observed, this was most likely due to degradation of the phenol, **H₂L**⁶, by thionyl chloride rather than formation of the acid chloride. From previous work in this thesis it was found that the C-C bond linking the phenol “body” to the “arm” is susceptible to attack by HCl (**Section 2.3.1.1** and **Section 2.3.1.2**).

Using the mononucleating ligands generated 4 new mono-Cu^{II} complexes were generated. In all 1,10-phenanthroline was used as a co-ligand. These complexes contain a targeting unit with pharmacological behaviour and the 1,10-phenanthroline would potentially allow for the complex to intercalate DNA and bring the active site into close target to the cellular target. The aim of this work was to generate new mono-Cu^{II} complexes as potential anticancer metallodrugs and so a future objective would be to determine and quantify their biological behaviour and to use this to rationally design more effective metallodrugs. Synthetically several different methods could be employed for the generation of these.

One: the use of other mononucleating ligands. In this work a phenylated dipicolylamine was used due to its relevance to other work presented in this thesis. But as was seen the phenolic oxygen was not involved in coordinating the Cu^{II} so dipicolylamine by itself could be used. This would be synthetically accessible by forming an amide bond between the secondary amine on dipicolylamine and the carboxylic acid moiety on the desired targeting unit. Also possible would be the use of other mononucleating ligands such as modified phenanthrolines, TACN, TACH and bipyridines (**Section 2.1.3.**) to name a few examples. All these generate mono-Cu^{II} complexes that have been shown to cleave polynucleotides¹³³⁻¹³⁶ by either hydrolytic, oxidative or combination mechanisms.

Two: the use of other co-ligands. In this work 1,10-phenanthroline due to its ability to allow the complexes to intercalate DNA but other large planar aromatic molecules could be used as a co-ligand., these include 5,6-dimethyl-1,10-phenanthroline (5,6-dmp), 1,10-phenanthroline-5,6-dione (dione), dipyrido[3,2-*f*:2',3'-*h*]quinoxaline (dpq), dipyrido[3,2-*a*:2',3'-*c*]phenazine (dppz) or benzo[*i*]dipyrido[3,2-*a*:2',3'-*c*]phenazine (dppn) (**Figure 3.26**). The Copper complexes of these have all been found to have enhanced DNA binding and cleavage than the corresponding 1,10-phenanthroline Copper complexes^{127,132,137}.

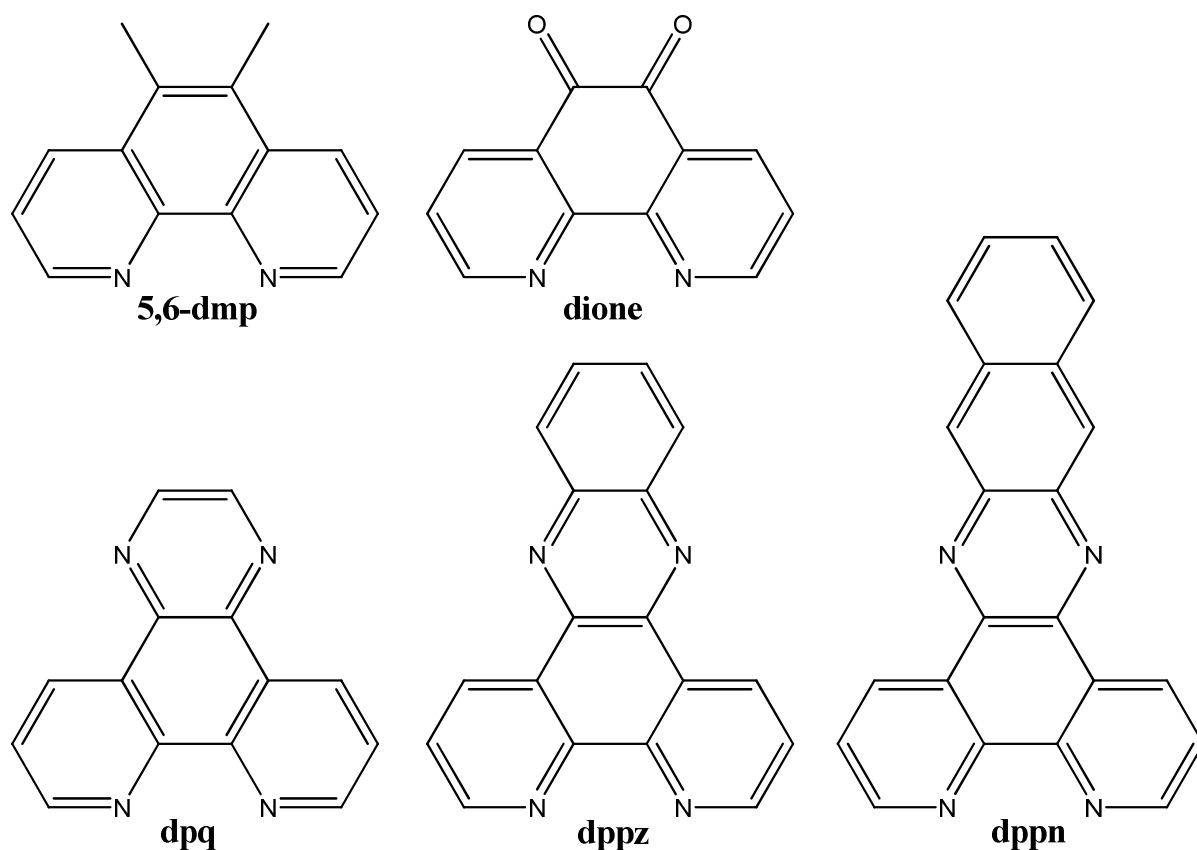


Figure 3.26: Structure of potential co-ligands.

Three: the use of other TSPO ligands. This method would allow for the generation of a greater number of potential metallodrugs. This is due to the number of structural groups to be exploited (**Section 3.1.3.1.**) and the large number of analogues of these that have been synthesised. In this work a PK11195 and Alpidem derivative were used due to the affinity and selectivity for TSPO^{65,96,102}, the potential ease to link them to mononucleating ligands and their relevance to other work being done within the group. While very few derivatives of the isoquinoline PK11195 have been generated a recent structure activity relationship (SAR) study has been performed with quinazoline analogues of PK11195¹³⁸ creating numerous TSPO ligands which could easily be linked to mononucleating ligands. Several SAR studies have also been performed on Alpidem⁹⁶⁻⁹⁸ and these have generated numerous TSPO ligands to be used as templates for synthesis of linkable molecules. But the main disadvantage of this method is the low overall yields, which is an obstacle that would need to be overcome so that usable amounts of potential metallodrugs could be generated efficiently.

All these methods either used singly or in combination would allow for the generation of a library of compounds and potentially an effective anti-cancer metallo-drug.

3.5 References

- (1) Maillard, J.-Y.; Hartemann, P. *Crit. Rev. Microbiol.* **2013**, *39*, 373-383.
- (2) Thompson, K. H.; Lichter, J.; LeBel, C.; Scaife, M. C.; McNeill, J. H.; Orvig, C. *J. Inorg. Biochem.* **2009**, *103*, 554-558.
- (3) Schwartz, J. A.; Lium, E. K.; Silverstein, S. J. *J. Virol.* **2001**, *75*, 4117-4128.
- (4) Dive, D.; Biot, C. *ChemMedChem* **2008**, *3*, 383-391.
- (5) Burger, R. M. *Chem. Rev.* **1998**, *98*, 1153-1170.
- (6) Sausville, E. A.; Peisach, J.; Horwitz, S. B. *Biochemistry* **1978**, *17*, 2740-2746.
- (7) Petering, D. H.; Byrnes, R. W.; Antholine, W. E. *Chem. Biol. Interact.* **1990**, *73*, 133-182.
- (8) Cancer in Ireland 2013: Annual report of the National Cancer Registry, *Dept. of Health* **2013**.
- (9) Galanski, M.; Jakupec, M. A.; Keppler, B. K. *Curr. Med. Chem.* **2005**, *12*, 2075-2094.
- (10) Poklar, N.; Pilch, D. S.; Lippard, S. J.; Redding, E. A.; Dunham, S. U.; Breslauer, K. J. *Proc. Natl. Acad. Sci. U.S.A.* **1996**, *93*, 7606-7611.
- (11) Kelland, L. *Nat Rev Cancer* **2007**, *7*, 573-584.
- (12) Dorr, R. In *Platinum and Other Metal Coordination Compounds in Cancer Chemotherapy 2* (Eds.: Pinedo, H. M., Schornagel, J. H.) Springer US: 1996, p 131-154
- (13) Bosslet, K.; Straub, R.; Blumrich, M.; Czech, J.; Gerken, M.; Sperker, B.; Kroemer, H. K.; Gesson, J.-P.; Koch, M.; Monneret, C. *Cancer Res.* **1998**, *58*, 1195-1201.
- (14) Bates, D.; Hillman, N.; Williams, B.; Neal, C.; Pocock, T. *J. Anat.* **2002**, *200*, 581-597.
- (15) Hobbs, S. K.; Monsky, W. L.; Yuan, F.; Roberts, W. G.; Griffith, L.; Torchilin, V. P.; Jain, R. K. *Proc. Natl. Acad. Sci. U.S.A.* **1998**, *95*, 4607-4612.
- (16) Gordon, A. N.; Tonda, M.; Sun, S.; Rackoff, W. *Gynecol. Oncol.* **2004**, *95*, 1-8.
- (17) Gradishar, W. J.; Tjulandin, S.; Davidson, N.; Shaw, H.; Desai, N.; Bhar, P.; Hawkins, M.; O'Shaughnessy, J. *J. Clin. Oncol.* **2005**, *23*, 7794-7803.

- (18) Rice, J. R.; Gerberich, J. L.; Nowotnik, D. P.; Howell, S. B. *Clin. Cancer Res.* **2006**, *12*, 2248-2254.
- (19) Tripisciano, C.; Kraemer, K.; Taylor, A.; Borowiak-Palen, E. *Chem. Phys. Lett.* **2009**, *478*, 200-205.
- (20) White, S. C.; Lorigan, P.; Margison, G. P.; Margison, J. M.; Martin, F.; Thatcher, N.; Anderson, H.; Ranson, M. *Brit. J. Cancer* **2006**, *95*, 822-828.
- (21) Dragovich, T.; Mendelson, D.; Kurtin, S.; Richardson, K.; Von Hoff, D.; Hoos, A. *Cancer Chemother. Pharmacol.* **2006**, *58*, 759-764.
- (22) Yang, F.; Zhang, Y.; Liang, H. *Int. J. Mol. Sci.* **2014**, *15*, 3580-3595.
- (23) Neumann, E.; Frei, E.; Funk, D.; Becker, M. D.; Schrenk, H.-H.; Müller-Ladner, U.; Fiehn, C. *Expert Opin. Drug Del.* **2010**, *7*, 915-925.
- (24) Kratz, F. *J. Control. Release* **2008**, *132*, 171-183.
- (25) Zheng, Y.-R.; Suntharalingam, K.; Johnstone, T. C.; Yoo, H.; Lin, W.; Brooks, J. G.; Lippard, S. J. *J. Am. Chem. Soc.* **2014**, *136*, 8790-8798.
- (26) Rademaker-Lakhai, J. M.; Terret, C.; Howell, S. B.; Baud, C. M.; de Boer, R. F.; Pluim, D.; Beijnen, J. H.; Schellens, J. H.; Droz, J.-P. *Clin. Cancer Res.* **2004**, *10*, 3386-3395.
- (27) Wu, C.-H.; Cao, C.; Kim, J. H.; Hsu, C.-H.; Wanebo, H. J.; Bowen, W. D.; Xu, J.; Marshall, J. *Nano Lett.* **2012**, *12*, 5475-5480.
- (28) Low, P. S.; Henne, W. A.; Doorneweerd, D. D. *Acc. Chem. Res.* **2007**, *41*, 120-129.
- (29) Chen, H.; Pazicni, S.; Krett, N. L.; Ahn, R. W.; Penner-Hahn, J. E.; Rosen, S. T.; O'Halloran, T. V. *Angew. Chem Int. Ed.* **2009**, *48*, 9295-9299.
- (30) Borgquist, S.; Holm, C.; Stendahl, M.; Anagnostaki, L.; Landberg, G.; Jirström, K. *J. Clin. Pathol.* **2008**, *61*, 197-203.
- (31) Descôteaux, C.; Leblanc, V.; Bélanger, G.; Parent, S.; Asselin, É.; Bérubé, G. *Steroids* **2008**, *73*, 1077-1089.
- (32) Lea, O. A.; Kvinnsland, S.; Thorsen, T. *Cancer Res.* **1989**, *49*, 7162-7167.
- (33) Kühnel, R.; de Graapf, J.; Rao, B. R.; Stolk, J. G. *J. Steroid Biochem.* **1987**, *26*, 393-397.
- (34) Hobisch, A.; Culig, Z.; Radmayr, C.; Bartsch, G.; Klocker, H.; Hittmair, A. *Cancer Res.* **1995**, *55*, 3068-3072.

- (35) Huxley, M.; Sanchez-Cano, C.; Browning, M. J.; Navarro-Ranninger, C.; Quiroga, A. G.; Rodger, A.; Hannon, M. J. *Dalton Trans.* **2010**, *39*, 11353-11364.
- (36) Ruiz-Sánchez, P.; König, C.; Ferrari, S.; Alberto, R. *J. Biol. Inorg. Chem.* **2011**, *16*, 33-44.
- (37) Kunze, S.; Zobi, F.; Kurz, P.; Spingler, B.; Alberto, R. *Angew. Chem. Int. Ed.* **2004**, *43*, 5025-5029.
- (38) Kramer, W.; Wess, G.; Schubert, G.; Bickel, M.; Girbig, F.; Gutjahr, U.; Kowalewski, S.; Baringhaus, K. H.; Enhsen, A.; Glombik, H. *J. Biol. Chem.* **1992**, *267*, 18598-18604.
- (39) Sreekanth, V.; Bansal, S.; Motiani, R. K.; Kundu, S.; Muppu, S. K.; Majumdar, T. D.; Panjamurthy, K.; Sengupta, S.; Bajaj, A. *Bioconjugate Chem.* **2013**, *24*, 1468-1484.
- (40) Albin, N.; Massaad, L.; Toussaint, C.; Mathieu, M.-C.; Morizet, J.; Parise, O.; Gouyette, A.; Chabot, G. G. *Cancer Res.* **1993**, *53*, 3541-3546.
- (41) Bolden, J. E.; Peart, M. J.; Johnstone, R. W. *Nat. Rev. Drug Discov.* **2006**, *5*, 769-784.
- (42) Minucci, S.; Pelicci, P. G. *Nat. Rev. Cancer* **2006**, *6*, 38-51.
- (43) Brabec, V.; Griffith, D. M.; Kisova, A.; Kostrhunova, H.; Zerzankova, L.; Marmion, C. J.; Kasparkova, J. *Mol. Pharm.* **2012**, *9*, 1990-1999.
- (44) Griffith, D.; Morgan, M. P.; Marmion, C. J. *Chem. Commun.* **2009**, 6735-6737.
- (45) Griffith, D. M.; Duff, B.; Suponitsky, K. Y.; Kavanagh, K.; Morgan, M. P.; Egan, D.; Marmion, C. J. *J. Inorg. Biochem.* **2011**, *105*, 793-799.
- (46) Parker, J. P.; Nimir, H.; Griffith, D. M.; Duff, B.; Chubb, A. J.; Brennan, M. P.; Morgan, M. P.; Egan, D. A.; Marmion, C. J. *J. Inorg. Biochem.* **2013**, *124*, 70-77.
- (47) Rademaker-Lakhai, J. M.; van den Bongard, D.; Pluim, D.; Beijnen, J. H.; Schellens, J. H. M. *Clin. Cancer Res.* **2004**, *10*, 3717-3727.
- (48) Jain, S. S.; Anderson, C. M.; DiRienzo, F.; Taylor, I. R.; Jain, K.; Guha, S.; Hoque, N. *Chem. Commun.* **2013**, *49*, 5031-5033.
- (49) Grinda, M.; Clarhaut, J.; Renoux, B.; Tranoy-Opalinski, I.; Papot, S. *MedChemComm* **2012**, *3*, 68-70.

- (50) Grinda, M.; Clarhaut, J.; Tranoy-Opalinski, I.; Renoux, B.; Monvoisin, A.; Cronier, L.; Papot, S. *ChemMedChem* **2011**, *6*, 2137-2141.
- (51) Sigel, E.; Barnard, E. A. *J. Biol. Chem.* **1984**, *259*, 7219-7223.
- (52) Braestrup, C.; Albrechtsen, R.; Squires, R. F. *Nature* **1977**, *269*, 702-704.
- (53) Mohler, H.; Okada, T. *Science* **1977**, *198*, 849-851.
- (54) Costa, E.; Guidotti, A. *Annu. Rev. Pharmacol. Toxicol.* **1979**, *19*, 531-545.
- (55) Costa, E.; Guidotti, A.; Mao, C. C. *Adv. Biochem. Psychopharmacol.* **1975**, 113-30.
- (56) Haefely, W.; Kulcsar, A.; Mohler, H.; Pieri, L.; Polc, P.; Schaffner, R. *Adv. Biochem. Psychopharmacol.* **1975**, 131-151.
- (57) Papadopoulos, V.; Baraldi, M.; Guilarte, T. R.; Knudsen, T. B.; Lacapère, J.-J.; Lindemann, P.; Norenberg, M. D.; Nutt, D.; Weizman, A.; Zhang, M.-R.; Gavish, M. *Trends Pharmacol. Sci.* **2006**, *27*, 402-409.
- (58) Anholt, R. R.; Pedersen, P. L.; De Souza, E. B.; Snyder, S. H. *J. Biol. Chem.* **1986**, *261*, 576-583.
- (59) Papadopoulos, V.; Amri, H.; Boujrad, N.; Cascio, C.; Culty, M.; Garnier, M.; Hardwick, M.; Li, H.; Vidic, B.; Brown, A. *Steroids* **1997**, *62*, 21-28.
- (60) Papadopoulos, V.; Guarneri, P.; Kreuger, K.; Guidotti, A.; Costa, E. *Proc. Natl. Acad. Sci. U.S.A.* **1992**, *89*, 5113-5117.
- (61) Hirsch, J. D.; Beyer, C. F.; Malkowitz, L.; Beer, B.; Blume, A. J. *Mol. Pharmacol.* **1989**, *35*, 157-163.
- (62) Nordenberg, J.; Fenig, E.; Landau, M.; Weizman, R.; Weizman, A. *Biochem. Pharmacol.* **1999**, *58*, 1229-1236.
- (63) Avital, A.; Richter-Levin, G.; Leschiner, S.; Spanier, I.; Veenman, L.; Weizman, A.; Gavish, M. *Neuropsychopharmacol.* **2001**, *25*, 669-678.
- (64) Braestrup, C.; Squires, R. F. *Proc. Natl. Acad. Sci. U.S.A.* **1977**, *74*, 3805-3809.
- (65) Awad, M.; Gavish, M. *J. Neurochem.* **1987**, *49*, 1407-1414.
- (66) Braestrup, C.; Nielsen, M.; Squires, R.; Laurberg, S. *Acta Psychiat. Scand.* **1978**, *58*, 27-32.
- (67) Diorio, D.; Welner, S. A.; Butterworth, R. F.; Meaney, M. J.; Suranyi-Cadotte, B. E. *Neurobiology Aging* **1991**, *12*, 255-258.
- (68) Meßmer, K.; Reynolds, G. P. *Neurosci. Lett.* **1998**, *241*, 53-56.

- (69) Gulyás, B.; Makkai, B.; Kása, P.; Gulya, K.; Bakota, L.; Várszegi, S.; Beliczai, Z.; Andersson, J.; Csiba, L.; Thiele, A. *Neurochem. Int.* **2009**, *54*, 28-36.
- (70) Schoemaker, H.; Morelli, M.; Deshmukh, P.; Yamamura, H. I. *Brain Res.* **1982**, *248*, 396-401.
- (71) Veenman, L.; Levin, E.; Weisinger, G.; Leschiner, S.; Spanier, I.; Snyder, S. H.; Weizman, A.; Gavish, M. *Biochem. Pharmacol.* **2004**, *68*, 689-698.
- (72) Miettinen, H.; Kononen, J.; Haapasalo, H.; Helén, P.; Sallinen, P.; Harjuntausta, T.; Helin, H.; Alho, H. *Cancer Res.* **1995**, *55*, 2691-2695.
- (73) Maaser, K.; Grabowski, P.; Sutter, A. P.; Höpfner, M.; Foss, H.-D.; Stein, H.; Berger, G.; Gavish, M.; Zeitz, M.; Scherübl, H. *Clin. Cancer Res.* **2002**, *8*, 3205-3209.
- (74) Hardwick, M.; Fertikh, D.; Culty, M.; Li, H.; Vidic, B.; Papadopoulos, V. *Cancer Res.* **1999**, *59*, 831-841.
- (75) Venturini, I.; Alho, H.; Podkletnova, I.; Corsi, L.; Rybnikova, E.; Pellicci, R.; Baraldi, M.; Peltó-Huikko, M.; Helén, P.; Zeneroli, M. L. *Life Sci.* **1999**, *65*, 2223-2231.
- (76) Katz, Y.; Ben-Baruch, G.; Kloog, Y.; Menczer, J.; Gavish, M. *Clin. Sci.* **1990**, *78*, 155-158.
- (77) Decaudin, D.; Castedo, M.; Nemati, F.; Beurdeley-Thomas, A.; De Pinieux, G.; Caron, A.; Pouillart, P.; Wijdenes, J.; Rouillard, D.; Kroemer, G.; Poupon, M.-F. *Cancer Res.* **2002**, *62*, 1388-1393.
- (78) Hans, G.; Wislet-Gendebien, S.; Lallemand, F.; Robe, P.; Rogister, B.; Belachew, S.; Nguyen, L.; Malgrange, B.; Moonen, G.; Rigo, J.-M. *Biochem. Pharmacol.* **2005**, *69*, 819-830.
- (79) Santidrián, A. F.; Cosiáls, A. M.; Coll-Mulet, L.; Iglesias-Serret, D.; de Frias, M.; González-Gironès, D. M.; Campàs, C.; Domingo, A.; Pons, G.; Gil, J. *Haematologica* **2007**, *92*, 1631-1638.
- (80) Mendonça-Torres, M. C.; Roberts, S. S. *Cancer Biol. Ther.* **2013**, *14*, 319-326.
- (81) Karam, J. A.; Jer-Tsong, H. *Apoptosis in Carcinogenesis and Chemotherapy* (Eds.: Chem, G. G., Lai, P.) **2009**, 25-50.
- (82) Büki, A.; Okonkwo, D. O.; Wang, K. K. W.; Povlishock, J. T. *J. Neurosci.* **2000**, *20*, 2825-2834.

- (83) Casellas, P.; Galiegue, S.; Basile, A. S. *Neurochem. Int.* **2002**, *40*, 475-486.
- (84) Joseph-Liauzun, E.; Delmas, P.; Shire, D.; Ferrara, P. *J. Biol. Chem.* **1998**, *273*, 2146-2152.
- (85) Jaremko, Ł.; Jaremko, M.; Giller, K.; Becker, S.; Zweckstetter, M. *Science* **2014**, *343*, 1363-1366.
- (86) Papadopoulou, V.; Boujrada, N.; Ikonomovica, M. D.; Ferrarab, P.; Vidica, B. *Mol. Cell. Endocrinol.* **1994**, *104*, 5-9.
- (87) McEnery, M. W.; Snowman, A. M.; Trifiletti, R. R.; Snyder, S. H. *Proc. Natl. Acad. Sci. U.S.A.* **1992**, *89*, 3170-3174.
- (88) Šileikytė, J.; Blachly-Dyson, E.; Sewell, R.; Carpi, A.; Menabò, R.; Di Lisa, F.; Ricchelli, F.; Bernardi, P.; Forte, M. *J. Biol. Chem.* **2014**, *289*, 13769-13781.
- (89) Bourguignon, J. J. *Peripheral Benzodiazepine Receptors* (Ed.: Glesen-Crouse, E.) **1993**, 59-85.
- (90) Lentini, G.; Bourguignon, J. J.; Wermuth, C. G. *QSAR: Rational Approaches to the Design of Bioactive Compounds* (Eds.: Silipo, C., Vittoria, A.) **1991**, 257.
- (91) Scarf, A. M.; Ittner, L. M.; Kassiou, M. *J. Med. Chem.* **2009**, *52*, 581-592.
- (92) Cappelli, A.; Anzini, M.; Vomero, S.; De Benedetti, P. G.; Menziani, M. C.; Giorgi, G.; Manzoni, C. *J. Med. Chem.* **1997**, *40*, 2910-2921.
- (93) Berson, A.; Descatoire, V.; Sutton, A.; Fau, D.; Maulny, B.; Vadrot, N.; Feldmann, G.; Berthon, B.; Tordjmann, T.; Pessayre, D. *J. Pharmacol. Exp. Ther.* **2001**, *299*, 793-800.
- (94) Langer, S. Z.; Arbilla, S.; Tan, S.; Lloyd, K. G.; George, P.; Allen, J.; Wick, A. E. *Pharmacopsychiatry* **1990**, *23*, 103-107.
- (95) Anzini, M.; Cappelli, A.; Vomero, S.; Giorgi, G.; Langer, T.; Bruni, G.; Romeo, M. R.; Basile, A. S. *J. Med. Chem.* **1996**, *39*, 4275-4284.
- (96) Nunzio, D.; Laquintana, V.; Pisu, M. G.; Dore, R.; Murru, L.; Latrofa, A.; Trapani, G.; Sanna, E. *J. Med. Chem.* **2008**, *51*, 6876-6888.
- (97) Trapani, G.; Franco, M.; Latrofa, A.; Ricciardi, L.; Carotti, A.; Serra, M.; Sanna, E.; Biggio, G.; Liso, G. *J. Med. Chem.* **1999**, *42*, 3934-3941.
- (98) Trapani, G.; Franco, M.; Ricciardi, L.; Latrofa, A.; Genchi, G.; Sanna, E.; Tuveri, F.; Cagetti, E.; Biggio, G.; Liso, G. *J. Med. Chem.* **1997**, *40*, 3109-3118.

- (99) Trapani, G.; Laquintana, V.; Denora, N.; Trapani, A.; Lopedota, A.; Latrofa, A.; Franco, M.; Serra, M.; Pisu, M. G.; Floris, I.; Sanna, E.; Biggio, G.; Liso, G. *J. Med. Chem.* **2004**, *48*, 292-305.
- (100) Kozikowski, A. P.; Ma, D.; Brewer, J.; Sun, S.; Costa, E.; Romeo, E.; Guidotti, A. *J. Med. Chem.* **1993**, *36*, 2908-2920.
- (101) Margiotta, N.; Denora, N.; Ostuni, R.; Laquintana, V.; Anderson, A.; Johnson, S. W.; Trapani, G.; Natile, G. *J. Med. Chem.* **2010**, *53*, 5144-5154.
- (102) Le Fur, G.; Vaucher, N.; Perrier, M. L.; Flamier, A.; Benavides, J.; Renault, C.; Dubroeuq, M. C.; Guérémy, C.; Uzan, A. *Life Sc.* **1983**, *33*, 449-457.
- (103) Tai, Y. F.; Pavese, N.; Gerhard, A.; Tabrizi, S. J.; Barker, R. A.; Brooks, D. J.; Piccini, P. *Brain Res. Bull.* **2007**, *72*, 148-151.
- (104) Manning, H. C.; Smith, S. M.; Sexton, M.; Haviland, S.; Bai, M.; Cederquist, K.; Stella, N.; Bornhop, D. J. *Bioconjugate Chem.* **2006**, *17*, 735-740.
- (105) Manning, H. C.; Goebel, T.; Thompson, R. C.; Price, R. R.; Lee, H.; Bornhop, D. J. *Bioconjugate Chem.* **2004**, *15*, 1488-1495.
- (106) Ibrahim, M. M.; Ramadan, A.-M. M.; Mersal, G. A. M.; El-Shazly, S. A. *J. Mol. Struct.* **2011**, *998*, 1-10.
- (107) Qian, J.; Wang, L.-P.; Tian, J.-L.; Yan, S.-P. *J. Coord. Chem.* **2011**, *64*, 1991-2001.
- (108) Belousoff, M. J.; Tjioe, L.; Graham, B.; Spiccia, L. *Inorg. Chem.* **2008**, *47*, 8641-8651.
- (109) Berthet, N.; Martel-Frchet, V.; Michel, F.; Philouze, C.; Hamman, S.; Ronot, X.; Thomas, F. *Dalton Trans.* **2013**, *42*, 8468-8483.
- (110) Veal, J. M.; Rill, R. L. *Biochemistry* **1991**, *30*, 1132-1140.
- (111) Wild, G. P.; Wiles, C.; Watts, P.; Haswell, S. J. *Tetrahedron* **2009**, *65*, 1618-1629.
- (112) Louie, M.-W.; Liu, H.-W.; Lam, M. H.-C.; Lau, T.-C.; Lo, K. K.-W. *Organometallics* **2009**, *28*, 4297-4307.
- (113) Wernerova, M.; Hudlicky, T. *Synlett* **2010**, *2010*, 2701-2707.
- (114) Jiang, J.-k.; Thomas, C. J.; Neumann, S.; Lu, X.; Rice, K. C.; Gershengorn, M. C. *Bioorg. Med. Chem. Lett.* **2005**, *15*, 733-736.
- (115) Manning, H. C.; Goebel, T.; Marx, J. N.; Bornhop, D. J. *Org. Lett.* **2002**, *4*, 1075-1078.

- (116) Janin, Y. L.; Roulland, E.; Beurdeley-Thomas, A.; Decaudin, D.; Monneret, C.; Poupon, M. F. *J. Chem. Soc. Perkin. Trans. 1* **2002**, 529-532.
- (117) Augeri, D. J.; O'Connor, S. J.; Janowick, D.; Szczepankiewicz, B.; Sullivan, G.; Larsen, J.; Kalvin, D.; Cohen, J.; Devine, E.; Zhang, H.; Cherian, S.; Saeed, B.; Ng, S.-C.; Rosenberg, S. *J. Med. Chem.* **1998**, *41*, 4288-4300.
- (118) Chan, T. Y.; Chen, A.; Allanson, N.; Chen, R.; Liu, D.; Sofia, M. J. *Tetrahedron Lett.* **1996**, *37*, 8097-8100.
- (119) Strauss, C.; Trainor, R. *Aust. J. Chem.* **1995**, *48*, 1665-1692.
- (120) Luis Miguel, L.-M.; Hisila, S.-O.; Navarro, R. E.; Lorena, M. L.; Sugich-Miranda, R.; Karen, O. L. *Polyhedron* **2014**, *79*, 338-346.
- (121) Queirós, C.; Leite, A.; Silva, A. M. G.; Gameiro, P.; de Castro, B.; Range, M. *Polyhedron*, **2015**, *87*, 1-7.
- (122) HOJO, K.; HARA, A.; ONISHI, M.; ICHIKAWA, H.; FUKUMORII, Y. In *Peptide science: proceedings of the. Japanese Peptide Symposium 2013*; Vol. 2012, p 173.
- (123) Audi, G.; Wapstra, A. H. *Nucl. Phys. A* **1993**, *565*, 1-65.
- (124) Audi, G.; Wapstra, A. H. *Nucl. Phys. A* **1995**, *595*, 409-480.
- (125) Wiesser, M. E.; N., H.; Coplen, T. B.; Bohlke, J. K.; Berglung, M.; Brand, W. A.; De Bièvre, P.; Groning, M.; Lass, R. D.; Meija, J.; Hirate, T.; Prohaska, T.; Schoenberg, R.; O'Connor, G.; Walcyk, T.; TYoneda, S.; Zhu, W. *Pure Appl. Chem.* **1999**, *85*, 1047-1078.
- (126) Berglund, M.; Weisser, M. E. *Pure Appl. Chem.* **2011**, *83*, 397-410.
- (127) Chen, Q.-Y.; Fu, H.-J.; Huang, J.; Zhang, R.-X. *Spectrochim. Acta A* **2010**, *75*, 355-360.
- (128) Ganeshpandian, M.; Ramakrishnan, S.; Palaniandavar, M.; Suresh, E.; Riyasdeen, A.; Akbarsha, M. A. *J. Inorg. Biochem.* **2014**, *140*, 202-212.
- (129) Maity, B.; Roy, M.; Chakravarty, A. R. *J. Organomet. Chem.* **2008**, *693*, 1395-1399.
- (130) Lu, J.; Li, J.-L.; Sun, Q.; Jiang, L.; Wang, B.-W.; Gu, W.; Liu, X.; Tian, J.-L.; Yan, S.-P. *J. Coord. Chem.* **2014**, *67*, 300-314.
- (131) Huang, G.-S.; Su, C.-C.; Wang, S.-L.; Liao, F.-L.; Lin, K.-J. *J. Coord. Chem.* **2000**, *49*, 211-226.
- (132) Ramakrishnan, S.; Palaniandavar, M. *J. Chem. Sci.* **2005**, *117*, 179-186.
- (133) Hegg, E. L.; Burstyn, J. N. *Inorg. Chem.* **1996**, *35*, 7474-7481.

- (134) Itoh, T.; Hisada, H.; Sumiya, T.; Hosono, M.; Usui, Y.; Fujii, Y. *Chem. Commun.* **1997**, 677-678.
- (135) Stern, M. K.; Bashkin, J. K.; Sall, E. D. *J. Am. Chem. Soc.* **1990**, *112*, 5357-5359.
- (136) Li, J.-H.; Wang, J.-T.; Hu, P.; Zhang, L.-Y.; Chen, Z.-N.; Mao, Z.-W.; Ji, L.-N. *Polyhedron* **2008**, *27*, 1898-1904.
- (137) Molphy, Z.; Prisecaru, A.; Slator, C.; Barron, N.; McCann, M.; Colleran, J.; Chandran, D.; Gathergood, N.; Kellett, A. *Inorg. Chem.* **2014**, *53*, 5392-5404.
- (138) Castellano, S.; Taliani, S.; Viviano, M.; Milite, C.; Da Pozzo, E.; Costa, B.; Barresi, E.; Bruno, A.; Cosconati, S.; Marinelli, L.; Greco, G.; Novellino, E.; Sbardella, G.; Da Settimo, F.; Martini, C. *J. Med. Chem.* **2014**, *57*, 2413-2428.

Chapter 4. Experimental

4.1. General information

^1H , ^{13}C and ^{31}P NMR spectra were recorded on Jeol ECX-400 and Varian 500 AR spectrometers. ^1H and ^{13}C spectra were referenced to TSP ($\delta = 0.00$) and residual solvent peaks. ^{31}P spectra were referenced to 85% H_3PO_4 in H_2O . Residual solvent peaks were assigned using published values¹. Peak assignment was performed using 1D and 2D NMR experiments (DEPT, COSY, HSQC and HMBC). When exact ^{13}C peak assignment could not be performed, the substitution on the C is indicated by C_{prim} , C_{sec} , C_{ter} and C_{quat} . Probe temperatures were 22 °C unless otherwise stated. For pD measurements, pH values of the solutions were measured by the use of a glass electrode and the pH value was converted to pD by the addition of 0.4 to the meter reading². The pD value was adjusted using 1 M DNO_3 and 1 M NaOD in D_2O .

Mass spectrometry was performed using a Waters LCT Premiere XE with electron spray ionisation (ESI) and time of flight (TOF) mass analyser. The presence and identification of any adducts was determined using literature values³. Predicted isotopic distributions were generated using the MassLynx mass spectrometry software. For high resolution mass spectrometry (HRMS) when molecular formula is quoted the most abundant isotope is used for calculation of masses. For elements with appreciable abundance of isotopes (Cl, Br or Cu) the specific isotope is quoted.

UV/Vis measurements were performed using a Varian Cary 50 spectrophotometer. The temperature of the sample carousel was controlled by a Grant thermostated water circulation bath coupled to the spectrophotometer.

Single crystal X-ray diffraction data was collected at room temperature (293 K) on an Oxford Diffraction Xcalibur S with Sapphire 2 CCD detector using graphite-monochromatic Mo-K_α radiation ($\lambda = 0.71069 \text{ \AA}$)⁴. The structures were solved by direct methods and Fourier syntheses and were refined by full-matrix least squares on F_2 using SHELXS-97⁵, SHELXL-97^{6,7} and Oscalil⁸. The scattering factors were those given in the SHELXL program. Hydrogen atoms except those for the solvent molecules of crystallisation were generated geometrically and refined as riding atoms with isotropic displacement factors equivalent to 1.2 times those of the atom to

which they are attached (1.5 for methyl groups). Graphics were produced with ORTEX⁹.

FT-IR spectra were recorded on a Perkin Elmer FT-IR spectrometer fitted with an ATR accessory. TGA and DSC were recorded on a Rheometric Scientific STA 625 instrument. Melting points were determined using a Stuart Scientific SMP3 melting point apparatus. Elemental analysis (Carbon, Nitrogen and Hydrogen) were performed with either a Perkin Elmer 2400 series II analyser at NUIG or with an Exeter Analytical CE-440 at University College Cork (UCC). Elemental analysis was performed in either duplicate or triplicate and the average used. Prior to elemental analysis samples were dried on high-vac overnight.

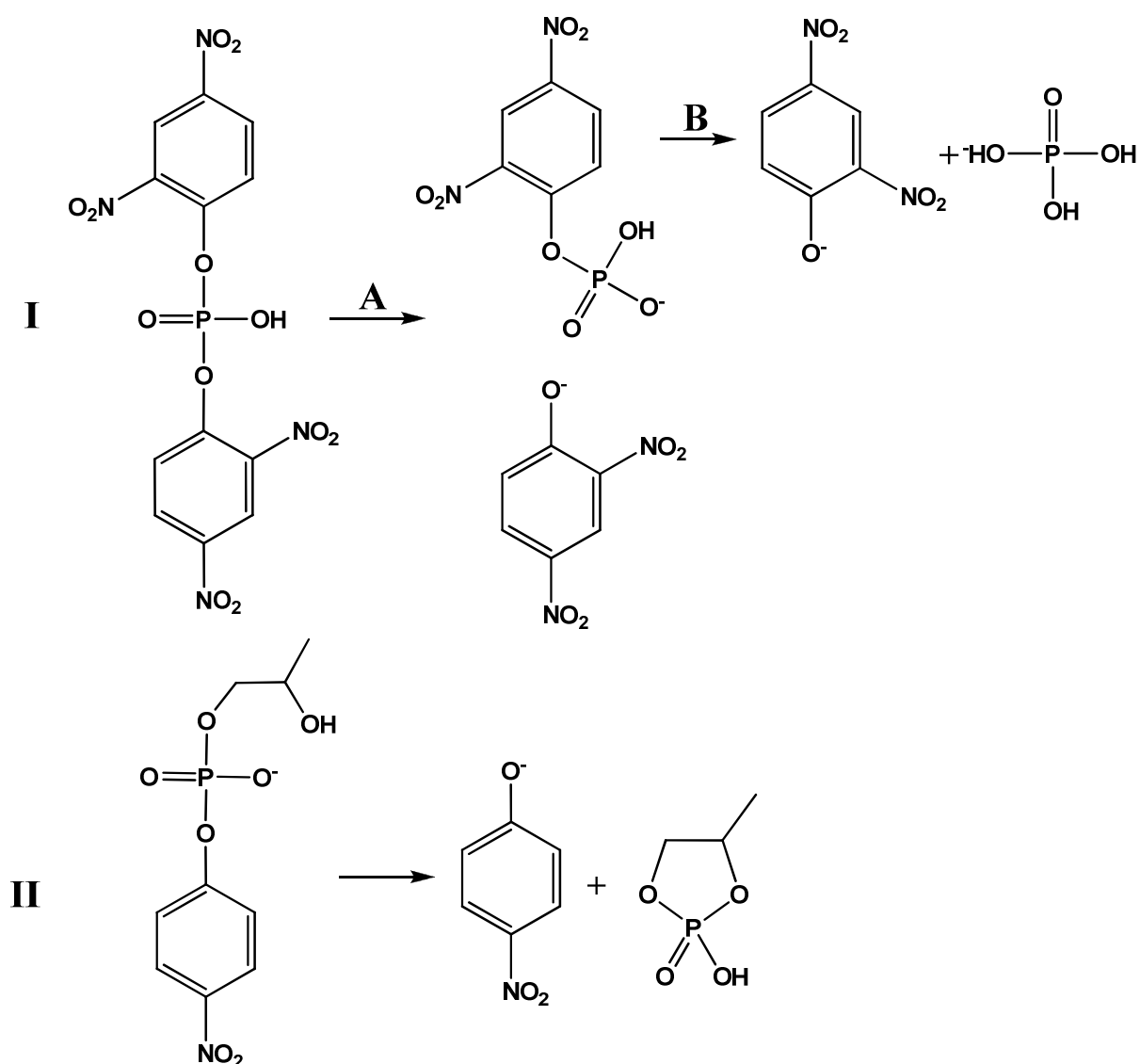
The pH of solutions was measured using a Jenway 3510 pH meter fitted with a Reflex Sensors Ltd. EC-1910-11 glass electrode. The pH meter was regularly calibrated using standard pH 4 and pH 7 buffers. Potentiometric titrations were performed in the pH range 5 – 11 with 10 ml solutions of complex at 1 mM concentration with an ionic strength of 0.1 M (KNO₃). The solutions of complex were titrated against a standard carbonate free 0.1 M NaOH solution purchased from Fisher Scientific. The program HYPERQUAD¹⁰ was used to calculate deprotonation constants from the titration data. Species diagrams were computed using a program based on the COMICS algorithm¹¹.

Microwave reactions were performed using a CEM Discover Microwave Reactor in 10 ml pressurized vials. Sonication reactions were performed using an Ultrawave precision ultrasonic cleaning bath at room temperature. Hydrogenation reactions were performed using a PARR 5500 series compact reactor coupled to a PARR 4836 controller unit.

Column chromatography was performed on either silica or where stated alumina gel. Technical grade silica gel with pore size 60 Å and activated, neutral, Brockman I alumina gel was used. Both were purchased from Sigma-Aldrich. Thin layer chromatography (TLC) was performed on TLC silica gel 60 F₂₅₄ plates. The presence or absence of compound was determined by visualising under UV lamp or by staining with either permanganate (KMnO₄) or vanillin stain. When R_f values are quoted, they are on silica gel plates.

4.2. Kinetic studies

The hydrolysis of phosphodiester analogues BDNP and HPNP were followed by measuring the release of 2,4-dinitrophenolate or 4-nitrophenolate, respectively (**Scheme 4.1**). This was done using a UV-Vis spectrophotometer monitoring the increase of absorbance at 400 nm. Concentrations of the released products were then calculated from their molar extinction co-efficients (ϵ): $12100 \text{ M}^{-1}\text{cm}^{-1}$ and $18700 \text{ M}^{-1}\text{cm}^{-1}$, respectively. The molar extinction coefficients were corrected for the degree of ionisation using the Henderson-Hasselbalch equation ¹²⁻¹⁴ ($\text{pK}_a = 4.0$ and 7.15 respectively¹⁵).



Scheme 4.1: I Hydrolysis of BDNP; II Hydrolysis of HPNP.

For both BDNP and HPNP the observed rate was corrected for the spontaneous hydrolysis of the substrate at the corresponding pH in the absence of the metal complex. Kinetic runs were done in duplicate to give a reproducibility of $\pm 20\%$.

Rate constants were obtained by the initial rates method (<5% conversion). The cut-off absorbance value, relating to 5% conversion, was calculated by the Beer-Lambert law using the corrected ϵ . Using initial rates method for BDNP minimised the contribution from the phosphomonoester hydrolysis (**Scheme 4.1 reaction I B**).

In a typical experiment UV-cuvettes containing 3ml of solution were prepared. The solution consisted of 50 mM buffer, 0.1 M ionic strength (NaOH and KNO₃), 1 mM complex (0.5 mM, 1 mM or 2 mM) and 50 μ M substrate. Each cuvette was prepared by adding portions of standard solutions of all the individual components. The resulting mixture was made up to the desired 3 ml by the addition of distilled water or solvent (DMSO or MeOH where stated). A selection of 'Goods' buffers¹⁶⁻¹⁸ were used: MES (pH 5.5 - 6.7), PIPES (pH 6.2 - 7.4), MOPS (pH 6.6 - 7.8), HEPES (pH 6.9 - 8.1), EPPS (pH 7.4 - 8.6), CHES (pH 8.7 - 9.9) and CAPS (pH 9.8 - 11.0). The pH was adjusted by addition of NaOH solution and the ionic strength was kept constant at 0.1 M using a KNO₃ solution. When the complex was generated in-situ, it was done by addition of separate ligand and metal salt solutions in appropriate amounts. Substrate was added just prior to the start of the kinetic run to ensure only the initial rate was measured. Metal salts used were Mg(CH₃COO)₂, Cu(NO₃)₂ and Ga(NO₃)₃. The concentration of the standard Mg²⁺ and Cu²⁺ solutions were confirmed by EDTA titration. The waters of crystallisation in the Ga(NO₃)₃.xH₂O salt was determined by elemental analysis and TGA analysis¹⁹.

BDNP²⁰ and HPNP²¹ were synthesised according to published procedures as their Na⁺ and Ba²⁺ salts respectively. Prior to use the purity of the substrates were confirmed by ¹H NMR, ³¹P NMR and elemental analysis.

4.3. Materials

Glycine ethyl ester, pyridine-2-carbaldehyde, picolyamine, p-cresol, diethyl iminodiacetate, formaldehyde solution, paraformaldehyde, NaBH₄, NaOH, KOH, NEt₃, SOCl₂, Mg(acetate)₂, Cu(NO₃)₂, Cu(Cl)₂, Ga(NO₃)₃.xH₂O, tyramine, di-*tert*-butyl dicarbonate, succinic anhydride, glutaric anhydride, cholic acid, DIC, dipropylamine, NEt₃, ethyl 1,2-dihydro-2-ethoxy-1-quinolinecarboxylate, 3-(4-chlorobenzoyl)propionic acid, Br₂, 2-amine-3-nitro pyridine, norephedrine, 2-chlorobenzoyl chloride, phosphorus pentoxide, SeO₂, AgNO₃, 1,10-phenanthroline and NH₄PF₆ were purchased from Sigma Aldrich, TCI and Alfa aesar and used as supplied. 6-Cl HOBt was purchased from Activotec and used as supplied. Solvents were of commercial grade and when needed to be H₂O free were dried according to literature methods²² or obtained from a Pure Solv MD-5 solvent purification system.

4.4. Synthetic procedures

4.4.1. Chapter 2: Synthesis of dinuclear complexes as artificial nucleases

4.4.1.1. Preparation of 1

Compound **1** was prepared following a literature procedure²³. ¹H NMR (400 MHz, DMSO): δ 8.27 (s, 1H, OH_F), 6.89 (s, 2H, C_CH), 5.14 (s, 2H, OH_H), 4.47 (s, 4H, C_GH₂), 2.15 (s, 3H, C_AH₃). ¹³C HMR (100 MHz, DMSO): δ 149.9 (C_E), 128.5 (C_B), 127.7 (C_D), 126.8 (C_C), 59.8 (C_G), 21.0 (C_A). ESI-LRMS *m/z* 167 [M-H]⁻. ESI-HRMS calcd for C₉H₁₁O₃ 167.0708 found *m/z* 167.0708 [M-H]⁻. IR (cm⁻¹) 3384 (m, O-H), 3303 (m, O-H), 3150 (br), 2952 (w), 2912 (w), 2877(m), 1604 (m, C=C), 1486 (m), 1462 (s), 1420 (m), 1369 (m), 1319 (m), 1263 (m), 1244 (w), 1197 (s, C_{Ar}-O), 1148 (m), 1060 (s, C-O), 1002 (w), 994 (s), 981 (m), 921 (s), 895 (w), 865 (s), 787 (m, C-H). Melting point: 130 - 131°C.

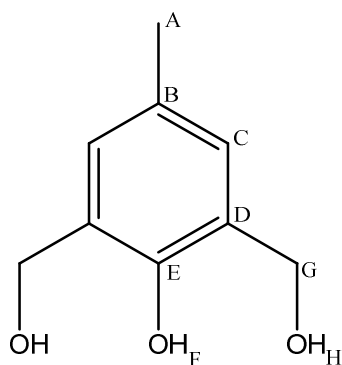


Figure 4.1: Structure of **1**.

4.4.1.2. Preparation of **2**

Compound **2** was prepared following a literature procedure²⁴. ¹H NMR and ¹³C NMR are similar to reported values²⁵. ¹H NMR (400 MHz, CDCl₃): δ 7.08 (s, 2H, C_CH), 5.54 (s, 1H, OH_F), 4.70 (s, 4H, C_GH₂), 2.26 (s, 3H, C_AH₃). ¹³C NMR (100 MHz, CDCl₃): δ 151.1 (C_E), 131.7 (C_C), 130.6 (C_B), 234.7 (C_D), 42.6 (C_G), 20.4 (C_A). ESI-LRMS *m/z* 205 [M-H]⁻. ESI-HRMS calcd for C₉H₁₁O³⁵Cl₂ 205.0187 found *m/z* 205.0198. IR (cm⁻¹) 3382 (m, O-H), 3305 (m), 3226 (m), 2920 (m), 287+ (m), 1647 (s), 1621 (w), 1596 (m), 1487 (m), 1466 (m), 1447 (w), 1437 (w), 1421 (w), 1371 (br), 1326 (m), 1301 (m), 1270 (m), 1248 (s), 1206 (s, C_{Ar}-O), 1169 (m), 1147 (m), 1130 (m), 1062 (w), 986 (s), 969 (w), 914 (m), 903 (w), 878 (w), 869 (m), 771 (s, C-Cl), 718 (m, C-H), 673 (s). Melting point 87 – 88 °C.

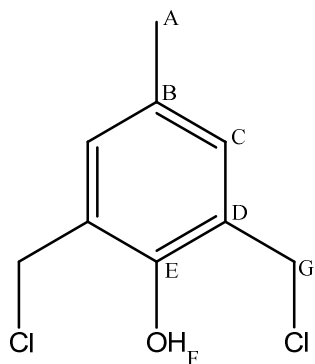


Figure 4.2: Structure of **2**.

4.4.1.3. Preparation of 3

Compound **3** was prepared using a modified literature procedure²⁶⁻²⁸. Pyridine-2-carbaldehyde (5.21 g, 48.7 mmol) was dissolved in 50 ml EtOH (anhydrous) and cooled to 0 °C. Picolyamine (5.27 g, 48.7 mmol) in 100 ml EtOH (anhydrous) was then added dropwise. After complete addition the reaction mixture was stirred at room temperature. After 4 hrs the mixture was cooled to 0 °C and sodium borohydride (3.68 g, 96.8 mmol) was added piecewise. After addition the reaction mixture was stirred at room temperature. After 16 hrs 100 ml of 10 M HCl was added dropwise and the reaction mixture was stirred at 0 °C. After 1 hr the MeOH was removed by evaporation and the pH of the mixture was adjusted to pH 11 using 2 M NaOH. The product was extracted into DCM and dried over Na₂SO₄. Evaporation of the solvent gave **3** (8.70 g, 43.7 mmol, 89.8% yield) as a brown viscous oil. ¹H NMR and ¹³C NMR peak positions agree with literature values^{28,29} but for ¹H the multiplet analysis differs. ¹H NMR (500 MHz, CDCl₃): δ 8.55 (dq, *J* = 4.8 Hz, 0.65 Hz, 2H, C_AH), 7.63 (td, *J* = 7.7 Hz, 1.8 Hz, 2H, C_CH), 7.36 (d, *J* = 8.3 Hz, 2H, C_DH), 7.14 (ddd, *J* = 7.5 Hz, 4.9 Hz, 1.0 Hz, 2H, C_BH), 3.99 (s, 4H, C_FH₂), 3.67 (s, 1H, NH_G). ¹³C NMR (100 MHz, CDCl₃): δ 159.7 (C_E), 149.4 (C_A), 136.4 (C_C), 122.7 (C_D), 122.5 (C_B), 53.7 (C_F). ESI-LRMS *m/z* 200 [M+H]⁺. ESI-HRMS calcd for C₁₂H₁₄N₃ 200.1188 found *m/z* 200.1182 [M+H]⁺. IR (cm⁻¹): 3050 (w, N-H), 3009 (w), 2824 (w), 1676 (br), 1589 (s, C=N), 1569 (s), 1518 (w, N-H), 1473 (m), 1432 (s), 1357 (w), 1293 (w), 1222 (w), 1147 (m, C-N), 1047 (m), 994 (m), 750 (s), 730 (s, C-H), 701 (w).

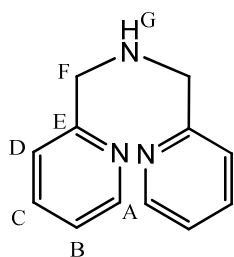


Figure 4.3: Structure of **3**.

4.4.1.4. Preparation of 4

Compound **4** was prepared by two separate means either by a known literature method³⁰ or by a novel schiff base method. Pyridine-2-carbaldehyde (5.35 g, 50 mmol) was dissolved in 100 ml MeOH. To this glycine-ethyl ester hydrochloride (6.86 g, 49 mmol) was added piecewise and the reaction mixture was stirred at room temperature. After 20 min the solution was cooled to 0 °C and sodium borohydride (1.92 g, 51 mmol) was added piecewise. After complete addition the reaction mixture was stirred at room temperature. After 16 hr 100ml of 1 M HCl was added and the reaction mixture was stirred at room temperature. After 20 min the MeOH was removed by evaporation and the resulting white precipitate was removed by filtration. The filtrate was neutralised using saturated sodium bicarbonate solution and the product was extracted into DCM and dried over Na₂SO₄. Evaporation of solvent gave **4** (7.24 g, 37.3 mmol, 74.5% yield) as a brown viscous oil. ¹H NMR agrees with previously reported data³¹. ¹H NMR (400 MHz, CDCl₃): δ 8.54 (d, *J* = 4.6 Hz, 2H, C_KH), 7.64 (td, *J* = 7.7 Hz, 1.8 Hz, C_IH), 7.32 (d, *J* = 7.8 Hz, 2H, C_HH), 7.16 (m, 2 H, C_JH), 4.14 (q, *J* = 7.2 Hz, 2 H, C_BH₂), 4.04 (s, 1 H, NH_E), 3.92 (s, 2 H, C_FH₂), 3.58 (s, 2 H, C_DH₂), 1.24 (t, *J* = 7.1 Hz, 3 H, C_AH₃). ¹³C NMR (125 MHz, CDCl₃): δ 171.1 (C_C), 158.9 (C_G), 149.2 (C_K), 136.7 (C_I), 122.4 (C_H), 122.2 (C_J), 60.5 (C_B), 54.2 (C_F), 50.1 (C_D), 14.2 (C_A). ESI-LRMS *m/z* 195 [M+H]⁺. ESI-HRMS calcd for C₁₀H₁₅N₂O₂ 195.1129, found *m/z* 195.1129 [M+H]⁺. IR (cm⁻¹): 2982 (w), 1735 (s, C=O), 1591 (m, C=N), 1570 (w, N-H), 1474 (m), 1434 (m), 1372 (m), 1187 (s, C-O), 1149 (m), 1095 (w, C-N), 1026 (s), 994 (m), 914 (w), 846 (w), 758 (m), 730 (s, C-H).

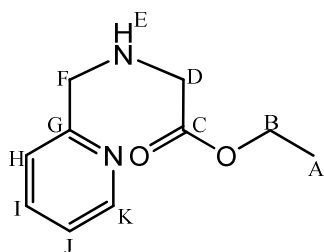


Figure 4.4: Structure of **4**.

4.4.1.5. Preparation of HL¹

Compound **HL¹** was prepared following a modified literature procedure³². The product was isolated by column chromatography in 100% Acetone. The R_f of the product in Acetone is 0. ¹H NMR broadly agrees with reported data³² but multiplet analysis in the aromatic region differs. ¹H NMR (400 MHz, CDCl₃): δ 8.51 (d, J = 4.8 Hz, 4H, C_MH), 7.60 (t, J = 7.6 Hz, 4H, C_KH), 7.49 (d, J = 7.8 Hz, 4H, C_JH), 7.11 (m, 4H, C_LH), 6.99 (C_CH), 5.5 (br, 1H, OH_F), 3.85 (s, 8H, C_HH₂), 3.76 (s, 4H, C_GH₂), 2.23 (s, 3H, C_AH₃). ¹³C NMR (100 MHz, CDCl₃): δ 159.4 (C_I), 153.7 (C_E), 149.0 (C_M), 136.6 (C_K), 130.8 (C_B), 129.8 (C_C), 123.9 (C_D), 123.0 (C_J), 122.0 (C_L), 59.9 (C_H), 54.9 (C_G), 22.4 (C_A). ESI-LRMS m/z 531 [M+H]⁺. ESI-HRMS calcd for C₃₃H₃₅N₆O 531.2872 found m/z 531.2867 [M+H]⁺. IR (cm⁻¹): 3063 (w), 3011 (w), 2928 (w), 2821 (m), 1588 (s, C=N), 1570 (m), 1474 (s), 1430 (s), 1363 (s), 1312 (w), 1296 (m), 1233 (s, C_{Ar}-O), 1134 (m, C-N), 1048 (m), 1001 (m), 980 (m), 871 (m), 790 (m), 754 (s, C-H).

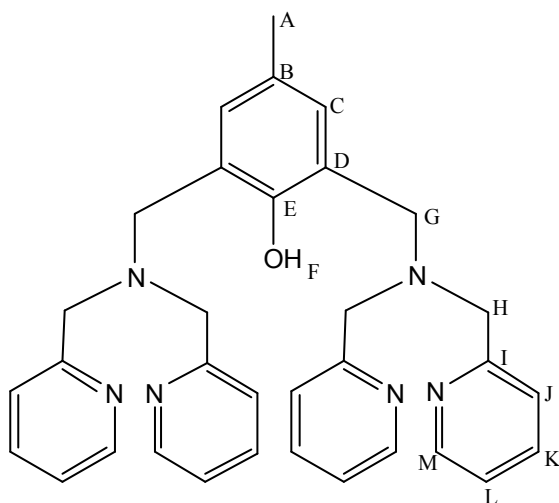


Figure 4.5: Structure of HL¹.

4.4.1.6. Preparation of 5

Compound **4** (2.42 g, 12.5 mmol) was dissolved in a solution of 70 ml THF (dry) and NEt₃ (7 ml, 50 mmol). To this compound **2** (1.27 g, 6.25 mmol) was added piecewise and the reaction mixture was stirred at room temperature. After 16 hrs the reaction mixture was filtered to remove the yellow precipitate (NEt₃HCl) and the filtrate was evaporated to dryness. The product was isolated by gradient column

chromatography 0 - 5% MeOH: DCM. The R_f of the product in 95:5 DCM: MeOH is 0.58. Evaporation of solvent gave **5** (2.72 g, 5.2 mmol, 84% yield) as a brown viscous liquid. ^1H NMR (500 MHz, CDCl_3): δ 8.48 (d, $J = 4.4$ Hz, 2H, $\text{C}_\text{J}\text{H}$), 7.62 (td, $J = 7.8$ Hz, 1.7 Hz, 2H, $\text{C}_\text{H}\text{H}$), 7.47 (d, $J = 3.8$ Hz, 2H, $\text{C}_\text{G}\text{H}$), 7.10-7.15 (m, 2H, $\text{C}_\text{I}\text{H}$), 6.90 (s, 2H, $\text{C}_\text{M}\text{H}$), 5.25 (s, 1H, OH_Q), 4.12 (q, $J = 7.2$ Hz, 4H, $\text{C}_\text{B}\text{H}_2$), 3.92 (s, 4H, $\text{C}_\text{E}\text{H}_2$), 3.83 (s, 4H, $\text{C}_\text{K}\text{H}_2$), 3.56 (s, 4H, $\text{C}_\text{D}\text{H}_2$), 2.18 (s, 3H, $\text{C}_\text{O}\text{H}_3$), 1.22 (t, $J = 7.1$ Hz, 6H, $\text{C}_\text{A}\text{H}_3$). ^{13}C NMR (125 MHz, CDCl_3): δ 171.4 (C_C), 158.2 (C_F), 153.5 (C_P), 148.7 (C_J), 136.8 (C_H), 130.1 (C_M), 127.6 (C_N), 123.3 (C_G), 123.1 (C_L), 122.2 (C_I), 60.5 (C_B), 59.3 (C_E), 54.8 (C_D), 54.4 (C_K), 20.5 (C_O), 14.2 (C_A). ESI-LRMS m/z 521 $[\text{M}+\text{H}]^+$, 543 $[\text{M}+\text{Na}]^+$, 519 $[\text{M}-\text{H}]^-$. ESI-HRMS calcd for $\text{C}_{29}\text{H}_{37}\text{N}_4\text{O}_5$ 521.2764 found m/z 521.2739 $[\text{M}+\text{H}]^+$. IR (cm^{-1}): 2982 (w, $\text{O}-\text{H}$), 2252 (w), 1736 (s, $\text{C}=\text{O}$), 1592 (w, $\text{C}=\text{N}$), 1571 (w), 1477 (m), 1435 (m), 1370 (m), 1296 (w), 1264 (w), 1191 (s, $\text{C}-\text{O}$), 1151 (m, $\text{C}_\text{Ar}-\text{O}$), 1095 (w), 1068 (w), 1028 (m), 909 (s), 866 (w), 849 (w), 761 (w), 726 (s, $\text{C}-\text{H}$)

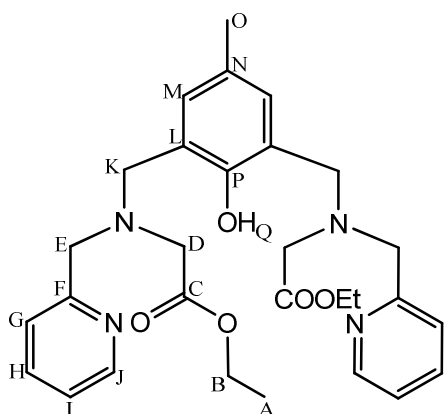


Figure 4.6: Structure of **5**.

4.4.1.7. Preparation of Na_3L^2

Compound **5** (0.69 g, 1.32 mmol) was dissolved in 20 ml EtOH. To this KOH (0.58 g, 10.36 mmol) was added and the reaction mixture was stirred at room temperature. After 72 hr the mixture was passed through an Amberlite 120 H^+ column. The effluent was evaporated, redissolved in MeOH and subsequently passed through an Amberlite 120 Na^+ column. Evaporation of MeOH gave H_3L^2 (0.45 g, 0.97 mmol, 64.3% yield) as the tri-sodium salt as a brown solid. ^1H NMR (500 MHz, DMSO): δ 8.47 (dq, $J = 4.8$ Hz, 0.8 Hz, 2H, $\text{C}_\text{J}\text{H}$), 7.72 (td, $J = 7.6$ Hz, 1.8 Hz, 2H, $\text{C}_\text{H}\text{H}$), 7.38 (d, $J = 7.8$ Hz, 2H, $\text{C}_\text{G}\text{H}$), 7.24 (ddd, $J = 7.5$ Hz, 4.8 Hz, 1.1 Hz, 2H, $\text{C}_\text{I}\text{H}$), 6.88 (s,

3H, $C_M\mathbf{H}$), 3.84 (s, 4H, $C_E\mathbf{H}_2$), 3.74 (s, 4H, $C_K\mathbf{H}_2$), 3.22 (s, 4H, $C_D\mathbf{H}_2$), 2.16 (s, 3H, $C_O\mathbf{H}_3$). ^{13}C NMR (125 MHz, DMSO- d_6): δ 172.8 (C_A), 159.0 (C_F), 153.7 (C_C), 149.1 (C_J), 137.2 (C_H), 130.1 (C_B), 126.8 (C_L), 123.6 (C_M), 123.2 (C_G), 122.7 (C_I), 58.8 (C_E), 54.6 (C_D), 54.1 (C_K), 20.7 (C_O). ESI-LRMS m/z 463 $[\text{M}-\text{H}]^-$. ESI-HRMS calcd for $\text{C}_{25}\text{H}_{27}\text{N}_4\text{O}_5$ 463.1981, found m/z 463.1999 $[\text{M}-\text{H}]^-$. IR (cm^{-1}): 2920 (br), 1715 (w, $\text{C}=\text{O}$), 1632 (m, $\text{C}=\text{N}$), 1592 (s), 1573 (m), 1482 (m), 1434 (m), 1387 (s), 1300 (m, $\text{C}_{\text{Ar}}-\text{O}$), 1218 (s, $\text{C}-\text{O}$), 1151 (m, $\text{C}-\text{N}$), 1049 (w), 996 (m), 863 (m), 760 (s, $\text{C}-\text{H}$), 694 (m). Anal calcd (%) for $\text{C}_{25}\text{H}_{25}\text{N}_4\text{Na}_3\text{O}_5$: C, 56.61; H, 4.75; N, 10.56; Found: C, 56.89; H, 5.01; N, 10.24. Melting point: 72 - 73 $^\circ\text{C}$.

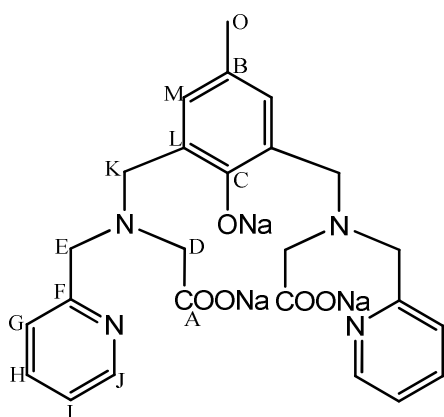


Figure 4.7: Structure of H_3L^2 .

4.4.1.8. Preparation of 6

Compound **6** was prepared following a literature procedure³³. ^1H and ^{13}C NMR match literature values³³. ^1H NMR (400 MHz, CDCl_3): δ 11.30 (s, 1H, CH_G), 9.85 (s, 1H, OH_I), 7.42 (s, 1H, $\text{C}_C\mathbf{H}$), 7.33 (s, 1H, $\text{C}_B\mathbf{H}$), 4.55 (s, 2H, $\text{C}_H\mathbf{H}_2$), 2.33 (s, 3H, $\text{C}_A\mathbf{H}_3$). ^{13}C NMR (100 MHz, CDCl_3): δ 196.5 (C_G), 157.5 (C_F), 139.0 (C_C), 123.4 (C_B), 129.4 (C_E), 126.1 (C_D), 120.6 (C_J), 26.8 (C_H), 20.3 (C_A). ESI-LRMS m/z 229 $[\text{M}+\text{H}]^+$. ESI-HRMS calcd for $\text{C}_9\text{H}_{10}^{79}\text{BrO}_2$ 228.9859 found m/z 228.228.9862 $[\text{M}+\text{H}]^+$. IR (cm^{-1}): 3177 (br, $\text{O}-\text{H}$), 2853 (w), 1750 (m, $\text{C}=\text{O}$), 1658 (s), 1596 (m), 1466 (m), 1419 (m), 1376 (m), 1295 (m), 1267 (m), 1209 (s, $\text{C}_{\text{Ar}}-\text{O}$), 1164 (m), 1121 (m), 1023 (w), 975 (m), 874 (m), 784 (m), 757 (m, $\text{C}-\text{H}$), 699 (s, $\text{C}-\text{Br}$).

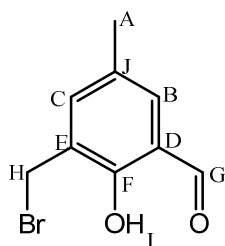


Figure 4.8: Structure of **6**.

4.4.1.9. Preparation of **7**

Compound **7** was prepared following a modified literature procedure³⁴. Procedure was similar to reported but compound **6** was used rather than the corresponding chloro analogue. ¹H NMR (400 MHz, CDCl₃): δ 10.43 (s, 1H, C_IH), 8.56 (d, *J* = 3.8 Hz, 2H, C_PH), 7.70 – 7.59 (m, 2H, C_NH), 7.44 (s, 1H, C_CH), 7.38 (d, *J* = 7.8 Hz, 2H, C_MH), 7.20 (s, 1H, C_DH), 7.19 – 7.14 (m, 2H, C_OH), 5.50 (br, 1H, OH_H), 3.88 (s, 4H, C_KH₂), 3.79 (s, 2H, C_JH₂), 2.26 (s, 3H, C_AH₃). ¹³C NMR (100 MHz, CDCl₃): δ 192.4 (C_I), 158.7 (C_L), 150.6 (C_G), 149.4 (C_P), 139.4 (C_D), 136.5 (C_N), 136.0 (C_E), 130.4 (C_F), 122.9 (C_C), 122.4 (C_B), 122.0 (C_M), 121.7 (C_O), 54.9 (C_K), 53.5 (C_J), 20.2 (C_A). ESI-LRMS *m/z* 348 [M+H]⁺, 346 [M-H]⁻. ESI-HRMS calcd for C₂₁H₂₂N₃O₂ 348.1712, found *m/z* 348.1695 [M+H]⁺. IR (cm⁻¹): 3063(w, O-H), 2924 (w), 2816 (br), 2706 (w), 1752 (m, C=O), 1648 (s), 1591 (s, C=N), 1570 (m), 1524 (m), 1467 (m), 1432 (m), 1376 (br), 1262 (m), 1241 (m), 1218 (m, C_{Ar}-O), 1165 (w), 1148 (m, C-N), 1109 (w), 1094 (w), 1048 (m), 994 (m), 941 (w), 869 (m), 841 (w), 808 (m), 754 (m), 730 (s, C-H), 701 (m), 670 (w).

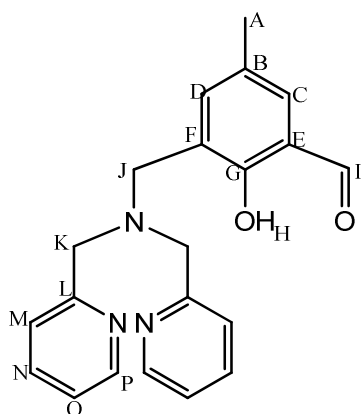


Figure 4.9: Structure of **7**.

4.4.1.10. Preparation of 8

Compound **8** was prepared following a modified literature procedure³⁵. It was found if the reaction mixture was stirred at the reported 2.5 hours only partial reduction took place so the reaction was stirred for 16 hrs. ¹H NMR similar to literature values³⁵ but multiplet analysis differs. ¹H NMR (400 MHz, CDCl₃) δ 11.31 (br, 1H, OH_H), 8.51 (d, *J* = 4.8 Hz, 2H, C_PH), 7.58 (td, *J* = 7.6, 1.4 Hz, 2H, C_NH), 7.27 (d, *J* = 8.2 Hz, 2H, C_MH), 7.16 – 7.05 (m, 2H, C_OH), 6.93 (s, 1H, C_CH), 6.78 (s, 1H, C_DH), 4.70 (s, 2H, C_IH₂), 3.93 (br, 1H, OH_Q), 3.82 (s, 4H, C_KH₂), 3.70 (s, 2H, C_JH₂), 2.19 (s, 3H, C_AH₃). ¹³C NMR (100 MHz, CDCl₃): δ 158.3 (C_L), 149.4 (C_G), 149.0 (C_P), 136.6 (C_N), 130.3 (C_D), 128.9 (C_C), 127.8 (C_E), 123.3 (C_F), 122.57 (C_B), 122.34 (C_M), 122.03 (C_O), 63.0 (C_I), 56.9 (C_K), 54.9 (C_J), 20.5 (C_A). ESI-LRMS *m/z* 350 [M+H]⁺. ESI-HRMS calcd for C₂₁H₂₄N₃O₂ 350.1869, found 350.1865. IR (cm⁻¹): 3012 (w, O-H), 2922 (w, O-H), 2832 (w), 1711 (br), 1671 (w), 1591 (m, C=N), 1570 (m), 1474 (m), 1432 (s), 1362 (m), 1289 (w), 1265 (w), 1221 (br, C_{Ar}-O), 1149 (m, C-N), 1123 (w), 1090 (w), 1049 (m, C-O), 994 (br), 878 (m), 861 (m), 753 (m), 731 (s, C-H), 704 (m), 663 (w).

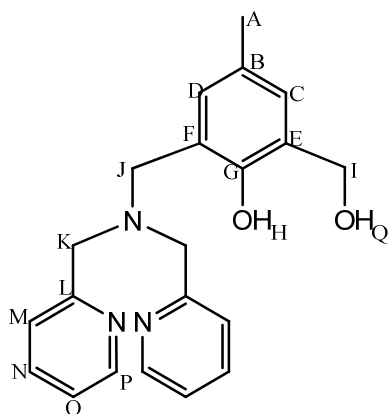


Figure 4.10: Structure of **8**.

4.4.1.11. Preparation of 10

Compound **10** was prepared following a literature procedure³⁶. ¹H NMR (400 MHz, CDCl₃): δ 4.08 (q, *J* = 6.9 Hz, 4H, C_BH₂), 3.36 (s, 4H, C_DH₂), 2.08 (br, 1H, NH_E), 1.18 (t, *J* = 7.4 Hz, 6H, C_AH₃). ¹³C NMR (100 MHz, CDCl₃): δ 171.8 (C_C), 60.8 (C_B), 50.1 (C_D), 14.2 (C_A). ESI-LRMS *m/z* 190 [M+H]⁺. ESI-HRMS calcd for C₈H₁₆NO₄ 190.1079 found *m/z* 190.1071 [M+H]⁺. IR (cm⁻¹): 3352 (br), 2983 (m),

1733 (s, C=O), 1682 (w), 1467 (w), 1446 (w), 1415 (w), 1370 (m), 1262 (w), 1183 (s), 1154 (s, C-O), 1096 (m), 1024 (s), 964 (m), 857 (m), 761 (br, C-H).

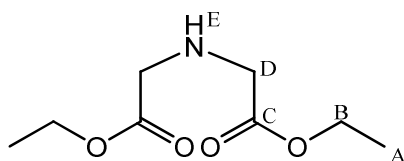


Figure 4.11: Structure of **10**.

4.4.1.12. Preparation of **11**

Compound **11** was prepared following a modified literature procedure³⁷. In a one-pot reaction compound **8** was converted to **9**³⁴ and subsequently reacted with **10** to give **11**. Compound **8** (5.73 g, 16.4 mmol) was dissolved in 150 ml DCM (anhydrous). To this SOCl₂ (7.2 ml, 0.1 mol) was added and the reaction mixture was stirred at room temperature under N₂. After 4 hr the excess SOCl₂ was removed by distillation and then washed with several portions of petroleum ether (5 x 50ml) to give compound **9**. This was then dissolved in 120 ml DCM (dry) and a mixture of NEt₃ (5 ml, 35.9 mmol) and compound **11** (3.02 g, 16mmol) in 20 ml DCM (dry) were added. Upon addition white gas was produced, this was removed by a N₂ gas stream and the reaction mixture was stirred at reflux under N₂. After 72 hr the reaction mixture was let cool and was stirred at room temperature. After 24 hr the reaction mixture was washed with saturated NaHCO₃ solution. The organic layer was dried with Na₂SO₄ and evaporated to dryness. The product was purified by gradient column chromatography 0 - 10% MeOH: DCM. Product R_f in 9:1 DCM: MeOH is 0. Evaporation of solvent gave **11** (5.2 g, 10 mmol, 62.5% yield) as a brown viscous oil. ¹H NMR (500MHz, CDCl₃): δ 8.50 (dq, *J* = 4.9 Hz, 0.9 Hz, 2H, C_TH), 7.60 (td, *J* = 7.7 Hz, 1.0 Hz, 2H, C_RH), 7.41 (d, *J* = 7.9 Hz, 2H, C_QH), 7.10 (ddd, *J* = 7.5 Hz, 4.9 Hz, 1.1 Hz, 2H, C_SH), 6.93 (s, 1H, C_GH), 6.91 (s, 1H, C_JH), 4.15 (q, *J* = 7.1 Hz, 4H, C_BH₂), 3.94 (s, 2H, C_EH₂), 3.83 (s, C_OH₂), 3.76 (s, 2H, C_NH₂), 3.54 (s, 4H, C_DH₂), 2.19 (s, 3H, C_IH₃), 1.22 (t, *J* = 7.1 Hz, 6H, C_AH₃). ¹³C NMR (125 MHz, CDCl₃): δ 171.3 (C_C), 158.7 (C_P), 153.6 (C_L), 148.8 (C_T), 136.6 (C_R), 130.3 (C_K), 130.2 (C_F), 127.6 (C_H), 123.3 (C_G), 123.1 (C_Q), 123.0 (C_J), 122.0 (C_S), 60.5 (C_B), 59.4 (C_O), 55.4 (C_N), 54.4 (C_D), 53.2 (C_E), 20.5 (C_I), 14.2 (C_A). ESI-LRMS 521 [M+H]⁺. ESI-HRMS calcd for C₂₉H₃₇N₄O₅ 521.2764, found *m/z* 521.2762 [M+H]⁺.

IR (cm⁻¹): 2992 (w), 2912 (w), 1733 (s, C=O), 1643 (w), 1591 (m), 1570 (m), 1476 (s), 1433 (s), 1374 (m), 1190 (s, C_{Ar}-O), 1148 (s, C-O), 1026 (s), 996 (m), 864 (m), 756 (s, C-H), 705 (w).

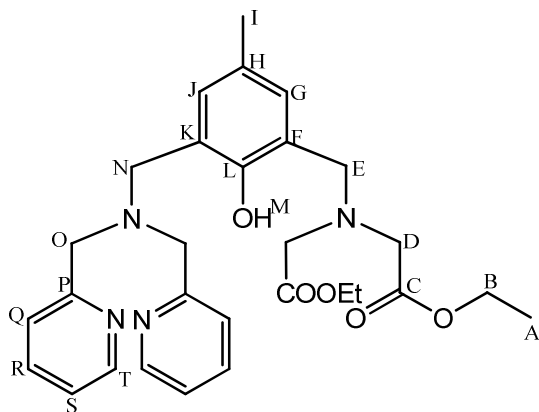


Figure 4.12: Structure of **11**.

4.4.1.13. Preparation of Na₃L³

Compound **11** (1.17 g, 2.24 mmol) was dissolved in 20 ml EtOH. To this KOH (1.16 g, 20.7 mmol) was added and the reaction mixture stirred at room temperature. After 24 hr the reaction mixture was passed through an Amberlite 120 H⁺ column. The effluent was evaporated to dryness, redissolved in MeOH and passed through an Amberlite 120 Na⁺ column. Evaporation of MeOH gave **H₃L³** (0.87 g, 1.9 mmol, 73% yield) as the tri-sodium salt as a brown solid. ¹H NMR (500 MHz, DMSO): δ 8.50 (dq, *J* = 4.8 Hz, 0.8 Hz, 2H, C_qH), 7.75 (td, *J* = 7.7 Hz, 1.7 Hz, 2H, C_cH), 7.40 (d, *J* = 7.2 Hz, 2H, C_mH), 7.24 (dd, *J* = 6.8 Hz, 5.1 Hz, 2H, C_bH), 6.91 (s, C_jH), 6.81 (s, C_gH), 3.77 (s, 2H, C_eH₂), 3.74 (s, 4H, C_oH₂), 3.64 (s, 2H, C_nH₂), 3.22 (s, 4H, C_dH₂), 2.15 (s, 3H, C_iH₃). ¹³C NMR (125 MHz, DMSO): δ 173.9 (C_a), 158.8 (C_p), 153.7 (C_l), 149.2 (C_q), 137.3 (C_c), 130.5 (C_k), 129.95 (C_h), 129.92 (C_g), 129.65 (C_f), 129.61 (C_j), 123.3 (C_m), 122.7 (C_b), 59.2 (C_o), 59.10 (C_d), 55.0 (C_n), 52.9 (C_e), 20.7 (C_i). ESI-LRMS *m/z* 463 [M-H]⁻, 456 [M+H]⁺. ESI-HRMS calcd for C₂₅H₂₉N₄O₅ 465.2138, found *m/z* 465.2124 [M+H]⁺. IR (cm⁻¹) 3367 (br), 3007 (w), 2821 (w), 1621 (s), 1593 (s), 1570 (m), 1482 (m), 1733 (m, C=O), 1391 (s), 1322 (m), 1289 (m, C-O), 1234 (m, C_{Ar}-O), 1150 (w, C-N), 1123 (w, C-N), 1091 (w), 1049 (m), 996 (m), 965 (m), 903 (m), 864 (m), 757 (s, C-H), 697 (m). Anal calcd (%) for C₂₅H₂₅N₄Na₃O₅: C, 56.61; H, 4.75; N, 10.56; Found: C, 56.27; H, 4.38; N, 10.54. Melting point: 69 - 71 °C.

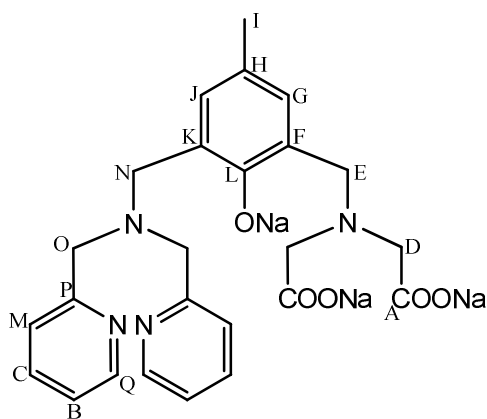


Figure 4.13: Structure of Na_3L^3 .

4.4.1.14. Preparation of $[\text{Mg}_2(\text{L}^1)(\text{acetate})_2]\text{BF}_4$

Compound HL^1 (0.26 g, 0.49 mmol) was dissolved in 15 ml MeOH. To this NEt_3 (0.14 ml, 1 mmol) and Magnesium Acetate (0.22 g, 1 mmol) was added. The reaction mixture was stirred at reflux under N_2 . After 2 hr the reaction mixture was let cool and NaBF_4 (0.056 g, 0.5 mmol) was added. The mixture was refrigerated overnight. After filtration and air-drying $[\text{Mg}_2(\text{L}^1)(\text{acetate})_2](\text{BF}_4)$ (0.116 g, 0.15 mmol, 30.6 % yield) was isolated as a white powder. ^1H NMR (500 MHz, DMSO-d_6): δ 8.58-8.61 (m, 2H, C_LH), 8.23-8.19 (m, 2H, C_LH), 7.99 (td, $J = 7.7$ Hz, 1.8 Hz, 2H, C_JH), 7.61 (d, $J = 7.8$ Hz, 2H, C_IH), 7.49 (dd, $J = 7.6$ Hz, 5.2 Hz, 2H, C_KH), 7.40 (td, $J = 7.7$ Hz, 1.7 Hz, 2H, C_JH), 7.08-7.12 (m, 2H, C_KH), 6.55 (d, $J = 7.8$ Hz, 2H, C_IH), 6.42 (s, 2H, C_CH), 4.42 (d, $^2J = 14.5$ Hz, 2H, C_GH_2), 4.03 (d, $^2J = 14.5$ Hz, 2H, C_GH_2), 3.68 (d, $^2J = 10.0$ Hz, 2H, C_FH_2), 3.53 (d, $^2J = 16.7$ Hz, 2H, C_GH_2), 3.37 (d, $^2J = 16.5$ Hz, 2H, C_GH_2), 3.14 (d, $^2J = 10.9$ Hz, 2H, C_FH_2), 2.02 (s, 6H, $\text{C}_{\text{acetate}}\text{H}_3$), 1.91 (s, 3H, C_AH_3). ^{13}C NMR (125 MHz, CDCl_3 , DMSO-d_6): δ 179.1 ($\text{C}_{\text{acetate}}$), 160.2 (C_E), 156.8 (C_H), 156.7 (C_H), 148.2 (C_L), 146.6 (C_L), 139.7 (C_J), 138.3 (C_J), 136.8 (C_D), 131.1 (C_C), 124.45 (C_I), 124.41 (C_B), 124.35 (C_K), 122.8 (C_K), 121.0 (C_I), 60.3 (C_G), 59.4 (C_F), 58.4 (C_G), 25.4 ($\text{C}_{\text{acetate}}\text{H}_3$), 20.3 (C_A). IR (cm^{-1}) 2844 (w), 1602(s, $\text{C}=\text{N}$), 1571 (m), 1481 (m), 1429 (s), 1365 (w), 1342 (w), 1324 (m), 1292 (w), 1281 (w), 1154 (m, $\text{C}-\text{N}$), 1091 (m), 1046 (s), 1012 (s), 975 (w), 954 (w), 910 (w), 882 (w), 859 (w), 828 (w), 807 (m), 759 (s, $\text{C}-\text{H}$), 742 (w), 730 (w). Anal calcd (%) for $\text{C}_{37}\text{H}_{41}\text{BF}_4\text{Mg}_2\text{N}_6\text{O}_5$: C, 56.60; H, 5.26; N, 10.70; found: C, 56.87; H, 4.97; N, 10.33 %. Melting point 264 – 265 °C.

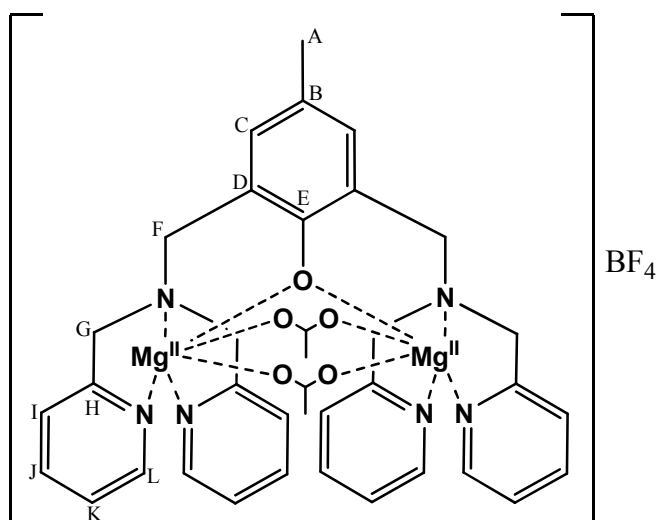


Figure 4.14: Structure of $[\text{Mg}_2(\text{L}^1)(\text{acetate})_2]\text{BF}_4$.

4.4.1.15. Preparation of $[\text{Cu}_2(\text{L}^2)(\text{H}_2\text{O})_2]\text{NO}_3$

The tri-sodium salt of H_3L^2 (106 mg, 0.2 mmol) was dissolved in 3.08 ml H_2O . To this 1.92 ml of a 0.207 M solution of $\text{Cu}(\text{NO}_3)_2$, (0.4 mmol) was added. The reaction mixture was heated to 60 °C in a sealed container. After 4 hr the reaction mixture was let cool and the pH was adjusted from 0.57 to 4.03 using 0.2 M NaOH. Slow evaporation of the solution over 1 week yielded $[\text{Cu}_2(\text{L}^2)(\text{H}_2\text{O})_2]\text{NO}_3$ (29 mg, 42 μmol , 21.1% yield) as dark green crystals. Crystals suitable for x-ray crystallography were obtained from repeating the same reaction at a 10 times smaller scale and leaving for 2 weeks. IR (cm^{-1}): 3222(br, **O-H**), 1648(m), 1606(s, **C=N**), 1475(s), 1450(w), 1425(m), 1374(s, **NO**₃), 1355(w), 1315(s), 1291(s, **C_{Ar}-O**), 1165(m, **C-N**), 1099(m), 1029(m), 959(m), 886(m), 867(m), 826(m), 772(m, **C-H**). Anal Calcd (%) for $\text{C}_{25}\text{H}_{29}\text{Cu}_2\text{N}_5\text{O}_{10}$: C, 43.73; H, 4.26; N, 10.20; found C, 43.44; H, 4.15; N, 10.13%. Melting point 222 °C.

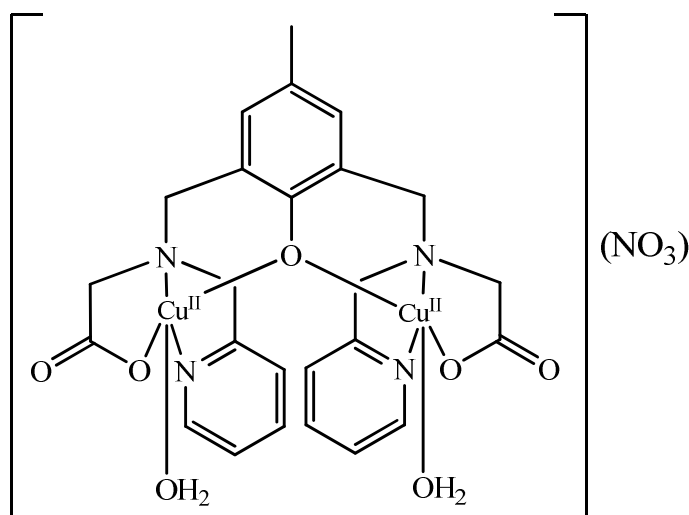


Figure 4.15: Structure of $[\text{Cu}_2(\text{L}^2)(\text{H}_2\text{O})_2]\text{NO}_3$.

4.4.1.16. Preparation of $[\text{Cu}_2(\text{L}^3)(\text{H}_2\text{O})_2]\text{NO}_3$

The tri-sodium salt of H_3L^3 (13.31 mg, 29 μmol) was dissolved in 39.5 μl H_2O . To this 210.8 μl of a 0.213 M solutions of $\text{Cu}(\text{NO}_3)_2$ (45 μmol) was added. The reaction mixture was heated to 60 $^\circ\text{C}$ in a sealed container. After 4 hr the reaction mixture was let cool and the pH was adjusted from 2.06 to 6.18 using 0.2 M NaOH. After standing for 2 days the solution was filtered. The product $[\text{Cu}_2(\text{L}^3)(\text{H}_2\text{O})_2]\text{NO}_3$ (8 mg, 12 μmol , 41.4% yield) was obtained as a black crystalline solid. IR (cm^{-1}): 3496 (w), 3371 (br, **O-H**), 2911 (w), 1650 (m), 1593 (s, **C=N**), 1530 (w), 1476 (s), 1439 (m), 1385 (s, **NO}_3**), 1355 (m), 1303 (w), 1295 (w), 1264 (m), 1231 (w), 1204 (w), 1153 (m, **C-N**), 1113 (w), 1096 (m), 1081 (m), 1053 (m), 1013 (m), 987 (w), 960 (m), 918 (s), 892 (m), 879 (m), 864 (m), 843 (w), 832 (w), 795 (m), 776 (m), 760 (s, **C-H**), 664 (m). ESI-LRMS (MeOH) m/z 619 $[\text{M}-(\text{H}_2\text{O})_2-(\text{NO}_3)+\text{MeOH}]^+$. ESI-LRMS (1:1 H_2O : ACN) m/z 605 $[\text{M}-\text{H}_2\text{O}-\text{NO}_3]^+$. ESI-HRMS (MeOH) calcd for $\text{C}_{26}\text{H}_{29}\text{N}_4\text{O}_6^{63}\text{Cu}_2$ 619.0679 found m/z 619.0660 $[\text{M}-(\text{H}_2\text{O})_2-(\text{NO}_3)+\text{MeOH}]^+$. ESI-HRMS (1:1 H_2O : ACN) calcd. for $\text{C}_{25}\text{H}_{27}\text{N}_4\text{O}_6^{63}\text{Cu}_2$ 605.0523 found m/z 605.0549 $[\text{M}-\text{H}_2\text{O}-\text{NO}_3]^+$. Anal Calcd (%) for $\text{C}_{25}\text{H}_{29}\text{Cu}_2\text{N}_5\text{O}_{10}$: C, 43.73; H, 4.26; N, 10.20; found C, 43.39; H, 4.71; N, 9.77%. Melting point 240 – 243 $^\circ\text{C}$.

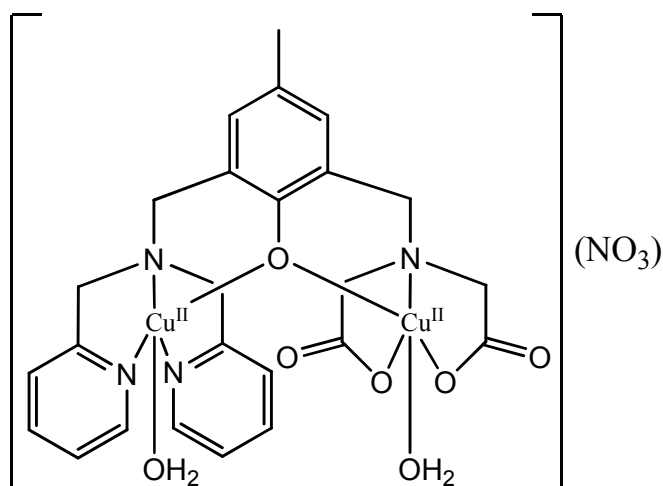


Figure 4.16: Structure of $[\text{Cu}_2(\text{L}^3)(\text{H}_2\text{O})_2]\text{NO}_3$.

4.4.1.17. Preparation of $[\text{Ga}_2(\text{L}^1)(\text{acetate})_2](\text{ClO}_4)_3$

Compound was prepared following a literature procedure³⁸. ^1H and ^{13}C spectra broadly match with literature values³⁸ but published spectra was in CD_3CN leading to a shift in value for some peaks. ^1H NMR (400 MHz, DMSO-d_6): δ 8.79 (d, $J = 5.3$ Hz, 2H, $\text{C}_\text{L}\text{H}$), 8.54 (s, $J = 5.2$ Hz, 2H, $\text{C}_\text{L}\text{H}$), 8.38 (t, $J = 7.8$ Hz, 2H, $\text{C}_\text{J}\text{H}$), 8.04 (d, $J = 7.8$ Hz, 2H, $\text{C}_\text{I}\text{H}$), 7.89 (t, $J = 7.8$ Hz, 2H, $\text{C}_\text{J}\text{H}$), 7.81 (t, $J = 6.7$ Hz, 2H, $\text{C}_\text{K}\text{H}$), 7.51 (t, $J = 6.5$ Hz, 2H, $\text{C}_\text{K}\text{H}$), 7.06 (d, $J = 8$ Hz, 2H, $\text{C}_\text{I}\text{H}$), 6.81 (s, 2H, $\text{C}_\text{C}\text{H}$), 4.86 (d, $^2J = 15.8$ Hz, 2H, $\text{C}_\text{G}\text{H}_2$), 4.76 (d, $^2J = 15.6$ Hz, 2H, $\text{C}_\text{G}\text{H}_2$), 4.24 (m, 4H, $\text{C}_\text{F}\text{H}_2$, $\text{C}_\text{G}\text{H}_2$), 3.99 (m, 4H, $\text{C}_\text{F}\text{H}_2$, $\text{C}_\text{G}\text{H}_2$), 2.41 (s, 6H, $\text{C}_\text{acetate}\text{H}_3$), 2.05 (s, 3H, $\text{C}_\text{A}\text{H}_3$). ^{13}C NMR (100 MHz, DMSO-d_6): δ 184.1 (C_acetate), 164.5 (C_E), 156.7 (C_H), 152.8 (C_H), 148.6 (C_L), 147.1 (C_L), 138.7 (C_J), 138.65 (C_J), 136.4 (C_D), 132.9 (C_C), 124.5 (C_I), 124.4 (C_B), 124.3 (C_K), 121.8 (C_K), 121.0 (C_I), 59.7 (C_F), 58.85 (C_G), 58.8 (C_G), 26.7 ($\text{C}_\text{acetate}\text{H}_3$), 21.8 (C_A). IR (cm^{-1}): 3554 (br), 3098 (w), 2980 (w), 1738 (w), 1611 (m), 1584 (s, $\text{C}=\text{N}$), 1482 (m), 1437 (s), 1308 (w), 1294 (w), 1262 (w), 1238 (w), 1207 (w), 1071 (s), 1053 (s, $\text{C}-\text{N}$), 1027 (s), 952 (w), 886 (w), 806 (w), 775 (m), 725 (w, $\text{C}-\text{H}$), 661 (m). Anal calcd (%) for $\text{C}_{37}\text{H}_{43}\text{N}_6\text{O}_{19}\text{Cl}_3\text{Ga}_2$: C, 39.62; H, 3.86; N, 7.49. found: C, 39.51; H, 3.93; N, 7.35 %.

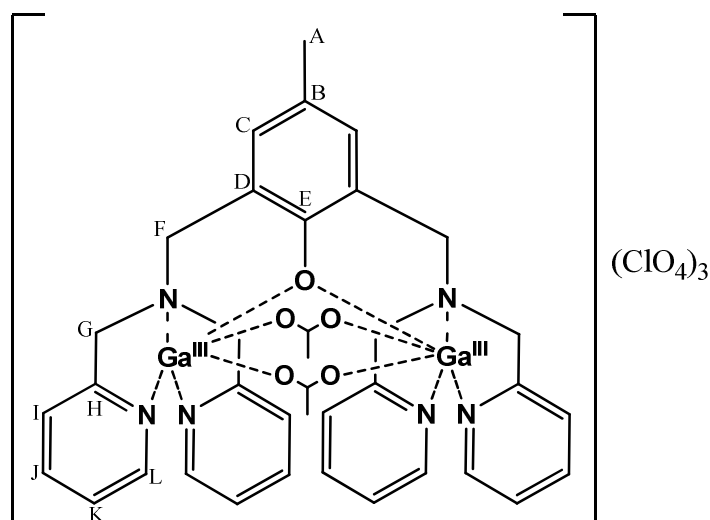


Figure 4.17: Structure of $[\text{Ga}_2(\text{L}^1)(\text{acetate})_2](\text{ClO}_4)_3$.

4.4.2. Chapter 3. Synthesis of mononucleating ligands linked to targeting units

The metal binding arm, **3**, was prepared as described previously (Section 4.4.1.3).

4.4.2.1. Preparation of **12**

A literature procedure³⁹ was followed but with the following differences: NaHCO_3 was used rather than Na_2CO_3 and the product was isolated by column chromatography 0 - 20% EtOAc:DCM. Product R_f in 2:8 EtOAc:DCM was 0.82. The desired product was isolated as a colourless viscous liquid which solidified to a white solid after 2 weeks. ^1H agrees but the ^{13}C spectrum differs with previously published data³⁹. ^1H NMR (400 MHz, CDCl_3): δ 6.99 (d, $J = 7.3$ Hz, 2H, $\text{C}_\text{H}\text{H}$), 6.75 (d, $J = 7.3$ Hz, 2H, $\text{C}_\text{I}\text{H}$), 6.5 (br, 1H, NH_D), 4.63 (br, 1H, OH_K), 3.31 (m, 2H, $\text{C}_\text{E}\text{H}_2$), 2.68 (m, 2H, $\text{C}_\text{F}\text{H}_2$), 1.43 (s, 9H, $\text{C}_\text{A}\text{H}_3$). ^{13}C NMR (100 MHz, CDCl_3): δ 169.8 (C_C), 154.8 (C_J), 130.4 (C_G), 129.9 (C_H), 115.6 (C_I), 79.4 (C_B), 42.1 (C_F), 35.3 (C_E), 28.5 (C_A). ESI-LRMS m/z 236 $[\text{M}-\text{H}]^-$. ESI-HRMS calcd for $\text{C}_{13}\text{H}_{18}\text{NO}_3$ 236.1287 found m/z 236.1295 $[\text{M}-\text{H}]^-$. IR (cm^{-1}): 3337 (br, $\text{O}-\text{H}$) 2978 (w) 2933 (w) 1678 (s, $\text{C}=\text{O}$) 1614 (w) 1595 (w) 1513 (s, $\text{N}-\text{H}$) 1450 (m) 1392 (w) 1366 (s) 1244 (s, $\text{C}-\text{O}$) 1161 (s) 1047 (m) 961 (m) 825 (m) 778 (m, $\text{C}-\text{H}$). Melting point: 63 – 64 $^\circ\text{C}$.

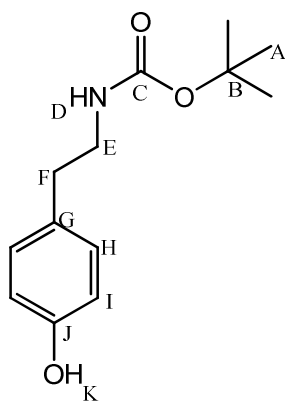


Figure 4.18: Structure of **12**.

4.4.2.2. Preparation of **13**

A modified literature procedure was used⁴⁰. Compound **3** (1.58 g, 7.9 mmol) was dissolved in 15 ml anhydrous EtOH. To this paraformaldehyde (0.35 g, 10.9 mmol) was added. The resulting mixture was heated at reflux until it became clear (approx. 4 hrs). To this clear solution compound **12** (2.5 g, 10.5 mmol) was added and the mixture heated at reflux. After 16 hrs the mixture was let cool and the product was isolated by column chromatography, firstly excess **12** was eluted in 8:2 DCM:EtOAc and the product was eluted in 95:5 DCM:MeOH. Product R_f in 1:1 DCM:EtOAc is 0. Evaporation of solvent gave **13** (2.21 g, 4.9 mmol, 62.4% yield) as a brown oil. ^1H (500 MHz, CDCl_3): δ 8.55-8.58 (m, 2H, $\text{C}_\text{A}\text{H}$), 7.63 (td, $J = 7.7$ Hz, 1.6 Hz, 2H, $\text{C}_\text{C}\text{H}$), 7.34 (d, $J = 7.9$ Hz, 2H, $\text{C}_\text{D}\text{H}$), 7.1-7.14 (m, 2H, $\text{C}_\text{B}\text{H}$), 6.98 (dd, $J = 8.5$ Hz, 1.8 Hz, 1H, $\text{C}_\text{L}\text{H}$), 6.87 (s, 1H, $\text{C}_\text{M}\text{H}$), 6.84 (d, $J = 8.2$ Hz, 1H, $\text{C}_\text{K}\text{H}$), 5.21 (br, 1H, OH_J), 4.63 (t, $J = 4.7$ Hz, 1H, NH_Q), 3.87 (s, 4H, $\text{C}_\text{F}\text{H}_2$), 3.76 (s, 2H, $\text{C}_\text{G}\text{H}_2$), 3.26-3.34 (m, 2H, $\text{C}_\text{P}\text{H}_2$), 2.66-2.70 (m, 2H, $\text{C}_\text{O}\text{H}_2$), 1.42 (s, 9H, $\text{C}_\text{T}\text{H}_3$). ^{13}C (125 MHz, CDCl_3): δ 158.2 (C_R), 156.6 (C_E), 156.1 (C_I), 148.9 (C_A), 136.8 (C_C), 130.8 (C_M), 130.4 (C_N), 129.2 (C_L), 123.2 (C_D), 122.2 (C_B), 121.4 (C_H), 115.1 (C_K), 78.8 (C_S), 59.2 (C_F), 56.0 (C_G), 41.8 (C_P), 34.1 (C_O), 28.4 (C_T). ESI-LRMS m/z 449 $[\text{M}+\text{H}]^+$. ESI-HRMS calcd for $\text{C}_{26}\text{H}_{33}\text{N}_4\text{O}_3$ 449.2553 found m/z 449.2554 $[\text{M}+\text{H}]^+$. IR (cm^{-1}): 3347 (br, O-H), 2979 (w), 2936 (w), 1736 (m), 1686 (m, C=O), 1615 (w, C=N), 1515 (m, N-H), 1447 (w), 1392 (w), 1366 (m), 1189 (s, $\text{C}_\text{Ar-O}$), 1164 (s, C-N), 1025 (s), 913 (m), 827 (m), 730 (m, C-H).

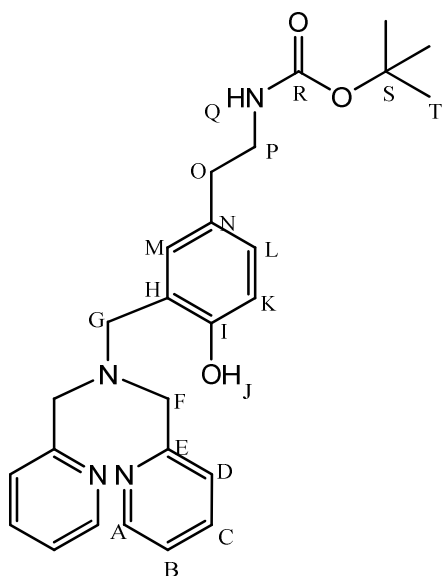


Figure 4.19: Structure of **13**.

4.4.2.3. Preparation of **HL**⁴

HL⁴ was prepared following a literature procedure⁴⁰. The product was isolated as a brown sticky oil. ¹H (500 MHz, CDCl₃): δ 8.42 (dq, *J* = 4.9 Hz, 0.8 Hz, 2H, C_AH), 7.50 (td, *J* = 7.7 Hz, 1.8 Hz, 2H, C_CH), 7.22 (d, *J* = 7.9 Hz, 2H, C_DH), 7.02-7.05 (m, 2H, C_BH), 6.90 (dd, *J* = 8.3 Hz, 2.1 Hz, 1H, C_LH), 6.86 (d, *J* = 1.9 Hz, 1H, C_MH), 6.70 (d, *J* = 8.2 Hz, 1H, C_KH), 5.24 – 5.17 (m, 3H, OH_J, N_QH₂), 3.74 (s, 4H, C_FH₂), 3.65 (s, 2H, C_GH₂), 3.02 (t, *J* = 7.5 Hz, 2H, C_PH₂), 2.81 (t, *J* = 7.3 Hz, 2H, C_OH₂). ¹³C (125 MHz, CDCl₃): δ 158.6 (C_I), 158.0 (C_E), 148.7 (C_A), 136.8 (C_C), 130.6 (C_M), 129.2 (C_L), 127.8 (C_N), 123.3 (C_D), 123.2 (C_B), 122.6 (C_H), 116.6 (C_K), 63.4 (C_G), 59.0 (C_F), 42.0 (C_P), 34.6 (C_O). ESI-LRMS *m/z* 349 [M+H]⁺. ESI-HRMS calcd for C₂₁H₂₅N₄O 349.2028 found *m/z* 349.2017 [M+H]⁺. IR (cm⁻¹): 2928 (w), 2829 (w), 1714 (w), 1590 (s, C=N), 1570 (s, N-H), 1499 (s), 1475 (m), 1433 (s), 1373 (m), 1250 (m), 1211(w, C_{Ar}-O), 1149 (m, C-N), 1049 (m), 994 (m), 874 (m), 757 (s), 731 (s, C-H).

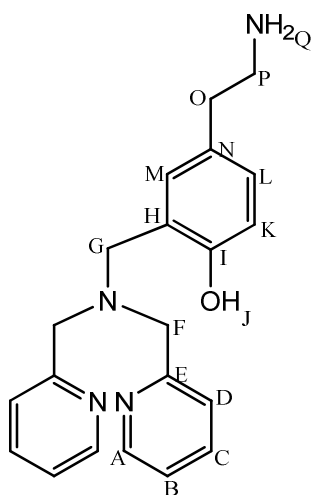


Figure 4.20: Structure of **HL**⁴.

4.4.2.4. Preparation of **H₂L**⁵

Compound **HL**⁴ (1.07 g, 3.1 mmol) was dissolved in 20 ml EtOH (dry). To this succinic anhydride (0.57 g, 5.7 mmol) was added and the reaction mixture was stirred at reflux under N₂. After 16 hr the mixture was let cool and evaporated to dryness. The product was isolated by gradient column chromatography 0-100% MeOH:DCM. Product R_f in 8:2 DCM:MeOH is 0. Evaporation of solvent gave **H₂L**⁵ (0.85 g, 61% yield) as a yellow sticky solid. ¹H NMR (500 MHz, DMSO-*d*₆): δ 10.39 (br, OH_V), 8.50 (dd, *J* = 5.1, 1.6 Hz, 2H, C_AH), 7.98 (t, *J* = 5.6 Hz, 1H, NH_Q), 7.74 (td, *J* = 7.7, 1.8 Hz, 2H, C_CH), 7.41 (d, *J* = 7.9 Hz, 2H, C_DH), 7.29 – 7.21 (m, 2H, C_BH), 7.00 (d, *J* = 2.2 Hz, 1H, C_MH), 6.90 (dd, *J* = 8.2, 2.2 Hz, 1H, C_LH), 6.67 (d, *J* = 8.1 Hz, 1H, C_KH), 5.76 (s, 1H, OH_J), 3.76 (s, 4H, C_FH₂), 3.64 (s, 2H, C_GH₂), 3.20 – 3.11 (m, 2H, C_PH₂), 2.54 (t, *J* = 7.5 Hz, 2H, C_OH₂), 2.30 (dd, *J* = 7.5, 5.7 Hz, 2H, C_TH₂), 2.23 (t, *J* = 6.7 Hz, 2H, C_SH₂). ¹³C NMR (126 MHz, DMSO-*d*₆): δ 174.9 (C_U), 171.8 (C_R), 158.8 (C_E), 155.5 (C_I), 149.2 (C_A), 137.3 (C_C), 130.7 (C_M), 129.8 (C_N), 128.9 (C_L), 123.5 (C_H), 123.2 (C_D), 122.7 (C_B), 116.0 (C_K), 59.0 (C_F), 55.1 (C_G), 41.0 (C_P), 34.9 (C_O), 31.4 (C_S), 31.0 (C_T). ESI-LRMS *m/z* 449 [M+H]⁺, 447 [M-H]⁻. ESI-HRMS calcd for C₂₅H₂₉N₄O₄ 449.2189, found *m/z* 449.2192 [M+H]⁺. IR (cm⁻¹): 3276 (w), 3075 (w), 3015 (w, O-H), 2926 (w), 2825 (w), 1711 (m, C=O), 1647 (s, C=O), 1591 (s, C=N), 1569 (s, N-H), 1499 (s), 1476 (m), 1433 (s), 1363 (m), 1248 (s, C-O), 1203 (m), 1150 (s, C-N), 1120 (m), 1090 (m), 1049 (m), 1025 (m), 1002 (m), 875 (m), 824 (m), 759 (s, C-H).

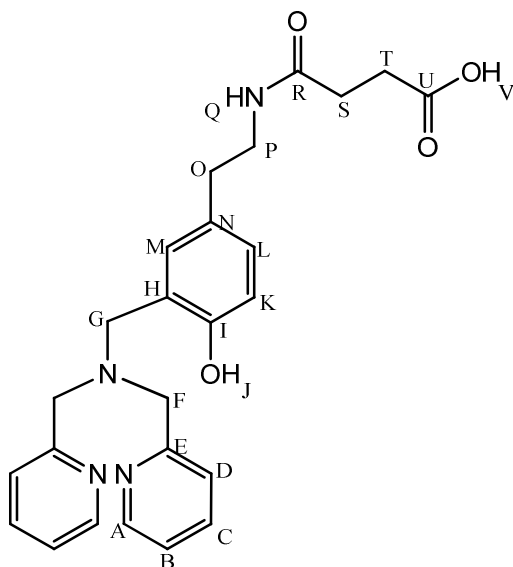


Figure 4.21: Structure of $\mathbf{H}_2\mathbf{L}^5$.

4.4.2.5. Preparation of $\mathbf{H}_2\mathbf{L}^6$

Compound \mathbf{HL}^4 (0.65 g, 1.86 mmol) was dissolved in 20 ml EtOH (dry). To this glutaric anhydride (0.21 g, 1.87 mmol) was added and the reaction mixture stirred at reflux under N_2 . After 24 hr the reaction mixture was let cool and evaporated to dryness. The product was isolated by gradient column chromatography 0-100% MeOH:DCM. The R_f of the product in 8:2 DCM:MeOH was 0. Evaporation of solvent gave $\mathbf{H}_2\mathbf{L}^6$ (0.60 g, 1.3 mmol, 70% yield) as a yellow sticky oil. ^1H NMR (500 MHz, DMSO- d_6): δ 10.37 (br, 1H, OH_W), 8.54 – 8.48 (m, 2H, C_AH), 7.82 (t, $J = 5.7$ Hz, 1H, NH_Q), 7.74 (td, $J = 7.7, 1.8$ Hz, 2H, C_CH), 7.41 (d, $J = 7.8$ Hz, 2H, C_DH), 7.24 (ddd, $J = 7.8, 4.7, 2.0$ Hz, 2H, C_BH), 6.99 (d, $J = 2.2$ Hz, 1H, C_MH), 6.90 (dd, $J = 8.2, 2.2$ Hz, 1H, C_LH), 6.67 (d, $J = 8.2$ Hz, 1H, C_KH), 5.74 (s, 1H, OH_J), 3.75 (s, 4H, C_FH_2), 3.64 (s, 2H, C_GH_2), 3.16 – 3.14 (m, 2H, C_PH_2), 2.55 (t, $J = 7.4$ Hz, 2H, C_OH_2), 2.10 (t, $J = 7.4$ Hz, 2H, C_UH_2), 2.02 (t, $J = 7.5$ Hz, 2H, C_SH_2), 1.65 (quint, $J = 7.4$ Hz, 2H, C_TH_2). ^{13}C NMR (125 MHz, DMSO- d_6): δ 174.7 (C_V), 172.0 (C_R), 158.8 (C_E), 155.5 (C_I), 149.2 (C_A), 137.3 (C_C), 130.7 (C_M), 129.8 (C_N), 129.0 (C_L), 123.5 (C_H), 123.2 (C_D), 122.7 (C_B), 116.0 (C_K), 58.9 (C_F), 55.1 (C_G), 40.9 (C_P), 35.1 (C_S), 34.9 (C_O), 34.1 (C_U), 21.4 (C_T). ESI-LRMS m/z 463 $[\text{M}+\text{H}]^+$, 461 $[\text{M}-\text{H}]^-$. ESI-HRMS calcd for $\text{C}_{26}\text{H}_{29}\text{N}_4\text{O}_4$ 461.2189, found m/z 461.2197 $[\text{M}-\text{H}]^-$. IR (cm^{-1}): 3285 (w), 3071 (w), 3007 (w, $\text{O}-\text{H}$), 2926 (w), 1713 (m, $\text{C}=\text{O}$), 1644 (s, $\text{C}=\text{O}$), 1592 (s, $\text{C}=\text{N}$), 1569 (m, $\text{N}-\text{H}$), 1548 (m), 1499 (s), 1476 (m), 1433 (s), 1364

(br), 1310 (w), 1247 (s, **C-O**), 1222 (m), 1197 (w), 1148 (m, **C-N**), 1091 (w), 1049 (w), 995 (w), 977 (w), 875 (w), 824 (m), 758 (s), 833 (w), 707 (w, **C-H**).

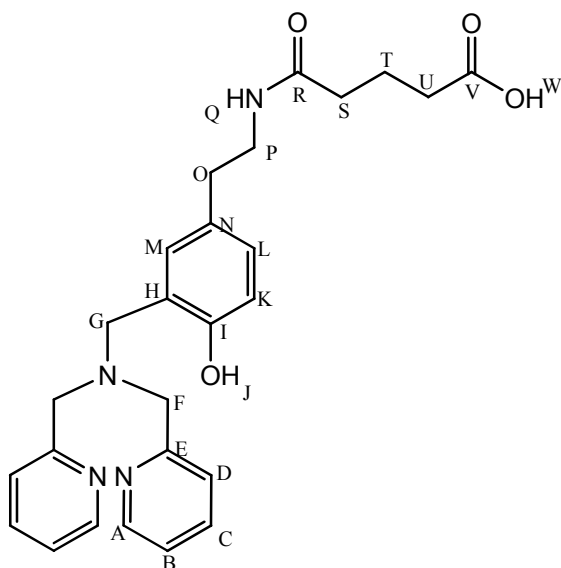


Figure 4.22: Structure of **H₂L⁶**.

4.4.2.6. Preparation of **14**

Compound **14** was prepared following a literature procedure⁴¹. The product was isolated by repeated column chromatography 20% EtOAc:Pet Spirits. The R_f of the product in 98:2 DCM:EtOAc is 0.29. Compound **14** was isolated as a colourless oil (79% yield). ¹H NMR similar to literature values⁴¹. ¹H NMR (400 MHz, CDCl₃): δ 7.92 (d, $J = 8.0$ Hz, 2H, **C_IH**), 7.39 (d, $J = 8.1$ Hz, 2H, **C_JH**), 3.34 – 3.17 (m, 6H, **C_CH₂**, **C_{C'}H₂**, **C_FH₂**), 2.75 (t, $J = 6.4$ Hz, 2H, **C_EH₂**), 1.69 – 1.57 (m, 2H, **C_BH₂**), 1.56 – 1.45 (m, 2H, **C_BH₂**), 0.93 (t, $J = 7.9$ Hz, 3H, **C_AH₃**), 0.84 (t, $J = 7.3$ Hz, 3H, **C_AH₃**). ¹³C NMR (125 MHz, CDCl₃): δ 171.1 (**C_G**), 167.8 (**C_D**), 137.5 (**C_K**), 136.8 (**C_H**), 129.8 (**C_I**), 128.8 (**C_J**), 53.4 (**C_{C'}**), 52.8 (**C_C**), 49.3 (**C_F**), 34.1 (**C_E**), 22.7 (**C_{B'}**), 21.0 (**C_B**), 11.6 (**C_{A'}**), 11.5 (**C_A**). ESI- LRMS m/z 294 [M+H]⁺. ESI-HRMS calcd for C₁₆H₂₃NO₂³⁷Cl 298.1388, found 298.1393 [M+H]⁺. IR (cm⁻¹): 2964 (m), 2932 (m), 2875 (m), 1686 (s, **C=O**), 1635 (s, **C=O**), 1589 (s), 1452 (m), 1427 (m), 1399 (s), 1362 (m), 1273 (br), 1231 (s), 1202 (m), 1141 (s, **C-N**), 1090 (s), 1013 (m), 989 (m), 948 (w), 895 (w), 829 (s, **C-H**), 795 (m), 768 (m), 746 (w, **C-H**).

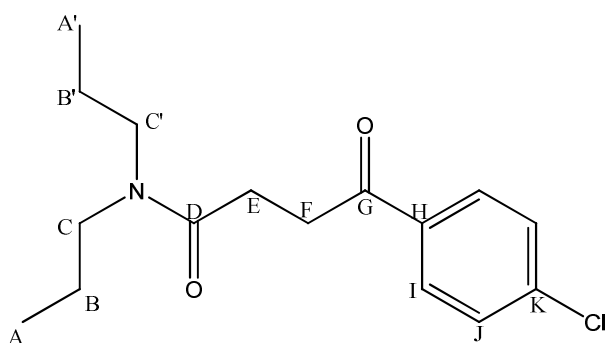


Figure 4.23: Structure of **14**.

4.4.2.7. Preparation of **15**

Compound **15** was prepared following a literature procedure⁴¹. The R_f of the product in 98:2 DCM:EtOAc is 0.57. ^1H NMR similar to literature values⁴¹. ^1H NMR (400 MHz, CDCl_3): δ 7.98 (d, $J = 8.4$ Hz, 2H, C_IH), 7.44 (d, $J = 8.4$ Hz, 2H, C_JH), 5.66 – 5.52 (m, 1H, C_FH), 3.33 – 2.96 (m, 6H, C_CH_2 , $\text{C}_C'\text{H}_2$, C_EH_2), 1.76 – 1.57 (m, 2H, C_BH_2), 1.48 (m, 2H, C_BH_2), 0.97 (t, $J = 7.4$ Hz, 3H, C_AH_3), 0.81 (t, $J = 7.9$ Hz, 3H, C_AH_3). ^{13}C NMR (125 MHz, CDCl_3): δ 183.4 (C_G), 164.7 (C_D), 138.8 (C_K), 136.2 (C_H), 130.4 (C_I), 129.0 (C_J), 50.6 (C_F), 49.4 (C_C'), 47.1 (C_C), 33.9 (C_E), 21.7 ($\text{C}_{B'}$), 19.6 (C_B), 11.3 ($\text{C}_{A'}$), 11.2 (C_A). ESI- LRMS m/z 374 $[\text{M}+\text{H}]^+$. ESI-HRMS calcd for $\text{C}_{16}\text{H}_{22}\text{NO}_2^{35}\text{Cl}^{79}\text{Br}$ 374.0522, found m/z 374.0516 $[\text{M}+\text{H}]^+$. IR (cm^{-1}): 2968 (m), 2936 (m), 2876 (m), 2253 (m), 1688 (s, $\text{C}=\text{O}$), 1639 (s, $\text{C}=\text{O}$), 1589 (m), 1472 (m), 1452 (m), 1423 (m), 1401 (m), 1361 (m), 1234 (s), 1143 (w), 1090 (m), 1002 (m), 973 (m), 899 (s), 806 (m, $\text{C}-\text{H}$), 725 (s, $\text{C}-\text{H}$).

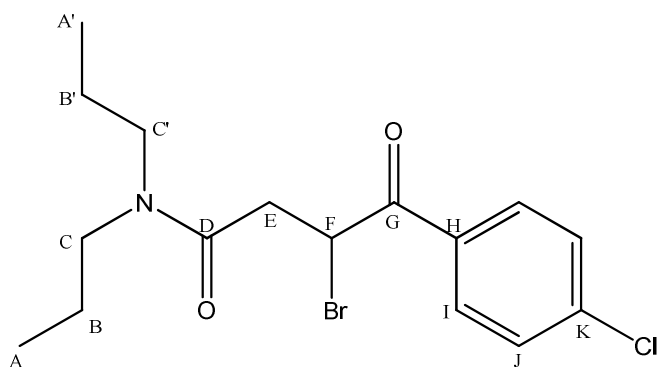


Figure 4.24: Structure of **15**.

4.4.2.8. Preparation of 16

Compound **16** was prepared using a modified literature procedure⁴². Compound **15** (4.29 g, 11.45 mmol) was dissolved in 40 ml of anhydrous Butan-1-ol. To this 3-nitropyridin-2-amine (1.56 g, 11.26 mmol) was added and the resulting mixture was stirred at reflux under N₂. After 48 hrs the mixture was evaporated to dryness. The crude product was isolated by gradient column chromatography 0% - 100% EtOAc:Pet Spirits. The pure product was isolated by subsequent gradient column chromatography 0%-20% EtOAc:DCM. The R_f of the product in 98:2 DCM:MeOH is 0.42. Evaporation of solvent gave **16** (290 mg, 0.7 mmol, 6.2% yield) as an orange solid. ¹H NMR (500 MHz, CDCl₃): δ 8.66 (dd, *J* = 6.7, 1.1 Hz, 1H, C_PH), 8.23 (dd, *J* = 7.6, 1.1 Hz, 1H, C_NH), 7.66 (d, *J* = 8.5 Hz, 2H, C_IH), 7.47 (d, *J* = 8.6 Hz, 2H, C_JH), 7.01 – 6.94 (m, 1H, C_OH), 4.15 (s, 2H, C_EH₂), 3.28 (t, *J* = 7.6 Hz, 2H, C_CH₂), 3.09 (t, *J* = 7.9 Hz, 2H, C_CH₂), 1.56 – 1.40 (m, 4H, C_BH₂, C_{B'}H₂), 0.84 (t, *J* = 7.4 Hz, 3H, C_AH₃), 0.74 (t, *J* = 7.4 Hz, 3H, C_AH₃). ¹³C NMR (125 MHz, CDCl₃): δ 166.9 (C_D), 145.2 (C_{quat}), 137.7 (C_O), 137.3 (C_{quat}), 134.8 (C_K), 131.9 (C_H), 130.8 (C_M), 130.7 (C_P), 130.3 (C_I), 129.0 (C_J), 123.4 (C_N), 116.9 (C_F), 49.9 (C_C), 48.0 (C_{C'}), 30.1 (C_E), 22.2 (C_B), 20.9 (C_{B'}), 11.3 (C_A), 10.9 (C_{A'}). ESI-LRMS *m/z* 415 [M+H]⁺. ESI- HRMS calcd for C₂₁H₂₄N₄O₃³⁵Cl 415.1537 found *m/z* 415.1523 [M+H]⁺. IR (cm⁻¹): 3084 (w), 2968 (m), 2934 (m), 2876 (m), 1734 (br), 1628 (s, C=O), 1555 (s, C-NO₂), 1524 (m), 1499 (m), 1482 (m), 1452 (w), 1427 (m), 1404 (w), 1373 (s, C-NO₂), 1353 (s), 1310 (br), 1255 (m), 1235 (m), 1209 (m), 1178 (w), 1144 (s, C-N), 1086 (s, C-N), 1011 (m), 963 (m), 925 (s), 901 (m), 885 (m), 831 (s, C-H), 820 (m), 788 (m), 738 (s), 729 (s, C-H), 687 (m). Melting point 202 – 204 °C, similar to literature value⁴².

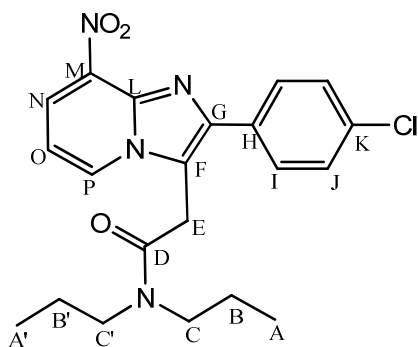


Figure 4.25: Structure of **16**.

4.4.2.9. Preparation of 17

Compound **16** was prepared following a modified literature procedure⁴². Compound **16** (290 mg, 0.7 mmol) was dissolved in 100 ml of anhydrous EtOH. To this a small portion (≈ 20 mg) of 5% Pd on C was added. The resulting mixture was stirred in a hydrogenator apparatus under 5 atm pressure of H₂. After 16 hrs the reaction was stopped and the resulting mixture filtered through Celite. Evaporation of filtrate gave **17** (238 mg, 0.62 mmol, 88% yield) as a dark green oil. After standing for 1 week at 4 °C the product solidified to a green powder. ¹H NMR (500 MHz, CDCl₃) δ 7.66 (dd, $J = 6.8, 1.0$ Hz, 1H, C_PH), 7.62 (d, $J = 8.5$ Hz, 2H, C_IH), 7.43 (d, $J = 8.5$ Hz, 2H, C_JH), 6.67 (t, $J = 7.1$ Hz, 1H, C_OH), 6.37 (dd, $J = 7.4, 1.0$ Hz, 1H, C_NH), 4.57 (br, 2H, N_QH₂), 4.04 (s, 2H, C_EH₂), 3.27 (t, $J = 7.7$ Hz, 2H, C_CH₂), 3.08 (t, $J = 7.81$ Hz, 2H, C_CH₂), 1.56 – 1.38 (m, 4H, C_BH₂, C_{B'}H₂), 0.83 (t, $J = 7.4$ Hz, 4H, C_AH₃), 0.71 (t, $J = 7.4$ Hz, 3H, C_AH₃). ¹³C NMR (125 MHz, CDCl₃) δ 167.6 (C_D), 139.0 (C_{quat}), 135.6 (C_M), 135.2 (C_K), 133.7 (C_{quat}), 131.4 (C_H), 129.9 (C_I), 128.8 (C_J), 115.7 (C_F), 114.7 (C_P), 113.6 (C_O), 102.8 (C_N), 49.7 (C_C), 47.9 (C_{C'}), 30.6 (C_E), 22.1 (C_{B'}), 20.9 (C_B), 11.3 (C_{A'}), 10.9 (C_A). ESI-LRMS m/z 385 [M+H]⁺. ESI-HRMS calcd for C₂₁H₂₆N₄O³⁵Cl 385.1795 found m/z 385.1781 [M+H]⁺. IR (cm⁻¹): 3332 (w, N-H), 2963 (m), 2931 (m), 2874 (w), 1633 (s, C=O), 1555 (s), 1488 (s), 1451 (m), 1429 (m), 1390 (s), 1310 (m), 1263 (m), 1232 (s), 1206 (w), 1137 (m, C-N), 1089 (s, C-N), 1050 (w), 1013 (s), 971 (w), 939 (w), 896 (m), 831 (s, C-H), 731 (s, C-H), 704 (s). Melting point 98 – 102 °C slightly higher than literature value of 97 – 99 °C⁴².

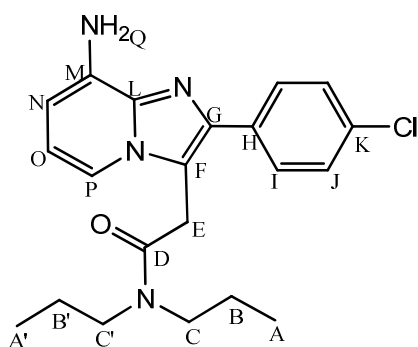


Figure 4.26: Structure of 17.

4.4.2.10. Preparation of 18

Compound **18** was prepared following a literature procedure⁴³. ¹H NMR (400 MHz, CDCl₃): δ 8.12 (br, 1H, NH_I), 7.72 – 7.61 (m, 2H, C_NH, C_OH), 7.51 (m, 1H, CMH), 7.45 – 7.30 (m, 6H, C_LH, C_CH, C_BH, C_AH), 5.18 – 5.09 (m, 1H, C_EH), 4.29 – 4.18 (m, 1H, C_GH), 3.71 (br, 1H, OH_F), 1.29 (d, J = 6.9 Hz, 3H, C_HH₃). ¹³C NMR (100 MHz, CDCl₃): δ 167.2 (C_J), 143.1 (C_D), 134.6 (C_P), 133.40 (C_K), 133.1 (C_N), 130.1 (C_O), 128.9 (C_L), 128.8 (C_B), 128.1 (C_C), 126.5 (C_M), 126.0 (C_A), 75 (C_E), 57 (C_G), 17.8 (C_H). No IR or MS data were recorded due to lack of sample.

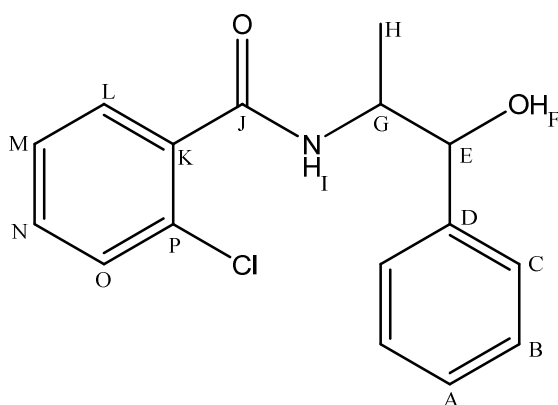


Figure 4.27: Structure of **18**.

4.4.2.11. Preparation of 19

Compound **19** was prepared following a literature procedure⁴³. ¹H and ¹³C NMR matches previously published data^{43,44}. ¹H NMR (400 MHz, CDCl₃): δ 7.77 (d, J = 9.7 Hz, 1H, C_HH), 7.56 – 7.36 (m, 8H, C_CH, C_EH, C_FH, C_GH, C_LH, C_MH, C_NH, C_OH), 2.73 (s, 3H, C_AH₃). ¹³C NMR (100 MHz, CDCl₃): δ 157.8 (C_J), 150.4 (C_B), 138.1 (C_D), 136.6 (C_K), 133.0 (C_H), 130.9 (C_O), 129.7 (C_P), 129.35 (C_M), 129.3 (C_F), 126.7 (C_L), 126.5 (C_N), 126.0 (C_E), 125.9 (C_G), 125.0 (C_I), 118.3 (C_C), 23.9 (C_A). No IR or MS data were recorded due to lack of sample.

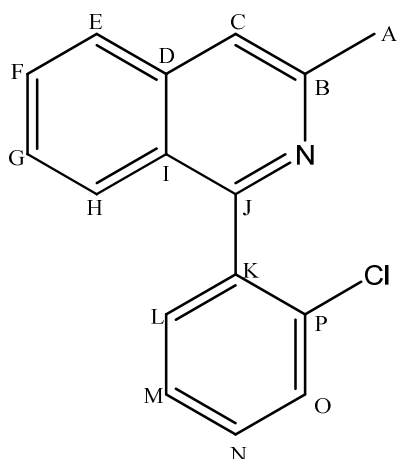


Figure 4.28: Structure of **19**.

4.4.2.12. Preparation of **20**

Compound **20** was prepared following a literature procedure⁴⁵. ¹H and ¹³C NMR agrees with previously published data^{44,45}. ¹H NMR (400 MHz, CDCl₃): δ 10.24 (s, 1H, C_AH), 8.44 (s, 1H, C_LH), 8.07 (d, *J* = 8.1 Hz, 1H, C_CH), 7.78 (m, 1H, C_HH), 7.72 – 7.62 (m, 2H, C_EH, C_OH), 7.58 – 7.51 (m, 1H, C_FH), 7.48 – 7.41 (m, 3H, C_MH, C_NH, C_GH). ¹³C NMR (100 MHz, CDCl₃): δ 194.0 (C_A), 160.1 (C_J), 146.5 (C_B), 137.9 (C_D), 136.2 (C_K), 133.7 (C_P), 131.65 (C_O), 131.6 (C_F), 130.7 (C_M), 130.6 (C_G), 130.4 (C_L), 129.8 (C_E), 129.5 (C_N), 127.9 (C_H), 127.5 (C_C), 121.5 (C_I). No IR or MS data were recorded due to lack of sample.

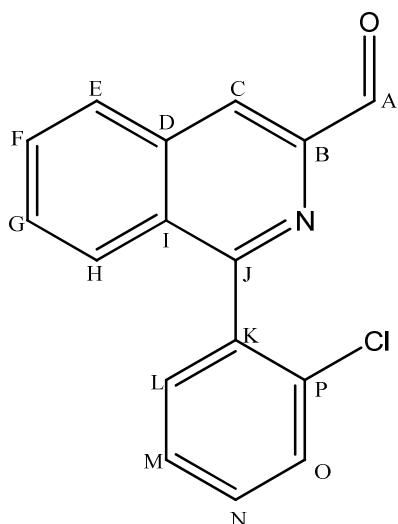


Figure 4.29: Structure of **20**.

4.4.2.13. Preparation of 21

Compound **21** was synthesised following a literature procedure⁴⁴. ¹H and ¹³C NMR match published values^{46,47} but no peak assignment was performed. ¹H NMR (400 MHz, CDCl₃): δ 10.6 (br, 1H, OH_A), 8.73 (s, 1H, C_DH), 8.11 (d, *J* = 8.2 Hz, 1H, C_FH), 7.85 (t, *J* = 7.5 Hz, 1H, C_GH), 7.79 – 7.75 (m, 1H, C_IH), 7.74 – 7.67 (m, 1H, C_PH), 7.59 (d, *J* = 7.9 Hz, 1H, C_MH), 7.57 – 7.42 (m, 3H, C_HH, C_NH, C_OH). ¹³C NMR (100 MHz, CDCl₃): δ 165.0 (C_B), 158.1 (C_C), 138.7 (C_{quat}), 136.80 (C_L), 136.75 (C_Q), 133.4 (C_N), 131.8 (C_G), 131.4 (C_H), 130.7 (C_P), 130.4 (C_J), 130.1 (C_I), 129.25 (C_F), 128.96 (C_E), 127.08 (C_M), 127.05 (C_O), 122.9 (C_D). ESI-LRMS *m/z* 282 [M-H]⁻, 284 [M+H]⁺. ESI-HRMS calcd for C₁₆H₉NO₂³⁵Cl 282.0322, found *m/z* 282.0311 [M-H]⁻. IR (cm⁻¹): 1701 (s, C=O), 1620 (w, C=N), 1590 (w), 1562 (w), 1501 (w), 1451 (w), 1428 (m), 1378 (m), 1299 (m, C-O), 1259 (m), 1221 (w), 1153 (w, C-N), 1127 (w), 1105 (w), 1054 (m), 1034 (m), 986 (w), 968 (m), 948 (br), 907 (m), 867 (w), 776 (s, C-H), 733 (s, C-H), 680 (m). Melting point 197 - 199 °C.

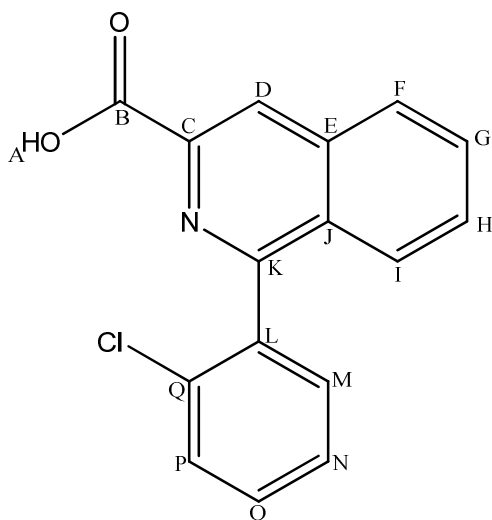


Figure 4.30: Structure of **21**.

4.4.2.14. Preparation of HL⁷

Compound HL⁴ (1.085 g, 3.1 mmol) was dissolved in 10 ml of 9:1 DCM: DIEA mixture. To this cholic acid (1.20 g, 2.9 mmol), 6-Cl HOBt (1.11 g, 6.53 mmol) and DIC (0.96 ml, 6.13 mmol) were added and the resulting mixture was stirred at room temperature. After 16 hr the mixture was evaporated to dryness. The product was isolated by gradient column chromatography (Alumina) 0% - 5% MeOH:DCM. The

R_f of the product in 90:10 DCM:MeOH is 0. Evaporation of solvent gave **HL**⁷ (1.44 g, 1.95 mmol, 67.3% yield) as a yellow solid. ¹H NMR (500 MHz, CDCl₃): δ 8.56 – 8.51 (m, 2H, C_AH), 7.63 (td, $J = 7.7, 1.8$ Hz, 2H, C_CH), 7.35 (dd, $J = 7.9, 1.1$ Hz, 2H, C_DH), 7.16 (ddd, $J = 7.6, 4.9, 1.1$ Hz, 2H, C_BH), 6.97 (dd, $J = 8.2, 2.2$ Hz, 1H, C_KH), 6.87 (d, $J = 2.2$ Hz, 1H, C_MH), 6.83 (d, $J = 8.1$ Hz, 1H, C_LH), 5.90 (t, $J = 5.8$ Hz, 1H, NH_Q), 3.94 (d, $J = 3.1$ Hz, 1H), 3.86 (s, 4H (C_FH₂)), 3.84 – 3.78 (m, 2H), 3.80 – 3.70 (m, 2H), 3.52 – 3.33 (m, 3H), 2.68 (t, $J = 6.8$ Hz, 2H), 2.27 – 2.10 (m, 4H), 2.06-1.97 (m, 1H), 1.96 – 1.87 (m, 2H), 1.81 – 1.69 (m, 4H), 1.68 - 1.61 (m, 2H), 1.61 – 1.46 (m, 4H), 1.45 – 1.30 (m, 3H), 1.29 – 1.18 (m, 1H), 1.14 – 1.01 (m, 2H), 0.91 (d, $J = 6.3$ Hz, 3H), 0.86 (s, 3H), 0.65 (s, 3H). ¹³C NMR (125 MHz, CDCl₃): δ 173.9 (C_R), 158.2 (C_E), 156.0 (C_I), 148.8 (C_A), 136.9 (C_C), 130.6 (C_M), 129.23 (C_K), 129.19 (C_H), 123.3 (C_D), 122.8 (C_N), 122.3 (C_B), 116.7 (C_L), 72.9 (C_{ter}), 71.9 (C_{ter}), 68.4 (C_{ter}), 59.1 (C_F), 57.1 (C_G), 46.6 (C_{ter}), 46.4 (C_{quat}), 41.7 (C_{ter}), 41.5 (C_{ter}), 40.7 (C_p), 39.7 (C_{sec}), 39.5 (C_{ter}), 35.3 (C_{ter}), 34.73 (C_{quat}), 34.68 (C_{sec}), 34.64 (C_O), 33.2 (C_{sec}), 31.8 (C_{sec}), 30.5 (C_{sec}), 28.2 (C_{sec}), 27.6 (C_{sec}), 26.6 (C_{sec}), 26.4 (C_{ter}), 23.3 (C_{sec}), 22.5 (C_{prim}), 17.4 (C_{prim}), 12.5 (C_{prim}). ESI-LRMS m/z 739 [M+H]⁺. ESI-HRMS calcd for C₄₅H₆₃N₄O₅ 739.4798, found m/z 739.4827 [M+H]⁺. IR (cm⁻¹): 3294 (br, O-H), 2925 (m), 2863 (m), 1643 (m), 1593 (m, C=N), 1570 (w), 1548 (w), 1499 (s), 1434 (s), 1367 (m), 1308 (w), 1249 (m), 1196 (w, C_{Ar}-OH), 1150 (m, C-N), 1115 (m), 1077 (s, C-OH), 1047 (s, C-OH), 1001 (m), 980 (s), 950 (w), 913 (m), 856 (w), 821 (w), 759 (s, C-H), 731 (w). Melting point 116 – 120 °C.

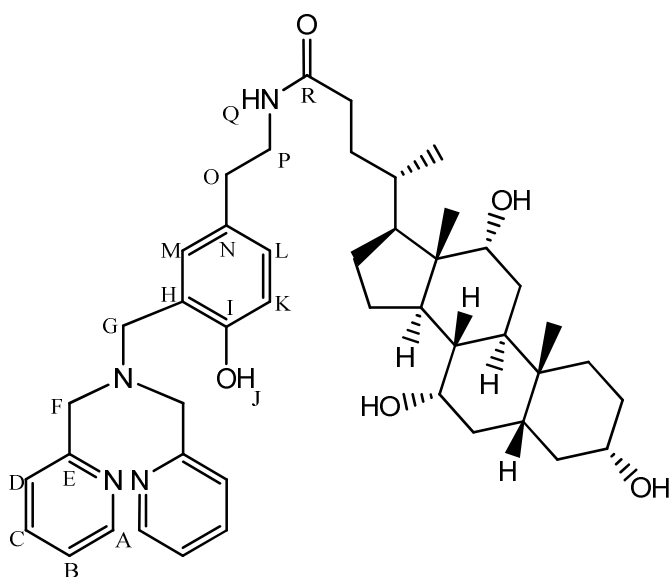


Figure 4.31: Structure of **HL**⁷ (there is no notation on the cholic acid unit as exact peak assignment was not possible).

4.4.2.15. Preparation of **HL**⁸

Compound **HL**⁴ (0.20 g, 0.57 mmol) was dissolved in 10 ml of 9:1 DCM: DIEA mixture. To this **23** (0.16 g, 0.56 mmol), 6-Cl HOBt (0.21 g, 1.24 mmol) and DIC (179 μ l, 1.14 mmol) were added and the resulting mixture was stirred at room temperature. After 16 hr the mixture was evaporated to dryness. The product was isolated by gradient column chromatography (Alumina) 0% - 5% MeOH: DCM. The R_f of the product in 90:10 DCM: MeOH is 0. Evaporation of solvent gave **HL**⁸ (0.25 g, 0.41 mmol, 71.4% yield) as a sticky brown solid. ¹H NMR (500 MHz, CDCl₃): δ 8.63 (s, 1H, C_TH), 8.57 – 8.51 (m, 2H, C_AH), 8.32 (t, J = 6.2 Hz, 1H, NH_Q), 8.02 (d, J = 8.4 Hz, 1H, C_VH), 7.73 (ddd, J = 8.2, 6.7, 1.5 Hz, 1H, C_WH), 7.65 (d, J = 8.4 Hz, 1H, C_{AC}H), 7.62 – 7.55 (m, 3H, C_YH, C_CH), 7.53 – 7.49 (m, 1H, C_{AF}H), 7.44 – 7.37 (m, 3H, C_XH, C_{AD}H, C_{AE}H), 7.32 – 7.29 (m, 2H, C_DH), 7.15 – 7.11 (m, 2H, C_BH), 7.03 (d, J = 8.1 Hz, 1H, C_LH), 6.92 (s, 1H, C_MH), 6.79 (dd, J = 8.2, 1.3 Hz, 1H, C_KH), 5.29 (s, 1H, OH_J), 3.82 (s, 4H, C_FH₂), 3.72 – 3.61 (m, 4H, C_GH₂, C_OH₂), 2.82 (t, J = 7.5 Hz, 2H, C_PH₂). ¹³C NMR (125 MHz, CDCl₃): δ 164.6 (C_S), 158.2 (C_E), 157.3 (C_R), 156.0 (C_I), 148.9 (C_A), 142.8 (C_{AA}), 137.8 (C_{AB}), 136.70 (C_C), 136.63 (C_{AG}), 131.4 (C_{AD}), 130.8 (C_W), 130.4 (C_M), 130.0 (C_X), 129.8 (C_{AF}), 129.36 (C_Z), 129.32 (C_L), 129.21 (C_N), 128.8 (C_Y), 128.5 (C_V), 128.2 (C_U), 127.3 (C_{AC}), 126.7 (C_{AE}), 122.8 (C_H), 122.22 (C_D), 122.16 (C_B), 120.2 (C_T), 116.5 (C_K), 59.1 (C_F), 56.9

(C_G), 41.2 (C_O), 35.1 (C_P). ESI-LRMS m/z 614 [M+H]⁺. ESI-HRMS calcd for C₃₇H₃₃N₅O₂³⁵Cl 614.2323 found m/z 614.2328 [M+H]⁺. IR (cm⁻¹): 3339 (m), 3063 (w), 2964 (m), 2920 (s), 2851 (m), 1664 (s, C=O), 1618 (m), 1591 (s, C=N), 1569 (s), 1521 (s, N-H), 1498 (s), 1474 (w), 1433 (s), 1383 (m), 1361 (m), 1325 (w), 1288 (w), 1248 (s), 1214 (m, C_{Ar}-O), 1167 (m), 1150 (m, C-N), 1128 (s, C-N), 1096 (m), 1050 (m), 1038 (w), 981 (m), 963 (w), 911 (m), 866 (m), 804 (m), 753 (s, C-H), 677 (m). Melting point: 146 – 148 °C.

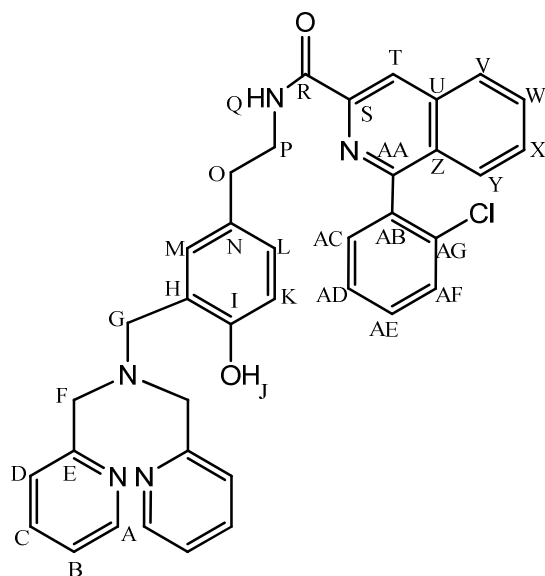


Figure 4.32: Structure of **HL**⁸.

4.4.2.16. Preparation of 22

In a sealed centrifuge tube compound **17** (32 mg, 83 μ mol) and succinic anhydride (30 mg, 300 μ mol) were dissolved in 2 ml of anhydrous Toluene. The mixture was sonicated for 120 mins at room temperature. The product was isolated by removal of the supernatant and washing the black solid with further portions of anhydrous toluene (2 x 2 ml). This gave **18** (28.6 mg, 59 μ mol, 71%) as a black sticky solid. ¹H NMR is similar to literature values⁴⁸ but multiplet analysis was incomplete in reported spectra. ¹H NMR (400 MHz, CDCl₃) δ 12.0 (br, 1H, OH_V), 9.67 (s, 1H, NH_Q), 8.26 (d, J = 7.5 Hz, 1 H, C_PH), 7.90 (d, J = 6.8 Hz, 1 H, C_NH), 7.51 (d, J = 8.4 Hz, 2 H, C_IH), 7.42 (d, J = 8.4 Hz, 2 H, C_JH), 6.90 (t, J = 7.2 Hz, 1 H, C_OH), 3.99 (s, 2 H, C_EH₂), 3.28 (t, J = 7.6 Hz, 2 H, C_CH₂), 3.11 (t, J = 7.7 Hz, 2 H, C_CH₂), 2.84 (t, J = 6.8 Hz, 2 H, C_TH₂), 2.72 (t, J = 6.8 Hz, 2 H, C_SH₂), 1.57 – 1.45 (m, 4H,

$C_{B'}H_2$, C_BH_2), 0.84 (t, $J = 7.4$ Hz, 3 H, $C_{A'}H_3$), 0.76 (t, $J = 7.4$ Hz, 3 H, C_AH_3). ^{13}C NMR (100 MHz, $CDCl_3$) δ 176.5 (C_U), 172.0 (C_R), 167.3 (C_D), 140.1 (C_{quat}), 138.6 (C_{quat}), 134.8 (C_K), 130.5 (C_M), 129.1 (C_I), 128.3 (C_J), 127.1 (C_H), 119.5 (C_N), 116.6 (C_F), 114.1 (C_P), 114.0 (C_O), 49.9 (C_C), 48.1 ($C_{C'}$), 32.3 (C_T), 29.7 (C_S), 28.5 (C_E), 22.3 ($C_{B'}$), 21.0 (C_B), 11.4 ($C_{A'}$), 11.1 (C_A). ESI-LRMS m/z 485 $[M+H]^+$. ESI-HRMS calcd for $C_{25}H_{30}N_4O_4^{35}Cl$ 485.1956, found m/z 485.1961 $[M+H]^+$. IR (cm^{-1}): 2963 (m), 2928 (m), 2884 (m), 2547 (br), 1863 (w), 1782 (m), 1710 (w, $C=O$), 1677 (s, $C=O$), 1636 (s), 1547 (s, $N-H$), 1491 (s), 1460 (w), 1419 (m), 1401 (m), 1362 (m), 1321 (w), 1290 (w, $C-O$), 1256 (m), 1233 (m), 1214 (s), 1160 (s), 1092 (s), 1049 (m), 1013 (m), 908 (m), 827 (m, $C-H$), 733 (s, $C-H$).

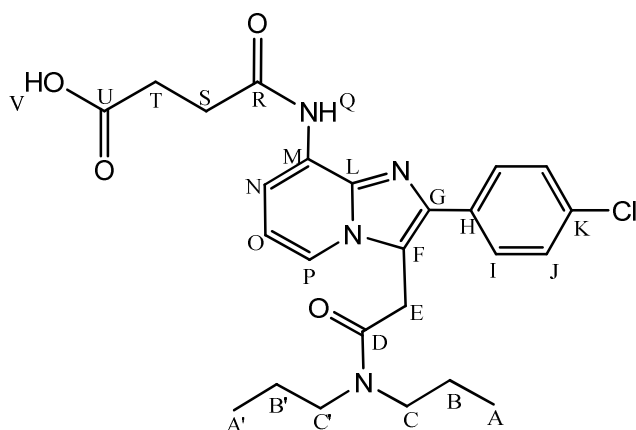


Figure 4.33: Structure of **22**.

4.4.2.17. Preparation of **23**

In a sealed centrifuge tube compound **17** (36.1 mg, 94 μ mol) and glutaric anhydride (27.8 mg, 244 μ mol) were dissolved in 2 ml of anhydrous Toluene. The mixture was sonicated for 120 mins at room temperature. The product was isolated by removal of the supernatant and washing the black solid with further portions of anhydrous toluene (2 x 2 ml). This gave **19** (30.21 mg, 61 μ mol, 65% yield) as a black sticky solid. 1H NMR is similar to literature values⁴⁸ but multiplet analysis was incomplete in reported spectra. 1H NMR (500 MHz, $CDCl_3$) δ 12.0 (br, OH_W), 9.80 (s, 1H, NH_Q), 8.30 (d, $J = 7.7$ Hz, 1H, $C_P H$), 7.92 (dd, $J = 6.8, 1.0$ Hz, 1H, $C_N H$), 7.51 (d, $J = 8.4$ Hz, 2H, $C_I H$), 7.45 (d, $J = 8.5$ Hz, 2H, $C_J H$), 6.92 (t, $J = 7.3$ Hz, 1H, $C_O H$), 4.00 (s, 2H, $C_E H_2$), 3.29 (t, $J = 7.6$ Hz, 2H, $C_{C'} H_2$), 3.11 (t, $J = 7.8$ Hz, 2H, $C_C H_2$), 2.70 (t, $J = 7.4$ Hz, 2H, $C_U H_2$), 2.46 (t, $J = 6.7$ Hz, 2H, $C_S H_2$), 2.14 – 2.04 (m, 2H,

$C_T H_2$), 1.63 – 1.44 (m, 4H, $C_B H_2$, $C_B' H_2$), 0.85 (t, $J = 7.4$ Hz, 7H, $C_A' H_3$), 0.77 (t, $J = 7.4$ Hz, 3H, $C_A H_3$). ^{13}C NMR (100 MHz, $CDCl_3$) δ 178.2 (C_V), 178.1 (C_R), 167.4 (C_D), 140.7 (C_{quat}), 138.5 (C_{quat}), 134.9 (C_K), 130.7 (C_M), 130.6 (C_I), 129.0 (C_J), 127.1 (C_H), 119.5 (C_N), 116.6 (C_F), 114.9 (C_P), 114.2 (C_O), 49.9 (C_C), 48.2 (C_C'), 35.9 (C_U), 33.2 (C_S), 29.9 (C_E), 22.3 ($C_{B'}$), 21.0 (C_B), 19.9 (C_T), 11.4 ($C_{A'}$), 11.1 (C_A). ESI-LRMS m/z 499 $[M+H]^+$. ESI-HRMS calcd for $C_{26}H_{32}N_4O_4^{35}Cl$ 499.2112, found m/z 499.2119 $[M+H]^+$. IR (cm^{-1}): 2964 (w), 2932 (w), 2567 (br), 1705 (s, $C=O$), 1635 (w, $C=O$), 1615 (m), 1549 (m), 1544 (m, $N-H$), 1492 (m), 1438 (s), 1406 (s), 1274 (m, $C-O$), 1232 (m), 1203 (m), 1144 (s, $C-N$), 1091 (m), 1051 (m), 1012 (m), 925 (w), 893 (w), 833 (s, $C-H$), 780 (m), 732 (s, $C-H$), 695 (m).

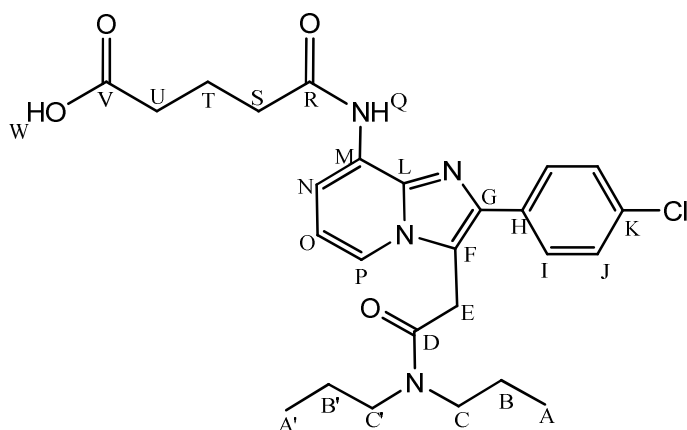


Figure 4.34: Structure of **23**.

4.4.2.18. Preparation of **HL**⁹

Compound **22** (28 mg, 58 μ mol) was dissolved in 10 ml of 9:1 DCM: DIEA. To this 6-Cl HOBt (21 mg, 124 μ mol), DIC (18 μ l, 115 μ mol) and **HL**⁴ (20 mg, 58 μ mol) were added and the resulting mixture was stirred at room temperature. After 16 hr the mixture was evaporated to dryness. The product was isolated by gradient column chromatography (Alumina) 0% - 10% MeOH:DCM. The R_f of the product in 90:10 DCM:MeOH is 0. Evaporation of solvent gave **HL**⁹ (29 mg, 35.6 μ mol, 61% yield) as a sticky brown solid. 1H (500 MHz, $CDCl_3$): δ 8.55 (d, $J = 5.2$ Hz, $C_{AL}H$), 8.11 (d, $J = 7.8$ Hz, 1H, $C_P H$), 7.91 (d, $J = 6.8$ Hz, 1H, $C_N H$), 7.65 – 7.57 (m, 3 H, $C_{AJ} H$, $C_I H$), 7.45 (d, $J = 8.3$ Hz, 2 H, $C_J H$), 7.35 (d, $J = 7.7$ Hz, 2H, $C_{AI} H$), 7.16 (t, $J = 6.3$ Hz, 2H, $C_{AK} H$), 7.01 (dd, $J = 8.2, 2.2$ Hz, 1H, $C_{AA} H$), 6.92 (d, $J = 2.2$ Hz, 1H, $C_Z H$), 6.85 – 6.77 (m, 2H, $C_{AB} H$, $C_O H$), 5.90 (t, $J = 5.7$ Hz, 1 H, NH_Q), 5.69 (t, $J = 4.6$ Hz,

4.4.2.19. Preparation of HL¹⁰

Compound **23** (19.5 mg, 39 μ mol) was dissolved in 10 ml of 9:1 DCM:DIEA. To this 6-Cl HOBt (14 mg, 83 μ mol), DIC (12.2 μ l, 78 μ mol) and **HL**⁴ (14 mg, 40 μ mol) were added and the resulting mixture was stirred at room temperature. After 16 hr the mixture was evaporated to dryness. The product was isolated by gradient column chromatography (Alumina) 0% - 10% MeOH:DCM. The R_f of the product in 90:10 DCM:MeOH is 0. Evaporation of solvent gave **HL**¹⁰ (26.5 mg, 31.95 μ mol, 82% yield) as a sticky brown solid. ¹H (500 MHz, CDCl₃): δ 8.58 – 8.52 (m, 2H, C_{AM}H), 8.12 (d, J = 7.7 Hz, 1H, C_PH), 7.89 (d, J = 6.8 Hz, 1H, C_NH), 7.66 – 7.57 (m, 3H, C_{AK}H, C_IH), 7.44 (d, J = 8.4 Hz, 2H, C_JH), 7.34 (d, J = 7.3 Hz, 2H, C_{AJ}H), 7.19 – 7.13 (m, 2H, C_{AL}H), 7.04 (dd, J = 7.9 Hz, 1.93 Hz, 1H, C_{AB}H), 6.93 (d, J = 2.1 Hz, 1H, C_{AA}H), 6.86 – 6.78 (m, 2H, C_{AC}H, C_OH), 5.83 (t, J = 5.6 Hz, 1H, NH_Q), 5.67 (br, 1 H, NH_W), 5.49 (s, 1H, OH_{AE}), 4.05 (s, 2H, C_EH₂), 3.86 (s, 4H, C_{AH}H₂), 3.77 (s, 2H, C_{AG}H₂), 3.51 (t, J = 7.2 Hz, 2H, C_XH₂), 3.32 – 3.26 (m, 2H, C_CH₂), 3.07 (t, J = 6.4 Hz, 2H, C_CH₂), 2.82 (t, J = 7.3 Hz, 2H, C_UH₂), 2.77 (t, J = 6.9 Hz, 2H, C_YH₂), 2.48 (t, J = 7.0 Hz, 2H, C_SH₂), 2.10 – 2.02 (m, 2H, C_TH₂), 1.58 – 1.41 (m, 4H, C_BH₂, C_{B'}H₂), 0.85 (t, J = 7.4 Hz, 3H, C_{A'}H₃), 0.75 (t, J = 7.4 Hz, 3H, C_AH₃). ¹³C NMR (125 MHz, CDCl₃) δ 177.5 (C_R), 171.1 (C_V), 167.4 (C_D), 158.20 (C_{AD}), 158.14 (C_{AI}), 148.8 (C_{AM}), 138.7 (C_{quat}), 136.80 (C_{quat}), 136.75 (C_K), 132.7 (C_{AK}), 131.7 (C_H), 130.5 (C_M), 130.40 (C_{AA}), 129.9 (C_I), 129.2 (C_{AB}), 129.0 (C_J), 127.9 (C_Z), 123.2 (C_{AJ}), 122.9 (C_{AF}), 122.2 (C_{AL}), 119.2 (C_N), 116.61 (C_{AC}), 116.58 (C_F), 114.5 (C_P), 114.0 (C_O), 59.2 (C_{AH}), 56.9 (C_{AG}), 49.8 (C_C), 48.0 (C_{C'}), 40.6 (C_X), 32.9 (C_Y), 32.6 (C_U), 31.4 (C_S), 30.2 (C_E), 23.5 (C_T), 22.2 (C_B), 20.9 (C_{B'}), 11.3 (C_{A'}), 11.0 (C_A). IR (cm⁻¹) 3336 (m, O-H), 2967 (s), 2927 (s), 2873 (w), 1638 (w, C=O), 1613 (w), 1590 (m), 1569 (s, N-H), 1552 (s, N-H), 1523 (w), 1499 (w), 1463 (m), 1433 (s), 1382 (m), 1361 (m), 1325 (m), 1247 (s), 1209 (w, C_{Ar}-H), 1147 (s), 1130 (s), 1049 (m), 995 (w), 977 (w), 957 (w), 892 (w), 866 (w), 827 (m, C-H), 758 (w). ESI-LRMS m/z 829 [M+H]⁺. ESI-HRMS calcd for C₄₇H₅₄N₈O₄³⁵Cl 829.3957 found m/z 829.3997 [M+H]⁺.

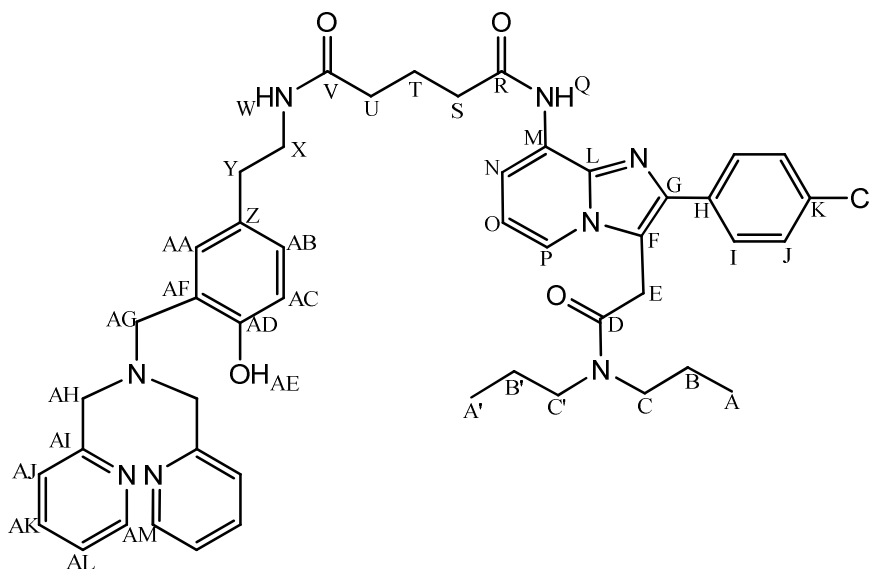


Figure 4.36: Structure of **HL¹⁰**.

4.4.2.20. Preparation of [Cu(HL⁷)(phen)](PF₆)₂

In a sealed centrifuge tube **HL⁷** (22.2 mg, 30 μmol), was dissolved in 0.2 ml MeOH. To this 0.283 ml of a 0.106 M CuCl₂ solution (30 μmol) and 0.254 ml of a 0.118 M 1,10-phenanthroline solution (30 μmol) were added and the tube was heated at 60 °C. After 4 hrs the tube was cooled, filtered and 0.375 ml of a 0.16 M NH₄PF₆ solution (60 μmol) was added. After standing for 2 days the solution was filtered and [Cu(HL⁷)(phen)](PF₆)₂ (9.92 mg, 7.8 μmol , 26% yield) was obtained as a light blue-green powder. ESI-LRMS m/z 499 [M+H₂O-2(PF₆)]²⁺. ESI-HRMS calcd for C₅₇H₇₂⁶³CuN₆O₆ 499.7405 found m/z 499.7378 [M+H₂O-2(PF₆)]²⁺. IR (cm⁻¹): 3063 (br, **O-H**), 1609 (w), 1587 (w), 1522 (s), 1431 (s), 1345 (w), 1312 (w), 1228 (w), 1149 (m, **C-N**), 1109 (m), 957 (w), 870 (m), 832 (s, **C-H**), 774 (m), 721 (s, **C-H**). Melting point 250 – 251 °C. Anal. Calcd (%) for C₅₇H₇₀CuF₁₂N₆O₅P₂: C, 53.79; H, 5.54; N, 6.60; found: C, 54.08; H, 5.41; N, 6.82%.

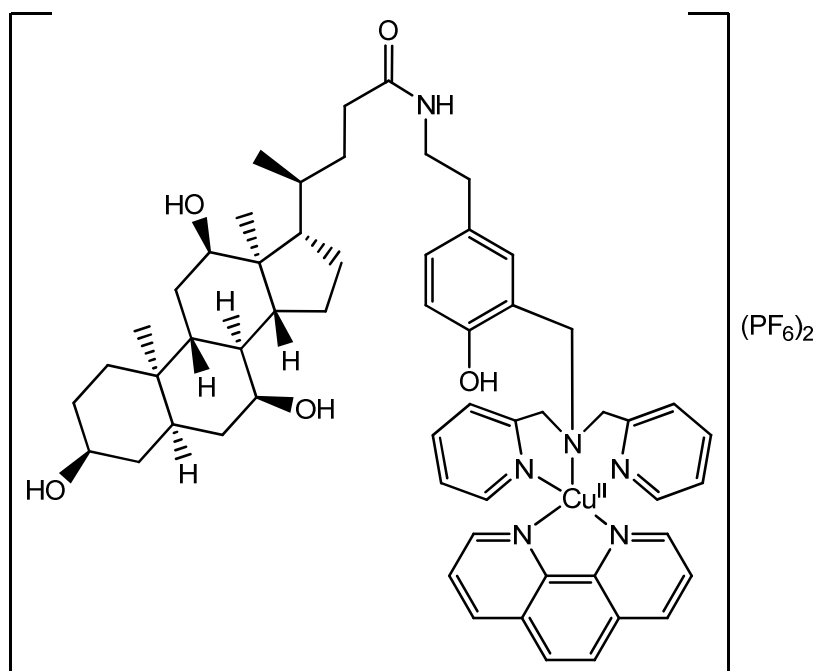


Figure 4.37: Structure of $[\text{Cu}(\text{HL}^7)(\text{phen})](\text{PF}_6)_2$.

4.4.2.21. Preparation of $[\text{Cu}(\text{HL}^8)(\text{phen})](\text{PF}_6)_2$

In a sealed centrifuge tube HL^8 (15.95 mg, 26 μmol), was dissolved in 0.2 ml MeOH. To this 0.245 ml of a 0.106 M CuCl_2 solution (26 μmol) and 0.22 ml of a 0.118 M 1,10-phenanthroline solution (26 μmol) were added and the tube was heated at 60 $^\circ\text{C}$. After 4 hrs the tube was cooled, filtered and 0.325 ml of a 0.16 M NH_4PF_6 solution (52 μmol) was added. After standing for 2 days the solution was filtered and $[\text{Cu}(\text{HL}^8)(\text{phen})](\text{PF}_6)_2$ (4.73 mg, 4.12 μmol , 15.8% yield) was obtained as a green powder. ESI-LRMS m/z 444 $[\text{M}+\text{MeOH}-2(\text{PF}_6)]^{2+}$. ESI-HRMS calcd for $\text{C}_{50}\text{H}_{44}^{35}\text{Cl}^{63}\text{CuN}_7\text{O}_3$ 444.1245 found m/z 444.1255 $[\text{M}+\text{MeOH}-2(\text{PF}_6)]^{2+}$. IR (cm^{-1}): 3059 (br, **O-H**), 1984 (w), 1625 (m), 1605 (m), 1583 (m), 1516 (m), 1431 (s), 1345 (m), 1310 (m), 1226 (m), 1201 (w), 1149 (s, **C-N**), 1107 (s), 1048 (w), 1028 (w), 961 (m), 870 (m), 828 (s, **C-H**), 792 (m), 776 (s), 735 (w), 719 (s, **C-H**). Melting point 264 - 266 $^\circ\text{C}$. Anal. Calcd (%) for $\text{C}_{49}\text{H}_{40}\text{ClCuF}_{12}\text{N}_7\text{O}_2\text{P}_2$: C, 51.27; H, 3.51; N, 8.54; found: C, 51.20; H, 3.80; N, 8.64%.

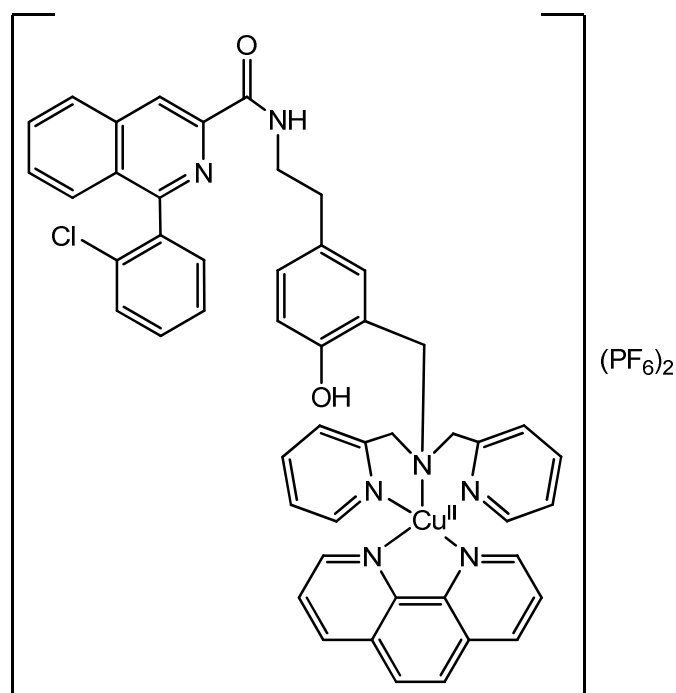


Figure 4.38: Structure of $[\text{Cu}(\text{HL}^8)(\text{phen})](\text{PF}_6)_2$.

4.4.2.22. Preparation of $[\text{Cu}(\text{HL}^9)(\text{phen})](\text{PF}_6)_2$

In a sealed centrifuge tube HL^9 (29 mg, 36 μmol), was dissolved in 0.2 ml MeOH. To this 0.24 ml of a 0.15 M CuCl_2 solution (36 μmol) and 0.28 ml of a 0.129 M 1,10-phenanthroline solution (36 μmol) were added and the tube was heated at 60 $^\circ\text{C}$. After 4 hrs the tube was cooled, filtered and 0.313 ml of a 0.23 M NH_4PF_6 solution (72 μmol) was added. After standing for 2 days the solution was filtered and $[\text{Cu}(\text{HL}^9)(\text{phen})](\text{PF}_6)_2$ (7.48 mg, 5.54 μmol , 15.4% yield) was obtained as a dark green powder. ESI-LRMS m/z 544 $[\text{M}+\text{MeOH}-2(\text{PF}_6)]^{2+}$. ESI-HRMS calcd for $\text{C}_{59}\text{H}_{63}^{35}\text{Cl}^{63}\text{CuN}_{10}\text{O}_5$ 544.6984 found m/z 544.6925 $[\text{M}+\text{MeOH}-2(\text{PF}_6)]^{2+}$. IR (cm^{-1}): 3675 (br), 3326 (w, **O-H**), 3200 (w), 2364 (m), 2146 (m), 2015 (m), 1977 (s), 1699 (m, **C=O**), 1537 (m, **N-H**), 1522 (w), 1423 (w), 1064 (m). 971 (w), 837 (s, **C-H**), 720 (s, **C-H**). Melting point 189 - 191 $^\circ\text{C}$. Anal. Calcd (%) for $\text{C}_{58}\text{H}_{59}\text{ClCuF}_{12}\text{N}_{10}\text{O}_4\text{P}_2$: C, 51.64; H, 4.41; N, 10.38; found: C, 51.52; H, 4.73; N, 10.59%.

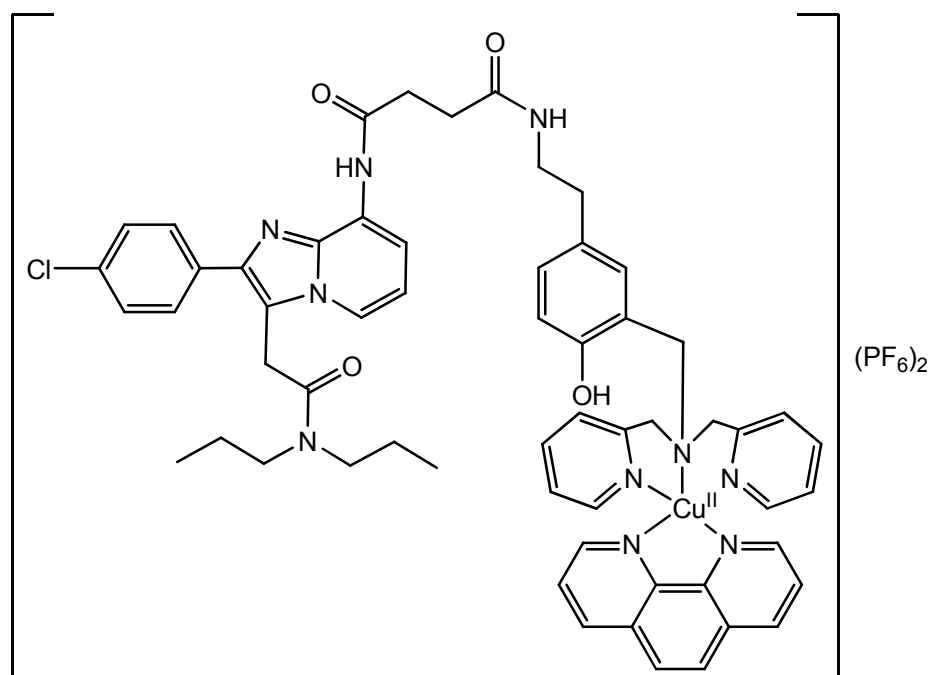


Figure 4.39: Structure of $[\text{Cu}(\text{HL}^9)(\text{phen})](\text{PF}_6)_2$.

4.4.2.23. Preparation of $[\text{Cu}(\text{HL}^{10})(\text{phen})](\text{PF}_6)_2$

In a sealed centrifuge tube HL^{10} (26.5 mg, 32 μmol), was dissolved in 0.2 ml MeOH. To this 0.213 ml of a 0.15 M CuCl_2 solution (32 μmol) and 0.248 ml of a 0.129 M 1,10-phenanthroline solution (32 μmol) were added and the tube was heated at 60 $^\circ\text{C}$. After 4 hrs the tube was cooled, filtered and 0.278 ml of a 0.23 M NH_4PF_6 solution (64 μmol) was added. After standing for 2 days the solution was filtered and $[\text{Cu}(\text{HL}^{10})(\text{phen})](\text{PF}_6)_2$ (6.40 mg, 4.7 μmol , 14.7% yield) was obtained as a blue-green powder. ESI-LRMS m/z 535 $[\text{M} - 2(\text{PF}_6)]^{2+}$. ESI-HRMS calcd for $\text{C}_{59}\text{H}_{61}^{35}\text{Cl}^{63}\text{CuN}_{10}\text{O}_4$ 535.6931 found m/z 535.6847 $[\text{M} - 2(\text{PF}_6)]^{2+}$. IR (cm^{-1}): 3670 (br, **O-H**), 3083 (br, **O-H**), 2349 (w), 2025 (w), 1699 (m, **C=O**), 1522 (m, **N-H**), 1428 (br), 1345 (w), 1246 (w), 1148 (w, **C-N**), 1029 (m), 870 (w), 837 (s, **C-H**), 723 (m, **C-H**). Melting point 198 – 200 $^\circ\text{C}$. Anal. Calcd (%) for $\text{C}_{59}\text{H}_{61}\text{ClCuF}_{12}\text{N}_{10}\text{O}_4\text{P}_2$: C, 51.99; H, 4.51; N, 10.28; found: C, 52.09; H, 4.81; N, 10.16%.

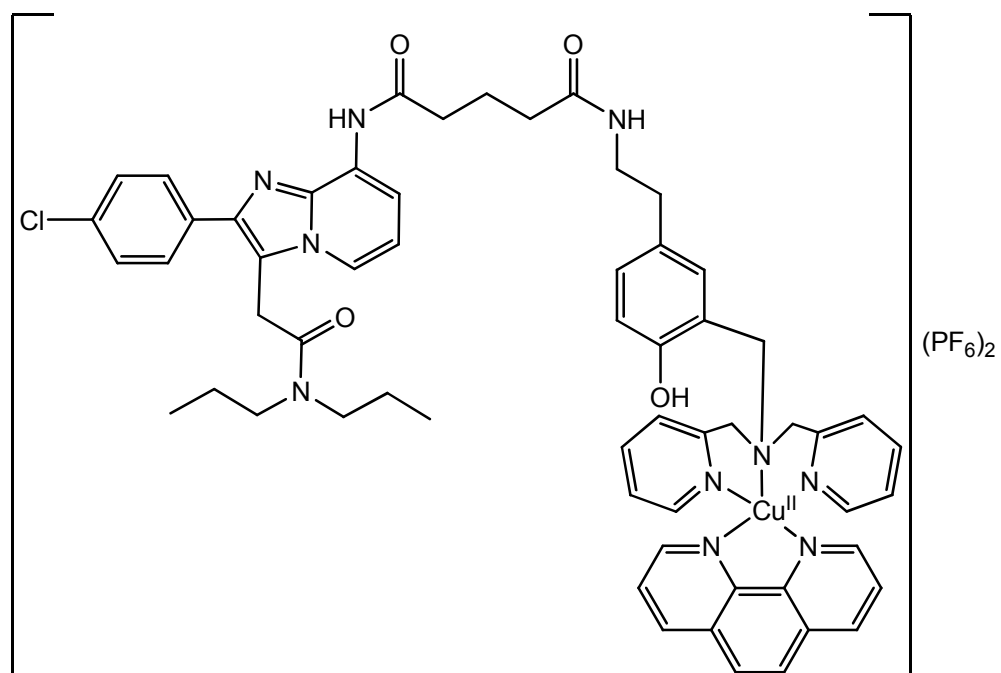


Figure 4.40: Structure of $[\text{Cu}(\text{HL}^{10})(\text{phen})](\text{PF}_6)_2$.

4.5. References

- (1) Gottlieb, H. E.; Kotlyar, V.; Nudelman, A. *J. Org. Chem.* **1997**, *62*, 7512-7515.
- (2) Glasoe, P. K.; Long, F. A. *J. Phys. Chem.* **1960**, *64*, 188-190.
- (3) Huang, N.; Siegel, M. M.; Kruppa, G. H.; Laukien, F. H. *J. Am. Soc. Mass Spectr.* **1999**, *10*, 1166-1173.
- (4) CrysAlisPro, Oxford Diffraction Ltd., Ver 1.171.33.31 (release 08-01-2009 CrysAlis171.NET).
- (5) Sheldrick, G. M. SHELXS-97. Program for crystal structure solution, University of Göttingen, Germany, 1997.
- (6) Sheldrick, G. M. SHELXL-97, Program for crystal structure refinement, University of Göttingen, Germany, 1997.
- (7) Sheldrick, G. M. SHELXTL-PLUS (VMS), Siemens Analytical X-Ray Instruments Inc., Madison, WI: 1990.
- (8) McArdle, P.; Gilligan, K.; Cunningham, D.; Dark, R.; Mahon, M. *CrystEngComm* **2004**, *6*, 303-309.
- (9) McArdle, P. *J. Appl. Crystallogr.* **1995**, *28*, 65.
- (10) Gans, P.; Sabatini, A.; Vacca, A. *Talanta* **1996**, *43*, 1739-1753.
- (11) Ginzburg, G. *Talanta* **1976**, *23*, 149-152.
- (12) Henderson, L. J. *Am. J. Physiol.* **1908**, *21*, 465.
- (13) Hasselbalch, K. A. *Biochem. Z. (FEBS J.)* **1916**, *78*, 112-144.
- (14) Po, H. N.; Senozan, N. M. *J. Chem. Educ.* **2001**, *78*, 1499.
- (15) Martell, A. E.; Smith, R. M. *Critical Stability Constants, Vol I*, Plenum Press **1977**.
- (16) Ferguson, W. J.; Braunschweiger, K. I.; Braunschweiger, W. R.; Smith, J. R.; McCormick, J. J.; Wasmann, C. C.; Jarvis, N. P.; Bell, D. H.; Good, N. E. *Anal. Biochem.* **1980**, *104*, 300-310.
- (17) Good, N. E.; Izawa, S. *Methods Enzymol.* **1972**; *24*, 53-68.
- (18) Good, N. E.; Winget, G. D.; Winter, W.; Connolly, T. N.; Izawa, S.; Singh, R. M. M. *Biochemistry* **1966**, *5*, 467-477.
- (19) Berbenni, V.; Milanese, C.; Bruni, G.; Marini, A. *J. Therm. Anal. Calorim.* **2005**, *85*, 401-407.
- (20) Bunton, C. A.; Farber, S. J. *J. Org. Chem.* **1969**, *34*, 767-772.

- (21) Brown, D. M.; Usher, D. A. *J. Chem. Soc.* **1965**, 6558-6564.
- (22) Williams, D. B.; Lawton, M. *J. Org. Chem.* **2010**, *75*, 8351-8354.
- (23) Van der Boom, M. E.; Liou, S. Y.; Ben-David, Y.; Shimon, L. J. W.; Milstein, D. *J. Am. Chem. Soc.* **1998**, *120*, 6531-6541.
- (24) Paine, R. T.; Tan, Y. C.; Gan, X. M. *Inorg. Chem.* **2001**, *40*, 7009-7013.
- (25) Lee, B.-L.; Kärkäs, M. D.; Johnston, E. V.; Inge, A. K.; Tran, L.-H.; Xu, Y.; Hansson, Ö.; Zou, X.; Åkermark, B. *Eur. J. Inorg. Chem.* **2010**, *2010*, 5462-5470.
- (26) Chomitz, W. A.; Minasian, S. G.; Sutton, A. D.; Arnold, J. *Inorg. Chem.* **2007**, *46*, 7199-7209.
- (27) Wong, Y.-L.; Mak, C.-Y.; Kwan, H. S.; Lee, H. K. *Inorg. Chim. Acta* **2010**, *363*, 1246-1253.
- (28) Pascaly, M.; Duda, M.; Rompel, A.; Sift, B. H.; Meyer-Klaucke, W.; Krebs, B. *Inorg. Chim. Acta* **1999**, *291*, 289-299.
- (29) Ho, Y.-H.; Chang, M.-C.; Yu, K.-H.; Liu, Y.-H.; Wang, Y.; Cheng, Y.-C.; Chen, J.-T. *Dalton Trans.* **2014**, *43*, 6287-6290.
- (30) Jarenmark, M.; Kappen, S.; Haukka, M.; Nordlander, E. *Dalton Trans.* **2008**, 993-996.
- (31) Policar, C.; Lambert, F.; Cesario, M.; Morgenstern-Badarau, I. *Eur. J. Inorg. Chem.* **1999**, *12*, 2201-2207.
- (32) Borovik, A. S.; Papaefthymiou, V.; Taylor, L. F.; Anderson, O. P.; Que, L. *J. Am. Chem. Soc.* **1989**, *111*, 6183-6195.
- (33) Wang, Q.; Wilson, C.; Blake, A. J.; Collinson, S. R.; Tasker, P. A.; Schröder, M. *Tetrahedron Lett.* **2006**, *47*, 8983-8397.
- (34) Lambert, E.; Chabut, B.; Chardon-Noblat, S.; Deronzier, A.; Chottard, G.; Bousseksou, A.; Tuchagues, J. P.; Laugier, J.; Bardet, M.; Latour, J. M. *J. Am. Chem. Soc.* **1997**, *119*, 9424-9437.
- (35) Huisman, M.; Koval, I. A.; Gamez, P.; Reedijk, J. *Inorg. Chim. Acta* **2006**, *359*, 1786-1794.
- (36) Park, H. S.; Lin, Q.; Hamilton, A. D. *J. Am. Chem. Soc.* **1999**, *121*, 8-19.
- (37) Camargo, M. A.; Neves, A.; Szpoganicz, B.; Bortoluzzi, A. J.; Fischer, F. L.; Terenzi, H.; Castellano, E. E. *Inorg. Chem.* **2010**, *49*, 3057-3063.

- (38) Smith, S. J.; Casellato, A.; Hadler, K. S.; Mitic, N.; Riley, M. J.; Bortoluzzi, A. J.; Szpoganicz, B.; Schenk, G.; Neves, A.; Gahan, L. R. *J. Biol. Inorg. Chem.* **2007**, *12*, 1207-1220.
- (39) Wild, G. P.; Wiles, C.; Watts, P.; Haswell, S. J. *Tetrahedron* **2009**, *65*, 1618-1629.
- (40) Louie, M.-W.; Liu, H.-W.; Lam, M. H.-C.; Lau, T.-C.; Lo, K. K.-W. *Organometallics* **2009**, *28*, 4297-4307.
- (41) Trapani, G.; Franco, M.; Ricciardi, L.; Latrofa, A.; Genchi, G.; Sanna, E.; Tuveri, F.; Cagetti, E.; Biggio, G.; Liso, G. *J. Med. Chem* **1997**, *40*, 3109-3118.
- (42) Trapani, G.; Franco, M.; Latrofa, A.; Ricciardi, L.; Carotti, A.; Serra, M.; Sanna, E.; Biggio, G.; Liso, G. *J. Med. Chem.* **1999**, *42*, 3934-3941.
- (43) Manning, H. C.; Goebel, T.; Marx, J. N.; Bomhop, D. J. *Org. Lett.* **2002**, *4*, 1075-1078.
- (44) Janin, Y. L.; Roulland, E.; Beurdeley-Thomas, A.; Decaudin, D.; Monneret, C.; Poupon, M.-F. *J. Chem. Soc., Perkin. Trans. 1* **2002**, 529-532.
- (45) Jiang, J. K.; Thomas, C. J.; Neumann, S.; Lu, X.; Rice, K. C.; Gershengorn, M. C. *Bioorg. Med. Chem. Lett.* **2005**, *15*, 733-736.
- (46) Gavish, M.; Veenman, J. A. Shterenberg, A.; Marek, I. *Heterocyclic derivatives, pharmaceutical compositions and methods of use thereof*, **2010**, US patent: US20090438291 20090924
- (47) Gavish, M.; Veenman, J. A.; Shterenberg, A.; Marek, I. *Heterocyclic derivatives binding to the peripheral-type benzodiazepine receptor*, **2008**, US patent: WO2006IL00979 20060822
- (48) Nunzio, D.; Laquintana, V.; Pisu, M. G.; Dore, R.; Murru, L.; Latrofa, A.; Trapani, G.; Sanna, E. *J. Med. Chem.* **2008**, *51*, 6876-6888.

Appendices

Appendix 1. pH rate profiles for auto hydrolysis of substrates

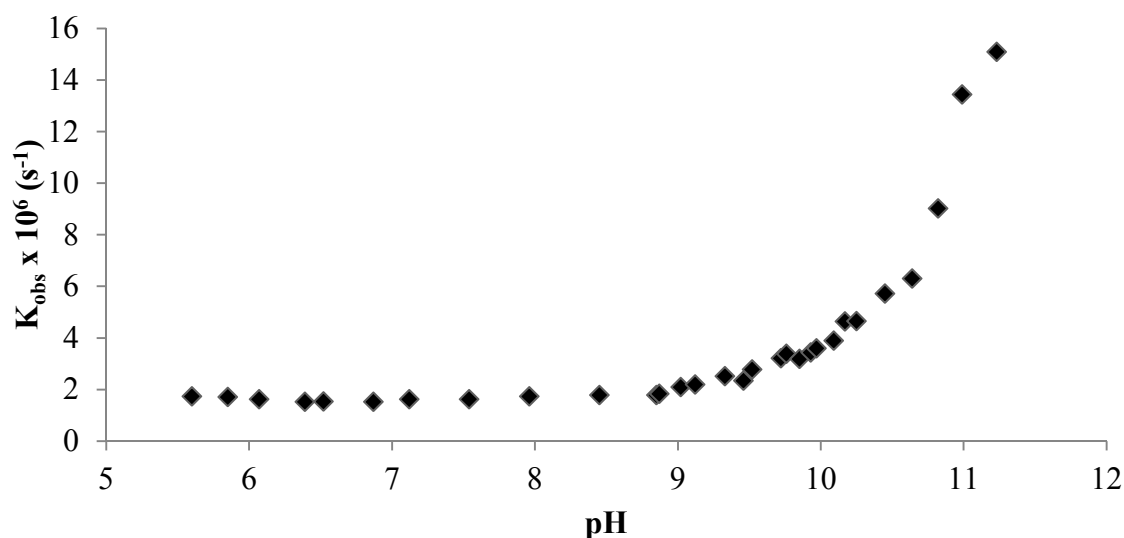


Figure A1.1: pH rate profile for auto-hydrolysis of BDNP [5×10^{-5} M] at 40 °C. $I = 0.1$ M (KNO_3), [buffer] = 50 mM (buffer = MES (pH 5.5 – 6.7), PIPES (pH 6.2 – 7.4), MOPS (pH 6.6 – 7.8), HEPES (pH 6.9 – 8.1), EPPS (pH 7.4 – 8.6), CHES (pH 8.7 – 9.9) and CAPS (pH 9.8 – 11.0)).

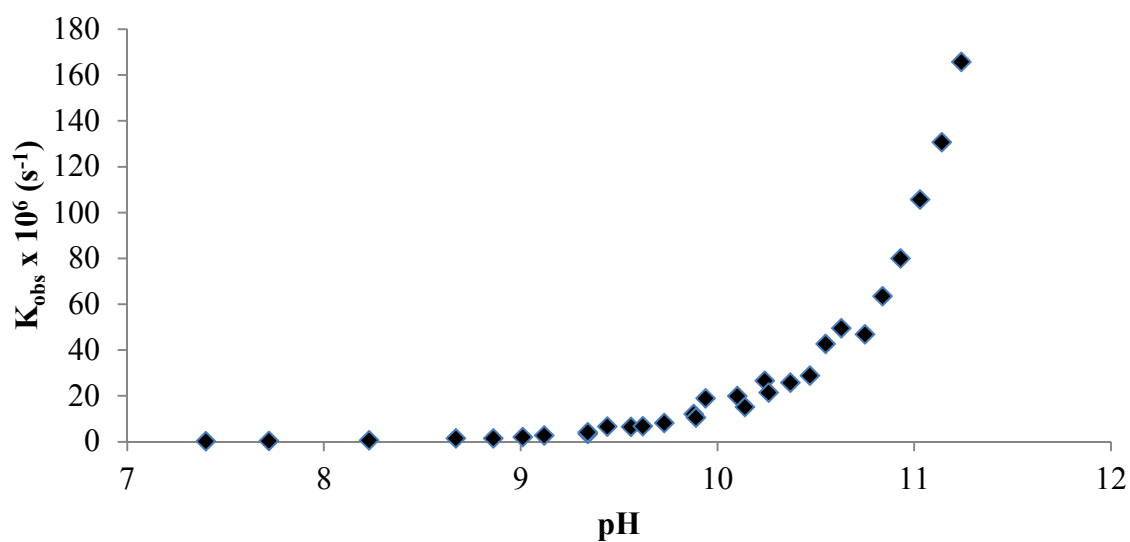
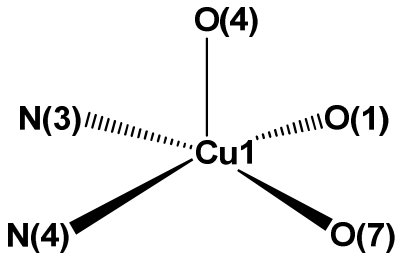
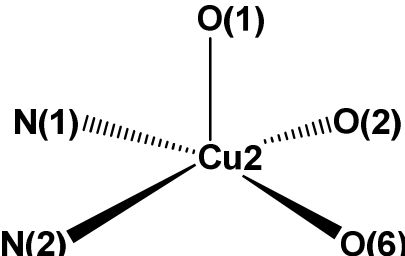


Figure A1.2: pH rate profile for auto hydrolysis of HPNP [5×10^{-5} M] at 40 °C. $I = 0.1$ M (KNO_3), [buffer] = 50 mM (buffer = MOPS (pH 6.6 – 7.8), HEPES (pH 6.9 – 8.1), EPPS (pH 7.4 – 8.6), CHES (pH 8.7 – 9.9) and CAPS (pH 9.8 – 11.0)).

Appendix 2. Cu coordination environment within $[\text{Cu}_2(\text{L}^2)(\text{H}_2\text{O})_2](\text{NO}_3)$.

Table A2.1: Coordination environment, bond lengths (Å), bond angles (°) and geometric parameter, τ^1 , for the Cu atoms in $[\text{Cu}_2(\text{L}^2)(\text{H}_2\text{O})_2](\text{NO}_3)$

Cu coordination environment	Bond distances (Å)		Bond angles (°)				τ^1
	Cu(1)-O(4)	2.179(2)	N(3)-Cu(1)-O(7)	176.17(10)	N(3)-Cu(1)-O(1)	94.62(10)	0.16
	Cu(1)-N(4)	2.001(3)	N(4)-Cu(1)-O(1)	166.51(10)	O(1)-Cu(1)-O(7)	89.21(9)	
	Cu(1)-O(7)	2.014(3)	O(4)-Cu(1)-N(4)	95.63(11)	O(7)-Cu(1)-N(4)	95.18(11)	
	Cu(1)-O(1)	1.945(2)	O(4)-Cu(1)-N(3)	82.38(10)	N(4)-Cu(1)-N(3)	81.08(11)	
	Cu(1)-N(3)	2.046(3)	O(4)-Cu(1)-O(1)	96.46(9)	O(4)-Cu(1)-O(7)	97.23(10)	
	Cu(2)-O(1)	2.185(2)	N(1)-Cu(2)-O(6)	173.12(12)	O(1)-Cu(2)-O(6)	91.85(10)	0.44
	Cu(2)-N(2)	1.985(3)	N(2)-Cu(2)-O(2)	146.64(10)	N(1)-Cu(2)-O(2)	83.10(11)	
	Cu(2)-O(6)	1.949(3)	O(1)-Cu(2)-N(2)	114.34(10)	O(2)-Cu(2)-O(6)	92.35(13)	
	Cu(2)-O(2)	2.034(3)	O(1)-Cu(2)-N(1)	93.84(9)	O(6)-Cu(2)-N(2)	96.71(13)	
	Cu(2)-N(1)	1.998(3)	O(1)-Cu(2)-O(2)	97.31(9)	N(2)-Cu(2)-N(1)	84.45(11)	

(1) Addison, A. W.; Rao, T. N.; Reedijk, J.; van Rijn, J.; Verschoor, G. C. *J. Chem. Soc. Dalton Trans.* **1984**, 1349-1356.

Appendix 3. Crystallographic data for $[\text{Cu}_2(\text{L}^2)(\text{H}_2\text{O})_2](\text{NO}_3)$.

Table 3.1: Crystallographic data for $[\text{Cu}_2(\text{L}^2)(\text{H}_2\text{O})_2](\text{NO}_3)$.

Formula	$\text{C}_{25}\text{H}_{25}\text{Cu}_2\text{N}_5\text{O}_{11}$
M_r	762.60
Crystal colour and habit	black block
Crystal size (mm)	0.20 x 0.30 x 0.30
Crystal System	Triclinic
Space group	P-1
Unit cell dimension	
a [Å]	9.6099(6)
b [Å]	12.7649(11)
c [Å]	13.4688(11)
α [°]	104.651(8)
β [°]	94.844(6)
γ [°]	97.413(7)
V [Å ³]	1573.3(2)
Z	2
D_{calc} (g cm ⁻³)	1.610
$\mu(\text{Mo K}\alpha)$ (μm^{-1})	1.430
F(000)	776
Temperature (K)	293
2θ range (°)	3.3 – 27.1
No. measd. reflections	12712
No. unique reflections (R_{int})	6775 (2.4 %)
No. of observed reflections	5219 ($I > 2\sigma(I)$)
No. of parameters	433
Final R_1^a	4.31%
wR_2 (all reflections) ^a	12.62%
Goodness-of-fit (observed reflections)	1.04

^a $R_1 = \sum ||F_o| - |F_c|| / \sum |F_o|$; $wR_2 = [\sum w(F_o^2 - F_c^2)^2 / \sum w(F_o^2)^2]^{1/2}$; $w^{-1} = \sigma^2(F_o^2) + (aP)^2$; $P = (F_o^2 + 2F_c^2)/3$

Appendix 4. MS characterisation of compounds **16**, **17**, **19**, **22** and **23**.

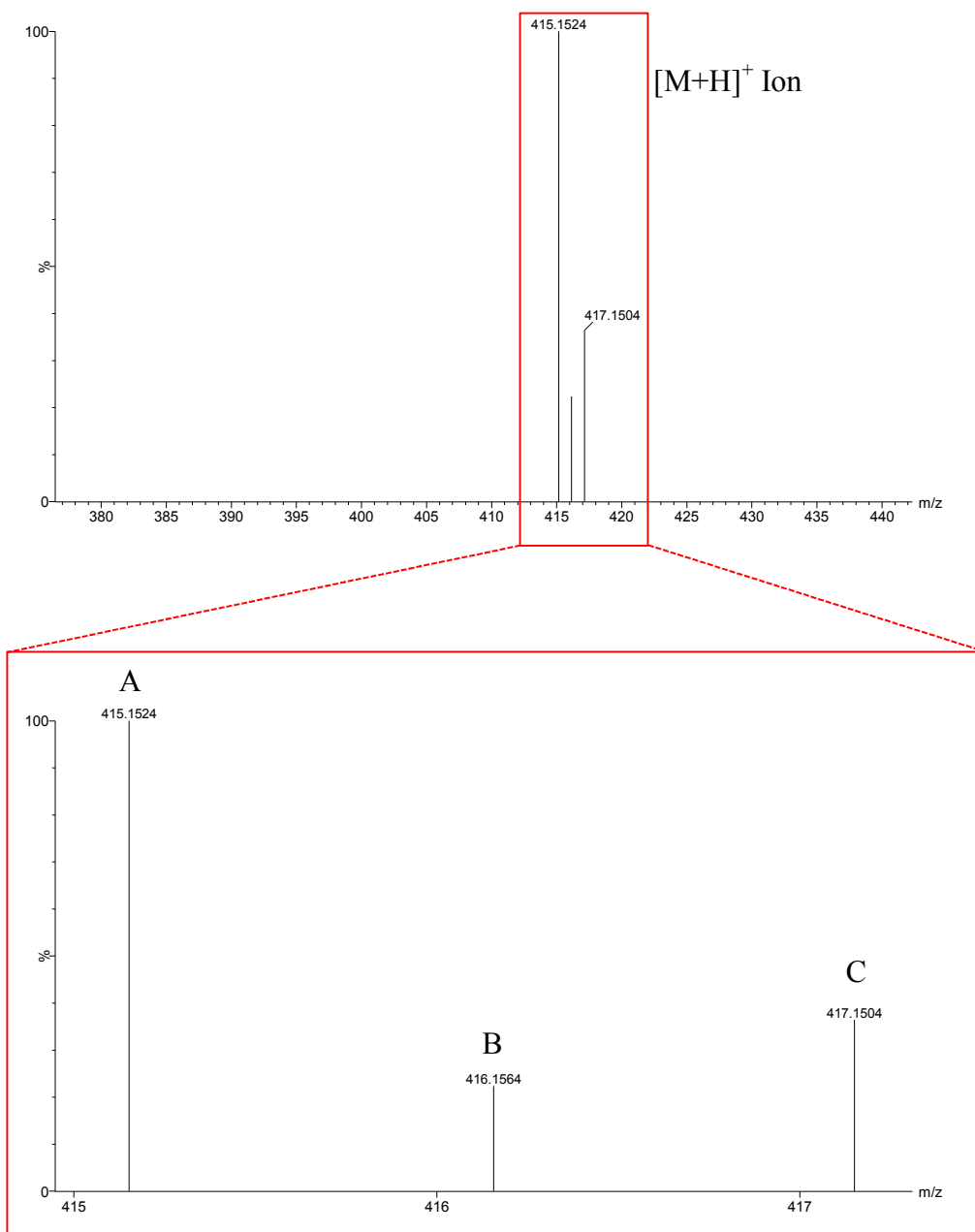
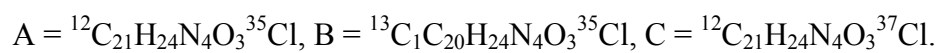


Figure A4.1: Expanded and zoomed positive ion MS for **16**, observed ion $[M+H]^+$.



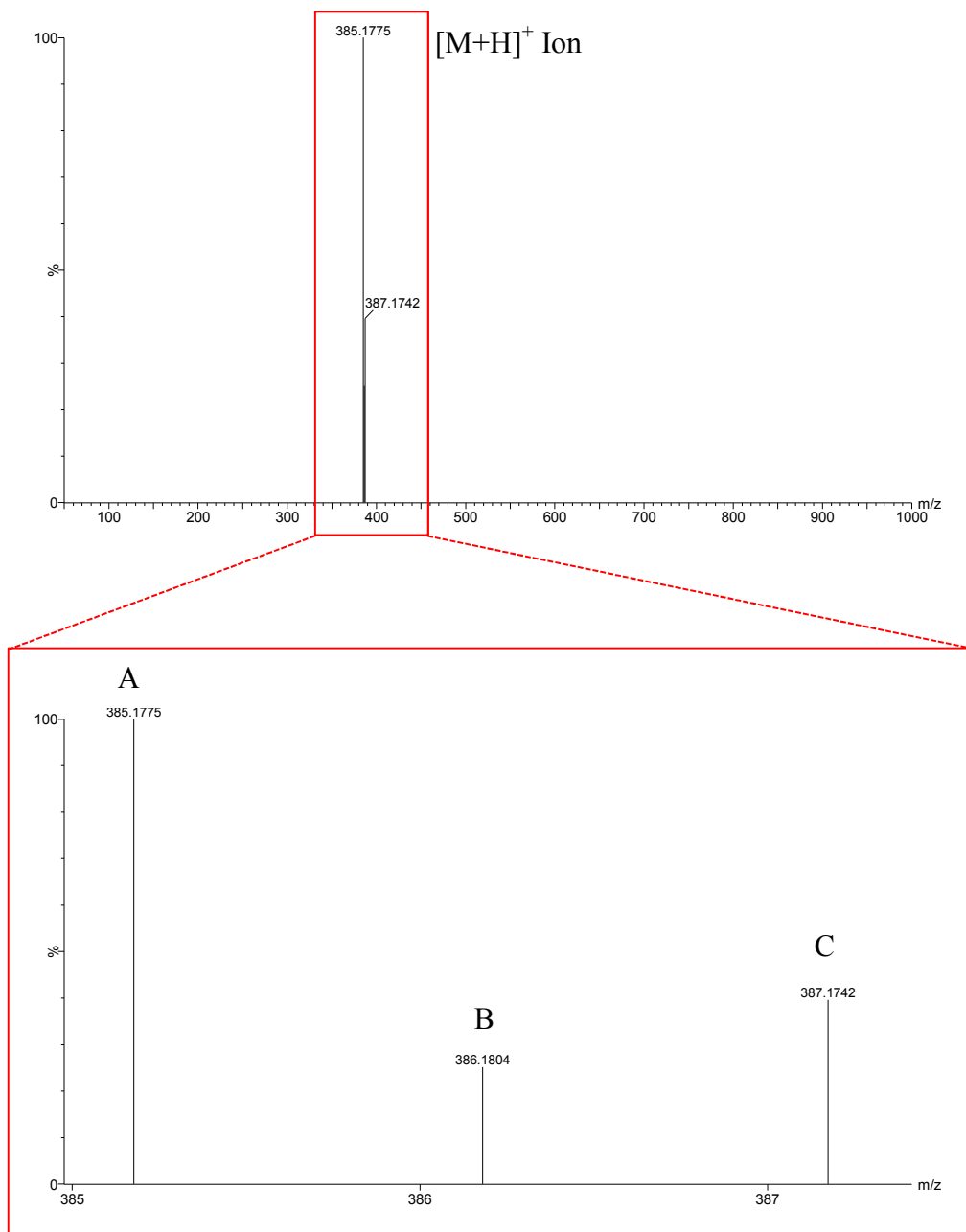


Figure A4.2: Expanded and zoomed positive ion MS for **17**, observed ion $[M+H]^+$.
 A = $^{12}\text{C}_{21}\text{H}_{26}\text{N}_4\text{O}^{35}\text{Cl}$, B = $^{13}\text{C}_1\text{C}_{20}\text{H}_{26}\text{N}_4\text{O}^{35}\text{Cl}$, C = $^{12}\text{C}_{21}\text{H}_{26}\text{N}_4\text{O}^{37}\text{Cl}$.

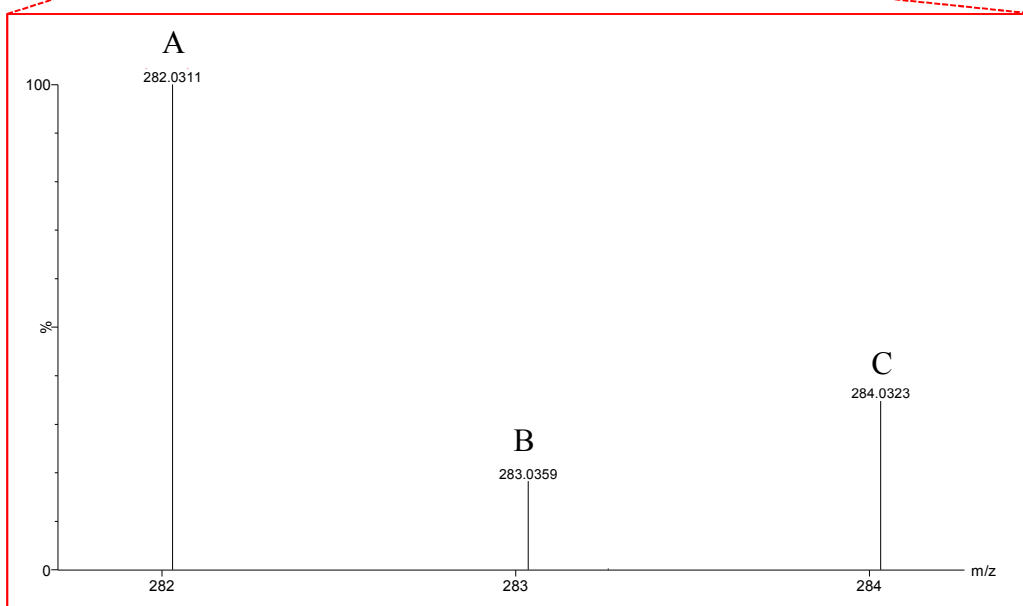
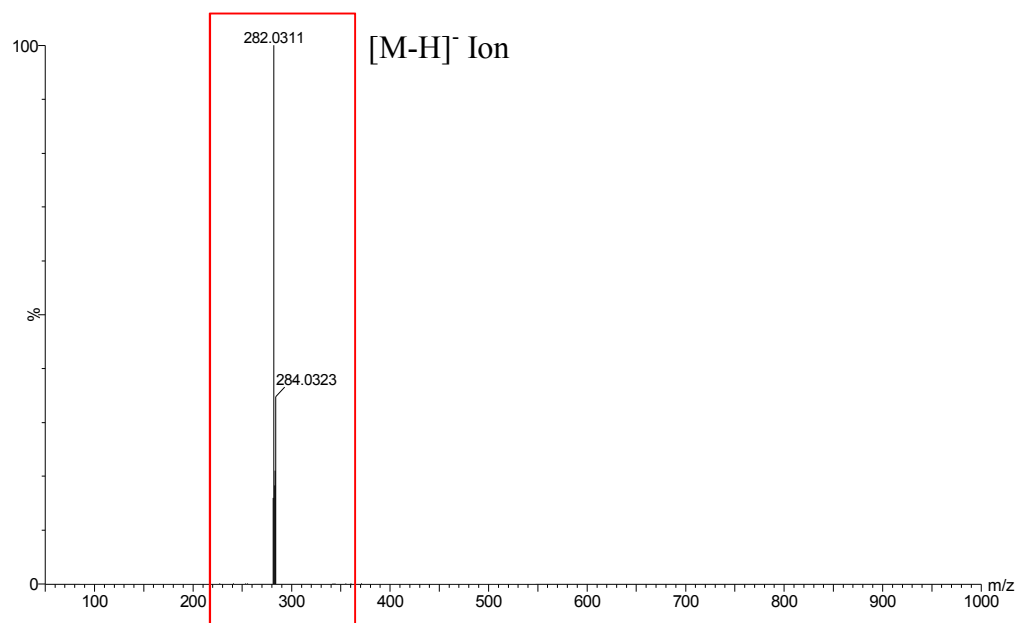


Figure A4.3: Expanded and zoomed positive/negative ion MS for **21**, observed ion $[M-H]^-$. A = $^{12}\text{C}_{16}\text{H}_9\text{NO}_2^{35}\text{Cl}$, B = $^{13}\text{C}^{12}\text{C}_{15}\text{H}_9\text{NO}_2^{35}\text{Cl}$ and C = $^{12}\text{C}_{16}\text{H}_9\text{NO}_2^{37}\text{Cl}$.

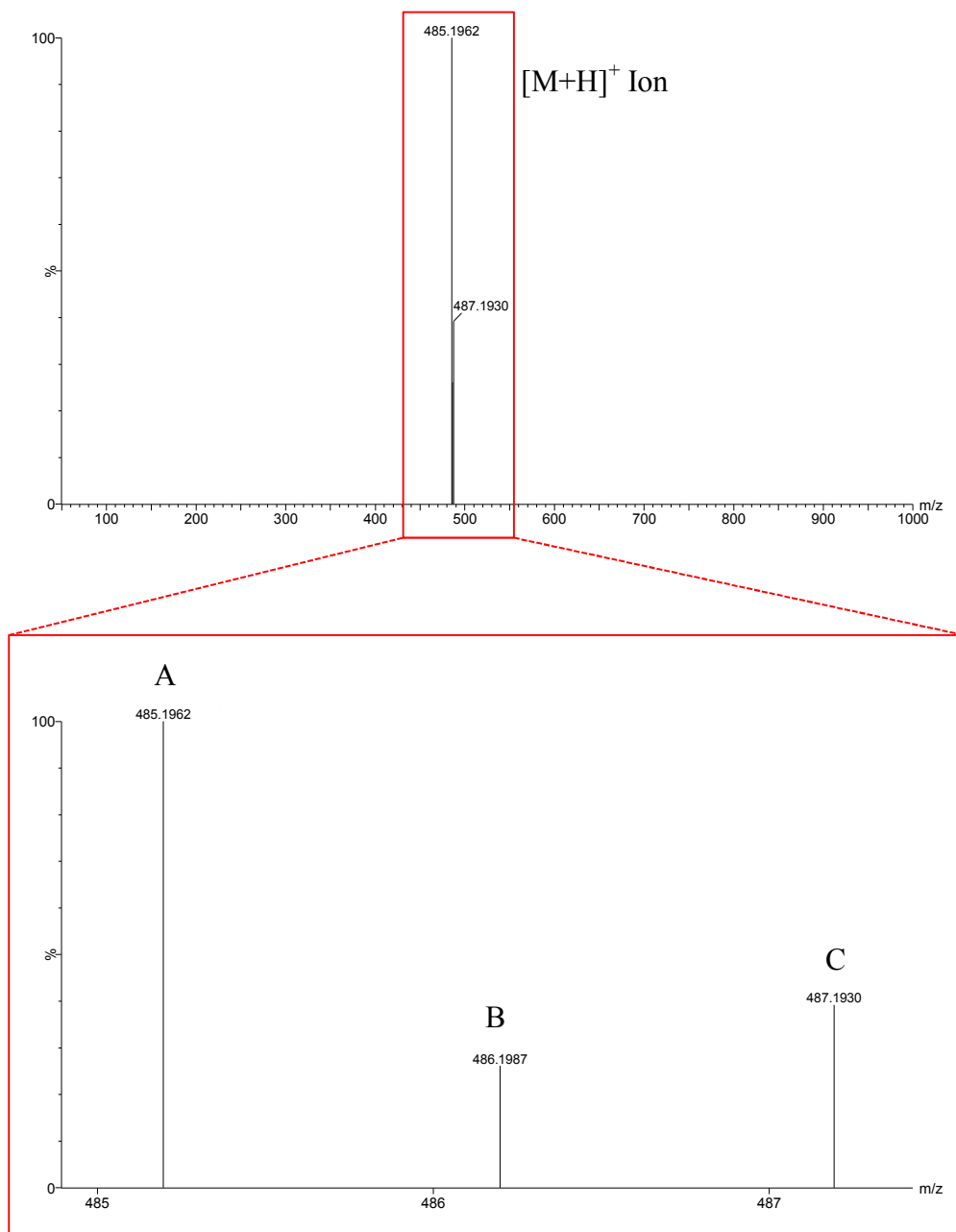


Figure A4.4: Expanded and zoomed positive ion MS for **22**, observed ion $[M+H]^+$.
 A = $^{12}\text{C}_{25}\text{H}_{30}\text{N}_4\text{O}_4^{35}\text{Cl}$, B = $^{13}\text{C}_1^{12}\text{C}_{24}\text{H}_{30}\text{N}_4\text{O}_4^{35}\text{Cl}$ and C = $^{12}\text{C}_{25}\text{H}_{30}\text{N}_4\text{O}_4^{37}\text{Cl}$.

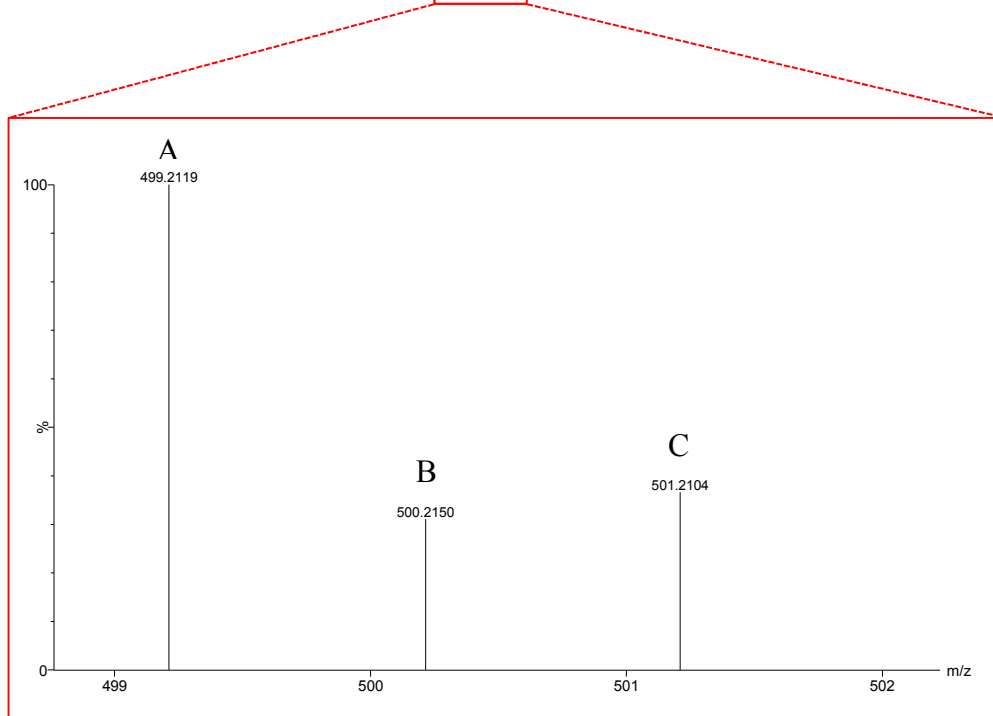
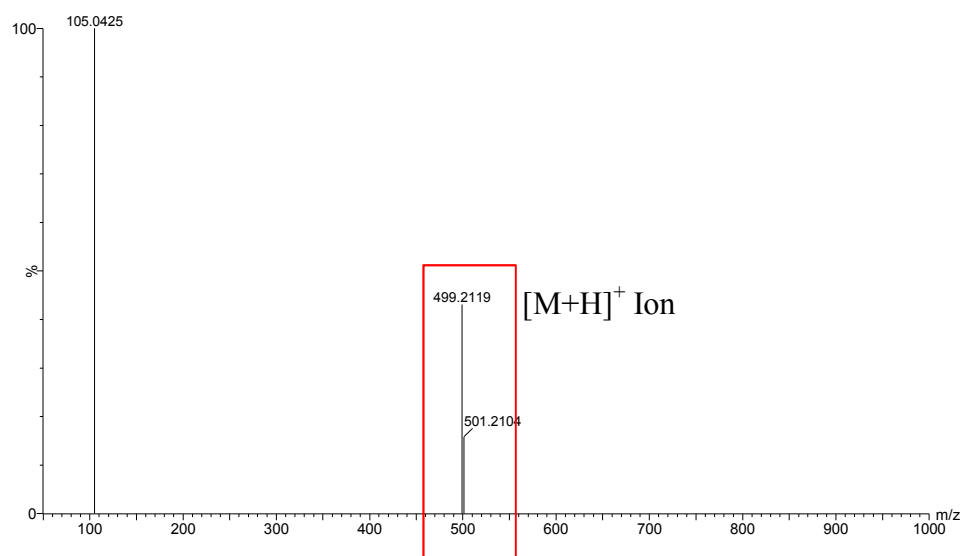


Figure A4.5: Expanded and zoomed positive ion MS for **23**, observed ion [M+H]⁺.
 A = ¹²C₂₆H₃₂N₄O₄³⁵Cl, B = ¹³C₁C₂₅H₃₂N₄O₄³⁵Cl and C = ¹²C₂₆H₃₂N₄O₄³⁷Cl.

Tables comparing measured and predicted MS values are included in **Appendix 5**.

Appendix 5. Tables of predicted versus measured MS data for generated ligands.

Table A5.1: Table of measured and predicted m/z for **HL⁷**, observed ion $[M+H]^+$.

Measured		Predicted		Species observed
m/z	intensity	m/z	intensity	
739.4811	100	739.4799	100	$^{12}\text{C}_{45}^{1}\text{H}_{63}^{14}\text{N}_4^{16}\text{O}_5$
740.4753	60.21	740.4831	52.64	$^{13}\text{C}_1^{12}\text{C}_{44}^{1}\text{H}_{63}^{14}\text{N}_4^{16}\text{O}_5$
741.4783	13.74	741.4861	14.58	$^{13}\text{C}_2^{12}\text{C}_{37}^{1}\text{H}_{63}^{14}\text{N}_4^{16}\text{O}_5$

Table A5.2: Table of measured and predicted m/z for **HL⁸**, observed ion $[M+H]^+$.

Measured		Predicted		Species observed
m/z	intensity	m/z	intensity	
614.2328	100	614.2323	100	$^{12}\text{C}_{37}^{1}\text{H}_{33}^{14}\text{N}_5^{16}\text{O}_2^{35}\text{Cl}$
615.2340	44.82	615.2354	43.54	$^{13}\text{C}^{12}\text{C}_{36}^{1}\text{H}_{33}^{14}\text{N}_5^{16}\text{O}_2^{35}\text{Cl}$
616.2298	44.82	616.2314	41.63	$^{12}\text{C}_{37}^{1}\text{H}_{33}^{14}\text{N}_5^{16}\text{O}_2^{37}\text{Cl}$
617.2302	15.65	617.2333	15.37	$^{13}\text{C}^{12}\text{C}_{36}^{1}\text{H}_{33}^{14}\text{N}_5^{16}\text{O}_2^{37}\text{Cl}$

Table A5.3: Table of measured and predicted m/z for **HL⁹**, observed ion $[M+H]^+$.

Measured		Predicted		Species observed
m/z	intensity	m/z	intensity	
815.3696	100	815.3800	100	$^{12}\text{C}_{46}^{1}\text{H}_{52}^{14}\text{N}_8^{16}\text{O}_4^{35}\text{Cl}$
816.3746	53.62	816.3831	55.02	$^{13}\text{C}^{12}\text{C}_{45}^{1}\text{H}_{52}^{14}\text{N}_8^{16}\text{O}_4^{35}\text{Cl}$
817.3705	44.17	817.3800	47.63	$^{12}\text{C}_{46}^{1}\text{H}_{52}^{14}\text{N}_8^{16}\text{O}_4^{37}\text{Cl}$
818.3680	19.14	818.3814	20.65	$^{13}\text{C}^{12}\text{C}_{45}^{1}\text{H}_{52}^{14}\text{N}_8^{16}\text{O}_4^{37}\text{Cl}$

Table A5.4: Table of measured and predicted m/z for **HL**¹⁰, observed ion $[M+H]^+$.

Measured		Predicted		Species observed
m/z	intensity	m/z	intensity	
829.4405	100	829.3956	100	¹² C ₄₇ ¹ H ₅₄ ¹⁴ N ₈ ¹⁶ O ₄ ³⁵ Cl
830.4423	57.16	830.3987	56.28	¹³ C ¹² C ₄₆ ¹ H ₅₄ ¹⁴ N ₈ ¹⁶ O ₄ ³⁵ Cl
831.4398	43.80	831.3958	48.36	¹² C ₄₇ ¹ H ₅₄ ¹⁴ N ₈ ¹⁶ O ₄ ³⁷ Cl
832.4418	24.76	832.3971	21.24	¹³ C ¹² C ₄₆ ¹ H ₅₄ ¹⁴ N ₈ ¹⁶ O ₄ ³⁷ Cl

Table A5.5: Table of measured and predicted m/z for **16**, observed ion $[M+H]^+$.

Measured		Predicted		Species observed
m/z	intensity	m/z	intensity	
415.1524	100	415.1537	100	¹² C ₂₁ H ₂₄ N ₄ O ₃ ³⁵ Cl
416.1564	22.33	416.1567	25.30	¹³ C ₁ C ₂₀ H ₂₄ N ₄ O ₃ ³⁵ Cl
417.1504	36.33	417.1516	35.65	¹² C ₂₁ H ₂₄ N ₄ O ₃ ³⁷ Cl

Table A5.6: Table of measured and predicted m/z for **17**, observed ion $[M+H]^+$.

Measured		Predicted		Species observed
m/z	intensity	m/z	intensity	
385.1777	100	385.1795	100	¹² C ₂₁ H ₂₆ N ₄ O ³⁵ Cl
386.1808	25.33	386.1826	25.25	¹³ C ₁ C ₂₀ H ₂₆ N ₄ O ³⁵ Cl
387.1743	40.08	387.1774	35.24	¹² C ₂₁ H ₂₆ N ₄ O ³⁷ Cl

Table A5.7: Table of measured and predicted m/z for **21**, observed ion $[M-H]^-$.

Measured		Predicted		Species observed
m/z	Intensity	m/z	Intensity	
282.0311	100	282.0322	100	$^{12}\text{C}_{16}\text{H}_9\text{NO}_2^{35}\text{Cl}$
283.0359	18.46	283.0354	18.37	$^{13}\text{C}^{12}\text{C}_{15}\text{H}_9\text{NO}_2^{35}\text{Cl}$
284.0323	34.68	284.0298	33.97	$^{12}\text{C}_{16}\text{H}_9\text{NO}_2^{37}\text{Cl}$

Table A5.8: Table of measured and predicted m/z for **22**, observed ion $[M+H]^+$.

Measured		Predicted		Species observed
m/z	Intensity	m/z	Intensity	
485.1963	100	485.1956	100	$^{12}\text{C}_{25}\text{H}_{30}\text{N}_4\text{O}_4^{35}\text{Cl}$
486.1985	25.87	486.1986	29.88	$^{13}\text{C}_1^{12}\text{C}_{24}\text{H}_{30}\text{N}_4\text{O}_4^{35}\text{Cl}$
487.1972	39.51	487.1938	37.09	$^{12}\text{C}_{25}\text{H}_{30}\text{N}_4\text{O}_4^{37}\text{Cl}$

Table A5.9: Table of measured and predicted m/z for **23**, observed ion $[M+H]^+$.

Measured		Predicted		Species observed
m/z	Intensity	m/z	Intensity	
499.2119	100	499.2112	100	$^{12}\text{C}_{26}\text{H}_{32}\text{N}_4\text{O}_4^{35}\text{Cl}$
500.2151	31.50	500.2143	31.02	$^{13}\text{C}_1\text{C}_{25}\text{H}_{32}\text{N}_4\text{O}_4^{35}\text{Cl}$
501.2105	35.93	501.2095	37.43	$^{12}\text{C}_{26}\text{H}_{32}\text{N}_4\text{O}_4^{37}\text{Cl}$